Molecular analysis of the cell-cell joining protein SepJ in *Anabaena* sp. PCC 7120

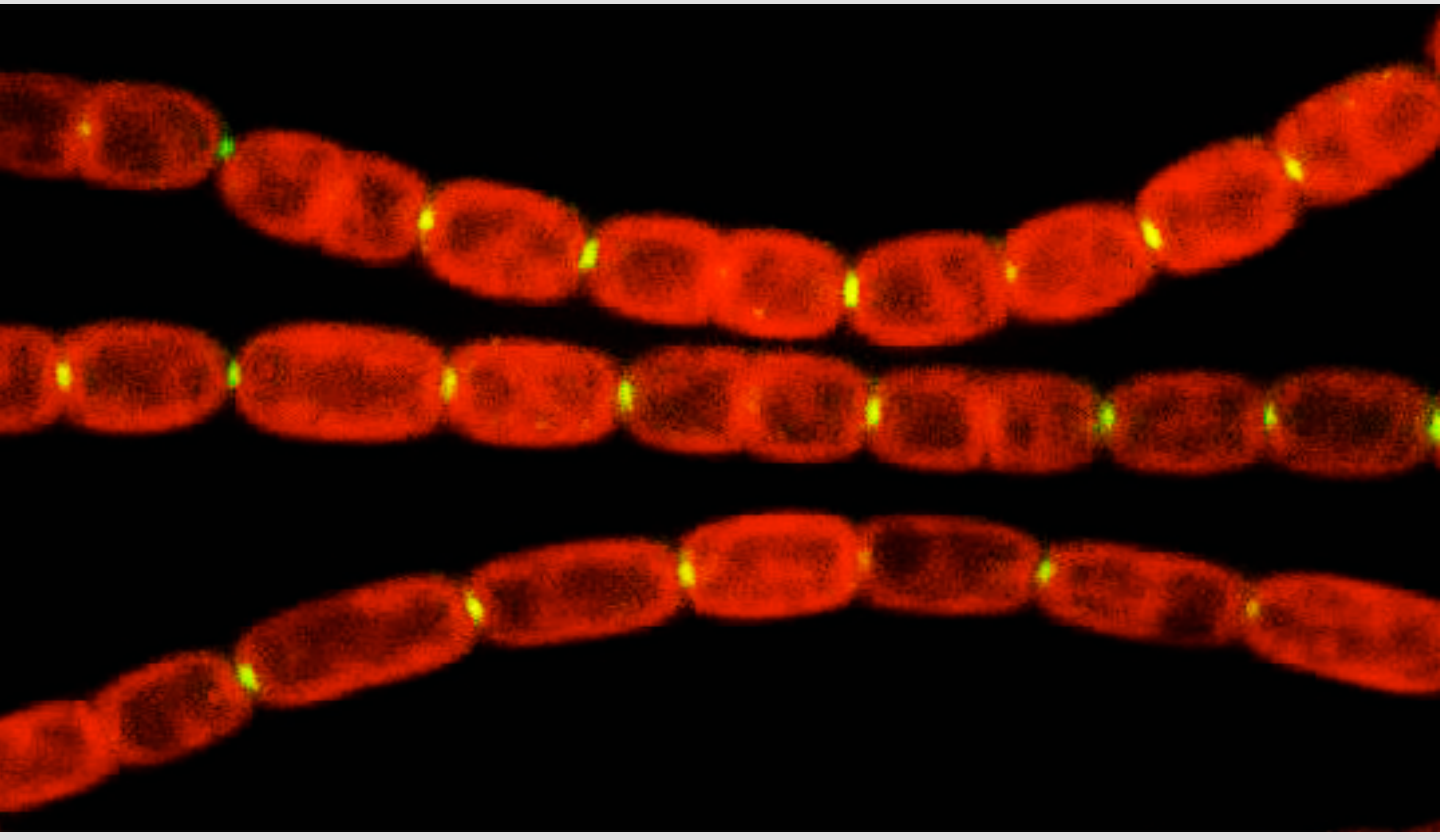

Félix Ramos León

Sevilla, 2017

Cover: micrograph of filaments of strain CSVM135 expressing the fusion protein SepJ-GFP-His_{10}. Red color corresponds to autofluorescence; green, GFP fluoresence.

CSIC
Consejo Superior de Investigaciones Científicas

Universidad de Sevilla

Molecular analysis of the cell-cell joining protein SepJ in *Anabaena* sp. PCC 7120

Trabajo presentado para optar al grado
de Doctor en Biología por el Licenciado
Félix Ramos León

Sevilla, Febrero de 2017

Director

Dr. Enrique Flores García
Profesor de Investigación del CSIC

Director

Dr. Vicente Mariscal Romero
Doctor en Bioquímica

Tutor

Dr. Manuel Hervás Morón
Catedrático de Bioquímica y Biología Molecular

AGRADECIMIENTOS

Esta tesis ha sido realizada en el Instituto de Bioquímica Vegetal y Fotosíntesis de Sevilla, centro mixto de la Universidad de Sevilla y el Consejo Superior de Investigaciones Científicas, gracias a una beca de Formación de Personal Investigador (BES-2012-052202) con financiación del proyecto BFU2011-22762, del que el Dr. Enrique Flores García ha sido el investigador principal.

Durante la realización de la tesis disfruté de una estancia de cuatro meses en la Universidad de Turku (Finlandia), trabajando en el grupo de investigación de la Profesora Eva-Mari Aro, bajo la supervisión de la Dra. Natalia Battchikova.

En primer lugar me gustaría agradecer a mi director de tesis, el Dr. Enrique Flores, y a la Dra. Antonia Herrero, por darme la oportunidad de formarme en su grupo. Gracias por esos consejos desde la experiencia y la sensatez. Este trabajo no sería lo que es sin la visión crítica de ambos.

En segundo lugar quisiera agradecer a mi co-director, el Dr. Vicente Mariscal, por formarme en el laboratorio y por toda su ayuda, tanto a nivel profesional como a nivel personal. ¡Creo que una página se quedaría corta para escribir todo lo que te debo! Gracias por todo.

Mil gracias también a todos mis compañeros del laboratorio 9-10, a los que aún siguen y a los que pasaron por aquí. No solo me llevo la experiencia de haber trabajado en un ambiente estupendo, también me llevo grandes amigos. A Leticia, Laura y Antonio, por todos esos tan buenos momentos que me han hecho pasar y por toda su ayuda. A Mireia, por esos abracitos, esas sentadillas cósmicas que siempre me sacarán una sonrisa. A Sergio Jr., por ser un gran compañero y mejor amigo aún. A Sergio Camargo, por los consejos que me ha dado y siempre manteniendo la calma. A Gracia, porque siempre ha estado ahí para cualquier cosa que he necesitado, ¡el laboratorio sin ti no sería lo mismo! A Silvia, porque mi estancia en el laboratorio 10 no hubiese sido lo mismo sin escuchar esa risa tan "salá". A Ana, por toda su ayuda y consejos cuando los geles de proteínas se ponían difíciles. A Mercedes, por compartir ratitos de desconexión por la tarde conmigo. A José Enrique, por pasarme XL1-Blue por la tarde… Todos saben que esta es la muestra de cariño más grande que existe ;) En general muchas gracias a todos por hacerme sentir querido, nunca olvidaré estos años con vosotros.

También me gustaría agradecer al Dr. Ignacio Luque, por todos los consejos y ayuda que me ha dado a lo largo de estos años. También a los chicos de su laboratorio, Javi y Miguel Ángel.

También me gustaría agradecer a toda la gente del IBVF que me ha prestado su ayuda en todo momento. Me he sentido como en casa siempre. A la gente de los desayunos, me gustó escuchar vuestras batallitas y experiencias. A todo el grupo de "los viernes ar zol" , esos ratitos de cervezas han sido la clave para desconectar en los momentos de más agobio. Mención especial para Valle, comentar resultados en el Holidays siempre fue el mejor final en los días de estrés.

I would like to thank Prof. Eva-Mari Aro for letting me train in her group, and Dr. Natalia Battchikova for supervising me during my stay in Turku. I would also like to thank all my friends from Turku: Luca, Martina, Anita, Julia and Juande. Thanks for taking care of me in Finland. You all made me feel like home there. Kiitos!! Love you guys! I would also like to thank the best Irish guy I have ever met, Sam. Thank you very much for teaching me the true English!

A toda mi familia. Quiero agradecer todo su apoyo en los momentos difíciles, y porque sin ellos esta tesis no podría haber empezado. Gracias a mis padres, mi hermana y mis abuelos. Soy muy afortunado de teneros, gracias por inculcarme los mejores valores. Todos mis triunfos serán para vosotros.

A mi amiga Carmen, su apoyo ha sido fundamental. Gracias por escucharme, comprenderme y ayudarme. Tu apoyo me ha ayudado a sobrellevar todos los contratiempos que han surgido en el transcurso de esta tesis. A mi Alba, porque siempre tenía un audio motivador en el momento oportuno, que me sacaba una sonrisa cuando lo necesitaba. Muchas gracias a las dos ¡Os quiero!

A Jose, por haberme escuchado y aconsejado tanto en los últimos meses. ¡Tú también has sido mi descubrimiento del 2016! Y por supuesto a Rob, Manuel y Chano, por haberme hecho sentir tan arropado en estos últimos meses tan duros. ¡Muchas gracias chicos!

Muchísimas gracias

INDEX

FIGURE INDEX

1. INTRODUCTION

2. MATERIAL & METHODS

3. RESULTS

4. DISCUSSION

TABLE INDEX

2. MATERIALS & METHODS

3. RESULTS

ABBREVATIONS

2-OG	2-oxoglutarate
5-CF	5-carboxifluorescein
A	Amperes
A_2pm	Meso-diaminopimelic acid
aa	Amino acid
Ap	Ampicillin
ATP	Adenosine triphosphate
BACTH	Bacterial adenylate cyclase two-hydrid
BN	Blue Native
bp	Base pair
BSA	Bovine serum albumin
CA	Carbonic anhydrase
cAMP	Cyclic adenosine monophosphate
CC	Coiled-coil
CCM	CO_2 concentrating mechanisms
Chl *a*	Chlorophyll *a*
Cm	Chloramphenicol
CM	Cytoplasmic Membrane
CPG	Cyanophycin plug
CS	Cyanophycin synthetase
Ct	Cycle threshold
DDM	n-Dodecyl β-D-maltoside
DEPC	Diethylpyrocarbonate
DME	Drug/Metabolite Exporter
DNA	Deoxyribonucleic acid
DNase	Deoxyribonuclease
dNTPs	Deoxyribonucleotides
ε	Molar extinction coefficient
E	Einstein
ECM	Extracellular matrix
EDTA	Ethylenediaminetetraacetic acid
FITC	Fluorescein isothiocyanate
FPLC	Fast protein liquid chromatography
FRAP	Fluorescence recovery after photobleaching
GFP	Green Fluorescent Protein
GlcNAc	N-acetylglucosamine
GOGAT	Glutamine oxoglutarate aminotransferase
GS	Glutamine synthetase
HEP	Heterocyst envelope polysaccharide
HGL	Heterocyst-specific glycolipids
HRP	Horseradish peroxidase
IM	Integral membrane
IPTG	Isopropyl β-D-1-thiogalactopyranoside
Km	Kanamycin
LB	Luria-Bertani medium
LPS	Lipopolysaccharide
MACS	Magnetic-activated cell sorting
MALDI-TOF	Matrix-Assisted Laser Desorption/Ionization – Time-Of-Flight
Mch	Multiple contiguous heterocysts phenotype
miliQ	Ultrapure water (Trademark)
MurNAc	*N*-acetylmuramic acid
Nm	Neomycin

nt	Nucleotide(s)
OM	Outer Membrane
ONP	*o*-Nitrophenol
ONPG	*ortho*-Nitrophenyl-β-galactoside
ORF	Open reading frame
PAGE	Polyacrilamide Gel Electrophoresis
PBP	Penicilin Binding Protein
PBS	Phosphate Buffered Saline
PBS-T	Phosphate Buffered Saline supplemented with 1% Tween-20
PCC	Pasteur Culture Collection
PCR	Polymerase Chain Reaction
PG	Peptidoglycan
P_{ND}	NtcA-dependent promoter
POTRA	Polypeptide Transport Associated
pp	Periplasm
PSI	Photosystem I
psi	Pounds-force per square inch
PSII	Photosystem II
PVDF	Polyvinylidene fluoride
RNA	Ribonucleic acid
RNase	Ribonuclease
rpm	Revolutions per minute
RT	Retrotranscription
RuBisCO	Ribulose-1,5-bisphosphate carboxylase/oxygenase
SD	Standard deviation
SDS	Sodium dodecyl sulphate
SEM	Standard error of the mean
Sm	Streptomycin
Sp	Spectinomycin
TBE	Tris-borate-EDTA buffer
TBS	Tris buffered saline
TBS-T	Tris buffered saline supplemented with 1% Tween-20
TCA	Trichloracetic acid
TEMED	Tetramethylethylenediamine
TM	Transmembrane
TMS	Transmembrane segment
μ	Specific growth rate constant
U	Enzymatic activity units
V	Volt
v/v	Volume/volume ratio
w/v	Weight/volume ratio
X-gal	5-bromo-4-chloro-3-indolyl-β-D-galactopyranoside

RESUMEN EN ESPAÑOL

La multicelularidad se ha desarrollado de forma independiente en el curso de la evolución en diversos grupos filogenéticos, incluidos diferentes grupos bacterianos, e implica universalmente fenómenos de adhesión, comunicación y diferenciación celular. Se encuentran organismos multicelulares en grupos bacterianos como las actinobacterias, las cianobacterias y las mixococcales. Los representantes multicelulares en las cianobacterias son aquellas que crecen formando filamentos de células o tricomas que, en condiciones de escasez de nitrógeno, presentan dos tipos celulares: las células vegetativas que fijan CO_2 mediante la fotosíntesis oxigénica y los heterocistos fijadores de nitrógeno atmosférico. La diferenciación de los heterocistos es un proceso que ha sido ampliamente estudiado desde los puntos de vista bioquímico y genético. Otros aspectos de la multicelularidad, como son los mecanismos de adhesión y comunicación intercelular, han sido menos estudiados.

En las cianobacterias formadoras de heterocistos, ante la ausencia de nitrógeno combinado en el medio, algunas células vegetativas del filamento se diferencian a heterocistos generando un patrón en el que dos heterocistos están separados por una media de diez células vegetativas. En la cianobacteria modelo *Anabaena* sp. PCC 7120, el proceso de diferenciación requiere la acción de numerosos reguladores, entre ls que destacan los factores de transcripción NtcA y HetR. NtcA controla la expresión de genes implicados en la asimilación de diferentes fuentes de nitrógeno incluyendo genes implicados en la diferenciación de los heterocistos. HetR parece ser específico de la diferenciación, y su actividad se inhibe por morfógenos derivados de PatS y HetR, que impiden la diferenciación de un número excesivo de heterocistos. Durante el crecimiento diazotrófico, los heterocistos y las células vegetativas intercambian nutrientes: compuestos reducidos de carbono son transferidos al heterocisto y nitrógeno fijado a las células vegetativas.

Morfológicamente, las cianobacterias se caracterizan por tener una envuelta celular de tipo Gram negativo, con una membrana externa por fuera de la capa de peptidoglicano que rodea a la membrana citoplasmática. En las cianobacterias filamentosas, la membrana externa es continua a lo largo del filamento, lo que determina la presencia de un periplasma que es funcionalmente continuo. Esto abre la posibilidad de que el espacio periplásmico sea una vía de comunicación entre las células del filamento. Además, la capa de peptidoglicano y la membrana externa continua también contribuyen a la integridad del filamento. Sin embargo, en el filamento cianobacteriano las células se encuentran conectadas por unas estructuras proteicas conocidas como *septal junctions*, que atraviesan las capas de peptidoglicano que se localizan entre las células a través de unas perforaciones en las mismas denominadas nanoporos. Estas estructuras podrían estar implicadas en la transferencia intercelular de compuestos además de jugar un papel en el mantenimiento de la integridad del filamento. La transferencia intercelular ha sido estudiada en cianobacterias formadoras de heterocistos usando sondas fluorescentes que incluyen la calceína, la 5-carboxifluoresceína y la esculina, un análogo fluorescente de la sacarosa. Entre los componentes propuestos de las *septal junctions* están las proteínas septales FraC, FraD y SepJ.

La localización de SepJ se ha estudiado mediante fusión con GFP y se localiza en el polo de forma focalizada, aunque se puede observar formando un anillo en células que se están dividiendo. Un mutante *sepJ* presenta un fenotipo de fragmentación y es incapaz de crecer diazotróficamente, ya que en él la diferenciación de heterocistos se aborta en una fase temprana. Además, el mutante *sepJ* está afectado en la transferencia intercelular de calceína y presenta un número reducido de nanoporos, mientras que la sobreexpresión de

SepJ resulta en un incremento en el número de nanoporos. SepJ contiene cuatro dominios: (i) una secuencia conservada de 26 aminoácidos en parte N-terminal; (ii) un dominio *coiled-coil* que podría estar implicado en interacciones proteína-proteína; (iii) un domino *linker* rico en prolina y serina; y (iv) un domino integral de membrana (domino permeasa) que muestra homología con proteínas de la superfamilia DMT (Drug/Metabolite Transporter).

El divisoma es un complejo multiproteico que se encarga de llevar a cabo la división celular en bacterias. Los genes implicados en la división celular en cianobacterias han sido identificados mediante análisis comparativos y solo algunos de ellos han sido objeto de estudio directo. Las cianobacterias presentan genes de división celular previamente identificados en bacterias Gram negativas, algunos presentes en bacterias Gram positivas y, además, otros exclusivos que no presentan homólogos en otras bacterias. En *Anabaena*, algunos de los genes identificados son *ftsZ*, que determina la proteína FtsZ encargada de formar el anillo Z, *ftsQ* y *ftsW*.

Basado en la observación de la proteína SepJ-GFP formando un anillo en el sitio de división celular, el primer objetivo de esta tesis fue estudiar la relación que podría tener SepJ con la maquinaria de división. Para ello se construyó un mutante condicional del gen esencial *ftsZ*. En la estirpe mutante, llamada CSFR18, el gen *ftsZ* se encuentra bajo un promotor regulado por NtcA y, consistentemente, los niveles de proteína FtsZ dependían de la fuente de nitrógeno presente en el medio. Cuando el amonio estaba presente en el medio, los niveles de FtsZ eran bajos, lo que dificultaba la división celular provocando que la estirpe mostrara una morfología aberrante y observándose, finalmente, la lisis de los cultivos. Cuando la fuente de nitrógeno era nitrato, los niveles de FtsZ eran algo más bajos que en la estirpe silvestre en las mismas condiciones, pero suficientes para permitir la división celular aunque el área celular se veía algo afectada. En condiciones diazotróficas, los niveles de FtsZ en la estirpe CSFR18 eran similares a los de la estirpe silvestre, permitiendo una morfología normal. La localización de SepJ fue analizada mediante inmunofluorescencia y se pudo ver cómo SepJ no se localizaba en el septo en la estirpe CSFR18 cuando ésta se incubaba en presencia de amonio como fuente de nitrógeno. Un análisis complementario, usando berberina, un inhibidor de la polimerización de FtsZ, corroboró que la localización de SepJ en el septo requería la maquinaria de división. También se generó un mutante condicional, llamado CSFR5, del gen *ftsQ* que se localiza justo aguas arriba de *ftsZ*. El promotor utilizado fue también el promotor sintético activado por NtcA. Desafortunadamente, la estirpe CSFR5 no mostró una alteración fenotípica evidente. Se encontró que *ftsQ* es un gen de baja expresión, haciendo que en la estirpe CSFR5 los niveles de expresión de *ftsQ* obtenidos con el promotor sintético regulado por NtcA fuesen siempre mayores que aquellos observados en la estirpe silvestre. De esto se puede concluir que la sobreexpresión de ftsQ no tiene efectos evidentes en la capacidad de división de las células de *Anabaena*.

Otra parte de la tesis doctoral se ha centrado en el estudio de la capacidad de SepJ para interaccionar consigo misma y con otras proteínas o estructuras celulares. La presencia de un extenso dominio *coiled-coil* en la proteína SepJ hacía pensar que ésta podría tener la capacidad de interaccionar con otras proteínas. Primero se analizó la capacidad de polimerización del dominio *coiled-coil* aislado mediante cromatografía de exclusión molecular, viendo que era capaz de formar multímeros. La presencia de complejos de SepJ en las membranas de *Anabaena* se analizó después usando una estirpe que expresaba la proteína de fusión SepJ-GFP-His_{10}. Mediante un procedimiento de doble

purificación, se comprobó que SepJ podría estar formando hexámeros en la membrana de *Anabaena*, pero no se obtuvo ninguna indicación de que en estos complejos pudiera participar otra proteína de forma estable. La capacidad de SepJ de interaccionar consigo misma también se estudió mediante el sistema del doble híbrido bacteriano. Nuestros resultados mostraron que SepJ puede interaccionar consigo misma y que tanto el dominio *coiled-coil* como el *linker* están involucrados en esta interacción. También se analizó mediante doble híbrido la interacción de SepJ con algunas proteínas implicadas en la división celular. SepJ resultó interaccionar fuertemente con la proteína FtsQ, encargada de reclutar componentes tardíos del divisoma. Esta interacción se corroboró mediante ensayos de co-purificación, en los que las dos proteínas fueron expresadas en *E. coli*. Otras proteínas que podrían interaccionar con SepJ son las proteínas FraC y FraD, que se localizan también en el septo, pero los ensayos de doble híbrido no mostraron interacción entre SepJ y estas proteínas. SepJ sí interaccionó en ensayos de doble híbrido con SjcF1, una proteína de unión a peptidoglicano que parece estar implicada en la regulación del tamaño de los nanoporos, la cual también interacciona con FraC. Además, fue analizada la interacción entre SepJ y peptidoglicano aislado de *Anabaena*. La proteína SepJ purificada mostró capacidad de unión a peptidoglicano, al igual que el dominio *coiled-coil* aislado. La capacidad de SepJ para formar hexámeros y su interacción con SjcF1 y con el peptidoglicano apoyan la idea de que SepJ forme parte de un tipo de septal junctions que intervendrían en el anclaje célula-célula y la transferencia intercelular de compuestos.

En la última parte de este trabajo se analizó el papel de SepJ en la transferencia intercelular de compuestos en *Anabaena*. Para ello, se construyeron una serie de mutantes de SepJ con alteraciones en el dominio permeasa. Primero se construyó una estirpe, llamada CSVM90, que expresaba una versión de SepJ que contaba solo con el primer segmento transmembrana. Esta estirpe mostró un fenotipo muy similar a un mutante de deleción de *sepJ*, aunque sus niveles de transferencia de calceína eran algo mayores. La estirpe CSVM90 también tenía un mayor número de nanoporos que una estirpe de deleción, aunque menos que una estirpe control en la que se reconstruyó el gen *sepJ*. A partir de la estirpe CSVM90 se construyó una serie de mutantes que contenían mutaciones puntuales de residuos conservados del dominio permeasa, deleciones de los dos y cuatro últimos segmentos transmembrana del mismo y pequeñas deleciones (una incluyendo un *loop* citoplásmico y otra la cola C-terminal de la proteína). Algunos mutantes mantenían el fenotipo de fragmentación de la estirpe parental CSVM90, pero otros recuperaron la capacidad de crecer formando filamentos largos. Entre estos últimos mutantes se distinguían dos grupos: los de un grupo estaban afectados en la transferencia de calceína y presentaban algunos heterocistos contiguos después de 48 h de incubación sin nitrógeno combinado (fenotipo MCH, de *multiple contiguous heterocysts*); los del otro grupo no estaban afectados en la transferencia de calceína pero presentaban fenotipo MCH tanto a las 24 h como a las 48 h de incubación sin nitrógeno combinado. El fenotipo MCH denota una alteración en la transferencia intercelular de los morfógenos PatS y HetN. Estos mutantes permiten por lo tanto discriminar entre las funciones de anclaje y comunicación de SepJ y apoyan la idea de que SepJ sea un componente de las *septal junctions* contribuyendo tanto al papel de anclaje como al papel funcional (comunicación célula-célula) de estas estructuras.

CONCLUSIONES

1. La localización subcelular de la proteína septal SepJ de la cianobacteria formadora de heterocistos *Anabaena* necesita la presencia de niveles normales de la proteína FtsZ en la célula y, por lo tanto, depende de la maquinaria de división. SepJ interacciona con la proteína FtsQ, y en esta interacción están involucrados los dominios periplásmicos de ambas proteínas.

2. SepJ forma oligómeros in vivo, probablemente hexámeros, y los dominios coiled-coil y linker están involucrados en la interacción homoespecífica.

3. Ensayos de doble híbrido en bacterias (BACTH) ponen de manifiesto que la proteína de unión a peptidoglicano SjcF1 puede interaccionar con SepJ y con FraC, otra proteína septal. SjcF1 podría constituir un nexo entre los dos tipos de *septal junctions* presentes en *Anabaena*, las que estarían formadas por SepJ y las formadas por las proteínas FraC/D.

4. SepJ interacciona directamente con el peptidoglicano, y el dominio *coiled-coil* está involucrado, al menos parcialmente, en esta interacción.

5. La región periplásmica de SepJ es importante para la formación de nanoporos, ya que la proteína SepJ es necesaria para formar un número normal de nanoporos y mutantes del dominio permeasa son capaces formar un número sustancial de los mismos.

6. El dominio permeasa de SepJ es necesario para la comunicación intercelular en el filamento de *Anabaena*, estando involucrado al menos en la transferencia de reguladores implicados en la formación del patrón de heterocistos.

7. Aunque las *septal junctions* carecen de una especificidad estricta de sustrato, algunos aminoácidos del dominio permeasa de SepJ aportan selectividad a las mismas.

1. INTRODUCTION

1.1. MULTICELLULARITY IN BACTERIA

Multicellularity is a form of biological organization in which individual cells aggregate in order to work coordinately as an organism. Multicellular organisms independently originated several times from unicellular ancestors in biological evolution (Bonner, 1998; Grosberg & Strathmann, 2007). The emergence of multicellular organisms involved new levels of organization that were reached by different mechanisms. All the multicellular forms have several features in common, including mechanisms for cell adhesion and cell-cell communication and coordination (Claessen *et al*., 2014).

Multicellularity is not a eukaryotic characteristic as it was thought for a long time. Among bacteria, many examples of multicellularity that go beyond the well-known *quorum* sensing can be found (Claessen *et al*., 2014). Different forms of multicellular bacteria are present in nature including biofilm-forming bacteria, swarming cells and bacteria forming filaments by syncytial or clustered growth. As long as is known, in each group of multicellular bacteria, the mechanism for cellular adhesion appears to be different bringing to light the independent origin of each form.

Biofilm formation is the simplest manifestation of multicellularity (Flemming *et al*., 2016). This process is based on the production of an extracellular matrix (ECM) that embeds the cells. Some of the cells can differentiate to carry out distinct functions, such as spore production in *Bacillus subtilis* biofilms. Physical connection does not usually occur between cells in a biofilm. However, it has been described that in early stages of biofilm formation *B. subtilis* and *Lactococcus lactis* form chains of cells that resolve into aggregates after ECM production.

Another example of bacterial multicellularity is present in swarming bacteria and myxobacteria. Myxobacteria dwell in soil and are able to move as a coordinated group of cells. They induce a developmental program in response to nutrient depletion, producing a spore-bearing structure called fruiting body. Intercellular signaling is essential for fruiting body formation, regulating gene expression and cell motility. To facilitate cellular cooperation during movement and the developmental process, an ECM is also produced (Muñoz-Dorado *et al*., 2016).

Filamentous growth of some bacteria may be considered the main evidence of multicellularity in prokaryotes. Syncytial growth is very well documented in Actinobacteria, concretely in Streptomycetes (Bush *et al*., 2015). These Gram-positive bacteria grow as a multicellular mycelium that originates after germination of spores. Under nutrient depletion, a developmental program leading to the formation of reproductive aerial hyphae that ultimately produce spores is triggered. Each multigenomic aerial hypha initiates a massive synchronous cell division event that forms a chain of unigenomic compartments that will become mature spores. After dispersion, spores germinate and a vegetative mycelium is produced again. Vegetative hyphae are divided in compartments separated by cross-walls. Channels are occasionally observed in these cross-walls suggesting that movement of nutrients and other compounds through the hyphae can take place (Jakimowicz & van Wezel, 2012).

Filamentous growth can also result from the incomplete separation of daughter cells after cell division. This type of growth can be found in different phylogenetic groups, such as *Desulfobulbaceae* (Pfeffer *et al*., 2012)*, Lachnospiraceae* (Thompson *et al*., 2012), the genera *Chloroflexus* (Pierson & Castenholz, 1974) or filamentous cyanobacteria, which are the best studied (Flores & Herrero, 2010). Some cyanobacteria belonging to taxonomic

groups IV and V of the classification of Ripkka *et al.* (1979) (see 1.2.1) are also able to differentiate specialized cells that, doing incompatible functions, coexist in the same filament. This is the case of heterocyst-forming cyanobacteria. Under nitrogen deprivation they differentiate heterocysts, which fix N_2 under anoxic conditions while the vegetative cells perform oxygenic photosynthesis. Other differentiation processes have been described in filamentous cyanobacteria, such as formation of hormogonia and akinetes involved in dispersion and persistence, respectively. (Meeks & Elhai, 2002; Flores & Herrero, 2010; Herrero *et al*., 2016).

1.2. CYANOBACTERIA

1.2.1. Classification and diversity of cyanobacteria

Cyanobacteria, considered the ancestors of plastids (Giovannoni *et al*., 1988), are the only bacteria able to perform oxygenic photosynthesis. They have an important ecological role, producing oxygen from oxygenic photosynthesis and contributing to the carbon cycle, removing CO_2 from the atmosphere and adding fixed carbon to organic matter. Some cyanobacteria can fix atmospheric nitrogen contributing to the nitrogen cycle. Cyanobacteria are considered the responsible of the accumulation of oxygen in the atmosphere that led to the Great Oxygenation Event about 2.4-2.2 billion years ago (Tomitani *et al*., 2006). Many organisms took then advantage of the available oxygen and forms of life based on aerobic metabolism evolved (Lyons *et al*., 2014).

Cyanobacteria are one of the most diverse prokaryotic phyla, showing a wide range of forms, from unicellular to multicellular filamentous species. Due to their diversity, cyanobacteria are present in almost every habitat on Earth, including soil, oceans, fresh water and even extreme environments. In addition, cyanobacteria of the order *Nostocales* are able to fix nitrogen in symbiosis with fungi and plants (Meeks & Elhai, 2002). Because of their ability to adapt to different media and their versatile metabolism, cyanobacteria are used for many biotechnological purposes including production of bioactive compounds, bioremediation, use of alternative energy sources or as fertilizers and healthy food (Abed *et al*., 2009).

The morphological diversity of cyanobateria has been traditionally used to classify these organisms in five sections (Rippka *et al.,* 1979). Section I includes unicellular forms that divide by binary fission or by budding; section II includes unicellular cyanobacteria that divide by multiple fission producing small cells (baeocytes) or by both multiple and binary fission; section III comprises filamentous cyanobacteria that divide in one plane; section IV includes filamentous cyanobacteria that are able of cell differentiation; and section V includes filamentous heterocyst-forming cyanobacteria that divide in more than one plane, resulting in branched filaments (Fig. 1.1).

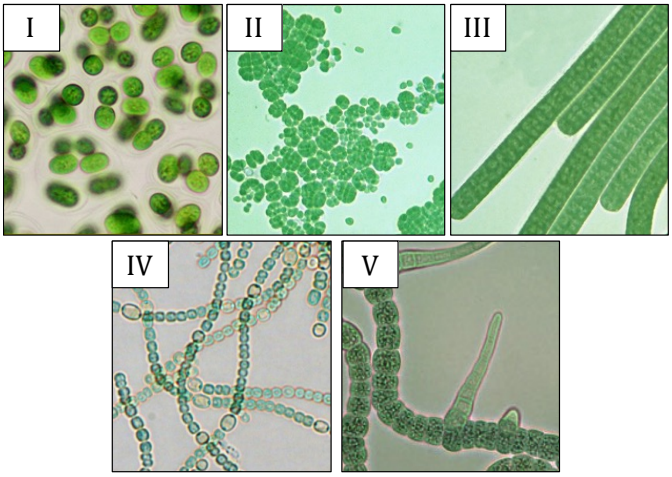

Fig. 1.1. Diversity of cyanobacteria. Classification of cyanobacteria based on morphological characteristics (Rippka *et al*., 1979). Some examples are shown: Section I: *Cyanothece* sp. PCC 9318; Section II: *Chroococcidiopsis* sp. PCC 7203; Section III: *Oscillatoria* sp. PCC 9325 (images cortesy of José E. Frías, CSIC and Universidad de Sevilla); Section IV: *Anabaena* sp. PCC 7120; Section V: *Fischerella muscicola* (images from Flores & Herrero, 2010).

Filamentous cyanobacteria are among the oldest multicellular organisms on Earth, and molecular phylogenetic analysis supports that filamentous heterocyst-forming cyanobacteria from sections IV and V have a monophyletic origin (Giovannoni *et al.*, 1988; Tomitani *et al*., 2006; Shih *et al*., 2013). All cyanobacteria share a unicellular common ancestor, and multicellularity has been dated to have evolved earlier than 2.0 billion years ago, coinciding with the Great Oxygenation Event (Schirrmeister *et al*., 2011; 2013). However, some current unicellular species are derived from filamentous forms, which appear to have lost the ability to form filaments (Schirrmeister *et al*., 2011).

This work has focused on the filamentous heterocyst-forming cyanobacterium *Anabaena* sp. strain PCC 7120, hereafter *Anabaena*.

1.2.2. Physiology of Cyanobacteria

The distinctive feature of cyanobacteria is that they perform oxygenic photosynthesis, fixing CO_2 through the reductive pentose phosphate cycle (Calvin-Benson-Bassham cycle). The enzyme that carries out CO_2 fixation is ribulose-1,5-bisphosphate carboxylase/oxygenase (RuBisCO). The low affinity of RuBisCO for CO_2 led cyanobacteria to develop CO_2 concentrating mechanisms (CCM), which include transporters that import CO_2 and bicarbonate into the cell, the enzyme carbonic anhydrase (CA) that catalyzes the interconversion of bicarbonate to CO_2 and water, and structures known as carboxysomes. Carboxysomes are micro-compartments in which RuBisCo is encapsulated together with carbonic anhydrase within a protein shell (Cameron *et al*., 2014). This co-localization of enzymes enables cyanobacteria to generate high levels of CO_2 at the site of carbon fixation. Moreover, the shell also provides a barrier that prevents CO_2 leakage into the cytosol.

Cyanobacteria are generally photoautotrophs. However, some cyanobacteria, including strains belonging to the *Nostocaceae*, can use sugars (mainly glucose, fructose and sucrose) as a carbon source (photoheterotrophs) or even as carbon and energy source (chemoheterotrophs) (Rippka, 1972; Ekman *et al*., 2013). Sugars might be important also for signaling in cyanobacteria. A glucose transporter from *Nostoc punctiforme* is important for colonization of the plant tissue in symbiosis (Ekman *et al*., 2013; Picossi *et al*., 2013).

Cyanobacteria can use different sources of combined nitrogen including ammonium, nitrate, nitrite, urea and some amino acids (Flores *et al*., 2005). In addition, under combined nitrogen limitation, some strains can fix atmospheric dinitrogen (N_2). Cyanobacteria take up the different combined nitrogen sources through specialized transporters (Hahn & Schleiff, 2014). Inside the cell, nitrate and nitrite are reduced to ammonium by nitrate reductase and nitrite reductase, respectively. Genes involved in nitrate and nitrite metabolism are found in an operon that includes genes encoding nitrite reductase (*nirA*), an ABC-type uptake transporter (*nrtABCD*) or a permease (*nrtP*), and nitrate reductase (*narB*) (Flores *et al*., 2005). Urea is hydrolyzed to ammonium and CO_2 by urease (Valladares *et al*., 2002). Ammonium that is produced in the cytoplasm or taken up from the medium through ammonium transporters (Paz-Yepes *et al*., 2007) is incorporated into organic compounds through the glutamine synthetase/glutamate synthase (GS/GOGAT) pathway (Luque & Forchhammer, 2008). GS synthesizes glutamine from ammonia and glutamate consuming ATP, and GOGAT catalyzes a reducing transamidation of glutamine to 2-oxoglutarate (2-OG) producing two molecules of glutamate. Because it is the intermediary of the Krebs cycle that is used for incorporation of nitrogen into carbon compounds, 2-OG is an important metabolite in cyanobacterial nitrogen and carbon metabolisms that is also used as indicative of the C/N balance in the cell (Muro-Pastor *et al*., 2001).

The enzyme responsible for nitrogen fixation is nitrogenase, which catalyzes the reduction of dinitrogen to two molecules of ammonia in an energy and reductant-dependent manner (Rubio & Ludden, 2008). The nitrogen fixation machinery is extremely sensitive to oxygen, which in cyanobacteria is produced by oxygenic photosynthesis. Thus, N_2-fixing cyanobacteria have developed different strategies to separate spatially or temporally N_2 fixation and oxygenic photosynthesis. Unicellular and some filamentous cyanobacteria perform nitrogen fixation in the dark when photosynthesis is not operative (Stal & Zehr, 2008). Other filamentous cyanobacteria are able to differentiate specialized cells –heterocysts– that maintain micro-oxic conditions and where nitrogenase is confined (Flores & Herrero, 2010).

Nitrogen metabolism has an important role in cyanobacterial physiology and it is acutely regulated. NtcA is a global transcription factor that influences the expression of many genes involved in nitrogen assimilation. In filamentous heterocyst-forming cyanobacteria, NtcA plays an essential role in heterocyst differentiation. NtcA is conserved among cyanobacteria and belongs to the CRP family of transcription factors (Herrero *et al*., 2013). NtcA acts as a homodimer in which each subunit presents a helix-turn-helix domain and binds to the DNA at sites with consensus sequence $GTAN_8TAC$ (Luque *et al*., 1994). The DNA binding activity of NtcA is enhanced in the presence of 2-OG, which in turn is necessary for transcriptional activation by NtcA (Tanigawa *et al*., 2002; Vázquez-Bermúdez *et al*., 2002; Valladares *et al*., 2008). Depending on the location of the NtcA-binding site in a gene promoter, NtcA can act as an activator or as a repressor of transcription (Picossi *et al*., 2014). Canonical NtcA-activated promoters have a consensus NtcA-binding site, centered at about 41.5 nucleotides upstream from the transcription start point (TSP) of the regulated gene, and a −10 box with the consensus sequence TAN_3T, thus matching the bacterial Class II activator-dependent promoters (Busby & Ebright, 1999). NtcA-activated promoters in which an NtcA-binding site is found further upstream from the -41.5 position have also been identified. In addition, there are some NtcA-dependent genes that do not show any NtcA-binding site in their promoters (Herrero *et*

al., 2001). In other cases, the NtcA-binding site differs from the consensus sequence (Fig. 1.2). On the other hand, when the NtcA-binding site overlaps the -10 box, NtcA acts as a repressor (Vázquez-Bermúdez *et al*., 2002).

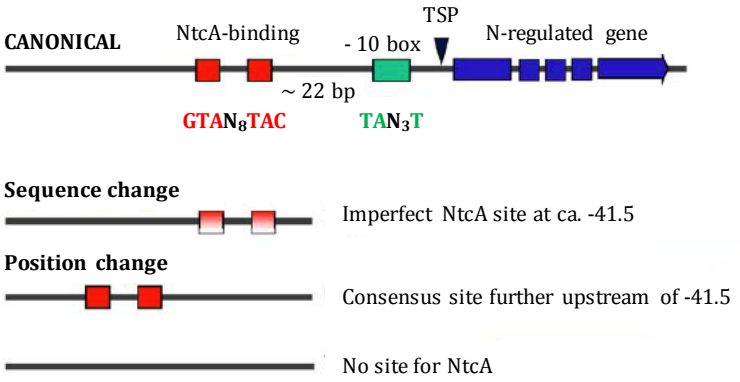

Fig. 1.2. NtcA-activated promoters. Schematic representation of different types of NtcA-activated promoters of genes involved in nitrogen metabolism and heterocyst differentiation (adapted from Herrero *et al*., 2004).

1.3. HETEROCYST DIFFERENTIATION

Filamentous cyanobacteria from Sections IV and V can differentiate specialized cells in response to changes in nutrient ability. In response to combined nitrogen limitation, some cells in the filament differentiate into heterocysts, which are terminal cells that perform N_2 fixation. Heterocysts are metabolically and morphologically different from the vegetative cells that perform oxygenic photosynthesis.

1.3.1. The heterocyst

Under the microscope, heterocysts are easily recognizable from vegetative cells since they have different size, shape and arrangement (Fig. 1.3.A). Their characteristic morphology results from a differentiation program that is triggered when the cells sense the absence of combined nitrogen. This process implies morphological and metabolic changes that aim at providing a micro-oxic environment for efficient nitrogen fixation.

1.3.1.1. Heterocyst morphology

Several characteristic morphological changes can be observed in heterocysts, such as (i) the loss of cellular inclusions including carboxysomes and glycogen granules, (ii) a marked rearrangement of thylakoids to the cell poles, where they develop a heavily contorted form (Lang & Fay, 1971), and (iii) the deposition of supplemental glycolipid and polysaccharide layers in the cell envelope that hamper the influx of gases. Additionally, large granules of cyanophycin (multi-L-arginyl-poly [L-aspartic acid]) are built at the heterocyst poles.

Heterocysts are protected from external oxygen by two chemically different layers outside of the outer membrane (Fig. 1.3.B): the inner layer is composed of heterocyst-specific glycolipids (HGL) and constitutes a permeability barrier for gases (Fay, 1992); the outermost layer, made up of polysaccharide (HEP), is thought to protect the glycolipid layer from physical damage (Xu *et al*., 2008). Diazotrophic growth is impaired if any of these layers is missing (Fan *et al*., 2005; Huang *et al*., 2005). The outermost layer is loosely

organized and of irregular thickness, and it is expanded toward the heterocyst poles making a structure that resembles a bottleneck. At the point of connection with the vegetative cell, the heterocyst acquires a shallow cup-like structure. The presence of the neck makes the heterocyst-vegetative cell septum narrower than a typical septum between vegetative cells, limiting gas entrance into the heterocyst (Walsby, 2007).

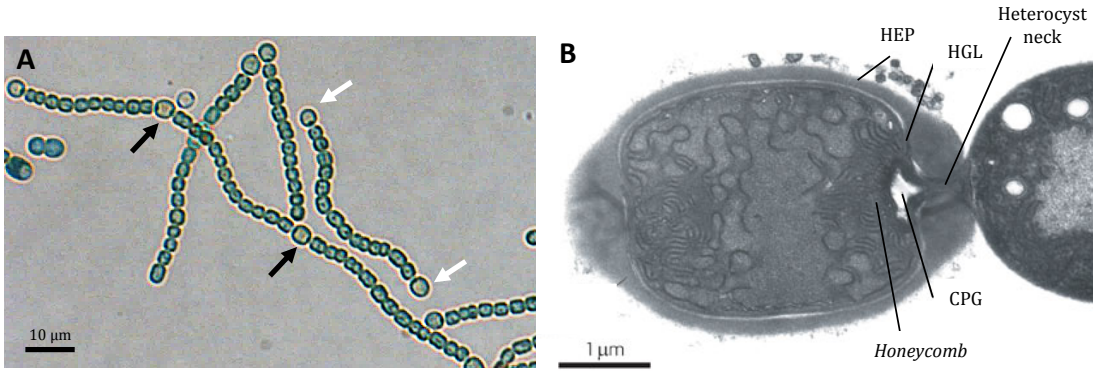

Fig. 1.3. The heterocysts. (**A**) N_2-grown filaments of *Anabaena* sp. PCC 7120 showing terminal heterocysts (white arrows) and intercalary heterocysts (black arrows). (**B**) Transmission electron micrograph showing a terminal heterocyst (left) and part of its adjacent vegetative cell (right) from a filament of *Anabaena*. In the preparation of samples for electron microscopy, the cyanophycin granule (CPG) is frequently lost, leaving a white, empty space in the micrographs. HEP, heterocyst polysaccharide layer; HGL, heterocyst glycolipid layer. Transmission electron micrograph by Iris Maldener, Universität Tübingen, Germany (taken from Flores & Herrero, 2010).

Terminal heterocysts contain a single polar granule, visible in the light microscope as a highly refractile round object. Intercalary heterocysts contain two polar granules. Electron micrographs of mature heterocysts show the granules as homogeneous plugs nearly filling the region of the cell adjacent to the septum. These granules contain cyanophycin in a structure known as the 'cyanophycin plug'. Cyanophycin is a biopolymer that serves as nitrogen cellular reserve and, as described earlier, is composed of arginine residues linked to a polyaspartate backbone (Sherman *et al*., 2000).

The reorganization of thylakoid membranes that takes place in the heterocysts also may involve generation of new membranes, and the produced structure is known as *honeycomb*. The *honeycombs* are located close to heterocyst poles, next to the cyanophycin plugs (Lang & Fay, 1971). Elements of the photosynthetic and respiratory apparatus are placed in these *honeycomb* membranes (Wolk *et al*., 1994). A protein called FraH has been shown to be involved in the formation of the *honeycomb* (Merino-Puerto *et al*., 2011a).

Heterocysts lose the ability to divide since they are terminally differentiated cells and cannot revert to a vegetative cell. The cell division machinery is down-regulated in heterocysts at both transcriptional and translational levels (Wang & Xu, 2005; Kuhn *et al*., 2000).

1.3.1.2. Heterocyst metabolism

Metabolic changes in the heterocysts include (i) the loss of photosystem II activity, thus avoiding photosynthetic oxygen production, (ii) an increased respiration rate for eliminating free oxygen, (iii) the loss of photosynthetic CO_2 fixation, and (iv) the expression of the N_2-fixing system (Golden and Yoon 2003; Herrero *et al*. 2004). Heterocysts contain GS, but lack GOGAT, implying that, for production of glutamine with

the ammonium resulting from N_2 fixation, glutamate has to be transferred from the vegetative cells to the heterocysts (Thomas *et al*., 1977; Martín-Figueroa *et al*., 2000).

Heterocysts adapt their metabolism to create a micro-oxic compartment required for nitrogen fixation. Thus, photosystem II (PSII), which produces O_2 from H_2O, is not operative in heterocysts. However, photosystem I (PSI), which relocates to *honeycomb* membranes, remains operative carrying out a non-cyclic electron that produces ATP for nitrogen fixation (Wolk *et al*., 1994). RuBisCO is also repressed in the heterocysts, so the Calvin-Benson-Bassham cycle is not operative. To reach the micro-oxic conditions required for nitrogen fixation, heterocysts also achieve a high rate of O_2 respiration resulting from induction of specific terminal oxidases, largely located in the *honeycomb* membranes (Valladares *et al*., 2003, 2007). Other proteins involved in photoprotection and O_2 uptake, such as flavodiiron proteins (Ermakova *et al*., 2014), appear to be also important for diazotrophic growth. All these changes make the heterocysts to rely on the vegetative cells to obtain reduced carbon. Sucrose appears to be one of the molecules transferred from vegetative cells to heterocysts, where sucrose is hydrolyzed by heterocyst-specific invertases (López-Igual *et al*., 2010; Vargas *et al.*, 2011).

As mentioned earlier, N_2 is reduced to NH_4^+ by nitrogenase. This enzyme complex is formed by a tetramer of the proteins encoded by the genes *nifD* and *nifK*, where the catalytic site is located, and two dimers of the protein encoded by *nifH,* which acts as electron donor (Rubio & Ludden, 2008). Nitrogenase activity requires reducing power that is provided by reduced sugars received from the vegetative cell. Ammonium produced by the nitrogenase complex is incorporated into a glutamate molecule to produce glutamine as described above, but other amino acids can also be synthesized in the heterocyst (Wolk *et al.*, 1976; Meeks *et al.*, 1977) (Fig. 1.4).

Metabolism of cyanophycin also takes place in the heterocyst. Cyanophycin is non-ribosomically synthesized by cyanophycin synthetase, and in this polymer aspartate and arginine are present in an almost 1:1 ratio. (Herrero & Burnat, 2014). Degradation of cyanophycin is carried out by a specific serine-type protease called cyanophycinase. This enzyme can cleave cyanophycin producing the dipeptide β-aspartyl-arginine. Genes encoding cyanophycin synthetase and cyanophycinase are expressed in vegetative cells and heterocysts in *Anabaena*, but differential expression leads to levels of both enzymes that are much higher in heterocysts than in vegetative cells (Gupta & Carr, 1981; Picossi *et al.*, 2004). The β-aspartyl-arginine resulting from cyanophycin degradation is transferred from heterocysts to vegetative cells where the enzyme aspartyl-arginine dipeptidase hydrolases the peptide bond releasing L-arginine and L-aspartic acid, which can be used as nitrogen sources for vegetative cells (Burnat *et al*., 2014a) (Fig. 1.4).

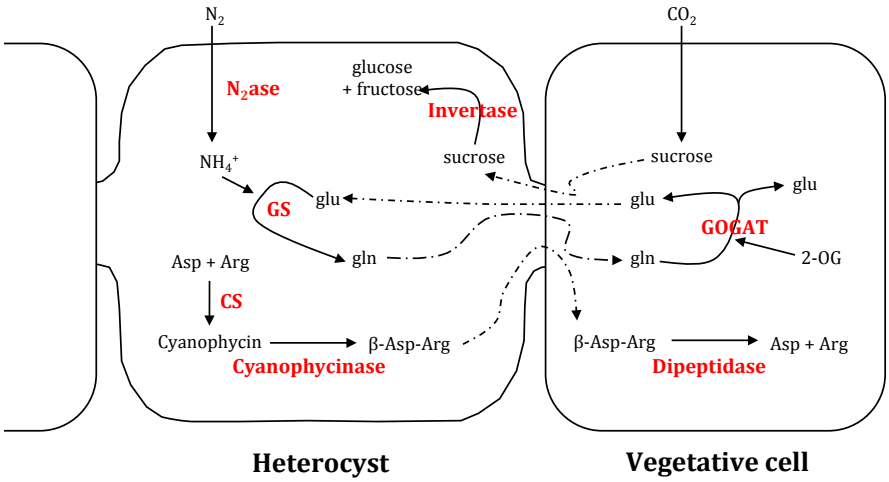

Fig. 1.4. Model of the carbon and nitrogen metabolism in heterocysts and vegetative cells. Nitrogen gas is reduced to NH_4^+ by nitrogenase (N_2ase) and then added to glutamate by glutamine synthetase (GS). The resulting glutamine is transported to the vegetative cells where glutamate-oxoglutarate amido transferase (GOGAT) yields two molecules of glutamate from glutamine and 2-oxoglutarate. Glutamate can return to the heterocyst to be amidated again by GS. Fixed N is also used to synthesize other amino acids in the heterocyst. Sucrose produced by CO_2 fixation is transferred to the heterocyst where it is hydrolyzed by invertase releasing glucose and fructose. Cyanophycin is synthesized by cyanophycin synthetase (CS) by adding aspartate and arginine residues to a cyanophycin primer. Cyanophycinase hydrolyses cyanophycin producing β-aspartyl-arginine (β-Asp-Arg) that is transferred to vegetative cells where it is hydrolyzed by isoaspartyl dipeptidase, releasing aspartate and arginine.

1.3.2. Regulation of heterocyst differentiation

Nitrogen deprivation induces 495 genes and inhibits expression of 196 genes in *Anabaena* (Xu *et al.*, 2008; Ehira & Ohmori, 2006). Expression of many of these genes is regulated by two main regulators involved in the cyanobacterial adaptation to nitrogen deprivation: NtcA and HetR. Whereas the global transcriptional regulator NtcA governs expression of many of the genes that respond to the N status of the cells (Picossi *et al.*, 2014), HetR regulates expression of genes involved in heterocyst development and function (Flaherty *et al.*, 2014).

When a source of combined nitrogen is absent from the medium, imbalance in C/N ratio increases levels of 2-oxoglutarate (2-OG) that activates the expression of NtcA (Li *et al.*, 2003; Frías *et al.*, 1994). NtcA fist promotes transcription of genes involved in assimilation of alternative nitrogen sources, and then genes involved in heterocyst differentiation. To promote heterocyst differentiation, the transcriptional regulator HetR is required. The *hetR* gene is one of the first genes induced in differentiating cells (Black *et al.*, 1993). During the initial steps of differentiation, *ntcA* and *hetR* are both positively autoregulated and induced in a mutually dependent manner (Black *et al.*, 1993; Muro-Pastor *et al.*, 2002). HetR controls subsequently the expression of genes involved in heterocyst differentiation and function. Genes induced in early steps of heterocyst differentiation include *patS* and *hetR* itself. Genes expressed after 6-12 h of nitrogen deprivation, corresponding to the intermediate phase of heterocyst differentiation, include those involved in synthesis of the heterocyst envelope (Maldener *et al.*, 2014). Among genes induced in late steps, we can find those encoding alternative oxydases and the nitrogenase enzyme (Herrero *et al.*, 2013). A tetrameric form appears to represent a functionally relevant form of HetR, whose abundance in the filament could be negatively

regulated by phosphorylation and by the negative regulator PatS (Feldmann *et al*., 2012; Valladares *et al*., 2016).

1.3.3. Establishment of the heterocyst pattern

Cyanobacterial heterocysts are distributed along the filament following a defined pattern that is governed by negative diffusible peptides (morphogens) produced in the differentiating cells. These morphogens inhibit heterocyst differentiation in the neighboring vegetative cells. In *Anabaena*, clusters of 3-4 cells initiate the process of differentiation by increasing the HetR intracellular concentrations (Black *et al.*, 1993), however only one of these cells complete the differentiation process. This mechanism establishes a semi-regular spaced pattern of heterocysts that are distributed between vegetative cells, with about 10-15 vegetative cells separating two heterocysts in *Anabaena*. Diffusible peptides containing at least 5 amino-acids of sequence RGSGR are the only diffusible negative signals that have been related so far to the maintenance of a heterocyst pattern in cyanobacteria. In *Anabaena*, this peptide is present in the sequence of two gene products, PatS and HetN, that influence heterocyst distribution in the filament (Yoon & Golden, 1998; Yoon & Golden, 2001; Callahan & Buikema, 2001).

The *patS* gene was first identified in a cosmid that suppressed heterocyst differentiation (Yoon & Golden, 1998). This gene encodes a small peptide of 17 amino acids that is produced by proheterocysts early during heterocyst differentiation (Yoon & Golden, 2001; Corrales-Guerrero *et al*., 2013). Inactivation of this gene leads to a multiple contiguous heterocyst (Mch) phenotype, and its overexpression abolishes differentiation (Yoon & Golden, 1998; Yoon & Golden, 2001). It has been hypothesized that PatS could act in a way similar to bacterial signaling peptides involved in quorum sensing and regulation of cellular differentiation (Wu *et al*., 2004). It is thought that PatS is produced in differentiating cells as a 17-amino acid peptide that is processed to a smaller C-terminal, active form that is transferred to the neighboring cells (Corrales-Guerrero *et al*., 2013). It has been found that the minimal active peptide contains the last 5 amino acids (RGSGR) of PatS (Wu *et al*., 2004). However, a processed form containing the last 8 amino acids has been proposed as the natural morphogen in *Anabaena* (Corrales-Guerrero *et al*., 2013). This active form appears to be distributed to the neighboring cells through channels connecting the cells, called septal junctions (Mariscal *et al*., 2016). Diffusion of PatS has been also demonstrated by immunofluorescence (Corrales-Guerrero *et al*., 2013). In the vegetative cells, PatS binds to HetR preventing HetR oligomerization and induction of heterocyst development (Feldmann *et al*., 2012; Valladares *et al*., 2016).

HetN, another protein containing the RGSGR peptide, is also a negative regulator of heterocyst differentiation. It is a predicted membrane protein located first all over the cytoplasm of the proheterocysts and later in the cell poles of the mature heterocysts, in the *honeycomb* membranes (Corrales-Guerrero *et al*., 2014a). HetN is not necessary for proper de novo pattern formation, but is required for stabilization and maintenance of the pattern over time. In *Anabaena*, HetN is encoded by the ORF *alr5358*. Deletion of the *hetN* gene causes a delayed MCH phenotype (Callahan & Buikema, 2001; Corrales-Guerrero *et al*., 2014). Although basal levels of *hetN* mRNA are present in cultures with combined nitrogen, its expression is induced 12 h after N step-down (Flaherty *et al*., 2011). Diffusion of a HetN-related signal has been suggested to take place (Corrales-Guerrero *et al*., 2014a), but the mechanism of action of HetN remains unknown.

1.4. CYANOBACTERIAL CELL ENVELOPE

The cyanobacteria are diderm bacteria bearing an outer membrane (OM) outside of the cytoplasmic membrane (CM) and peptidoglycan layers (PG) (Figure 1.5). The space between the outer and cytoplasmic membranes is called periplasm and is where the peptidoglycan layers reside. Although cyanobacteria bear a Gram-negative type of cell envelope, they show some unusual features. In filamentous cyanobacteria, the outer membrane is continuous along the filament, not entering the septa between adjacent cells (Flores *et al.*, 2006; Wilk *et al.*, 2011). Hence, all cells in the filament share a common periplasm (Mariscal *et al.*, 2007). It has been described that the cell envelope of filamentous cyanobacteria contributes to filament integrity (Burnat *et al.*, 2014b). Some cyanobacteria can produce a paracrystalline layer outside of the OM called S-layer. This surface layer is a non-membranous lattice of protein or glycoprotein (Hahn & Schleiff, 2014), and its functions are protection, cell integrity, adhesion and, in some cyanobacteria, swimming motility (Liberton & Pakrasi, 2008).

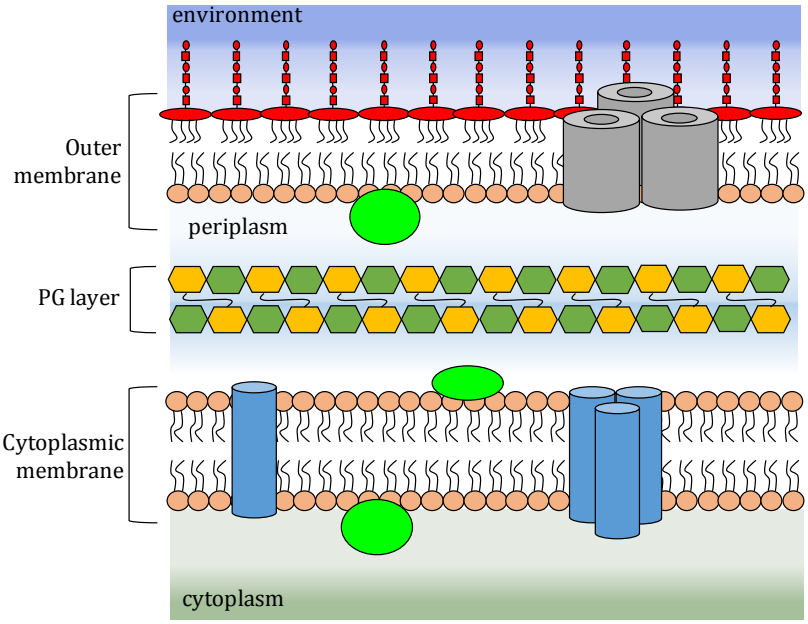

Fig. 1.5. General structure of the cell envelope in Gram-negative bacteria. The cell envelope is composed of the cytoplasmic membrane (CM), the peptidoglycan (PG) layer and the outer membrane (OM). The CM is a symmetric lipid bilayer composed of phospholipids, represented in pink, and integral membrane proteins (blue). The periplasm is the aqueous space between the CM and OM where the peptidoglycan layer resides (PG depicted as a line of hexamers that represent N-acetyl glucosamine [GlcNAc] and N-acetyl muramic acid [MurNAc]). The OM is an asymmetric lipid bilayer containing phospholipids in its inner leaflet and rich in lipopolysaccharide (LPS), depicted in red, in its outer leaflet. Integral proteins of the OM are called porins (represented in grey). Both membranes, CM and OM, contain lipoproteins represented in green.

1.4.1. The outer membrane

The outer membrane (OM), characteristic of Gram-negative bacteria, is an asymmetrical bilayer. The inner leaflet consists of phospholipids and the outer leaflet is rich in lipopolysaccharide (LPS) (Bos *et al*., 2007). The structure of LPS can be divided in three parts: (a) the lipid A membrane anchor, (b) the core region and (c) the O-specific antigen (Sperandeo *et al*., 2016). Lipid A is the most conserved part of LPS and generally consists of a β-1,6-linked D-glycosamine phosphorylated disaccharide. The core region connects lipid A with the polysaccharide of the O-antigen, which is the most diverse part of the LPS. The O-antigen consists of polysaccharide chains of variable length and sugar composition. The study of LPS from some cyanobacteria has suggested that cyanobacterial LPS is an ancient form of LPS that could be the origin of a more complex LPS, such as that of enterobacteria (Snyder *et al*., 2009).

The OM also contains integral membrane proteins structured with antiparallel amphipathic β-strands that fold into cylindrical β-barrels (Koebnik *et al*., 2000). Permeability selectivity of these proteins, called porins, makes the outer membrane a selective barrier for several molecules (Nikaido, 2003). Nine putative porins are encoded in the *Anabaena* genome (Nicolaisen *et al*., 2009). Four of them (Alr4550, All4499, Alr0834 and Alr3608) could be identified in the outer membrane fraction by proteomic analysis (Moslavac *et al*., 2005).

Some outer membrane proteins are involved in multidrug resistance. One of these proteins is TolC (tolerance to colicin) (Nagel de Zwaig & Luria, 1967). TolC is a trimeric protein, anchored in the outer membrane by beta strands and with a very long periplasmic part, that can serve as an outer membrane component for several processes such as protein export via a type I pathway and drug export via RND (resistance, nodulation, division) type systems. The only TolC homolog in *Anabaena* is HgdD (Alr2887), which is essential for the formation of mature heterocysts (Moslavac *et al*., 2007). The same phenotype has been observed for the ABC-transporter DevBCA (Fiedler *et al*., 1998). Physical interaction between HgdD and the ABC transporter DevBCA has been observed (Staron *et al*., 2011) indicating that both components are likely to form a Type I secretion system that exports glycolipids for heterocyst layer formation.

1.4.2. The periplasm

The periplasm is a compartment somewhat more viscous than the cytoplasm (Mullineaux *et al.*, 2006) that contains peptidoglycan and many soluble proteins, and it is an oxidizing environment (Gennaris *et al.*, 2015; Lippa & Goulian 2012). Periplasmic proteins include proteins participating in transport, proteins involved peptidoglycan metabolism, and chaperons involved in protein folding. Most of these functions occur in the absence of an obvious energy source since no ATP is found in the periplasmic space (Ruiz *et al*., 2006).

The peptidoglycan (PG) (also known as murein sacculus) is a polymeric macromolecule made of glycan chains interconnected through peptide bridges. The resulting structure is very stable and robust, being one of its main functions to protect bacteria from osmotic lysis. Moreover, it also serves as a scaffold for other envelope structures. PG is made by β-1,4-linked *N*-acetylmuramic acid (MurNAc) and *N*-acetylglucosamine (GlcNAc) polymerized into long glycan strands that are crosslinked with peptides (Figure 1.6.A) (Ruiz, 2016). These peptides are generally made of L-alanine

(L-Ala), D-glutamic acid (D-Glu), meso-diaminopimelic acid (A_2pm) and D-alanine (D-Ala) residues (Turner *et al*., 2014).

In *Anabaena*, the murein sacculus is made of two or three PG layers that surround each cell of the filament (Wilk *et al*., 2011). Transmission electron microscopy and electron tomography show multiple layers at the intercellular septa (Flores *et al*., 2006; Wilk *et al*., 2011). Since sacculi from several cells together can be isolated from *Anabaena* filaments (Fig. 1.6.B), it has been proposed that PG layers from adjacent cells are fused (Herrero *et al*., 2016). Analysis by transmission electron microscopy of septal peptidoglycan sacculi from some filamentous cyanobacteria, such as *Nostoc punctiforme* and *Anabaena*, revealed the presence of rigid disk-shaped septal structures, which appear to be composed by septal peptidoglycan layers from two adjacent cells (Fig. 1.6.B). These structures contain an array of perforations that have been named "nanopores" (Lehner *et al*., 2013). Nanopores are located in the central part of the septal peptidoglycan disk and their diameter is about 15-20 nm (Lehner *et al*., 2013; Nürnberg *et al*., 2015). Nanopores might allow proteinaceous structures to pass through and connect adjacent cells (Mariscal, 2014).

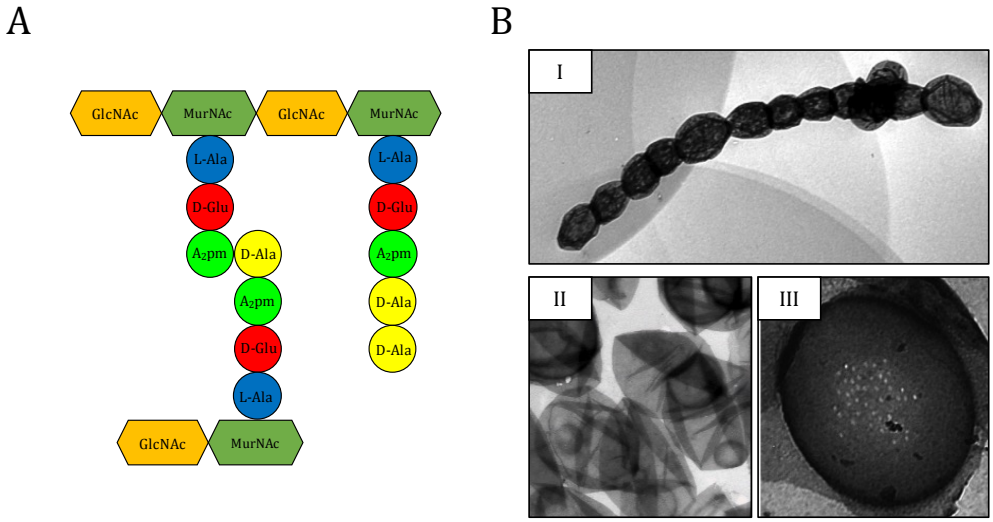

Fig. 1.6. Cyanobacterial peptidoglycan. (**A**) Simplified peptidoglycan structure. GlcNAc, *N*-acetylglucosamine; MurNAc, *N*-acetylmuramic acid; L-Ala, L-alanine; D-Glu, D-glutamic acid; A_2pm, meso-diaminopimelic acid; D-Ala, D-Alanine. (**B**) (I) Transmission electron microscopy of purified peptidoglycan sacculi from *Anabaena* corresponding to about 10 cell units. (II) Isolated murein sacculi corresponding to cells from filaments of *Anabaena* showing septal disks as more electron-dense ellipses. (III) Septal peptidoglycan disk from *Anabaena* illustrating the presence of nanopores (I and II taken from Mariscal *et al*. [2016]).

Peptidoglycan elongation during cell growth requires the cleavage of covalent bonds in the sacculus to allow incorporation of new material. The proteins involved in this degradation are located in the periplasm and are called autolysins (Typas *et al*., 2012). Studies in a range of bacteria have indicated that autolysins sculpt the shape, size and thickness of peptidoglycan and are essential for separation of daughter cells during cell division (Typas *et al*., 2012). In cyanobacteria, genes homologous to autolysins have been identified (Hahn & Schleiff, 2014).

In *E. coli*, AmiA, AmiB and AmiC, autolysins generally called amidases, are involved in hydrolysis of the septal PG to allow daughter cell separation (Vollmer *et al*., 2008; Typas *et al*., 2012). Heterocyst-forming cyanobacteria have two AmiC amidases, AmiC1 and

AmiC2 (Zhu *et al*., 2001). However, they do not generally participate in septal peptidoglycan separation during cell division, since in filamentous cyanobacteria peptidoglycan hydrolysis and outer membrane invagination does not normally take place (Herrero *et al*., 2016). Although function of other cyanobacterial AmiC amidases remains unknown, AmiC2 from *N. punctiforme* and AmiC1 from *Anabaena* are required for heterocyst differentiation (Lehner *et al*., 2011; Berendt *et al*., 2012).

A novel peptidoglycan-binding protein regulating nanopore size has been recently identified in *Anabaena* (Rudolf *et al*., 2015). SjcF1, conserved in filamentous cyanobacteria, contains two PG-binding domains and an SH3 domain, which is involved in protein-protein interactions. An *Anabaen*a *sjcF1* mutant shows an altered morphology of the septal nanopores, which are wider and of a more variable diameter than in the wild type.

1.5. SEPTUM STRUCTURE IN FILAMENTOUS CYANOBACTERIA

The fact that filamentous cyanobacteria grow as chains of cells has called the attention of microscopists, who focused on the structure and morphology of the filament including the septum between cells. Wildon & Mercer (1963) were among the first who addressed the structure of intercellular septa and described the presence of some structures connecting adjacent cells in the filament. These structures, later named "microplasmodesmata" by Lang & Fay (1971), were observed as thin strings perpendicular to the cytoplasmic membranes (Fig. 1.7.B). Giddings & Staehelin (1978) used freeze-fracture electron microscopy to analyze septal structure and observed "microplasmodesmata" as pits and protrusions on the exoplasmic and protoplasmic fracture faces of the membranes, respectively. These structures showed a diameter of less than 20 nm and they were observed usually located at the center of the septum (Giddings & Staehelin, 1978, 1981).

The septum between vegetative cells of filamentous cyanobacteria has been studied recently by electron tomography. Wilk *et al*. (2011) investigated the structure of the septum between vegetative cells of *Anabaena* in samples chemically fixed and stained with potassium permanganate or osmium tetraoxyde. The structures connecting the cells were described to be proteinaceous and termed 'septosomes' (Wilk *et al*., 2011). Depending on the method of staining, septosomes could be positively stained (using potassium permanganate; 5.5 nm in diameter, 18 nm in length) or negatively stained (using osmium tetroxide; 14 nm in diameter, 26 nm in length [Fig. 1.7.A]) (Wilk *et al*., 2011).

Samples of *Anabaena* prepared by cryo-fixation and stained with osmium tetraoxyde have also been analyzed by electron tomography (Omairi-Nasser *et al*., 2014). The septa contained structures, called 'channels', traversing the septal peptidoglycan between vegetative cells but also between a heterocyst and a vegetative cell (Fig. 1.7.C) (Omairi-Nasser *et al*., 2014). These channels were reported to be of different size depending on the septum: 12 nm long and 12 nm in diameter in the septa between vegetative cells, and 21 nm long and 14 nm diameter in the septa between vegetative cells and heterocysts (Omairi-Nasser *et al*., 2014). These data suggest that remodeling of the septa occurs during heterocyst development, and the width of the septum between vegetative cell and heterocyst is wider than that of the septum between two vegetative cells. These structures seem to pierce the septal peptidoglycan disks and would correspond to the perforations named 'nanopores' described above (Lehner *et al*., 2013).

An array of about 75 nanopores (each about 15 nm in diameter) has been reported in *Anabaena* (Nürnberg *et al*., 2015).

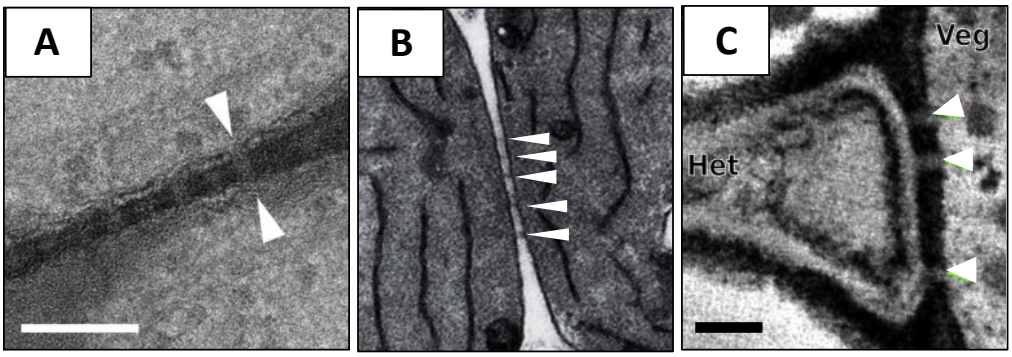

Fig. 1.7. Septal structures in *Anabaena* sp. PCC 7120. (**A**) Transmission electron micrograph of the septum between vegetative cells. Sample stained using an osmium tetroxide-based protocol making septal junctions (indicated by white arrows) negatively stained (micrograph from Wilk *et al*., 2011). Size bar, 100 nm. (**B**) Transmission electron micrograph showing an intercellular septum in a filament of *Anabaena*, in which thin structures perpendicular to the cytoplasmic membranes of the two adjacent cells can be observed (white arrows). Septal junctions are positively stained using potassium permanganate (micrograph by Iris Maldener, Universität Tübingen, Germany, taken from Flores & Herrero, 2010). (**C**) Transmission electron micrograph of the septum between a vegetative cell (Veg) and a heterocysts (Het). Septal junctions are highlighted by white arrows (micrograph from Omairi-Nasser *et al*., 2014). Size bar, 40 nm.

1.6. SEPTAL PROTEINS

Although, as mentioned earlier, the continuous outer membrane and the cell wall contribute to maintain cells together in the filament, several proteins, located at the septum between cells, have been identified to participate in maintaining filament integrity (Bauer *et al*., 1995; Flores *et al*., 2007; Nayar *et al*., 2007; Merino-Puerto *et al*., 2010). Lack of these proteins produce filament fragmentation making *Anabaena* to grow as short filaments.

1.6.1. The Fra proteins

The Fra proteins, so-called because their mutation causes filament fragmentation, are encoded by a gene cluster that contains an operon constituted by the *fraC*, *fraD* and *fraE* genes (Merino-Puerto *et al*., 2010). The cluster also contains another gene, called *fraF*, which is located downstream from the operon in the opposite orientation. Whereas deletion of each gene of the *fra* operon causes filament fragmentation and inability to grow under diazotrophic conditions, deletion of *fraF* results in increased frequencies of long filaments and impaired diazotrophic growth on solid medium (Merino-Puerto *et al*., 2013). The *fra* operon is conserved in most filamentous cyanobacteria, and the cluster (the *fra* operon together with the *fraF* gene) is frequently conserved in heterocyst-forming cyanobacteria. The *fra* operon is expressed at a low and constitutive level, whereas *fraF* is induced by nitrogen deprivation producing mRNAs that overlap as antisense RNAs *fraE* and, partly, *fraD* (Merino-Puerto *et al.*, 2013; Ehira & Ohmori, 2014).

FraC, FraD and FraE are integral membrane proteins. FraC and FraD fused to GFP are found at the cell poles spread in the intercellular septa (Merino-Puerto *et al*., 2010) (Fig. 1.8.A). FraC is a 179-amino acid residue protein that is predicted to have three transmembrane segments (TMSs), and its C terminus is predicted to be located in the

cytoplasm (Fig. 1.8.B) (Herrero *et al.*, 2016). FraD is a 343-residue protein that contains five TMSs with a predicted cytoplasmic N-terminus and periplasmic C-terminus. The C-terminal 167 residues of FraD contain two strongly predicted, albeit short, coiled-coil motifs that may be involved in protein-protein interactions (Fig. 1.8.B). The last protein encoded by the *fra* operon is FraE, which is a 267-residue protein that is predicted to bear six TMSs (Fig. 1.8.B). FraE shows homology to the permeases of some ABC transporters.

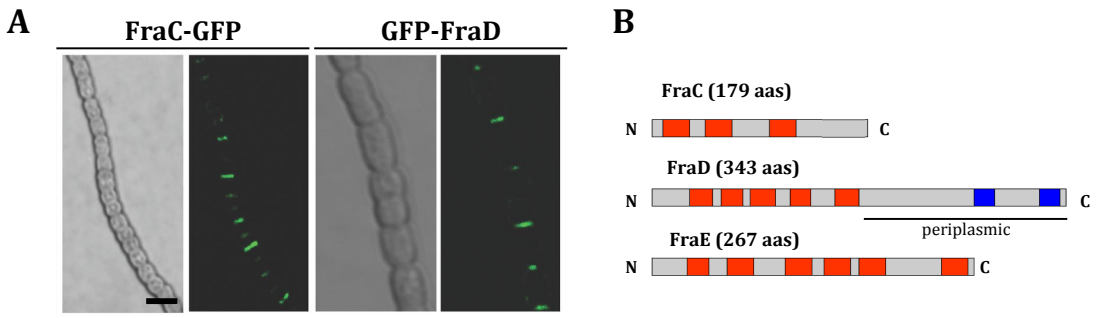

Fig 1.8. The Fra proteins. (**A**) Bright field (left) and GFP fluorescence (right) micrographs of filaments of *Anabaena* strains expressing FraC fused to GFP by its C-terminus (FraC-GFP) and FraD fused to GFP by its N-terminus (GFP-FraD) (from Herrero *et al.*, 2016). Size bar, 5 μm. (**B**) Schemes of the FraC, FraD and FraE proteins. Orange boxes denote transmembrane segments; blue boxes correspond to coiled-coil motifs.

In addition to the fragmentation phenotype, mutants of *fra* genes are also impaired in heterocyst differentiation and intercellular molecular exchange. The *fraE* mutant differentiates immature heterocysts that lack a well-formed neck. The *fraC* and *fraD* mutants make heterocysts showing the septal region corresponding to the heterocyst neck with the heterocyst cytoplasmic membrane withdrawn towards the heterocyst interior (Merino-Puerto *et al.*, 2011b; Omairi-Nasser *et al.*, 2015). A double *fraC fraD* mutant shows a very similar phenotype to that of *fraC* or *fraD* single mutants. This observation together with the coincident location of both proteins at the intercellular septa and the conservation of gene arrangement suggest that FraC and FraD work together (Merino-Puerto *et al.*, 2011b).

FraF is a pentapeptide-repeat protein expressed at high levels in the heterocysts (Ni *et al.*, 2009; Merino-Puerto *et al.*, 2013). The mechanism through which this protein restricts filament length remains unknown.

1.6.2. SepJ

Mutants in the *sepJ* gene were repeatedly isolated in rounds of transposon mutagenesis looking for mutants of *Anabaena* unable to grow diazotrophycally (Ernst *et al.*, 1992; Buikema *et al.*, 1991). Disruption of *sepJ* produces aberrant heterocyst differentiation, which is arrested at an early stage, and filament fragmentation that is exacerbated under diazotrophic conditions (Flores *et al.*, 2007; Nayar *et al.*, 2007; Mariscal *et al.*, 2011). The *sepJ* gene is ORF *alr2338* of the *Anabaena* genome (Kaneko *et al.*, 2001). This gene is proximal to *hetR* (alr2339), and this genomic organization is conserved in most heterocyst-forming cyanobacteria. The *sepJ* gene is transcribed in filaments grown with combined nitrogen, and its expression increases upon N step-down but does not require the regulators NtcA or HetR (Flores *et al.*, 2007).

Anabaena SepJ is a 751 amino-acid protein that is predicted to have four well-differentiated domains (Herrero *et al.*, 2016) (Fig 1.9.A):

1. N-terminal region: it comprises the first 27 amino acid residues and is strongly conserved. It could to bear topological signals for proper localization of SepJ in the membrane.
2. Coiled-coil domain: it comprises residues 28 to 207. This domain consists of two strongly predicted coiled-coil motifs and might be involved in protein-protein interactions. Tridimensional structure prediction of this domain shows a very similar folding to that of the coiled-coil domain of PcsB from *Streptococcus pneumoniae*, a peptidoglycan hydrolysis protein involved in separation of daughter cells during bacterial cell division (Bartual *et al*., 2014).
3. Linker domain: it comprises residues 208 to 411. This domain is present in SepJ from all filamentous cyanobacteria but its length is very variable (from 67 to 317 amino acids). However, amino acid composition of the linker domain is very conserved containing high percentages of Pro (15-20%) and Ser (10-20%), in addition to Thr (6-15%) and, in some cases, Glu (about 10%) (Herrero *et al*., 2016).
4. Integral membrane domain (permease domain): it comprises residues 412-751. Analysis of the sequence of this domain indicates that it can be divided into two subdomains, IM1 and IM2 (Herrero *et al*., 2016). IM2 comprises the last eight TMSs of the protein and is topologically conserved in all SepJ sequences except that of *Cylindrospermopsis raciborskii* (Plominsky *et al*., 2015). The IM2 subdomain shows similarity to proteins of the drug/metabolite exporter (DME) family. The IM1 subdomain is more variable in predicted topology than IM2, and it may bear one, two or three TMSs.

SepJ is restricted to the cyanobacterial clade and its general structure is strongly conserved in the protein from heterocyst-forming cyanobacteria. SepJ-like proteins from non-heterocyst formers show a very similar architecture but in many cases the linker domain is short. A protein homologous to the permease domain is also encoded in the genome of many unicellular cyanobacteria. The distribution of SepJ proteins among cyanobacteria suggests that evolution of SepJ may have comprised the acquisition of new domains starting from a DME family protein (Mariscal *et al*., 2011). A unique case of a different SepJ protein has been recently reported (Plominsky *et al*., 2015). In the heterocyst-forming cyanobacterium *Cylindrospermopsis raciborskii* the *sepJ* gene is split into two genes, *Crc_03186* (enconding a SepJ protein that lacks the four last TMSs) and *Crc_03185* (encoding a protein containing two TMSs similar to the last TMSs of regular SepJ proteins).

SepJ localization has been studied by fusions with the GFP (Flores *et al*., 2007). SepJ-GFP localizes to the cell poles in the intercellular septa (Fig. 1.9). SepJ-GFP is very focalized in the middle of the septum, and a single fluorescence spot is seen in the intercellular septa because SepJ-GFP proteins from two adjacent cells are very close together. In a *fraCD* mutant, SepJ-GFP is located in the intercellular septa but not focused, indicating that the Fra proteins are needed for proper localization of SepJ (Merino-Puerto *et al*., 2010). Additionally, SepJ-GFP is seen to position at a ring, similar to a Z ring, in the middle of the cells when cell division starts (Flores *et al*., 2007; Mariscal & Flores, 2010).

The domain organization of SepJ has been studied by mutational analysis (Mariscal *et al*., 2011). A SepJ version lacking the coiled-coil domain can be incorporated into the membrane but is not properly located at the cell poles indicating that the coiled-coil

domain is needed for polar localization of SepJ. A strain carrying a deleted version of SepJ lacking the entire periplasmic part also fails in septal localization. Both types of mutants show filament fragmentation. Deletion of the linker domain results in a slight fragmentation of the filaments and does not significantly impair the septal localization of the protein, heterocyst differentiation or diazotrophy. On the other hand, an *Anabaena* SepJ chimeric construct containing the periplasmic section of SepJ from *Anabaena* fused to the permease domain of SepJ from *Trichodesmium* (a non-heterocyst forming cyanobacterium) does alleviate the filament fragmentation phenotype but fails in diazotrophic growth (Mariscal *et al.*, 2011). All these studies suggest that whereas the periplasmic section of SepJ plays an important role in filamentation, its permease domain may be involved in intercellular molecular transfer required for diazotrophic growth.

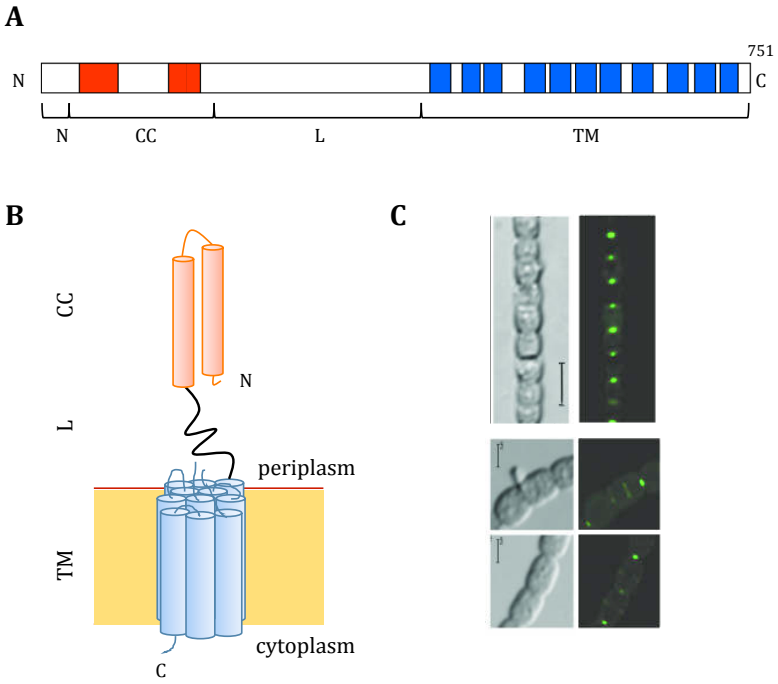

Fig 1.9. SepJ protein in *Anabaena*. (**A**) Predicted structure of *Anabaena* SepJ. N, conserved N-terminal region; CC, coiled-coil domain; L, linker domain; TM, transmembrane domain. Red boxes indicate the predicted coil-coil motifs. Blue boxes indicate TMSs predicted by TMHMM program. (**B**) Proposed model for the topology of the different domains of SepJ. The coiled-coil domain (CC) is shown in orange, the linker domain (L) as a black line, and the transmembrane domain (TM) in blue (9 TMSs are depicted, but there could be 11). (**C**) Micrograph of strain CSAM137 producing SepJ-GFP; bright field and GFP fluorescence are shown. SepJ-GFP can be seen forming a ring in the middle of dividing cells as shown in the bottom panels (Micrograph from Flores *et al.*, 2007). Size bar, 6 μm.

Examination of peptidoglycan sacculi from a Δ*sepJ* mutant shows that it contains a decreased number of nanopores, indicating that SepJ could be involved in nanopore formation (Nürnberg *et al.*, 2015). This finding was corroborated by electron tomography studies (Omairi-Nasser *et al.*, 2015). All these evidences led to the hypothesis that SepJ is a component of the proteinaceous structures –septal junctions– that connect neighboring cells through nanopores.

1.7. INTERCELLULAR COMMUNICATION

Intercellular molecular exchange plays a crucial role in the physiology of heterocyst-forming cyanobacteria, since exchange of regulators and nutrients is essential in heterocyst development and diazotrophic growth. Diffusible regulatory molecules that control heterocyst distribution in the filament include the PatS and HetN morphogens. Cellular distribution of a morphogen including the RGSGR sequence has been studied by immunofluorescence (Corrales-Guerrero *et al*., 2013). On the other hand, specific enzymes involved in nitrogen and carbon metabolism are expressed exclusively or preferentially in vegetative cells or heterocysts implying the intercellular transfer of some intermediates of the metabolic pathways. The following are well-known examples: the GS-GOGAT pathway (Martín-Figueroa *et al*., 2000) and the catabolic pathways of cyanophycin (Gupta & Carr, 1981; Picossi *et al*., 2004; Burnat *et al*., 2014a), sucrose (López-Igual *et al*., 2010; Vargas *et al*., 2011), and alanine (Jüttner, 1983; Pernil *et al*., 2010).

For the last decades, many studies have been carried out in search of the routes through which the transferred molecules are exchanged between vegetative cells and heterocysts. Different structural and physiological studies have suggested the existence of two possible pathways for intercellular molecular exchange: the continuous periplasm and cell-cell joining structures (Mariscal *et al*., 2007; Mullineaux *et al*., 2008).

1.7.1. The continuous periplasm

The presence of a continuous outer membrane along the filament makes the periplasm a shared compartment for all the cells in the filament that might serve as a communication conduit. The continuity of the periplasm is not only structural but also functional. The production of GFP protein (27 kDa) in the periplasm from pro-heterocysts showed that diffusion of small proteins in this compartment can take place (Mariscal *et al*., 2007). However, the existence of a dense peptidoglycan mesh may impair the diffusion of large proteins (Zhang *et al*., 2008, 2013).

The use of this conduit would involve the presence of membrane transporters mediating substrate export from the producing cell and import into the recipient cell. ABC transporters involved in the uptake of amino acids and glucosides have been identified in *Anabaena*, and some of them are required for optimal diazotrophic growth (Picossi *et al*., 2005; Pernil *et al*., 2008; Nieves-Morión *et al.*, 2017a). Movement of metabolites through the periplasm would require a low permeability of the OM for those metabolites to avoid significant leakage from the filament. Indeed, it has been shown that the outer membrane of *Anabaena* has low permeability for certain amino acids and sugars that are exchanged in diazotrophic conditions, including glutamate, glutamine and sucrose (Nicolaisen *et al*., 2009).

1.7.2. Septal junctions involved in intercellular molecular exchange

As in the case of metazoan gap junctions, intercellular molecular exchange in filamentous cyanobacteria has been studied using small fluorescent probes (Mullineaux *et al*., 2008; Nürnberg *et al*., 2015). These probes include fluorescein derivatives, calcein (623 Da) and 5-carboxyfluorescein (5-CF; 376 Da), and the fluorescent sucrose analog esculin (340 Da) (Mullineaux *et al*., 2008; Mariscal *et al*., 2011; Nürnberg *et al*., 2015). Fluorescein derivatives are used as acetoxymethyl ester forms that are membrane

permeable but not fluorescent. These forms permeate into the cell, where they are hydrolyzed by esterases producing the fluorescent and hydrophilic forms that are retained inside the cells. Intercellular molecular exchange can then be studied by FRAP (Mullineaux et al., 2008). This technique has been used for determining the kinetics of diffusion through gap junctions (Haugland, 2005). It allows quantification of diffusion in living cells of a fluorescently labeled probe. The general method is to label a filament with a fluorescent molecule, photobleach a specific cell of the filament, and then image the recovery of fluorescence over time (Mullineaux *et al.*, 2008). Diffusion or active movement of molecules replaces bleached fluorophore with unbleached molecules from neighboring cells. Over time, fluorescence recovers in the bleached cell and decreases in its neighbors.

Mutants of septal proteins are differentially impaired in the transfer of fluorescent probes. Thus, whereas mutants lacking FraC and FraD are strongly impaired in the transfer of esculin and 5-CF, mutants lacking SepJ are mainly affected in calcein transfer (Mariscal *et al.*, 2011; Merino-Puerto *et al.*, 2011; Nürnberg *et al.*, 2015). This suggests that at least two different types of conduits may be present between cells. Putting together all the data available, it has been suggested that septal proteins may constitute functional analogs of metazoan gap junctions, and thus, have been named septal junctions (Mariscal, 2014; Flores *et al.*, 2016). Septal junctions might promote nanopore formation since, as mentioned above, the occurrence of nanopores in the septal peptidoglycan disks is decreased in mutants lacking SepJ and/or FraC and FraD (Nürnberg *et al.*, 2015). However, a *sepJ fraC fraD* triple mutant still shows some activity of intercellular molecular transfer and the presence of a few nanopores per septum, indicating that other type(s) of septal junctions might exist.

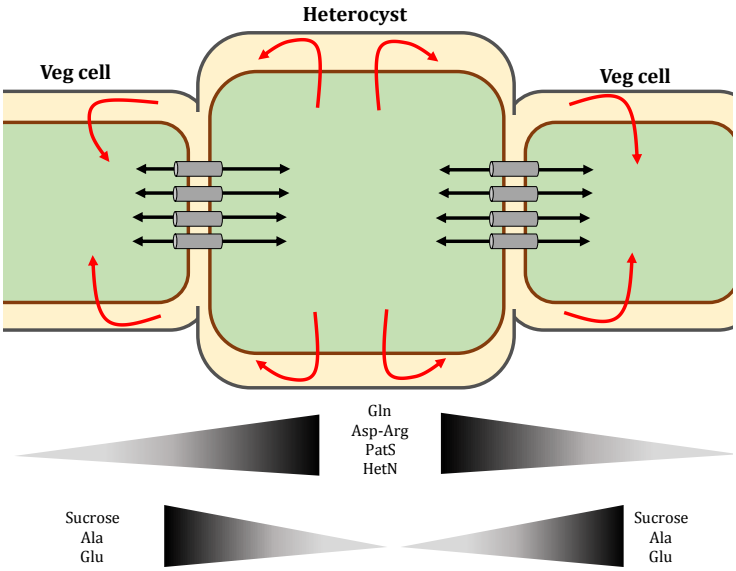

Fig. 1.10. Proposed pathways for intercellular molecular exchange in *Anabaena*. Scheme of part of a filament of *Anabaena*. The continuous periplasm pathway is represented by red arrows. This pathway would involve exporters that move metabolites from the cytoplasm to the periplasm, and importers that introduce these metabolites into the cells from the periplasm. The septal junction pathway is represented by black arrows and involves septal junctions represented as grey cylinders. Molecules that have been shown to be transferred are indicated below the producer cell: sucrose, alanine (Ala) and glutamate (Glu) are moved from vegetative cells to the heterocysts; and glutamine (Gln), β-isoaspartyl-arginine (Asp-Arg) and PatS and HetN morphogens are transferred from the heterocysts to vegetative cells.

Mutants of some putative inner membrane import systems are also impaired in intercellular molecular exchange of fluorescent tracers such as esculin or calcein (Escudero *et al*., 2015; Nieves-Morión *et al*., 2017a). These results suggest that the full operation of the septal junctions might depend on a correct setting of the different transporters present in the intercellular septa.

1.8. CELL DIVISION IN BACTERIA

In nearly all bacteria, cytokinesis is initiated by the polymerization into a ring-like structure (Z-ring) at mid-cell of the tubulin homolog FtsZ (Kirkpatrick & Viollier, 2011). FtsZ is a GTPase that is conserved in almost all bacteria. Polymerization of FtsZ is modulated by its GTPase activity. FtsZ monomers start to accumulate underneath the cytoplasmic membrane but they need a tether to interact with the cytoplasmic face of the membrane, since FtsZ lacks membrane-interacting domain. In *E. coli,* this task is achieved through a partnership between FtsA and ZipA, both of which participate in cytokinesis and simultaneously associate with the membrane and bind to FtsZ (Rico *et al*., 2013). Alternative tethers for FtsZ exists in other bacteria, such as SepF, a conserved protein among Gram-positive bacteria. SepF is non-essential and it has been demonstrated that overexpression of this protein can compensate the lack of FtsA in *Bacillus subtilis* (Ishikawa *et al*., 2006). Once the Z-ring is tethered to the membrane, it acts as a scaffold for the recruitment of further division components that extend to the periplasm. The macromolecular complex formed by all the proteins involved in cell division is known as divisome.

The divisome matures through the incorporation of FtsK, FtsQ, FtsL, FtsB, FtsW, FtsI, and FtsN (Aarsman *et al*., 2005). Among these late proteins, FtsQ has an important role driving the localization of the subsequent proteins. FtsQ is a low abundance membrane protein (about 22 copies per cell in *E. coli*) whose recruitment to the division site depends on FtsK (Carson *et al*., 1991). The FtsQ structure includes a cytoplasmic N-terminal tail, a membrane-spanning helix and a longer periplasmic section, which is composed of two domains: α and β. The α domain corresponds to a POTRA domain presumably involved in chaperone-like functions, and the β domain includes a region involved in the interactions with FtsB/FtsL (Villanelo *et al*., 2011). In Gram-positive bacteria such as *B. subtilis*, an FtsQ homolog called DivIB (Robson & King, 2006) is present. Another important late protein is FtsW, an integral membrane protein that appears to be involved in PG biogenesis. FtsW is a member of the SEDS (shape, elongation, division and sporulation) family of proteins. In *E. coli,* FtsW has ten transmembrane spans and the gene is present in the same operon as *ftsI*, which encodes a penicillin-binding protein. FtsW has been recently shown to be a PG glycosyltransferase (Meeske *et al.*, 2016).

The final steps of cell division include constriction and cell separation. Constriction is presumably an energy-dependent process. There are at least two potential drivers. One is constriction of the cytosolic Z ring, with associated factors and membrane anchor. The other is inward growth of an annulus of PG. However, the ability of certain wall-less organisms to divide suggests that PG synthesis is not essential for division, although an equivalent extracellular mechanism substituting for PG synthesis cannot be ruled out in these organisms (Errington *et al*., 2003). Cell separation occurs later by the action of various cell wall autolysins. Splitting of septal peptidoglycan is accomplished by three

amidases, AmiA, AmiB and AmiC, and the LytM-domain proteins EnvC and NlpD (de Boer, 2010). Moreover, in Gram-negative bacteria, invagination of the outer membrane must occur. In E. coli, this process requires the action of the Tol-Pal complex that is composed of three proteins located in the cytoplasmic membrane (TolQAR), one periplasmic protein (TolB) and the outer membrane lipoprotein Pal (Typas *et al*., 2012).

1.8.1. Cell division in cyanobacteria

Cyanobacterial cell division has been studied mainly in unicellular strains such as *Synechococcus* sp. PCC 7942 (*S. elongatus*) and *Synechocystis* sp. PCC 6803. The cyanobacterial genes involved in cell division have been identified by comparative and mutational analysis, which have shown that these organisms contain some cell division genes previously identified in Gram-negative bacteria, some in Gram-positive bacteria and some others that are specific to cyanobacteria (Miyagishima *et al*., 2005; Cassier-Chauvat & Chauvat, 2014). Components of the cyanobacterial divisome currently know are summarized in Fig. 1.11.

All the cyanobacterial genomes sequenced so far bear a gene encoding FtsZ. In most bacteria, the *ftsZ* gene is found in a cluster with *ftsQ* and *ftsA.* In cyanobacteria *ftsZ* and *ftsQ* are usually located close to each other, but they lack *ftsA*. Although neither FtsL nor FtsB is present in cyanobacteria, a protein structurally similar to FtsB, named CyDiv, has been described recently (Mandakovic *et al*., 2016). No homologs of ZipA can be either recognized in cyanobacterial genomes. The role of these proteins anchoring FtsZ to the plasma membrane in other bacteria might be carried out in some cyanobacteria by SepF, the alternative FtsZ tether in Gram-positive bacteria, which has been found in *Synechocystis.* SepF interacts with FtsZ and increases the stability of FtsZ polymers (Marbouty *et al*., 2009a). Moreover, a cyanobacterial specific gene, *zipN* (also known as *ftn2*), has been identified in *S. elongatus* (Miyagishima *et al*., 2005). ZipN is a self-interacting protein that also interacts with other division components including FtsZ, FtsI and FtsQ (Marbouty *et al*., 2009b; Cassier-Chauvat & Chauvat, 2014).

Other components exclusive of the cyanobacterial divisome have been identified. ZipS (also known as Ftn6) is a protein that also interacts with FtsZ and bears a DnaD-like domain which is predicted to physically interact with DNA (Marbouty *et al*., 2009c). Thus, ZipS could be a molecular link between cell division and DNA metabolism (Herrero *et al*., 2016).

Concerning proteins involved in PG synthesis and remodeling, cyanobacterial genomes contain genes encoding penicillin-binding proteins (PBP) and autolysins. *Anabaena* possesses at least 12 genes encoding PBP and *Synechocystis* at least 9. Amidases are also present in cyanobacteria (Cassier-Chauvat & Chauvat, 2014; Hahn & Schleiff, 2014).

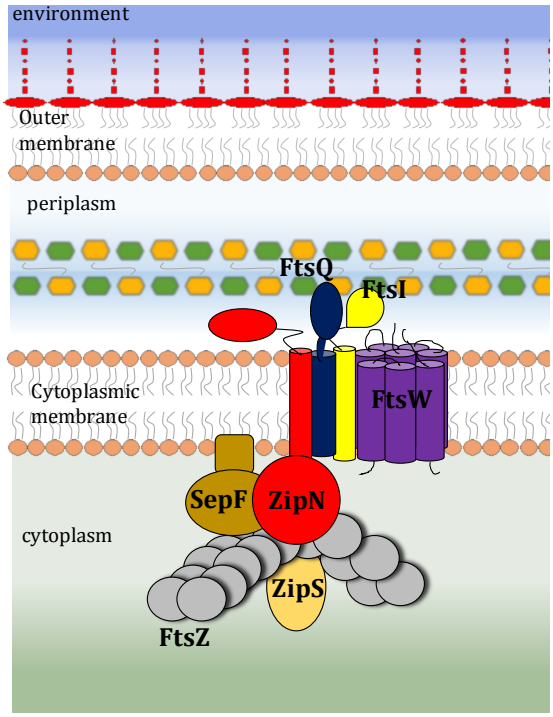

Fig. 1.11. Model of the cyanobacterial divisome. FtsZ polymers could be tethered to the membrane by ZipN and SepF. FtsQ, involved in recruitment of late components, interacts with ZipN, FtsI and FtsW (Marbouty *et al.*, 2009b). The cyanobacterial specific protein ZipS can interact with FtsZ directly and bears a DNA-binding domain that may link cell division and DNA segregation (Adapted from Chaisser-Chauvat & Chauvat, 2014).

Filamentous cyanobacteria represent an obvious example of variations on the theme of binary fission. In these organisms, cell division has been poorly studied. Localization of FtsZ in *Anabaena* has been studied using GFP fusions and immunogold labeling, which showed that this protein polymerizes in a ring at midcell starting the process of division (Sakr *et al.*, 2006; Klint *et al.*, 2007). Moreover, FtsZ appears to be at low levels or absent in heterocysts (Kuhn *et al.*, 2000; Klint *et al.*, 2007), but further details on its regulation are unknown.

Filamentous cyanobacteria terminate cell division generally without OM constriction and cell separation, since only a small fraction of cell division events appear to terminate with two separated cells giving rise to independent filaments. On the other hand, in these organisms, the cell division machinery might recruit septal junction proteins involved in cell-cell adhesion. As mentioned in chapter 1.5, AmiC-type amidases are involved in nanopore formation, which is related to a correct placement of cell-cell-connecting structures (Hahn & Schleiff, 2014).

1.9. OBJECTIVES OF THIS WORK

In this work, we have studied in depth the septal protein SepJ in order to elucidate mechanisms responsible for cell-cell adhesion and intercellular communication in the filaments of the cyanobacterium *Anabaena* sp. PCC 7120. The main objectives have been:

1. To study the mechanism for SepJ localization in the septum and its relationship with the cell division machinery
2. To study the ability of SepJ to form oligomers and to interact with other proteins and cellular structures related to cell division and nanopore formation.
3. To study of the role of the SepJ permease domain in intercellular molecular exchange, including transfer of fluorescent tracers and heterocyst differentiation regulators.

The results of this work are included in the following articles:

Ramos-León F, Mariscal V, Frías JE, Flores E & Herrero A (2015) Divisome-dependent subcellular localization of cell-cell joining protein SepJ in the filamentous cyanobacterium Anabaena. Mol Microbiol 96: 566-580.

Rudolf M, Tetik N, Ramos-León F, Flinner N, Ngo G, Stevanovic M, Burnat M, Pernil R, Flores E & Schleiff E (2015) The peptidoglycan-binding protein SjcF1 influences septal junctions function and channel formation in the filamentous cyanobacterium *Anabaen*a. mBio 6: e00376-15.

Ramos-León F, Mariscal V & Flores E (2017) Specific mutations in the SepJ permease discriminate between the cell-cell binding and communication functions of cyanobacterial septal junctions. Submitted.

Ramos-León F, Mariscal V, Battchikova N, Aro EM & Flores E (2017) Septal protein SepJ from the heterocyst-forming cyanobacterium *Anabaena* forms oligomers and interacts with peptidoglycan. In preparation.

2. MATERIALS & METHODS

2.1. ORGANISMS AND GROWTH CONDITIONS

2.1.1. *Escherichia coli*

2.1.1.1. Strains

The *Escherichia coli* strains used in this work are described in Table 2.1.

Table 2.1. *E. coli* strains used in this work

Strain	Genotype	Uses	Ref.
BL21	F- *ompT gal dcm lon hsdS$_B$(r_B-m_B-) λ(DE3[lacI lacUV5-T7 gene 1 ind1 sam7 nin5])*	Protein production	Studier & Moffatt (1986)
BTH101	F- *cya-99 araD139 galE15 galK16 rpsL1 (Sm^r) hsdR2 mcrA1 mcrB1*	Bacterial Two Hybrid analysis	Karimova *et al.* (1998)
DH5α	F- *supE44 hsdR17(r_k-m_k+) recA1 girA96 (Nal^r) endA1 thi-1 relA1 Δ(lacaya-argF) (Ø80lacZΔM15) U59*	Gene cloning and plasmid construction	Hanahan (1983)
ED8654	*Lac-3 o LacY1 supE44 supF58 hsdR514 (r_k-m_k-) recA56mcrA1 metB1 lacY galk2 galT22 trpR55*	*Anabaena* conjugation	Murray *et al.* (1977)
HB101	F- hsdS20 *(r_B-m_B-) leu supE44 ara14 galK2 lacY1 proA2 rpsL20 xyl-5 mtl-1 recA13 mcrB*	*Anabaena* conjugation	Boyer & Roulland-Dussoix (1969)

2.1.1.2. Culture conditions

E. coli strains were grown in Luria-Bertani medium (LB), containing 10 g·L^{-1} NaCl, 10 g L^{-1} tryptone and 5 g L^{-1} yeast extract (Sambrook & Russell, 2001). LB medium was supplemented with 1.5% (w/v) agar (Merck) for solid media. Sterilization was performed in autoclave. Competent cells of strains DH5α and BL21 were obtained from the Servicio de Cultivos Biológicos del Centro de Investigaciones Científicas Isla de la Cartuja.

Liquid cultures were incubated in orbital shakers at 200 rpm and 37°C. 10-mL tubes were used for small cultures (3-5 mL) and 1-L flasks for large-scale cultures (500 mL). Solid cultures were grown in Petri dishes at 37°C. Cultures were supplemented with antibiotics sterilized by filtration. Final concentrations of antibiotics were: ampicilin (Ap), 50 μg mL^{-1}; chloramphenicol (Cm), 30 μg mL^{-1} (dissolved in ethanol); streptomycin sulfate (Sm), 25 μg mL^{-1} or 100 μg mL^{-1} for strain BTH101; spectinomycin dihydrochloride pentahydrate (Sp), 100 μg mL^{-1}; and kanamycin sulfate (Km), 50 μg mL^{-1}. Antibiotic stocks were prepared in water except chloramphenicol, which was dissolved in ethanol.

2.1.2. Cyanobacteria

2.1.2.1. Strains

Anabaena sp. (also known as *Nostoc* sp.) strain PCC 7120 (ATCC 27893) has been the focus of this work. It belongs to section IV of the taxonomic classification of Rippka *et*

al. (1979). All the cyanobacterial strains used in this work are described in Tables 2.2 and 2.3.

Table 2.2. Cyanobacterial strains used that were not generated in this work

Strain	**Genotype**	**Resistance**	**Reference**
Anabaena sp. PCC 7120	wild-type	None	Rippka *et al.* (1979)
CSAM137	*sepJ-gfpmut2*::pCSV3	SmSp	Flores *et al.* (2007)
CSVM135	*sepJ-gfpmut2-his10*::pCSV3	SmSp	V. Mariscal, unpublished

Table 2.3. Mutant strains of *Anabaena* generated in this work

Strain	**Genotype**	**Description**	**Resistance**
CSFR5	C.S3-P_{ntcA}::*alr3857*	*ftsQ* conditional mutant	SmSp
CSFR18	C.S3-P_{ntcA}::*alr3858*	*ftsZ* conditional mutant	SmSp
CSFR11	CSVM90::pCSFR53	CSVM90 strain complemented with the wild-type *sepJ* gene	SmSp
CSFR12	CSVM90::pCSFR54	Mutant expressing the $SepJ_{\Delta 498-507}$ version	SmSp
CSFR13	CSVM90::pCSFR55	Mutant expressing the $SepJ_{R617A}$ version	SmSp
CSFR14	CSVM90::pCSFR56	Mutant expressing the $SepJ_{E663A}$ version	SmSp
CSFR15	CSVM90::pCSFR57	Mutant expressing the $SepJ_{S667A}$ version	SmSp
CSFR16	CSVM90::pCSFR58	Mutant expressing the $SepJ_{H624A}$ version	SmSp
CSFR19	CSVM90::pCSFR59	Mutant expressing the $SepJ_{G579A}$ version	SmSp
CSFR20	CSVM90::pCSFR60	Mutant expressing the $SepJ_{G724A}$ version	SmSp
CSFR21	CSVM90::pCSFR61	Mutant expressing the $SepJ_{A542R}$ version	SmSp
CSFR22	CSVM90::pCSFR62	Mutant expressing the $SepJ_{\Delta 739-751}$ version	SmSp
CSFR23	CSVM90::pCSFR63	Mutant expressing the $SepJ_{\Delta 626-751}$ version	SmSp
CSFR24	CSVM90::pCSFR64	Mutant expressing the $SepJ_{\Delta 690-751}$ version	SmSp
CSFR25	CSVM90::pCSFR65	Mutant expressing the $SepJ_{Y612A}$ version	SmSp
CSFR26	CSVM90::pCSFR66	Mutant expressing the $SepJ_{T616A}$ version	SmSp
CSFR27	CSVM90::pCSFR67	Mutant expressing the $SepJ_{R562A}$ version	SmSp
CSFR28	CSVM90::pCSFR68	Mutant expressing the $SepJ_{E580A}$ version	SmSp
CSVM90	*sepJ(Δbp1,387-bp2,244)*	Mutant expressing the $SepJ_{\Delta 463-748}$ version	None

2.1.2.2. Culture conditions

Anabaena strains were grown under photoautotrophic axenic conditions in a slightly modified $BG11_0$ medium (Rippka *et al.*, 1979). This medium contains 0.2 mM Na_2CO_3, 0.3 mM $MgSO_4$, 0.24 mM $CaCl_2$, 0.2 mM K_2HPO_4, 28.5 µM citric acid, 6 mg·L^{-1} iron(III) citrate hydrate (19% Fe), 2.4 µM H_3BO_3, 9.1 µM $MnCl_2$, 1.6 µM Na_2MoO_4, 0.8 µM $ZnSO_4$, 0.3 µM $CuSO_4$ and 0.2 µM $CoCl_2$. Growth media was prepared using a 100x solution containing all the components except K_2HPO_4, which was added just before sterilization. BG11 medium was prepared adding 17.2 mM $NaNO_3$, and $BG11_0$+ NH_4^+ medium was prepared adding 4 mM NH_4Cl buffered with 8 mM TES·NaOH (pH 7.5).

50-mL and 25-mL liquid cultures were incubated in 100-mL and 50-mL flasks, respectively, in an orbital incubator set at 100 rpm in a 30°C chamber, and illuminated from above at 30 µE m^{-2} s^{-1}.

Bubbled cultures were used in certain experiments. In these cases, 1-L cultures were grown in BG11 medium supplemented with 10 mM $NaHCO_3$ ($BG11_C$), and were illuminated laterally (40 µE m^{-2} s^{-1}) and bubbled with a sterile mixture of air and CO_2 (99:1) that additionally allowed for a correct stirring of the culture.

Solid medium was prepared by adding 1% (w/v) Bacto-Agar (Difco) sterilized in autoclave separately from the nutrients. Solid cultures were incubated at 30°C and illuminated from above at 15-30 µE m^{-2} s^{-1}.

Antibiotics were added to the media when it was required. The final concentrations of antibiotics were: streptomycin sulfate and spectinomycin dihydrochloride pentahydrate (SmSp), 2 µg·mL^{-1} for liquid and 5 µg·mL^{-1} for solid cultures. Antibiotics were sterilized by filtration.

Cultures were routinely collected by centrifugation at 4,000 rpm for 5 min, washed three times and diluted to 1 µg chlorophyll *a* (Chl) mL^{-1} in the desired medium. Alternatively, cells were collected by filtration through 0.45-µm pore diameter filters with a vacuum system.

2.2. MANIPULATION AND ANALYSIS OF DNA

2.2.1. Plasmids

Table 2.4. Plasmids used that were not generated in this work

Name	Resistance	Description	Reference
pCSAL33	Ap	*gfp-mut2* in a modified pMBL-T vector (without the NheI site)	A. López-Lozano, unpublished
pCSE221	Ap	Plasmid derived from pUT18 producing a SepJ-T18 translational fusion	Ramos-León et *al.* (2015) by JE. Frías
pCSE222	Km	Plasmid derived from pKNT25 producing a SepJ-T25 translational fusion	Ramos-León et *al.* (2015) by JE. Frías

pCSE226	Ap	Plasmid derived from pUT18 producing a SepJ(ΔCC)-T18 translational fusion	Ramos-León *et al*. (2015) by JE. Frías
pCSE227	Ap	Plasmid derived from pUT18 producing a SepJ(Δpp)-T18 translational fusion	Ramos-León *et al*. (2015) by JE. Frías
pCSE228	Ap	Plasmid derived from pUT18 producing a SepJ(ΔTM)-T18 translational fusion	Ramos-León *et al*. (2015) by JE. Frías
pCSE231	Km	Plasmid derived from pKNT25 producing a SepJ(ΔCC)-T25 translational fusion	Ramos-León *et al*. (2015) by JE. Frías
pCSE236	Km	Plasmid derived from pKNT25 producing a SepJ(ΔTM)-T25 translational fusion	Ramos-León *et al*. (2015) by JE. Frías
pCSE237	Km	Plasmid derived from pKNT25 producing a SepJ(Δpp)-T25 translational fusion	Ramos-León *et al*. (2015) by JE. Frías
pCSE239	Ap	Plasmid derived from pUT18 producing a SepJ(Δlinker)-T18 translational fusion	Ramos-León *et al*. (2015) by JE. Frías
pCSE240	Km	Plasmid derived from pKNT25 producing a SepJ(Δlinker)-T25 translational fusion	Ramos-León *et al*. (2015) by JE. Frías
pCSRO	SmSp	Derived from pCSV3 and pRL278 containing the polylinker and resistance cassette from pCSV3 and the *sacB* gene from pRL278	R. López-Igual
pCSV3	SmSp	Plasmid derived from pRL500, used for conjugation to *Anabaena*	Olmedo-Verd *et al*., (2006)
pCSVM98	Km	Derived from pET28-b producing the coiled-coil domain of SepJ fused to a His_6-tag	V. Mariscal, unpublished
pCSVM100	Km	Derived from pET28-b producing the entire SepJ protein fused to a His_6-tag	V. Mariscal, unpublished
pMBL-T	Ap	Commercial vector for cloning purposes	Dominion MBL
pRL278	Km	Vector used for positive selection of double recombinants in *Anabaena*	Black *et al*. (1993)
pRL443	ApTc	Conjugative plasmid, mobilizes ColE1-derived plasmids	Elhai & Wolk (1988a)
pRL623	Cm	Derived from CoIK, helper plasmid for conjugation	Elhai *et al*. (1997)
pSpark	Ap	Commercial vector for cloning purposes	Canvax

Table 2.5. Plasmids generated in this work

Name	Resistance	Description
pCSFR1	Ap Sm Sp	Plasmid generated by obtaining the gene-cassette C.S3 from pCSE33 with BamHI and cloned in pMBL-T digested with the same enzyme
pCSFR2	Ap	Plasmid containing a fragment including the upstream region of *alr3858* obtained by PCR with primers alr3858-3 and alr3858-4 cloned in pMBL-T digested with ApaI and SalI
pCSFR3	Ap	Plasmid containing a fragment that includes the 5' region of *alr3858* obtained by PCR with primers alr3858-1 and alr3858-2, cloned in pSpark digested with SacI and XhoI
pCSFR5	Ap	Plasmid containing a synthetic NtcA-regulated promoter obtained by PCR with primers Pro-sNtcA-1 and Pro-sNtcA-2 and cloned in pMBL-T digested with SpeI and EcoRV
pCSFR8	Ap Sm Sp	Plasmid generated by obtaining an ApaI-SalI fragment from pCSFR2 that contains the upstream region of *alr3858* and cloned in pCSFR1 with the same enzymes
pCSFR10	Ap Sm Sp	Plasmid generated by obtaining a SpeI-EcoRV fragment of pCSFR5 that contains the synthetic NtcA-regulated promoter and cloned in pCSFR8 with the same enzymes
pCSFR15	Ap Sm Sp	Plasmid generated by obtaining a SacI-XhoI fragment from pCSFR3 that contains the 5' region of *alr3858*, cloned in pCSFR10 with the same enzymes
pCSFR18	Km Sm Sp	Plasmid generated by obtaining PvuII fragment from pCSFR15 that contains promoter-*ftsZ* construction and cloned in pRL278 digested with XhoI and treated with Klenow
pCSFR22	Km	Plasmid generated by obtaining a PCR product with primers alr3858-7 and alr3858-8 that includes the *alr3858* gene and cloned in pCOLADuet-1
pCSFR30	Km	Plasmid generated by obtaining a PCR product with primers alr3857-7 and alr3857-8 that includes the *alr3857* gene and cloned in pKT25 digested with BamHI and PstI
pCSFR31	Km	Plasmid generated by obtaining a PCR product with primers all0154-10 and all0154-9 that contains the *all0154* gene and cloned in pKT25 digested with BamHI and PstI
pCSFR32	Km	Plasmid generated by obtaining a PCR product with primers alr3858-13 and alr3858-14 that contains the *alr3858* and cloned in pKNT25 digested with BamHI and PstI
pCSFR34	Ap Sm Sp	Plasmid generated by obtaining a PCR product with primers alr3857-3 and alr3857-4 than contains the 5' region of *alr3857* and cloned in pCSFR15 digested with SacI and XhoI
pCSFR35	Ap Sm Sp	Plasmid generated by obtaining a PCR product with primers alr3857-5 and alr3857-6 that contains the upstream region of *alr3857* and cloned in pCSFR34 digested with ApaI and SalI

pCSFR36	Km Sm Sp	Plasmid generated by cloning PvuII-digested fragment from pCSFR35, that contains promoter-*ftsQ* construction, in pRL278 digested with XhoI and treated with Klenow
pCSFR45	Km	Plasmid generated by cloning the PCR product obtained with primers all1861-1 and all1861-2, that contains the ORF *all1861*, in pKT25 with BamHI and KpnI
pCSFR46	Ap	Plasmid generated by cloning the PCR product obtained with primers all1861-1 and all1861-2, that contains the ORF *all1861*, in pUT18C with BamHI and KpnI
pCSFR50	Cm	Plasmid generated by cloning the PCR product obtained with primers alr3857-13 and alr3857-14, that contains the ORF *alr3857*, in pACYCDuet-1 with BamHI and XhoI
pCSFR51	Ap	Plasmid generated by cloning the SacI-EcoRI fragment from pCSAL3, containing the *gfp* gene, in pCSE221 with the same enzymes
pCSFR52	Ap	Plasmid generated by cloning the PstI-KpnI fragment of pCSE227, containing periplasm-deleted version of SepJ, in pCSFR51 with the same enzymes
pCSFR53	Sm Sp	Plasmid generated by cloning the PCR product, containing 379 bp of *alr2338*, obtained with primers alr2338-37 and alr2338-38, in pCSV3 digested with EcoRI
pCSFR54	Sm Sp	Plasmid generated by cloning the PCR product that contains the C-terminal part of *alr2338* gene deleted in nucleotides encoding residues 498-507, obtained by PCR with primers alr2338-37, alr2338-40, alr2338-39, alr2338-38 (overlapping PCR), in pCSV3 digested with EcoRI
pCSFR55	Sm Sp	Plasmid generated by cloning a fragment containing 379 bp of *alr2338* modified to substitute Arg617 for Ala obtained by PCR with primers alr2338-37, alr2338-42, alr2338-38, alr2338-41 (overlapping PCR), in pCSV3 with EcoRI
pCSFR56	Sm Sp	Plasmid generated by cloning a fragment containing 379 bp of *alr2338* modified to substitute Glu663 for Ala obtained by PCR with primers alr2338-37, alr2338-44, alr2338-38, alr2338-43 (overlapping PCR), in pCSV3 with EcoRI
pCSFR57	Sm Sp	Plasmid generated by cloning a fragment containing 379 bp of *alr2338* modified to substitute Ser667 for Ala obtained by PCR with primers alr2338-37, alr2338-46, alr2338-38, alr2338-45 (overlapping PCR), in pCSV3 with EcoRI
pCSFR58	Sm Sp	Plasmid generated by cloning a fragment containing 379 bp of *alr2338* modified to substitute His624 for Ala obtained by PCR with primers alr2338-37, alr2338-48, alr2338-38, alr2338-47 (overlapping PCR), in pCSV3 digested with EcoRI
pCSFR59	Sm Sp	Plasmid generated by cloning a fragment containing 379 bp of *alr2338* modified to substitute Gly579 for Ala obtained by PCR with primers alr2338-37, alr2338-50, alr2338-38, alr2338-49 (overlapping PCR), in pCSV3 digested with EcoRI

pCSFR60	Sm Sp	Plasmid generated by cloning a fragment containing 379 bp of *alr2338* modified to substitute Gly724 for Ala obtained by PCR with primers alr2338-37, alr2338-52, alr2338-38, alr2338-51 (overlapping PCR), in pCSV3 digested with EcoRI
pCSFR61	Sm Sp	Plasmid generated by cloning a fragment containing 379 bp of *alr2338* modified to substitute Ala542 for Arg obtained by PCR with primers alr2338-37, alr2338-54, alr2338-38, alr2338-53 (overlapping PCR), cloned in pCSV3 digested with EcoRI
pCSFR62	Sm Sp	Plasmid generated by cloning the PCR product obtained with primers alr2338-37 and alr2338-55, containing part of *alr2338* deleted in nucleotides encoding residues 739-751, in pCSV3 digested with EcoRI
pCSFR63	Sm Sp	Plasmid generated by cloning the PCR product obtained with primers alr2338-37 and alr2338-56, containing part of *alr2338* deleted in nucleotides encoding residues 626-751, in pCSV3 digested with EcoRI
pCSFR64	Sm Sp	Plasmid generated by cloning the PCR product obtained with primers alr2338-37 and alr2338-57, containing part of *alr2338* deleted in nucleotides encoding residues 690-751 in pCSV3 digested with EcoRI
pCSFR65	Sm Sp	Plasmid generated by cloning a fragment containing 379 bp of *alr2338* modified to substitute Tyr612 for Ala obtained by PCR with primers alr2338-37, alr2338-58, alr2338-38, alr2338-59 (overlapping PCR), in pCSV3 digested with EcoRI
pCSFR66	Sm Sp	Plasmid generated by cloning a fragment containing 379 bp of *alr2338* modified to substitute Tre616 for Ala obtained by PCR with primers alr2338-37, alr2338-60, alr2338-38, alr2338-61 (overlapping PCR), in pCSV3 digested with EcoRI
pCSFR67	Sm Sp	Plasmid generated by cloning a fragment containing 379 bp of *alr2338* modified to substitute Arg562 for Ala obtained by PCR with primers alr2338-37, alr2338-62, alr2338-38, alr2338-63 (overlapping PCR), in pCSV3 with EcoRI
pCSFR68	Sm Sp	Plasmid generated by cloning a fragment containing 379 bp of *alr2338* modified to substitute Glu580 for Ala obtained by PCR with primers alr2338-37, alr2338-64, alr2338-38, alr2338-65 (overlapping PCR), in pCSV3 digested with EcoRI
pCSVM90	Sm Sp	Plasmid generated by cloning a fragment containing part of *alr2338* obtained by PCR with primers alr2338-25, alr2338-30 and alr2338-29, alr2338-34 (overlapping PCR), in pCSRO digested with SpeI and XbaI

2.2.2. DNA isolation

2.2.2.1. Isolation of plasmids from *E. coli*

Plasmidic DNA from overnight-grown *E. coli* cultures was isolated using the *Nucleospin Plasmid* kit (Macherey Nagel), following the manufacturer's instructions.

2.2.2.2. Isolation of total DNA from *Anabaena*

Cells from 50-mL liquid cultures were harvested by filtration and resuspended in a final volume of 500 µL $T_{1/10}E$ (10 mM Tris-HCl, 0.1 mM EDTA-Na_2, pH 8) in an Eppendorf tube. 150 µL of sterile glass beads (250-300 µm diameter, sterilized at 180°C), 20 µL of 10% sodium dodecyl sulfate and 450 µL of phenol-chloroform (1:1, v/v) were then added. The mixture was shaken in a vortex for 1 min and incubated in ice for 1 min. This process was repeated three times. After that, the lysate was centrifuged at (16,100 *x g*, 15 min, 4°C) and the resulting clear supernatant was transferred to a new Eppendorf tube for successive extractions with 1 volume of phenol, phenol:chloroform, and twice with chloroform. Then, DNA was precipitated with 2.5 volumes of ethanol and 0.1 volumes of 3 M potassium acetate, pH 5.2. Tubes were incubated for 1 h at -20°C to allow for DNA precipitation. After centrifugation (16,100 x *g*, 30 min, 4°C), the pellet containing genomic DNA was washed with 70% ethanol (v/v), dried and resuspended with 50 µL of double-distilled water.

2.2.3. DNA quantification

The concentration of DNA was determined using a *NanoDrop Spectrophotometer ND-1000*. Absorbance was measured at 260 nm (extinction coefficient ε = 0.020 mL mg^{-1} cm^{-1}). DNA concentration was also estimated by comparison with samples of known concentration after agarose gel electrophoresis.

2.2.4. PCR

Polymerase Chain Reaction (PCR) was performed in a *Tpersonal* (Whatman-Biometra) thermal cycler using BioTaq DNA Polymerase (for routine analysis) and iProof (high fidelity polymerase for cloning purposes) following the manufacturer's instructions. Primers used in this work are summarized in Table 2.6.

Table 2.6. Oligodeoxynucleotide primers used in this work. The restriction sites are underlined in the sequence. Nucleotides used insertion of specific-site mutations are shown in bold.

Primer	Sequence (5'>3')
all0154-9	TAATCTGCAGTGAAGCTACGCA
all0154-10	CTGTGGATCCTTAAAACATCCG
all2707-1	ATTACTGCAGGTTGATCACGGTGC
all2707-2	TCATGGATCCTTTATAGCGGCTGA
all5167-1	GCTCAAGCAATTCGTCACTGTTCC
all5167-2	AAAGATTGCGTCGGTCTGGTGT
alr0599-1	CCAAATAGCTGGGCCAGTGTTAGT

alr0599-2	GGAATTGCTTTGCCAGTTGTCAG
alr2338-10	TGAGCCAGAAGTCCAGAG
alr2338-13	GAATTCAGAGCTTGGGGGTTGTA
alr2338-17	TCCATGGGGCGATTTGAGAAGCGA
alr2338-20	ACTCTCGAGATTGGCAGGTTTGT
alr2338-25	ATCAACAACGAGATGGGGCGATTTGAG
alr2338-29	ATCAACAACGAGATGCAAGATCAGGTAAA
alr2338-30	GGTCTCCGCGCTTGATGTTTCTTGGATAG
alr2338-34	CGTTTTTCCTGATCGGTACCTTAACCTTCTGCATT
alr2338-35	AAGCTCTGCAGGCGATTTGAGAAGCGA
alr2338-36	GGTTTAACCCGGGCTTCTGCATTGG
alr2338-37	ATCAGAATTCCCATTAGAGGAGACTAGC
alr2338-38	TACGAATTCATAGAGCGTTCTTATCTGC
alr2338-39	TGAAGCAATCACAGCCACAGAGATTTG
alr2338-40	TGGCTGTGATTGCTTCAGGTTTTGC
alr2338-41	ATCCTGACC**GC**CGTATGTGC
alr2338-42	ACATACG**GC**GGTCAGGATGAG
alr2338-43	TAAGTTACTGG**C**AATTGTGTTAAGTGC
alr2338-44	GCACTTAACACAATT**G**CCAGTAACTTAG
alr2338-45	GAAATTGTGTTA**GC**TGCTTTTATTTTGGG
alr2338-46	CAAAATAAAAGCA**GC**TAACACAATTTCCAG
alr2338-47	GGCTAAAGTC**GC**TCCAGTATCTTTGTC
alr2338-48	AAAGATACTGGA**GC**GACTTTAGCCGCAC
alr2338-49	ATTTTCTGTG**C**TGAGGTGCTAGTTTTTG
alr2338-50	TAGCACCTCA**G**CACAGAAAATAGCG
alr2338-51	CAAATATTCG**C**AGTTTTATTCGTCACTTTTG
alr2338-52	GAATAAAACT**G**CGAATATTTGGGCAATG
alr2338-53	ACCGGAGTG**CGT**ATCGCCCTTTTC
alr2338-54	AAGGGCGAT**ACG**CACTCCGGTGGG
alr2338-55	TACGAATTC**TTA**GCCAATACCAAAAGC
alr2338-56	TACGAATTC**TTA**TACTGGATGGACTTTAGC
alr2338-57	TACGAATTC**TTA**ACCTAATTTATTGATCCC
alr2338-58	AGGATGAGG**GC**ACAAGCAAAGG
alr2338-59	TGCTTGT**GC**CCTCATCCTGAC
alr2338-60	GCGGG**C**CAGGATGAGG
alr2338-61	ATCCTG**G**CCCGCGTATGTG
alr2338-62	GGGCGATC**AGC**GAACAGAAGCCAG
alr2338-63	TTC**GCT**GATCGCCCCGGTGTATTTC
alr2338-64	TGTGGTG**C**GGTGCTAGTTTTTG
alr2338-65	TAGCACC**G**CACCACAGAAAATAGC
alr3857-1	CGGCGATCGCTGACTCTT
alr3857-2	CACTGCGACAGGTATTCTTTCTT
alr3857-3	TACAGAGCTCACACAAGCCTAGTGAA
alr3857-4	TATACTCGAGCATTGGCATCGATTAAA
alr3857-5	TCTAGGGCCCCAATTTGACTGTACTAT
alr3857-6	TCTAGTCGACTGGTTAATTTCAGCAGC
alr3857-7	ATATCTGCAGTGCCTGGTATAGCG
alr3857-8	CTACGGATCCTTATGGCGTTTGAT
alr3857-13	TATTGGATCCTGGTATAGCGTCGG

alr3857-14	ATTCTCGAGACATGATTATGGCG
alr3858-1	ATAGTGAGCTCCTAGATGTGTAACA
alr3858-2	CTCGAGCCCGCACGTCAGCAA
alr3858-3	GGGCCCAGAGTTAGCCGTTAG
alr3858-4	GTCGACTATTAAGTTTGACAGCAC
alr3858-6	CTCGAGGACGTGTTACCACTCCAACAG
alr3858-7	GAACGGATCCGACACTTGATAATAA
alr3858-8	TAAACTCGAGTTAATTTTTGGGTGGT
alr3858-9	TTTGGTGCCGTGATTGATGATAG
alr3858-10	CGTTTTGGGGGAGCAGA
CS3-5	TCCGCGCTGTAGAAGTCACC
Pro-sNtcA-1	GACACTAGTAATTGTAGCAATCGCTACAATACAGAAACCAGTC
Pro-sNtcA-2	GTGATATCGTGATCTTAGGAGCGTGACTGGTTTCTGTATTGTAGC

Real-time PCR was performed in an *iCycler iQ* (BioRad) with the *SensiFAST SYBR & Fluorescein Kit* (BIOLINE) using 1/10 volumes of the cDNA resulting from the previous reverse-transcription step (see 2.3.3). Three technical replicates were performed for each condition and gene. First a master mix was prepared following the manufacturer's instructions and then 20-µL reactions were loaded in a 96-well plate. The efficiencies of the primer pairs were tested previously with different concentrations of genomic DNA as template. The optimal annealing temperature was selected from real-time PCR experiments using a gradient of temperatures. Efficiencies were calculated using the LinRegPCR software (Ramakers *et al*., 2003). The Ct values obtained were analyzed with the REST 2009 Software (Pfaffl *et al*., 2002). The mathematical treatment of data to calculate relative gene expression was performed using the formula: Relative gene expression = $2^{-\Delta\Delta Ct}$ (Pfaffl, 2001); where ΔΔCt corresponds to the increase in the threshold cycle of the problem gene with respect to the increase in the threshold cycle of the housekeeping genes.

2.2.5. Enzymatic treatments of DNA

2.2.5.1. Restriction

DNA was digested for 30 min to 2 h using endonucleases supplied by New England Biolabs. Digestions were carried out according to manufacturer's recommendations in the appropriate buffers.

2.2.5.2. Ligation

T4 bacteriophage DNA ligase (Dominion MBL) or the ligase provided with the pSpark DNA Cloning System were used for ligation of different fragments of DNA. 10-µL reactions were performed at 21°C for 1-24 h. The buffer supplied in the cloning kit was used and the vector:insert concentration ratio used was approximately 1:3, or 1:5 for ligations with pMBL-T and pSpark plasmids.

2.2.5.3. Dephosphorylation

Dephosphorylation of 5' protruding extremes was carried out in order to prevent re-circularization of linearized vectors. DNA was incubated with rAPid alkaline phosphatase (Roche) following the manufacturer's instructions.

2.2.6. DNA electrophoresis

DNA fragments were separated by agarose gel electrophoresis (Sambrook & Russell, 2001). Gels were prepared with 0.8% or 2% agarose (w/v) in TBE buffer (90 mM Tris-Borate, 2 mM EDTA-Na_2, pH 8), supplemented with 0.03% (v/v) *GelRed Nucleic Acid* Gel Stain (Biotium). Before loading samples into the gel, they were mixed with 0.1 volumes of 10x sample buffer (50% glycerol [v/v], 0.4% bromophenol blue [w/v] and 0.4% xylene cyanol FF [w/v]). The size of the fragments was estimated by using the commercial size marker *1kb ladder* (Biotools). The electrophoresis was carried out using a *Mini-Sub Cell GT* or *Wide Mini-Sub Cell GT* (BioRad), and the DNA was visualized with ultraviolet light on the *Bio-Rad Gel-Doc XR* system using the *BioRad Quantity One* 4.6.2 software.

2.2.7. Purification of DNA from gels and PCR reactions

DNA was isolated from gels or from enzymatic reactions using the commercial Gel Band Purification Kit (GE Healthcare) according to the provided protocol.

2.2.8. DNA sequencing

PCR products or isolated plasmids were sequenced by the Secugen S.L. Company service (Ramino de Maeztu 9, Madrid, Spain).

2.3. MANIPULATION AND ANALYSIS OF RNA

2.3.1. RNA isolation

Cells from 50-mL cultures were collected by filtration (see 2.1.2.3), washed with 5 mL of $T_{50}E_{100}$ buffer (50 mM Tris-HCl, 100 mM EDTA-Na_2, pH 8) and resuspended in 2 mL of the same buffer. Cell suspensions were transferred to 2-mL Eppendorf tubes, centrifuged and the resulting pellets were frozen with liquid nitrogen and stored at -20°C until use.

Cells were resuspended in 300 µL of buffer containing 300 mM sucrose and 10 mM sodium acetate (pH 4.5) supplemented with 100 µL of 250 mM EDTA-Na_2 and 400 µL of lysis buffer (2% SDS, 10 mM sodium acetate, pH4.5). After homogenization, 1 mL of 65°C pre-heated acid phenol (pH4.5) was added. The resulting mixture was shaken for 30 s in a vortex and incubated at 65°C for 2 min. This process was repeated 3 times. Then, the mixture was centrifuged for 5 min (4°C, 14,000 *x g*). The resulting supernatant was transferred to a clean Eppendorf tube and treated subsequently with 1 mL of acid phenol, 1 mL of acid phenol:chloroform (1:1), and finally with 1 mL of chloroform. The mixture

was shaken in a vortex for 30 s, incubated at 65°C for 2 min and centrifuged for 5 min (16,100 x *g*, 4°C), and the process was repeated. After chloroform treatment, the supernatant was transferred to a clean Eppendorf tube, 1 mL of isopropanol was added and the mixture was incubated at -20°C for at least 1 h. After centrifugation for 30 min, the supernatant was discarded and the pellet was washed with 70% ethanol. The pellet was dried and resuspended in 200 µL of DEPC-treated water at 4°C for at least 2 h. Then, 200 µL of phenol:chloroform (1:1) was added and the resulting mix was shaken in a vortex for 30 s and centrifuged for 5 min. the supernatant was transferred to a clean Eppendorf tube containing 200 µL of chloroform, shaken and centrifuged again. The supernatant was transferred to a clean tube and 500 µL of absolute ethanol and 50 µL of 3 M sodium acetate (pH 5.2) were added and the mix was incubated at -20°C for 20 min. After 30-min centrifugation, the pellet was washed with 70% ethanol, dried and resuspended in 45 µL of DEPC-treated water at 4°C for at least 2 h. In order to remove traces of DNA, 5 µL of DNase 10x buffer (Ambion) and 1 µL (2 U) of *TurboDNase* (Ambion) were added and incubated at 37°C for 30 min. After that, 1 µL of *TurboDNase* was re-added and the mixture was incubated for 30 min. To inactivate the reaction, 5 µL of inactivation reactive was added and left to act during 2 min. Then, a 90-s centrifugation was carried out and the resulting supernatant was transferred to a clean tube. The presence of contaminating DNA was tested by PCR (no PCR product was obtained in any of the RNA samples).

2.3.2. RNA quantification

The concentration of RNA was determined using a NanoDrop Spectrophotometer ND-1000. The absorbance was measured at 260 nm (ε= 0.025 mL mg^{-1} cm^{-1}).

2.3.3. Reverse-transcription

Reverse-transcription was carried out with the *QuantiTect Reverse Transcription Kit* (QUIAGEN), using 600 ng of RNA as template and 100 ng of *Random Hexamer Primers* (BIOLINE) instead of those provided by the kit.

2.4. GENETIC METHODS

2.4.1. Transformation of *E. coli*

2.4.1.1. Transformation by heat shock

E. coli strains DH5α and HB101 were subjected to transformation by heat shock. 100 µL of competent cells were mixed with 10 µL of ligation product or 1 µL of purified plasmid. The mixture was incubated on ice for 15 minutes, then at 42°C for 90 s, and then incubated again on ice for 5 min. After that, 1 mL of LB was added and the cells were incubated at 37°C for 1 h in a shaker in order to permit expression of the antibiotic-resistance gene. The cells were harvested by centrifugation and the pellet was spread atop solid LB medium with the appropriate antibiotics to select cells carrying the construct. For pSpark or pMBL-T derived constructs, 40 µg mL^{-1} X-Gal was added to the plates in order to facilitate selection of correct clones (α complementation assay) (Sambrook & Russell, 2001).

2.4.1.2. Transformation by electroporation

Competent cells of *E. coli* strains BL21 or BTH101 were mixed with 1 µL of isolated plasmid or mix of pKT25/pUT18-derived plasmids, respectively, and incubated for at least 1 min on ice. The mix was subjected to electroporation using a 2-mm cuvette in an EasyjecT Optima electroporation system (EQUIBIO) (2500 V, 15 µF, 335 Ω). After that, 1 mL of LB was added quickly, and the cells were incubated at 37°C for 1 h in a shaker. Later on, the cells were spread atop LB plates containing the appropriate antibiotics.

2.4.2. Conjugation to *Anabaena*

The conjugation protocol is described in Elhai & Wolk (1988b). ED8654 strain bearing pRL443 plasmid (which provides conjugation functions) was transferred to *E. coli* HB101 strain that carried the *cargo* plasmid and the helper plasmid pRL623. This last plasmid bears genes that encode methylases for AvaI, AvaII and AvaIII restriction sites (Elhai *et al*., 1997), which protect the cargo plasmid from digestion by the *Anabaena* restriction endonucleases, as well as the *mob* gene. In a second step, the cargo plasmid is transferred to *Anabaena*.

The conjugation was carried out as follows: 250 µL of a stationary-phase culture of *E. coli* ED8654 (pRL443) and 350 µL of a stationary-phase culture of *E. coli* HB101 (pRL623 and *cargo* plasmid) were inoculated in 10 mL of fresh LB medium with appropriated antibiotics and incubated at 37°C for 2.5 h in a shaker. Cells were collected by centrifugation, washed three times with LB in order to remove antibiotics, and mixed together in a final volume of 0.5 to 1 mL. After incubating cell suspension at room temperature for at least 2 h, an *Anabaena* suspension containing 10 µg of Chl was added, and the resulting suspension was spread on a nitrocellulose filter (Nucleopore) set atop on solid BG11 + 5% (v/v) LB medium in a Petri dish. This plate was incubated at 30°C with white light (10 µE s^{-1} m^{-2}) for at least 3 h and then at standard light intensity (30 µE s^{-1} m^{-2}) overnight. The filter was then transferred to a plate with BG11 medium, and one day later, to a plate with BG11 medium supplemented with antibiotics. After that, the filter was transferred to fresh medium with antibiotics every second day until resistant colonies appeared.

Single cross-over mutants were normally obtained by homologous recombination of a plasmid which does not have a replication origin for *Anabaena* (Fig. 2.1).

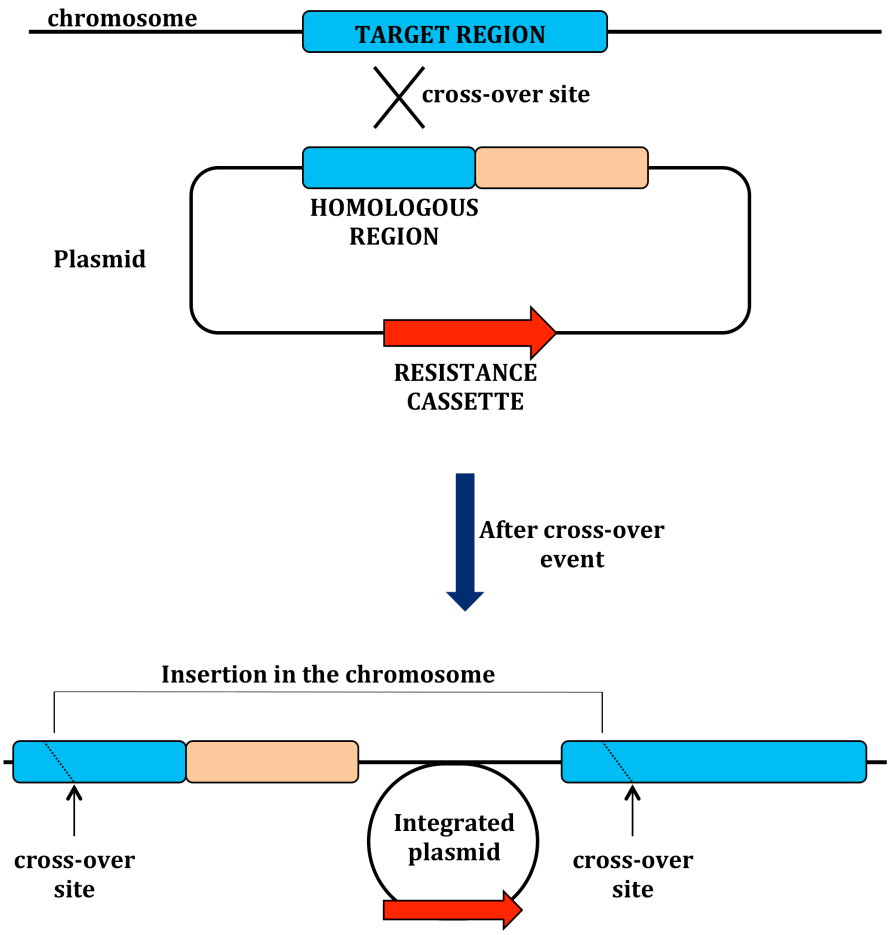

Fig. 2.1. Schematic representation of single cross-over mutant construction.

For obtaining double cross-over exconjugants, segregation of single cross-over exconjugants was first checked by PCR, and after that, they were transferred to a new plate containing BG11 medium + 5% sucrose. A pRL278-derivative plasmid was used in this case, which bears the *sacB* gene, encoding the *Bacillus subtilis* levansucrase. This enzyme converts sucrose to levan, which accumulates in the periplasm and is toxic to *Anabaena*. Thus, *sacB*-carrying plasmids provide sucrose sensitivity, and double cross-over exconjugants were those that had lost the plasmid (Fig. 2.2). Sucrose-resistant clones were tested by growth in the presence of Nm (the plasmid bears a Nm-resistance cassette).

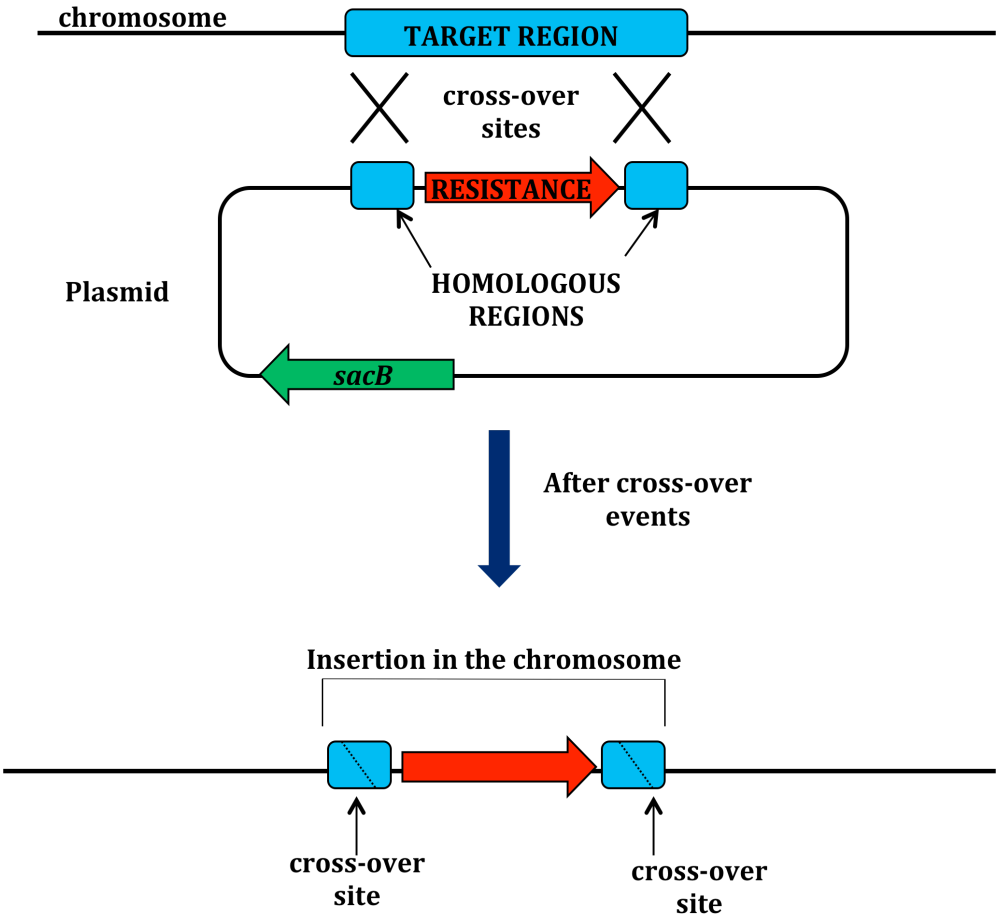

Fig. 2.2. Schematic representation of double cross-over mutant construction.

In order to facilitate segregation of the mutants, in some cases the mutants were grown in liquid medium, subjected to sonication in a bath and spread at low density on plates to get isolated colonies. Segregation was checked by PCR and those clones that did not have the wild-type gene were selected.

2.5. PROTEIN ANALYSIS

2.5.1. Production of proteins in *E. coli*

E. coli strain BL21carrying plasmids to produce proteins of interest (see Table 2.5) were grown in 30 mL of LB medium containing appropriate antibiotics and 2% glucose at 37°C overnight. The next day, cells were collected by centrifugation and resuspended in 1 mL of LB medium. 500 µL of this cell suspension were used to inoculate 500 mL of LB medium supplemented with antibiotics. When absorbance at 600 nm was 0.6, 1 mM of isopropyl β-D-1-thiogalactopyranoside (IPTG) was added in order to induce heterologous protein expression. After incubation at 37°C for at least 2 h, cells were collected by centrifugation at 5,000 *x g* for 15 min, washed, and resuspended in a buffer, which depended on the aim of the study.

2.5.1.1. Purification of His-tagged FtsZ

Anabaena FtsZ fused to a His-tag was overproduced in *E. coli* (pCSFR22) (see Table 2.5) to obtain antibodies. Induction of the protein was made as described above (2.5.1). After induction, cells were resuspended in 10 mL of a buffer containing 50 mM Tris-HCl (pH 8.0), 200 mM NaCl, 10% glycerol and supplemented with 5 μg μL^{-1} DNase I and protease inhibitors (*complete Mini EDTA-free* from Roche). Cells were broken by passage through a French Pressure cell SLM-AMINCO (twice at 20,000 psi). The resulting suspension was centrifuged at 15,000 x *g* for 10 min. Both precipitate (containing inclusion bodies) and supernatant were analyzed for the presence of FtsZ. Because an overproduced band corresponding to molecular size of FtsZ was observed in the supernatant, this fraction was subjected to affinity chromatography.

Total protein extract was subjected to FPLC (Fast Protein Liquid Chromatography) using a *5-mL HisTrap* column (GE Healthcare). Retained proteins were eluted with an increasing concentration of imidazole (Fig. 2.3). After two purification steps, imidazole was removed from the samples by dialysis. Finally, purified FtsZ preparations were concentrated to 1 mg·mL^{-1} using a *Stirred Ultrafiltration Cell* (Millipore).

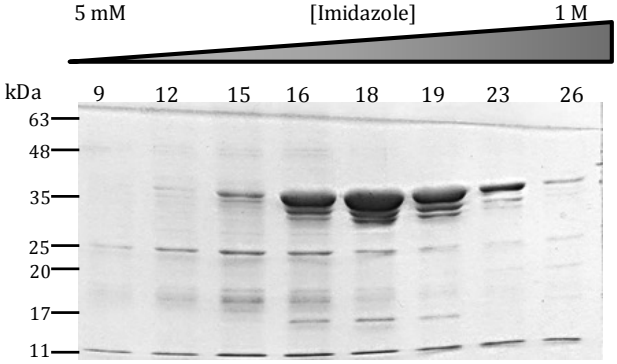

Fig. 2.3. Purification of His-tagged *Anabaena* FtsZ protein. Samples subjected to affinity chromatography were eluted with increased amounts of imidazole and analyzed by SDS PAGE. Each lane in the gel corresponds to the number of a fraction eluted from the column.

700 μg of purified FtsZ were first injected subcutaneously to a *New Zeland* rabbit (weight around 2-2.5 kg). 350 μg of purified protein were used for the second and third injections. Rabbit antiserum was produced by the Centro de Producción y Experimentación Animal (University of Seville). Different dilutions of the serum were tested against the purified protein in order to determine the best dilution for western blot analysis.

2.5.1.2. Purification of His-tagged SepJ

His-tagged SepJ versions were also purified from *E. coli* bearing plasmids pCSVM98 and pCSVM100. Induction was carried out as described earlier, cells were collected by centrifugation and resuspended in 10 mL of PBS (5.5 mM Na_2HPO_4, 1.8 mM KH_2PO_4, 137 mM NaCl, 2.7 mM KCl) buffer supplemented with 5 μg·μL^{-1} DNase I and protease inhibitors. Cells were broken as previously described for FtsZ. For SepJ-His_6 the

supernatant was then subjected to centrifugation (150,000 x *g*, 1 h, 4°C) to separate soluble proteins from membranes. The precipitated membranes were then resuspended in 1 mL of PBS buffer containing 1% n-Dodecyl β-D-maltoside (DDM). For His_6-tagged SepJ coiled coil domain (SepJCC-His_6) the cell lysate was used directly in solubilization with DDM. Solubilized proteins, containing SepJ-His_6 or SepJCC-His_6 were subjected to a His SpinTrap (GE Healthcare) column following the instructions of the supplier. SepJ-His_6 and SepJCC-His_6 proteins were eluted from the column with 300 µL of Elution buffer (PBS buffer containing 1% DDM and 300 mM imidazole).

2.5.2. Protein purification from *Anabaena* membranes

2.5.2.1. Cell fractionation and extraction of membranes from *Anabaena*

Filaments from 300-mL cultures were harvested by centrifugation at 7,000 *x g*, washed twice with PBS buffer (5.5 mM Na2HPO4, 1.8 mM KH2PO4, 137 mM NaCl, 2.7 mM KCl). Harvested cells were resuspended in 2 mL of PBS buffer containing 30 mM CaCl2, 800 mM sorbitol, 1 mM ε-amino-n-caproic acid, and the cells were broken by vortexing 6 x 1 min at 4°C in the presence of glass beads. The total cell extract was obtained by centrifugation at 3000 *x g* for 5 min to remove the glass beads and unbroken cells. The membranes were then pelletted at 18,000 *x g* for 30 min, and resuspended in PBS buffer containing 600 mM sucrose, 30 mM $CaCl_2$, 1 M glycinbetaine and 5 mg mL-1 Pefabloc. In order to solubilize membranes to purification assay, isolated membranes were collected by centrifugation at 18,000 xg for 15 min. The membrane fraction was resuspended in 1 mL of storage buffer (50 mM Hepes-NaOH [pH 7.5], 600 mM sucrose, 30 mM $CaCl_2$ and 1 M glycerol).

2.5.2.2. Purification of SepJ complexes from *Anabaena* membranes

Membranes from strains CSVM135 (producing SepJ-GFP-His_{10}), PCC 7120 (wild type) and CSAM137 (producing SepJ-GFP) were subjected to the following protocol. Precipitated membranes were resuspended in PBS buffer supplemented with 1% DDM and incubated for 15 min at 4°C. Non-solubilized proteins were removed by centrifugation at 15,000 *x g* for 20 min. The supernatant, containing solubilized protein complexes, was subjected to a first step of purification using a His SpinTrap (GE Healthcare) column under native conditions following the instructions of the supplier. Proteins bound to the column were eluted with 200 µL of elution buffer (PBS buffer containing 1% DDM and 300 mM of imidazole). This first-eluted fraction was analyzed by SDS-PAGE and BN-PAGE.

After the first isolation step, the eluted fraction was diluted to 1 mL with PBS buffer containing 1% DDM and incubated with *µMACS Anti-GFP MicroBeads* (Miltenyi Biotec) at 4°C for 1 h. The mixture was then loaded into a *MACS* column (Miltenyi Biotec), washed with 3 mL of PBS (containing 1% DDM) and eluted with 100 µL of elution buffer (50 mM Tris-HCl [pH 6.8], 50 mM DTT, 1% SDS, 1 mM EDTA, 0.0005% bromophenol blue and 10% glycerol). Eluted fractions were analyzed by SDS-PAGE.

2.5.3. Protein biochemical methods

2.5.3.1. TCA (trichloracetic acid) protein precipitation

Cells from liquid cultures were collected by filtration as described above. Cells were washed once with Buffer A, containing 50 mM Tris-HCl (pH 7.5), 500 mM NaCl and 10% glycerol. After resuspension to reach 10 µg of Chl per mL, 500 µL of sample (5 µg of Chl) were mixed with 500 µL of 20% trichloroacetic acid (10% final concentration) and incubated on ice for at least 30 min. After that, total proteins were pelleted by centrifugation at 13,200 *x g* for 30 min, washed with 300 µL of cold acetone and centrifuged again for 10 min (all steps carried out at 4°C). The protein pellet was dried at room temperature for 15 min and then resuspended in 25 µL of buffer A. After that, samples were mixed with 1 volume of 2x sample buffer, incubated at 95°C for 15 min and loaded into a SDS-polyacrylamide gel (see 2.5.3.3).

2.5.3.2 Protein quantification

Protein was routinely quantified using the method described by Bradford (1976), measuring the absorbance at 595 nm. BSA was used as a standard.

The method of Lowry *et al*. (1951) with the modifications introduced by Markwell *et al.* (1978) was used to determine protein in *Anabaena* cultures for calculation of growth rates (see 2.8.2), for protein quantification in BATCH analysis (see 2.6.2) or for quantification of membrane fractions. 200-µL samples were supplemented with 50 µL of 0.5 N NaOH and 750 µL of solution C (a 100:1 mixture of Solution A and Solution B; Solution A contained 2% [w/v] Na_2CO_3, 0.4% [w/v] NaOH, 0.16% [w/v] potassium sodium tartrate and 1% [w/v] SDS; Solution B contained 4% [w/v] $CuSO_4 \cdot 5H_2O$). Samples were shaken with a vortex and incubated at 37°C for 5 min. After that, 75 µL of Folin-Ciocalteus reagent diluted 1:1 (v/v) in water were added, samples were shaken again in a vortex and then incubated at 37°C for 5 min. Finally, the absorbance at 750 nm was measured. Samples containing different amounts of BSA were used as standards.

2.5.3.3 SDS-PAGE

The procedure of Laemmli (1970) was followed as described in Sambrook & Russell (2001) in order to separate proteins by electrophoresis in polyacrylamide gels. *Miniprotean3 Cell* (BioRad) system was used. The running gel was prepared with acrylamide:bisacrylamide (29:1) at 10 or 12% in 375 mM Tris-HCl (pH 8.8). The stacking gel was prepared at 4% acrylamide:bisacrylamide (29:1) in 125 mM Tris-HCl (pH 6.8). 0.1% (w/v) SDS was added to gels in order to facilitate protein denaturalization. 0.05% APS (Ammonium persulfate) and 0.1% TEMED were added just before protein casting to start acrylamide polymerization.

One volume of sample buffer 2x, containing 125 mM TrisHCl (pH 6.8), 20% (v/v) glycerol, 4% (w/v) SDS, 10% (v/v) 2-mercaptoethanol and 0.0025% (w/v) bromophenol blue, was mixed with samples before loading into the gel. Samples were only heated in the case of FtsZ protein analysis.

The electrophoresis buffer was prepared with 25 mM Trizma base, 192 mM glycine and 0.1% SDS (pH 8.3). The protein size standard used was *Prestained Ladder* (gTPbio).

2.5.3.4. Blue Native-PAGE

Anabaena membranes containing 200 μg of total protein were collected by centrifugation at 16,100 *x g* for 20 min. Then, 10 μL of resuspension buffer (25 mM BisTris [pH 7.0], 20% glycerol, 500 mM $MgCl_2$, 5 mg mL^{-1} Pefabloc) were added to the pellet. The tubes were dragged across the holes of a tube rack to disrupt the solution in order to resuspend the membranes. They then were incubated on ice for 10 min. After that, 10 μL of resuspension buffer supplemented with β-dodecylmaltoside (DDM) in order to get 1% (w/v) as a final concentration was added. Samples were incubated in ice for 10 min. Preparations were then centrifuged at 16,100 *x g* for 20 min and the supernatant, containing the solubilized membranes (about 10 $\mu g \cdot \mu L^{-1}$ final concentration), was transferred to a new tube. 5 μL of 4x BN Sample Buffer (100 mM Bis-Tris, 500 mM ε-amino-n-caproic acid, 37.5% sucrose and 50 mg ml^{-1} Serva G Blue) were added to the samples, which were then subjected to native electrophoresis.

Native Gels were prepared according Schamel (2008), with some modifications. Recipes for acrylamide gels are detailed in Table 2.7. The composition of stock solutions was the following: 3x Gel Buffer BN (150 mM Bis-Tris, 1.5 M 6-aminohexanoic acid), 75% (w/v) glycerol, Acrylamide solution (48% (w/v) acrylamide and 1.5% bisacrylamide), TEMED and 10% (w/v) APS (ammonium persulfate). Heavy (10% [w/v] acrylamide) and Light (4% [w/v] acrylamide) solutions were prepared in order to make a gradient gel. All the solutions were kept in ice during the preparation of the gel in order to avoid precocious polymerization.

Table 2.7. Recipes for making gradient acrylamide gels

Stock solution	**Light Solution (4%)**	**Heavy Solution (10%)**	**Stacking Gel (3.5%)**
Double distilled water	1077.4 μL	420 μL	121 μL
3x Gel Buffer BN	700 μL	700 μL	500 μL
75% (w/v) glycerol	140 μL	560 μL	-
Acrylamide solution (48% AA, 1.5% BIS)	169.6 μL	407 μL	121 μL
TEMED	11 μL	11 μL	16 μL
10% (w/v) APS	2 μL	2 μL	3 μL

For running BN-gels, a cathode buffer, containing 15 mM BisTris (pH 7.0), 50 mM Tricine and 0.005% (w/v) Coomasie Blue G250, and an anode buffer, containing (50 mM BisTris [pH 7.0]) were used. The gel was run using a PowerPac Power Supply (BioRad) device and the following protocol: 50 V (30 min), 75 V (30 min), 100 V (60 min), 125 V (30 min), 150 V (60 min), 175 V (60 min) and 200 V (60-90 min). After 1.5-h running, the blue cathode buffer was replaced by a clear cathode buffer (the same composition as cathode buffer but without Coomasie blue).

2.5.3.5. Staining of polyacrylamide gels

For Coomasie blue staining, SDS-PAGE gels were incubated for 1 h in a solution containing 0.25% (w/v) Coomasie blue R-250, 10% (v/v) acetic acid and 45 % (v/v) methanol. After staining, excess of die was eliminated incubating the gel in a destaining solution containing 10% (v/v) acetic acid and 45 % (v/v) methanol for 4 h.

For silver staining, the *Silver Staining kit* (GE Healthcare) was used. Gels were fixed using Fixation Solution (40% [v/v] ethanol and 10% [v/v] acetic acid) for 30 min and then they were incubated in Sensibilization Solution (30% [v/v] ethanol, 0.2% [w/v] sodium thiosulfate and 6.8% [w/v] sodium acetate) for 30 min. After three 5-min washes with Milli-Q water, gels were incubated in 0.25% (w/v) silver nitrate for 20 min and washed quickly twice with water. Developing reaction was then carried out by incubating the gels in Develop solution (2.5% [w/v] sodium carbonate and 0.0296% [v/v] formaldehyde) until bands of interest appeared. Gels were then transferred quickly to Stop Solution, containing 1.46% (w/v) Na_2-EDTA.

2.5.3.6. Size-exclusion chromatography

The His-tagged coiled-coil domain of SepJ was purified as described in section 2.5.1.2. 500 µl of purified protein at 1 mg mL^{-1} were dialyzed against 50 mM Tris-HCl pH 8.0 and 200 mM NaCl. 100 µL of the protein was then passed through a 0.45-µm pore-size filter and loaded into a Superdex 200 10/300 column (GE Healthcare) using a FPLC (Fast Protein Liquid Chromatography) device at constant flow (0.4 mL min^{-1}). Eluted fractions were collected in 400-µL samples and subjected to SDS-PAGE. The presence of the coiled-coil domain in the different fractions was detected by western blot using an anti-His-HRP-conjugated antibody (Qiagen) (see 2.5.3.7.). For size estimation, the same procedure was carried out using a mixture of known-size proteins including thyroglobulin (670 kDa), gamma globulin (158 kDa), albumin (67 kDa), ovalbumin (43 kDa), chymotrypsinogen A (25 kDa), myoglobin (17 kDa), ribonuclease A (13.5 kDa) and vitamin B12 (1.35 kDa). To ascertain which fraction corresponded to each protein, eluted fractions were loaded into a polyacrylamide gel, subjected to SDS-PAGE and stained using Coomassie blue. The retention time was plotted versus the known size of the standards, and the slope was used to calculate the molecular size of fractions containing the SepJ coiled-coil domain.

2.5.3.7. Transference of proteins to PVDF membranes and Western Blot analysis

Proteins were transferred from polyacrylamide gels to *PVDF Hybond-P* 0.45-µm pore-size membranes (GE Healthcare) with *ECL Semi-dry* blotters TE 77 and TE 70 PWR (GE Healthcare) systems. Current was calculated using the formula: $I=S \cdot t$; where I is the current in mA, S is the surface of the gel in cm^2 and t is the thickness of the gel in mm. Transference buffer contained 478 mM Trizma base (pH 8.0), 0.03% (w/v) SDS, 39 mM glycine and 5% (v/v) methanol. Native gels were previously incubated in transference buffer for 30 min.

For Western blot analysis, the membranes were incubated in blocking buffer (5% (w/v) semi-skimmed milk powder in TBS buffer [15 mM Tris-HCl (pH 7.5), 200 mM NaCl] at 30°C for 1 h or at 4°C overnight. The PVDF membranes were then incubated at 30°C for at least 90 min or at 4°C overnight with a primary antibody diluted in blocking buffer (1:2,000 for anti-GFP [A6455 from Invitrogen]; 1:1,000 for anti-FtsZ serum; 1:500 for anti-SepJCC; 1:5,000 for anti-His HRP-conjugated [Qiagen]). The membranes were then washed 3 times for 5 min with TBS-T buffer (TBS buffer containing 0.05% [v/v] Tween-20) and incubated with a secondary antibody (Anti-Rabbit IgG [whole molecule]-Peroxidase antibody produced in goat [Sigma]) diluted 1:10,000 in blocking buffer. The membrane was washed twice with TBS-T for 5 min and once with TBS buffer. Detection was carried out using *WesternBright ECL* (Advansta) and exposure to *Hyperfilm* (GE Healthcare).

2.6. PROTEIN INTERACTION PROCEDURES

2.6.1. Co-purification of SepJ and FtsQ from *E.coli*

For co-purification assays we co-expressed SepJ-GFP and His_6-FtsQ in the same BL21 *E. coli* strain (Table 2.1). Protein expression was induced as described in section 2.5.6. Then, cells were resuspended in 10 mL of PBS buffer containing protease inhibitors and disrupted by passage twice through a French pressure cell at 20,000 psi. After centrifugation at 15,000 x *g* for 10 min, total protein extract, which was obtained as the supernatant, was incubated with *µMACS Anti-GFP MicroBeads* (Miltenyi Biotec) at 4°C for 1 h. The mixture was then loaded into a *MACS* column (Miltenyi Biotec), and the column was washed with 3 mL of PBS buffer. 100 µL of elution buffer (50 mM Tris-HCl [pH 6.8], 50 mM DTT, 1% SDS, 1 mM EDTA, 0.0005% bromophenol blue and 10% glycerol) were used in order to release proteins from the column. The presence of SepJ and FtsQ in the elutions was analyzed by SDS-PAGE and western blot (see 2.5.3.7).

2.6.2. Bacterial two-hybrid assay (BACTH)

Bacterial Adenylate Cyclase Two-Hybrid Assay (BACTH) has been described by Karimova *et al*. (1998). *E. coli* strain BTH101 was co-transformed by electroporation with two plasmids, one of them derived from pKT25 and the other one derived from pUT18 (Tables 2.4 and 2.5). Cells were spread atop an LB plate containing Ap, Km, Sm and 2% (w/v) glucose. After incubation at 30°C overnight, four different clones from different plasmid combinations were transferred to a new plate containing 0.5 mM IPTG, 40 $\mu g \cdot mL^{-1}$ 5-bromo-4-chloro-3-indolyl-β-D-galactopyranoside (X-gal) and antibiotics. As negative

control a replica of this plate containing glucose and antibiotics (LB Ap/Km/Sm/gluc) was prepared.

For quantification of β-galactosidase activity, bacteria carrying a pair of plasmids were grown in 3-mL LB medium in the presence of 0.5 mM IPTG and antibiotics at 30°C overnight. 0.5 mL of overnight cultures were added to 2 mL of buffer Z (60 mM Na_2HPO_4, 40 mM NaH_2PO_4, 10 mM KCl and 1 mM $MgSO_4$). Then, to permeabilize the cells, they were supplemented with 30 µL of toluene and 35 µL of 0.1% SDS, vortexed for 10 s and incubated with shaking at 37°C for 45 min for evaporation of toluene.

For the enzymatic reaction, 875 µL of permeabilized cells were added to 2.5 mL of buffer Z containing β-mercaptoethanol (25 mM final concentration). The tubes were incubated at 30°C in a water bath for at least 5 min. The reaction started by addition of 875 µL of 0.4 mg·mL^{-1} *o*-nitrophenol-β-galactoside diluted in buffer Z. 1-mL samples were taken at 0, 1, 3 and 5 min, and added to 0.5 mL of 1 M Na_2CO_3 in order to stop the reaction. Absorbance at 420 nm was measured. The amount of o-nitrophenol (ONP) produced was calculated from $Abs_{420\ nm}$ using an extinction coefficient ε= 4.5 mM^{-1} cm^{-1}.

2.6.3. Peptidoglycan binding

2.6.3.1. Peptidoglycan isolation

Murein sacculi (peptidoglycan, PG) was isolated by a protocol modified from that of de Pedro *et al.* (1997). Cells grown in 2 L of BG11C medium (bubbled cultures) were collected by filtration and resuspended in 15 mL of PBS buffer (5.5 mM Na_2HPO_4, 1.8 mM KH_2PO_4, 140 mM NaCl, 2.7 mM KCl [pH 7.4]). The cell suspension was concentrated to 50 µg Chl mL^{-1} and 3 mL (corresponding to 150 µg Chl) were used to isolate PG. Filaments were fragmented by sonication in a bath in order to obtain a homogenous cellular suspension (single cells or 2 to 3-cells long filaments). Then, cells were harvested by centrifugation at 3,000 *x g* for 10 min and resuspended in 1 mL of PBS buffer. Drops of the cell suspension were slowly added to 10 mL of boiling 6% (w/v) SDS solution. The suspension was boiled under strong stirring for 1 h. After that, samples were incubated at 37°C overnight (gently stirred). Then, samples were boiled for 1 h and the PG was sedimented by centrifugation at 320,000 *x g*, 25°C, for 30 min in a *Beckman XL-80* ultracentrifuge using 80Ti rotor. The pellet was resuspended in 3 mL of 3% (w/v) SDS and then boiled for 2 h. PG was sedimented again by centrifugation (320,000 *x g*, 25ºC, 30 min). The pellet was resuspended in 2 mL of 0.05% (w/v) SDS and boiled for 2 h. After sedimentation, the pellet was resuspended in 1.5 mL of 50 mM sodium phosphate buffer (pH 6.8) containing 50 µg (corresponding to 2 U) of α-chymotrypsin (from bovine pancreas, Sigma). The suspension was incubated at 37°C overnight.

After adding 0.5 mL of water and 0.75 mL of 6% SDS, the samples were boiled for 2 h and then sedimented by centrifugation as above. The pellet was washed three times using double distilled water in order to remove SDS (after resuspending the pellet, PG was collected by centrifugation at 320,000 *x g* for 15 min at 25°C). Finally, the pellet was resuspended in 120 µL of water.

2.6.3.2. Peptidoglycan binding assay

SepJ-His_{10} and SepJCC-His_6 were purified as described earlier (2.6.3.1). Bovine serum albumin (BSA) and horseradish peroxidase (HRP) were used as negative controls. A volume of protein preparation to give 5 μM final concentration of protein (1% DDM) and 30 μL of OD_{600} 0.83 peptidoglycan solution were mixed in a final volume of 50 μL. The mixture was incubated at room temperature for 1 h with gentle shaking. After that, the mixture was centrifuged (135,000 *x g,* 30 min, 4°C). The pellet, containing peptidoglycan and the putative interacting proteins, was washed with 50 μL of PBS buffer (containing 1% DDM), collected again by centrifugation as above and resuspended in 50 μL of the same buffer. All the fractions were analyzed by SDS-PAGE, and the protein was quantified by the Lowry procedure.

2.7. MICROSCOPY

2.7.1. Light microscopy

An Olympus BX60 microscope (using an UplanFI 40x/0.75Ph2 objective or an UplanFI 100x/1.30 oil objective) was used to visualize *Anabaena* filaments.

2.7.2. Immunofluorescence

Cells from 1.5 ml of liquid cultures were collected by centrifugation, placed atop a poly-L-lysine pre-coated microscope slide (Sigma) and covered with a 45-μm pore-size Millipore filter. Afterwards, the filter was removed and the slide was let to dry at room temperature and, then, immersed in 70% ethanol at -20°C for 30 min and dried 15 min at room temperature. The cells were washed twice by covering the slide with PBS-T containing 5.5 mM Na_2HPO_4, 1.8 mM KH_2PO_4, 140 mM NaCl, 2.7 mM KCl (pH 7.4) and 0.05% (v/v) Tween-20 (2 min each time, room temperature). Subsequently, the slides were treated with blocking buffer (5% milk powder in PBS-T) for 15 min. Cells on the slides were then incubated with a primary antibody (anti-SepJ-CC diluted in blocking buffer 1:250, or anti-FtsZ serum, diluted 1:100) for 90 min, washed three times with PBS-T, incubated 45 min in the dark with secondary anti-rabbit antibody conjugated to fluorescein isothiocyanate (FITC) (Sigma, 1:500 dilution in PBS-T) and washed three times with PBS-T. After dried, several drops of FluorSave (Calbiochem) were added atop the slide, which was then covered with a coverslip and sealed with nail lacque. Fluorescence was monitored using a FITC L5 filter (excitation, band-pass (BP) 480/40 filter; emission, BP 527/30 filter) and imaged with a Leica DM6000B fluorescence microscope and an ORCA-ER camera (Hamamatsu). Images were analyzed using the ImageJ software (http://imagej.nih.gov/ij).

2.7.3. Confocal microscopy, calcein labelling and FRAP experiments

For calcein staining, filaments grown in BG11 medium were collected and grown overnight at 1 µg Chl mL^{-1} under standard growth conditions. After that, 20 µL of a 1 mg mL^{-1} calcein-AM solution were added to 1 mL of culture. After incubation for 90 min at 30° in darkness, filaments were harvested and washed with BG11 medium twice. The filament suspension was then spotted onto BG11 solid medium and placed in a custom-built temperature-controlled sample holder with a glass coverslip on top. Cells were imaged using an immersion objective HCX PLAM-APO 63x 1.4 NA in a Leica TCS SP2 microscope. A 488-nm line argon laser was used as the excitation source. Fluorescent emission was monitored by collection across a window of 500-520 nm using a 50-µm pinhole. After an initial image was recorded, the bleach was carried out by switching the microscope to X-scanning mode, increasing the laser intensity by a factor of 10 and scanning a line across one cell for 1-2 seconds. The laser intensity was then reduced, the microscope was switched back to XY-imaging mode and a sequence of images was recorded at 1 s intervals.

FRAP data analysis was carried out by creating stacks of images and quantifying fluorescence density for the specific cell that had been bleached using the program *ImageJ*. The obtained data were used in order to calculate the recovery rate constant *R* from the formula $C_B = C_0 + C_R (1 - e^{-2Rt})$, where C_B is fluorescence in the bleached cell, C_0 is fluorescence immediately after the bleach and tending towards $(C_0 + C_R)$ after fluorescence recovery, t is time, and *R* is the recovery rate constant due to transfer of the marker from one neighbor cell (Merino-Puerto *et al.*, 2011b).

2.7.4. Visualization of murein sacculi by transmission electron microscopy

The sacculi from filaments grown in BG11 medium were isolated as described in section 2.6.3.1. The purified sacculi were deposited on formvar/carbon film-coated copper grids and stained with 1% (w/v) uranyl acetate. After that, samples were examined with a ZEISS LIBRA 120 PLUS electron microscope at 120 kV.

2.8. PHYSIOLOGICAL PARAMETERS MEASURED IN *Anabaena*

2.8.1. Quantification of chlorophyll *a*

A method derived from that described by Mackinney (1941) was used to determine chlorophyll *a* (Chl) concentration. Cells from 1 mL of liquid culture were collected by centrifugation and resuspended in 100 µL of medium. This cellular suspension was mixed with 900 µL of methanol, shaken in a vortex for 1 min and sedimented by centrifugation for 1 min. The absorbance of the supernatant was then measured at 665 nm (ε= 74.46 mL mg^{-1} cm^{-1}).

2.8.2. Determination of growth rate constants

Cells from 50-mL liquid cultures were collected by centrifugation and washed 3 times with $BG11_0$ medium. After determination of Chl, cells corresponding to 0.2 µg Chl·mL^{-1} were inoculated in flasks containing 25 mL of $BG11_0$, $BG11_0$+NH_4^+ or BG11 medium without antibiotics. 200-µL samples were taken twice a day for 5 days after homogenizing the culture with a 1000-µL micropipette tip and stored at -20°C. The concentration of protein in the samples was measured by the Lowry method (2.5.3.2). The growth rate constant (µ) was calculated as $\mu=\ln 2/t_d$ where t_d is the duplication time.

2.8.3. Growth tests in solid medium

Cells grown in liquid BG11 medium were collected, washed 3 times with $BG11_0$ medium and, after Chl determination, cell suspensions were diluted to 1, 0.5, 0.25, 0.125 and 0.0625 µg Chl mL^{-1}. Ten µL of each suspension were spotted on plates containing $BG11_0$, $BG11_0$+NH_4^+ or BG11 without antibiotics. Spots (containing initially 10, 5, 2.5, 1.25 and 0.625 ng Chl) were incubated under standard growth conditions for up to 14 days.

2.8.4. Nitrogenase activity

Determination of nitrogenase activity was carried out by a method based on that described by Stewart *et al*. (1967). 50 mL of $BG11_0$ medium were inoculated with cells from BG11 medium corresponding to 1 µg Chl mL^{-1}. After incubation for 48 h at standard growth conditions, cells were collected by centrifugation. 2-mL cell suspensions were prepared at a final concentration of 10 µg Chl mL^{-1} in small flasks. Rubber flask caps were placed in order to block air exchange. After incubating cultures for 1 h, 2 mL of acetylene were injected into the flasks using a syringe with a needle. 1-mL gas samples were taken every 30 min for 3 h, and the ethylene produced was determined by gas chromatography. After the assay, the concentration of Chl was determined to express nitrogenase activity as nmol ethylene (µg Chl)$^{-1}$ h^{-1}.

2.8.5. Filament length, cell morphology and heterocyst frequency

Anabaena strains were grown in 50-mL BG11 medium. After 7 days of growth, cells were harvested by centrifugation and washed 3 times with $BG11_0$ medium. 25-mL cultures of the different strains (containing 1 µg Chl mL^{-1}) were prepared in $BG11_0$, $BG11_0$+NH_4^+ and BG11 medium. Cells were visualized under the microscope, photographed with a Leica DFC 300 FX camera associated to the microscope at 24 and 48 h or 5 days (only for experiments with strain CSFR18). In order to distinguish heterocysts, 100 µL of culture were mixed 1:10 with 1% (w/v) Alcian Blue in water. Alcian blue stains bacterial polysaccharides, permitting to visualize the thick envelope polysaccharide layer of heterocysts.

2.8.6. Treatment with berberine

BG11 cultures containing about 1 µg Chl mL^{-1} were incubated in the presence of 0.1-1 mM berberine hemisulfate (Sigma) at 30°C. 1-mL samples were harvested by centrifugation at 24 and 72 h. After washing once with BG11, cells were fixed in poly-L-lysine slides for FtsZ and SepJ immunolocalization as described above (2.7.2).

2.9. *IN SILICO* ANALYSIS OF DNA AND PROTEIN SEQUENCES

2.9.1. Analysis of DNA sequences

The genome of *Anabaena* sp. PCC 7120 (Kaneko *et al*., 2001) is available in the Cyanobase website (http://genome.microbedb.jp/cyanobase) and the Intregrated Microbial Genomes (IMG) page of the Joint Genome Institute (https://img.jgi.doe.gov). Gene sequences were taken from these pages and analyzed using *SerialCloner* software in order to design plasmids. *Lasergene DNASTAR* software was used to design PCR primers and analyze DNA sequencing chromatograms.

2.9.2. Analysis of protein sequences

Protein sequences were taken from the Cyanobase website, the IMG page and NCBI.

3. RESULTS

3.1. SepJ LOCALIZATION AND ITS DEPENDENCE ON THE DIVISOME

3.1. SepJ LOCALIZATION AND ITS DEPENDENCE ON THE DIVISOME

In the filaments of *Anabaena* sp. PCC 7120 (hereafter *Anabaena*), SepJ-GFP fusions localize GFP fluorescence as a focused spot at the intercellular septa between the vegetative cells (Fig. 3.1.A). In cells in the process of division, GFP fluorescence is also observed in what appears to be the site of division. To get further information of SepJ-GFP localization in cells in the process of division, 3d fluorescence microscopy was carried out. For that purpose, Z sections covering an entire cell that had already started division were obtained. Images were subjected to a de-convolution step and three-dimensionally reconstructed (Fig. 3.1.B). SepJ-GFP localized as a ring in the division plane that resembles the localization of proteins involved in cell division such as FtsZ (Sakr *et al*., 2006).

To get a deeper insight on the mechanism of SepJ localization in the septum, conditional mutants of the cell division proteins FtsZ and FtsQ were generated and localization of SepJ was studied.

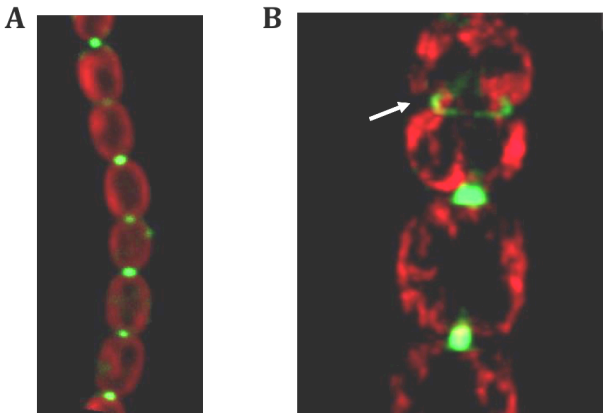

Fig. 3.1. Localization of SepJ-GFP in *Anabaena*. (**A**) SepJ-GFP is located at the intercellular septa as a focused spot. Micrograph from Flores *et al*. (2007). Red fluorescence corresponds to autofluorescence of photosynthetic pigments. (**B**) In dividing cells, SepJ-GFP is located as a ring in the middle of the cells, indicated by a white arrow in the figure. Micrograph by V. Mariscal.

3.1.1. Genomic context of *ftsQ* and *ftsZ* in *Anabaena*

ORF *alr3858* of the *Anabaena* genome is annotated as *ftsZ* and extends from position 4,655,902 to 4,657,188 of the chromosome. Homology searches using the sequence of the *E. coli* FtsQ protein identified the product of ORF *alr3857* (from position 4,653,866 to 4,654,711 in the chromosome) as FtsQ from *Anabaena*. Thus, the *Anabaena ftsQ* and *ftsZ* genes are nearby in the chromosome, separated by a 1,191bp-long intergenic region.

Analysis of this intergenic region in *Anabaena* and other cyanobacteria is shown in Fig. 3.2. Cyanobacteria from taxonomic groups I and III (unicellular and filamentous cyanobacteria) show a shorter intergenic region (with a mean length of 250 bp). This intergenic region is enlarged in heterocyst-forming cyanobacteria, and some of them contain an uncharacterized ORF (Fig. 3.2). In *Anabaena*, this putative ORF is not annotated. However, homology searches using the *Anabaena variabilis* predicted protein identified in the genome of *Anabaena* this ORF, which would encode a 130-residue protein of unknown

function. No known domain could be found in the sequence of this hypothetical protein. According to data in Flaherty *et al*. (2011), *ftsQ* and *ftsZ* do not seem to be co-transcribed in *Anabaena*, and no transcripts are detected in the intergenic region. Although this information questions the presence of the intergenic ORF as an active gene, it cannot be discarded that this hypothetical gene is expressed under some culture conditions.

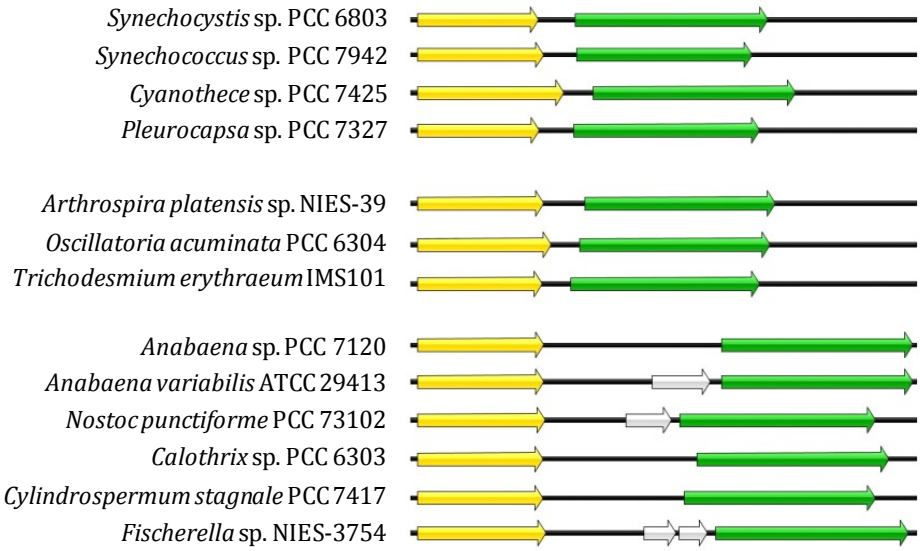

Fig 3.2. Schematic (to scale) of the *ftsQ-ftsZ* gene cluster in some cyanobacteria. The *ftsQ* gene is represented in yellow and *ftsZ* in green. In some of cyanobacteria, an ORF, represented in light grey, is annotated between both genes. *Synechocystis* sp. PCC 6803, *Synechococcus* sp. PCC 7942 and *Cyanothece* sp. PCC 7425 belong to Section I (unicellular cyanobacteria); *Pleuracapsa* sp. PCC 7327 belongs to Section II; *Arthrospira platensis* sp. NIES-39, *Oscillatoria acuminata* PCC 6304 and *Trichodesmium erythraeum* IMS101 belong to Section III (non-heterocyst forming filamentous cyanobacteria); *Anabaena* sp. PCC 7120, *Anabaena variabilis* ATCC 29413, *Nostoc punctiforme* PCC 73102, *Calothrix* sp. PCC 6303 and *Cylindrospermum stagnale* PCC 7417 belong to Section IV; and *Fischerella* sp. NIES-3754 belongs to Section V (branching heterocyst-forming cyanobacteria).

3.1.2. Construction and characterization of a conditional *ftsZ* mutant

Because *ftsZ* is generally an essential gene in bacteria and, to the best of our knowledge, *ftsZ* insertional mutants have never been obtained in *Anabaena*, *ftsZ* appears to be an essential gene. Nonetheless, some studies on FtsZ function in *Anabaena* have been performed impairing FtsZ polymerization (Sakr *et al*., 2006).

In order to generate an *Anabaena* mutant of *ftsZ*, a construct in which a synthetic promoter substituted for the native promoter of the gene was designed. This synthetic promoter, P_{ND}, was based on known features of the Class II NtcA-activated promoters (Herrero et al., 2001) and contained a consensus NtcA-binding site located 23 bp upstream from a -10 promoter box (Fig. 3.3). Thus, expression levels of the genes under this promoter could be controlled using different nitrogen sources. To avoid possible polar effects on the promoter, the C.S3 gene cassette including the well-known Ω cassette, conferring resistance to Sm and Sp and containing transcriptional terminators at both ends, was inserted just upstream of P_{ND} (Fig. 3.3). The C.S3-P_{ND} construct was flanked by sequences corresponding to flanking regions of the *ftsZ* gene.

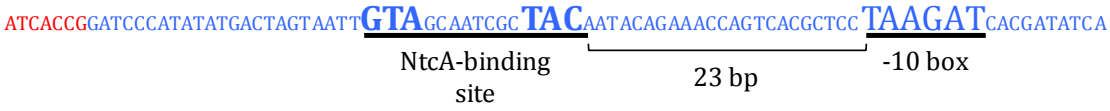

Fig. 3.3. Sequence and elements of the synthetic NtcA-dependent promoter, P_{ND}. The nucleotide sequence of the synthetic NtcA-dependent promoter is shown in blue with the NtcA-binding site and -10 promoter hexamer highlighted. Sequence in red corresponds to the end of C.S3 which includes the Ω cassette that encodes resistance to Sm and Sp and bears transcriptional terminators in both ends (Elhai & Wolk, 1988a).

To create a conditional mutant of *ftsZ* in *Anabaena* following the described strategy, fragments upstream and downstream of the *ftsZ* promoter were obtained by PCR and used to construct a plasmid to be transferred to *Anabaena* for integration into the chromosome by double cross-over events. The procedure is schematized in Fig. 3.4. A fragment upstream of the *ftsZ* promoter was amplified using primers alr3858-3 and alr3858-4 and cloned in vector pMBL-T between ApaI and SalI sites generating pCSFR2. A fragment downstream of the *ftsZ* promoter was amplified using primers alr3858-1 and alr3858-2 and cloned in vector pSpark between SacI and XhoI sites generating pCSFR3. The synthetic promoter was obtained by PCR using overlapping primers Pro-sNtcA-1 and Pro-sNtcA-2 and cloned in vector pMBL-T using SpeI and EcoRV. After getting the three plasmids, the fragments of interest were cloned using the same restriction enzymes as before in pCSFR1, a pMBL-based plasmid that contains the C.S3 cassette cloned into a BamHI site (Fig. 3.4). The resulting plasmid was called pCSFR15. This plasmid was corroborated by sequencing. A PvuII-digested fragment from pCSFR15 was transferred to pRL278, previously digested with XhoI and filled in with the Klenow enzyme, generating plasmid pCSFR18.

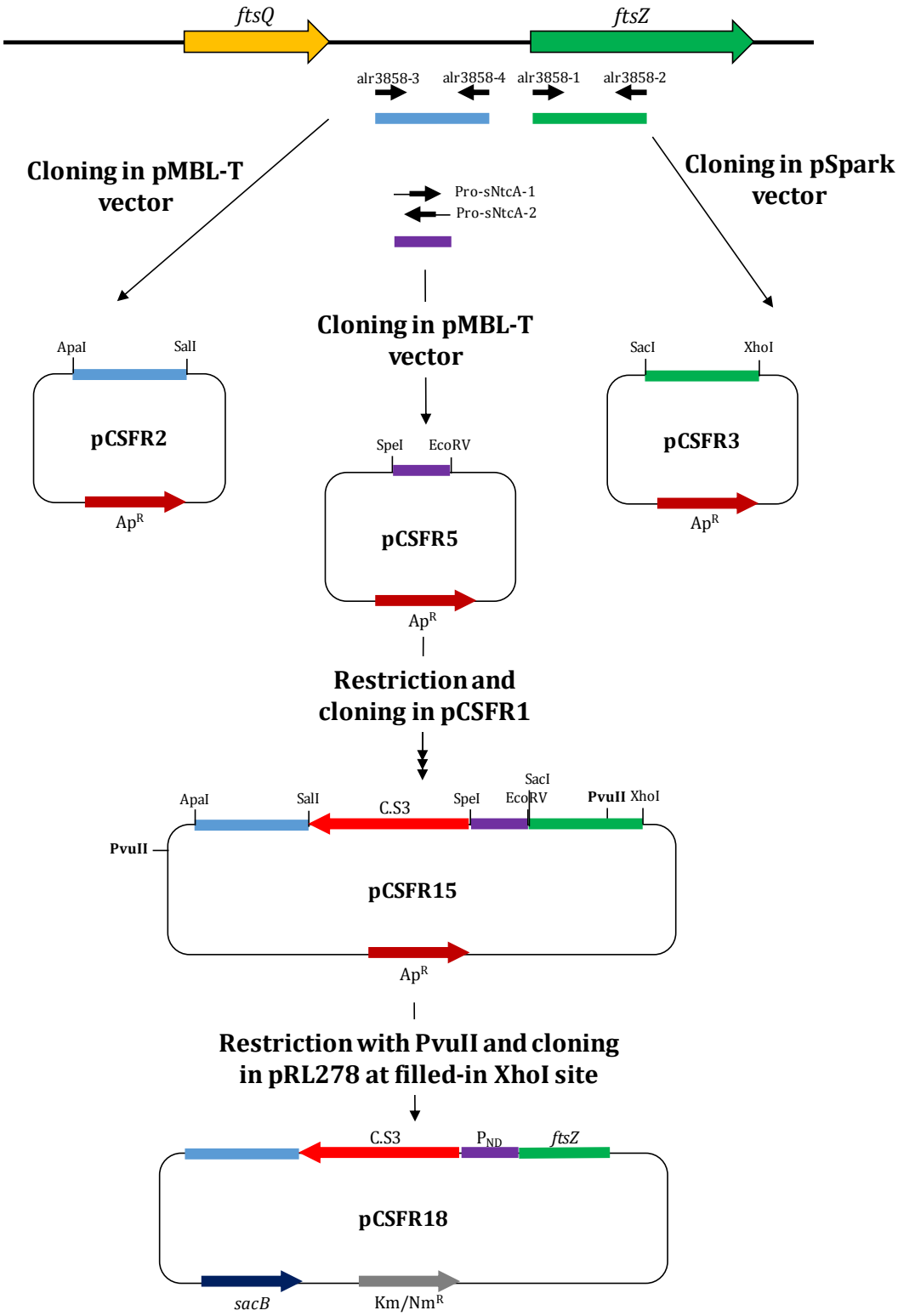

Fig. 3.4. Construction of plasmid pCSFR18. The *ftsQ* gene is represented in yellow and the *ftsZ* gene in green. An amplification product containing the upstream *ftsZ* region is represented in light blue, a product containing the 5' region of *ftsZ* in green, and the synthetic promoter in purple. The gene conferring resistance to ampicillin (Ap^R) is represented in garnet. The C.S3 cassette is represented as a red arrow that also indicates the orientation of the Sm^R/Sp^R gene in the Ω cassette. The *sacB* gene, which confers sensitivity to sucrose, is represented in dark blue, and the gene conferring resistance to kanamycin (Km) for *E. coli* or neomycin (Nm) for *Anabaena* is represented by a grey arrow.

Plasmid pCSFR18 was transferred to *Anabaena* by conjugation, and exconjugants were selected as Sm^R/Sp^R clones as described in section 2.4.2. A clone homozygous for the chromosomes bearing the C.S3-P_{ND}-*ftsZ* construct was selected for further analysis and named strain CSFR18. The genomic structure of the mutant was analyzed by PCR. Segregation was checked in cells from media containing nitrate, ammonia or no source of combined nitrogen. To do this, filaments grown in BG11 medium with antibiotics were harvested, washed and inoculated in BG11, $BG11_0$+NH_4^+ and $BG11_0$ media at 1 µg Chl mL^{-1}. After 48 h of incubation under standard conditions, filaments from each culture were collected and DNA was isolated. The presence of wild-type chromosomes was checked using primers alr3858-3 and alr3858-6, which would produce a 1,112-bp long product. This pair of primers would also generate a PCR product when mutant chromosomes were present, but its length would correspond to 3,200 bp and the efficiency of amplification could not be comparable to that of wild-type chromosomes. Therefore, the presence of mutant chromosomes was checked using primers C.S3-5 and alr3858-6, which would generate a 1,647-bp long product (Fig. 3.5.A). Mutant chromosomes were detected in strain CSFR18 but not in the wild type, in which only unspecific amplification could be seen. On the other hand, wild-type chromosomes could not be detected in strain CSFR18, and the 3,200-bp product could be seen when the alr3858-3/alr3858-6 primer pair was used, corroborating the absence of wild-type chromosomes. (Fig. 3.5.B).

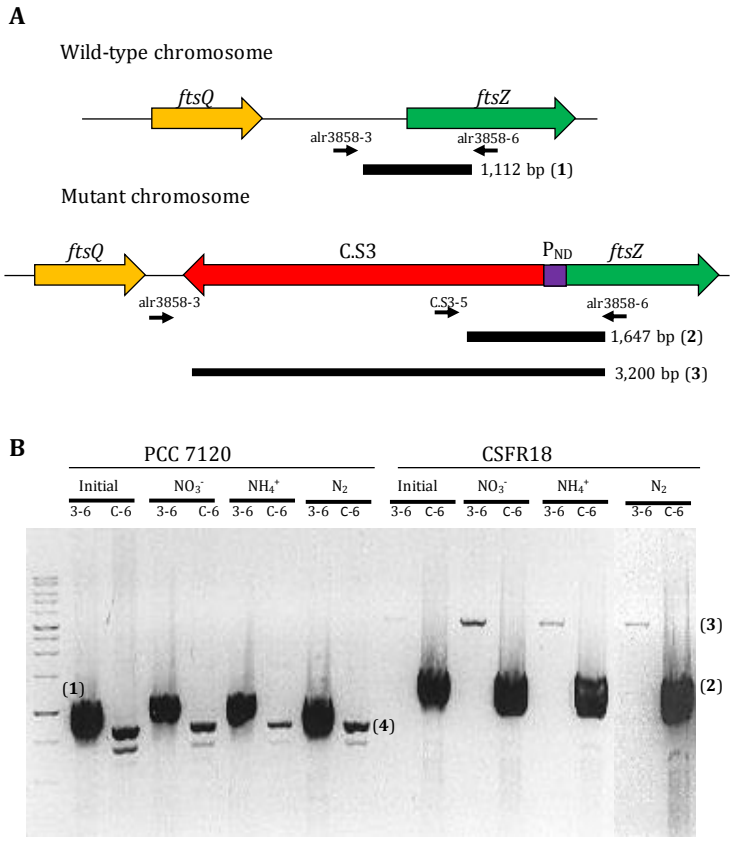

Fig. 3.5. PCR analysis of the genomic structure of strain CSFR18. (**A**) Schematic of the *ftsQ-ftsZ* genomic region in the wild-type and mutant chromosomes, with indication of primers used in the PCR reactions and expected PCR product sizes. (**B**) Products of the PCR reactions performed with the indicated primers ("C" stands for primer C.S3-5; bands identified by numbers in bold as in A) and, as template, DNA from the indicated strain grown in BG11 medium ("initial") or incubated for 48 hours with the indicated nitrogen source. (**4**) is a non-specific amplification product.

Canonical NtcA-dependent promoters drive high gene expression when the cells are incubated in the absence of combined nitrogen and repress expression in the presence of combined nitrogen sources, especially ammonium (Herrero *et al*., 2001). To know whether our synthetic NtcA-type promoter, P_{ND}, drives expression of the *ftsZ* gene with the expected regulation, nitrate-grown filaments of the wild type and strain CSFR18 were washed and incubated for 2 days in media with nitrate or ammonium or without combined nitrogen. RNA samples were isolated from each condition and reverse-transcribed. Levels of the *ftsZ* transcript were quantified by real-time PCR using primers alr3858-9 and alr3858-10. The expression of *alr0599* and *all5167*, which is not affected by nitrogen deprivation (Flaherty *et al*., 2011), was used to normalize the values obtained for *ftsZ*. Primer pairs used for expression of these two genes were alr0599-1/alr0599-2 and all5167-1/all5167-2 respectively. We found that in the wild type, *ftsZ* expression was up-regulated in diazotrophic conditions (almost 2-fold higher compared to ammonium- or nitrate-containing media). Strain CSFR18 showed 23%, 60% and 89% of the wild-type *ftsZ* expression levels in media with ammonium or nitrate or without combined nitrogen, respectively (Fig. 3.6.A, Table 3.1). These results are consistent with the expected activity of the P_{ND} promoter and showed that *ftsZ* expression could be repressed in strain CSFR18 by incubation in the presence of ammonium.

To corroborate that FtsZ levels were regulated by the nitrogen source in strain CSFR18, we studied FtsZ by western blot analysis. Antibodies against *Anabaena* FtsZ were obtained after heterologous expression of a His-tagged protein in *E. coli*. We first amplified the *ftsZ* gene from *Anabaena* DNA using primers alr3858-7 and alr3858-8. The resulting product was cloned in vector pCOLADuet-1 using BamHI and XhoI, producing pCSFR22. After growing overnight in the presence of glucose, cells of *E. coli* BL21 bearing pCSFR22 were collected and grown in LB medium supplemented with IPTG in order to induce the production of the protein. After incubation for 2 h, the soluble fraction was obtained by breaking the cells and centrifugation and loaded into a nickel column, and the retained *Anabaena* FtsZ protein was eluted using imidazole. This purified protein was used to produce antibodies (see *Mat&Meth* section 2.5.1.1).

The levels of FtsZ in *Anabaena* were investigated using the FtsZ antibodies. BG11-grown filaments from the wild type and strain CSFR18 were incubated with different nitrogen sources for 48 h. After harvesting the filaments, total protein was precipitated with cold trichloracetic acid (10%) and resuspended in a Tris-based buffer. Samples containing 60 μg of protein were subjected to SDS-PAGE and western blot analysis using the antibodies. The results obtained are shown in Fig. 3.6.B. Similar levels of the FtsZ protein were detected in the three different conditions for the wild type. The FtsZ levels in strain CSFR18 were higher in diazotrophic than in nitrate-containing cultures, and lowest in ammonium-containing cultures, with the levels in the absence of combined nitrogen being similar in the mutant and the wild type. Although, compared to levels in nitrate-grown filaments, protein levels were relatively lower than transcript levels under diazotrophic conditions for both strains (Table 3.1), the results of western blot analysis are consistent with the regulation observed at the transcriptional level.

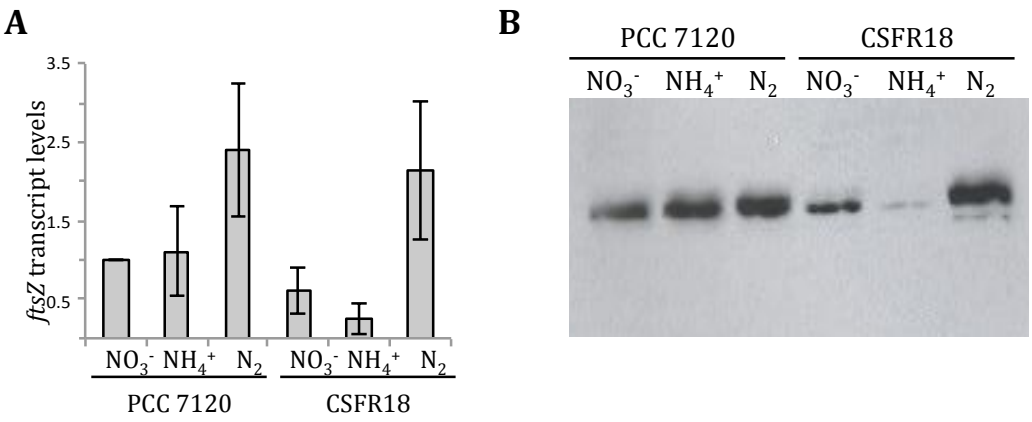

Fig. 3.6. Expression of *ftsZ* in *Anabaena* strains PCC 7120 and CSFR18. (**A**) Levels of the *ftsZ* transcript relative to those in nitrate-grown wild-type cells. RNA was isolated from BG11-grown filaments incubated for 48 hours under culture conditions with the indicated nitrogen source, and RT-qPCR was performed as described in *Mat&Meth* sections 2.2.4 and 2.3.3. (**B**) Levels of the FtsZ protein analyzed by western blot using antibodies against *Anabaena* FtsZ. Total protein was obtained from filaments incubated for 48 h under culture conditions with the indicated nitrogen source, and 60 μg of protein were loaded per lane in the SDS-PAGE gels.

Table 3.1. Expression of *ftsZ* at transcriptional and protein levels. Levels of the *ftsZ* transcript in *Anabaena* (PCC 7120) and strain CSFR18 are presented relative to those in nitrate-grown wild-type cells. Mean ± SD (*n*) of fold change is shown for each strain in each culture condition. Levels of FtsZ protein were determined by quantifying the integrated density of each band observed in western blot and normalizing to that in nitrate-grown wild-type cells.

Strain	Nitrogen source	*ftsZ* transcript levels	FtsZ protein levels
PCC 7120	NO_3^-	1.00 ± 0.00 (6)	1.00
	NH_4^+	1.11 ± 0.58 (6)	1.31
	N_2	2.40 ± 0.85 (6)	1.29
CSFR18	NO_3^-	0.60 ± 0.30 (3)	0.76
	NH_4^+	0.25 ± 0.21 (3)	0.08
	N_2	2.13 ± 0.88 (3)	1.63

Subcellular localization of FtsZ was addressed by immunofluorescence analysis with the *Anabaena* FtsZ antibodies (Fig. 3.7). In the wild type, FtsZ could be seen forming a ring at the middle of vegetative cells, but not in heterocysts. Although a poor labeling was found in ammonium-grown wild-type cells, FtsZ rings could be also seen in these cells. In strain CSFR18, FtsZ rings were clearly labeled in diazotrophic filaments, but this labeling was only detected in vegetative cells, not in heterocysts. In this strain, FtsZ rings could also be seen in filaments incubated with nitrate but they were detected with difficulty. However, no FtsZ rings were observed in the big cells produced after incubation in the presence of ammonium. These results are consistent with the different levels of FtsZ observed by western blot analysis and illustrate that strain CSFR18 showed a regulated expression of *ftsZ* leading to production of low FtsZ cellular levels under well-established culture conditions.

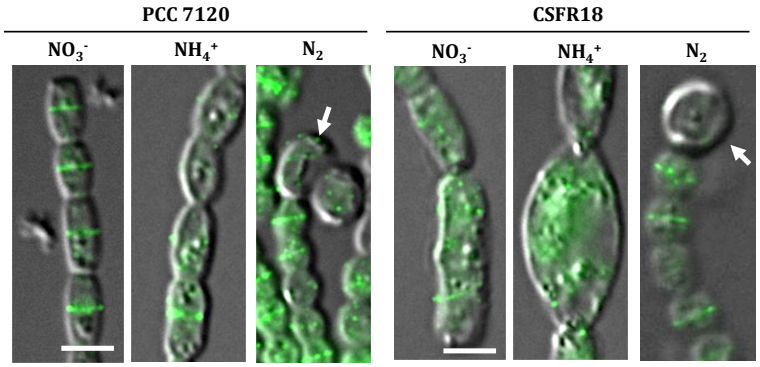

Fig. 3.7. Immunolocalization of FtsZ in *Anabaena* strains PCC 7120 and CSFR18. Filaments from BG11 medium were incubated for 48 h with the indicated nitrogen source. Immunofluorescence analysis using anti-*Anabaena* FtsZ protein antibodies was then carried out as described in *Mat&Meth* section 2.7.2. Merged bright-field and fluorescence images are shown. Arrows point to heterocysts. Size bar, 3 μm.

In order to know whether the growth rate of *Anabaena* is influenced by the cellular levels of FtsZ, we studied growth of strain CSFR18 in comparison to the wild type in solid and liquid media with different nitrogen sources. For the growth test on solid medium, filaments from BG11-grown cultures were collected, washed and spotted at different dilutions on solid media containing nitrate, ammonium or no source of combined nitrogen. Growth of CSFR18 was impaired in the three conditions, but especially in the presence of ammonium (Fig. 3.8). Nitrate was the nitrogen source that allowed less impaired growth. Hence, strain CSFR18 was routinely maintained on solid BG11 medium (which contains nitrate as nitrogen source) supplemented with Sm and Sp at 5 μg mL^{-1} each.

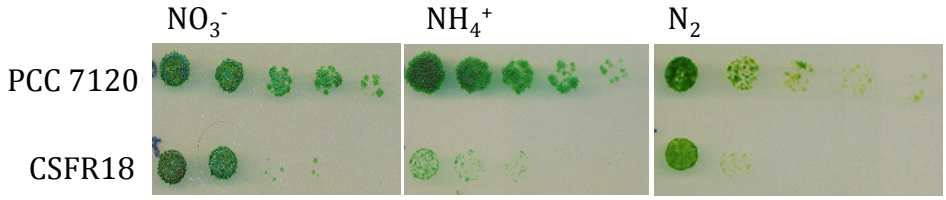

Fig. 3.8. Growth test of strain CSFR18 on solid media. Samples from BG11-grown filaments of strains PCC 7120 and CSFR18 were spotted at different dilutions (spots containing 5, 2.5, 1.25, 0.625 and 0.3125 ng of Chl *a* respectively) on solid media with the indicated nitrogen source, incubated under standard growth conditions and photographed after 7 days.

To test growth in liquid medium, cultures of strain CSFR18 grown in liquid BG11 medium were washed and inoculated in liquid BG11, $BG11_0$+ammonium or $BG11_0$ medium, respectively, at 0.2 μg Chl mL^{-1}. The amount of protein in the cultures was quantified in samples taken every 8 hours during 5 days, and the growth rate constants were calculated (Fig. 3.9, Table 3.2). Although the growth rates were somewhat slower than those of the wild type, exponential growth was not much affected (Fig. 3.9). However, in strain CSFR18, the cells showed an altered morphology under the microscope, mainly in ammonium-containing media but also in nitrate-containing media, in which they were significantly larger than the wild-type cells (Fig. 3.10.A; Table 3.2). Moreover, after 7 days of incubation, the appearance of the cultures was very different. The culture of strain

CSFR18 containing nitrate became yellowish, which is indicative of an altered physiology; the culture with ammonium was lysed since it showed lack of turbidity and blue color due to release of phycobiliproteins; only the diazotrophic culture was similar to the corresponding wild-type culture (Fig. 3.10.B).

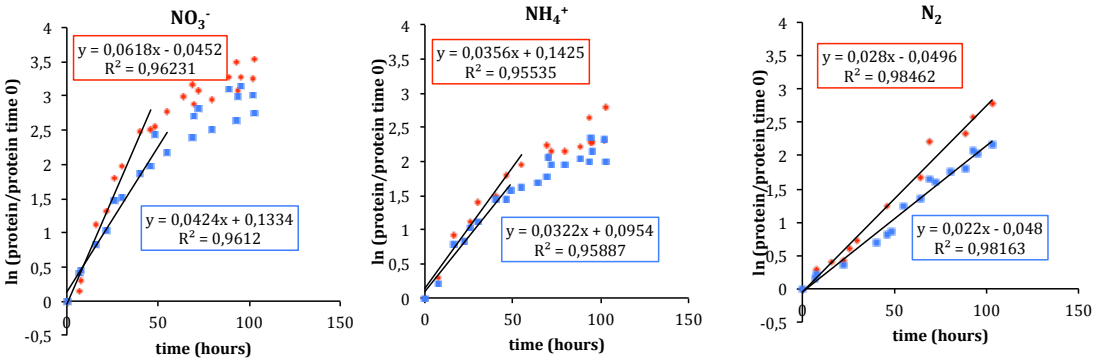

Fig. 3.9. Growth curves of strains PCC 7120 and CSFR18. BG11-grown filaments were incubated with the indicated nitrogen source, the protein concentration was measured in samples from the cultures, and the growth rate constants were determined (see Table 3.2). Strain PCC 7120 is represented by red diamonds, and strain CSFR18 by blue squares.

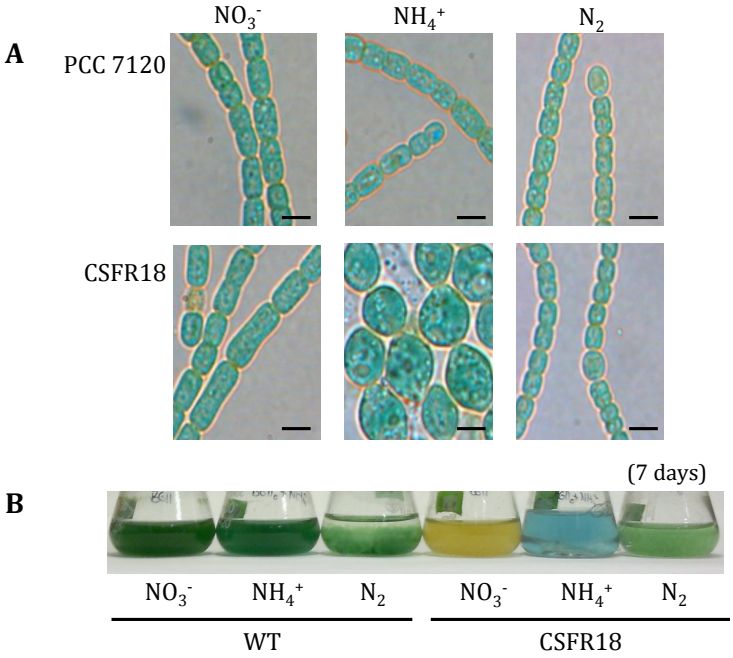

Fig. 3.10. Phenotype of strain CSFR18 in liquid medium. (**A**) After 5 days of growth in medium containing the indicated nitrogen source, filaments were visualized by light microscopy. The area of the cells was determined in the different liquid cultures (see Table 3.2 for more details). Size bars, 3 µm. (**B**) Photographs of cultures after 7 days of growth in media with the indicated nitrogen source.

Table 3.2. Growth rates of strains PCC 7120 and CSFR18 in liquid medium containing the indicated nitrogen sources. The area of the cells observed under the microscope is also indicated (mean ± SD; 37 cells measured in each culture) for cultures grown in liquid medium containing the indicated nitrogen source for 5 days. Student's *t* test indicated that the differences between the mutant and the wild type were significant in the cultures containing nitrate ($P < 10^{-11}$) and ammonium ($P < 10^{-12}$).

Strain	Nitrogen source	Growth rate constant, μ (day^{-1})	Cellular area (μm^2)
PCC 7120	NO_3^-	1.48	12.51 ± 0.53
	NH_4^+	0.85	13.36 ± 0.68
	N_2	0.67	12.18 ± 0.33
CSFR18	NO_3^-	1.02	22.90 ± 1.14
	NH_4^+	0.77	45.37 ± 3.61
	N_2	0.53	10.90 ± 0.50

The results obtained in the phenotypic characterization of strain CSFR18 are consistent with NtcA-dependent expression of *ftsZ*. A low level of FtsZ protein was produced in ammonium-containing cultures impairing cell division and disrupting cell morphology.

3.1.3. Construction of conditional *ftsQ* mutants

The *ftsQ* gene from *Anabaena* has not been studied previously but, based on knowledge in other organisms, it is predicted to be also an essential gene. It is a very conserved gene that, as mentioned earlier, is located just upstream of *ftsZ* in the genomes of cyanobacteria. An *ftsQ* conditional mutant was constructed following the same strategy as for strain CSFR18. In this case, plasmid pCSFR15 was used as scaffolding. The fragments encompassing upstream and 5' regions of *ftsZ* were substituted by regions of *alr3857* (*ftsQ*). The 5' region of *ftsQ* was amplified by PCR using primers alr3857-3 and alr3857-4 and *Anabaena* DNA as template. The PCR product was digested with SacI and XhoI and cloned into pCSFR15 digested with the same enzymes, rendering pCSFR34. The upstream region of *ftsQ* was obtained by PCR using primers alr3857-5 and alr3857-6. The PCR product was digested with ApaI and SalI and cloned into pCSFR34 digested with the same enzymes, rendering pCSFR35. This plasmid was then digested with PvuII and the fragment containing the P_{ND}-*ftsQ* fusion was cloned into pRL278 digested with XhoI and filled in with Klenow enzyme. The resulting plasmid was called pCSFR36 (Fig. 3.11).

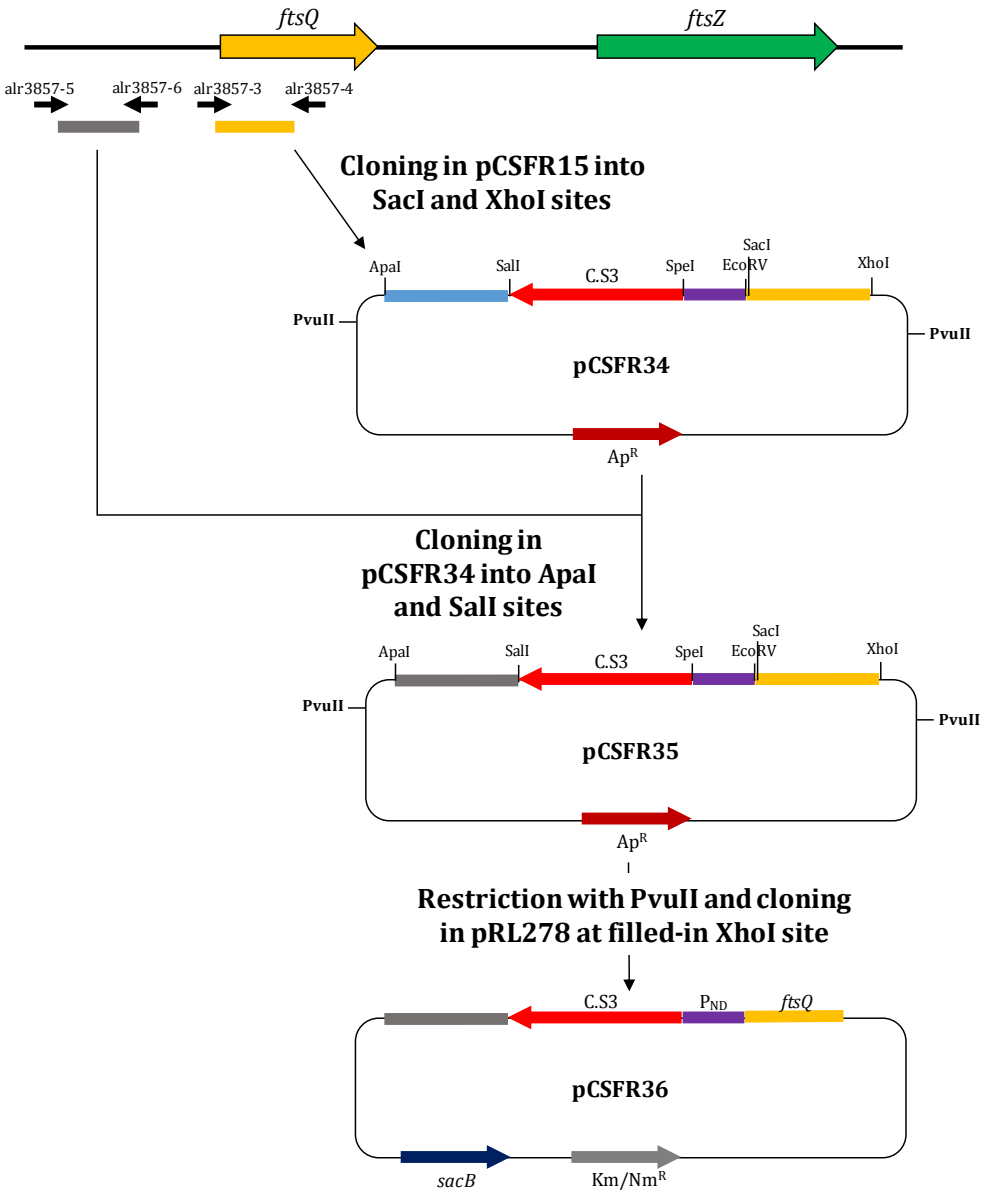

Fig. 3.11. Construction of plasmid pCSFR36. The *ftsQ* gene is represented in yellow and *ftsZ* in green. The amplification product containing the upstream *ftsQ* region is represented in grey, the product containing the 5' region of *ftsQ* in yellow, and the synthetic promoter in purple. The gene conferring resistance to ampicillin (Ap^R) is represented in garnet The C.S3 cassette is represented as a red arrow that also indicates the orientation of the Sm^R/Sp^R gene. The *sacB* gene, which confers sensitivity to sucrose, is represented in dark blue, and the gene conferring resistance to kanamycin (Km) for *E. coli* or neomycin (Nm) for *Anabaena* is represented by a grey arrow. See the text for details.

The pCSFR36 plasmid was transferred to *Anabaena* by conjugation (see *Mat&Meth* section 2.4.2), and the selection of exconjugants and further procedures for obtaining mutants generated by double cross-over was carried out as for CFR18 (see *Mat&Meth* section 2.4.2). The resulting strain, which bears the *ftsQ* gene under the control of the NtcA-type promoter, was named CSFR5. Segregation was checked in different media to ensure that the construct was stable in the genome independently of the culture conditions. Filaments grown in BG11 medium with antibiotics were harvested, washed and inoculated in BG11, $BG11_0$ + NH_4^+ and $BG11_0$ media at 1 µg Chl mL^{-1}. After 48 h of growth under standard conditions, genomic DNA was isolated. The presence of wild-type

chromosomes was checked using primers alr3857-5 and alr3857-4, which generate a 988-bp long product. This pair of primers would generate a PCR product when mutant chromosomes were present, but its length would correspond to 3,134 bp and the efficiency of amplification could not be comparable to that of wild-type chromosomes. Hence, the presence of mutant chromosomes was also checked using primers C.S3-5 and alr3857-4, which generate a 1,549-bp long product (Fig. 3.12.A). Mutant chromosomes were detected in strain CSFR5 but not in the wild type. On the other hand, wild-type chromosomes could not be detected in strain CSFR5, but neither the 3,134-bp fragment probably due to a low efficiency of amplification of a large PCR product. However, a product could be seen using C.S3-5/alr3857-4 primers corroborating the presence of only mutant chromosomes (Fig. 3.12.B).

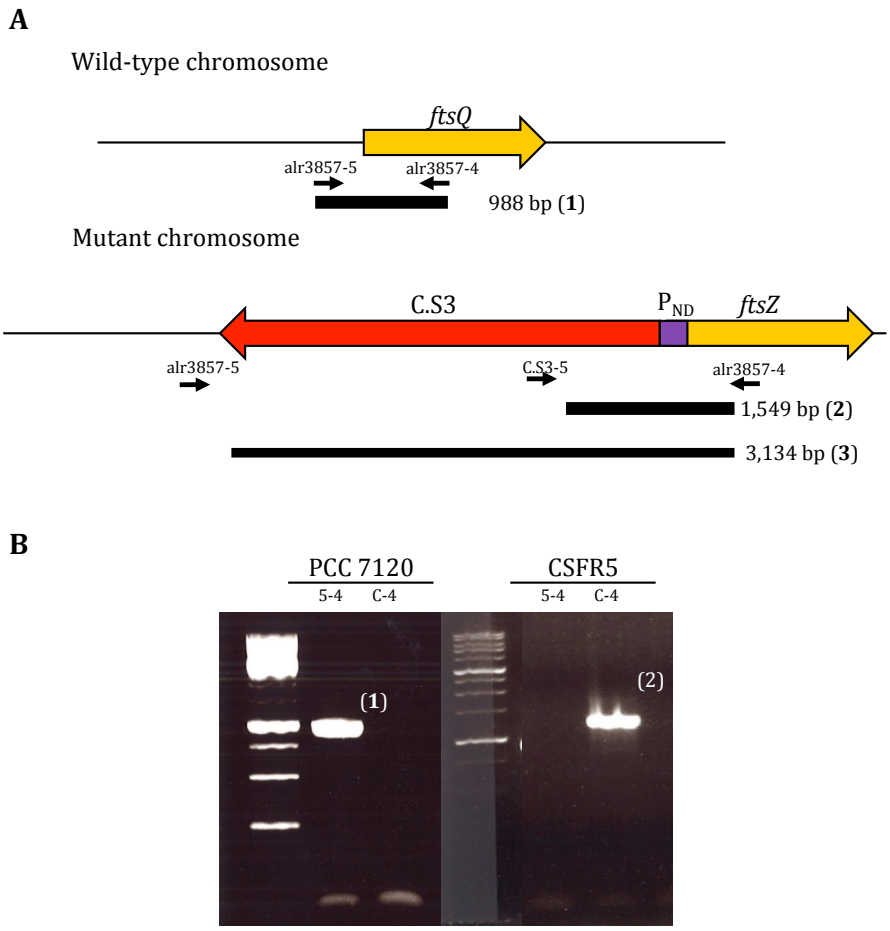

Fig. 3.12. PCR analysis of the genomic structure of strain CSFR5. (**A**) Schematic of the *ftsQ* genomic region in the wild-type and mutant chromosomes, with indication of primers used in the PCR reactions and expected PCR product sizes. (**B**) Products of the PCR reactions performed with the indicated primers ("C" stands for primer C.S3-5; bands identified by numbers in bold as in A) and, as template, DNA from the indicated strain grown in BG11 medium. (**3**) is a specific amplification product that could be predicted to appear when mutant chromosomes are present but it could not be detected in PCR reaction probably due to a low efficiency of amplification.

The expression pattern of *ftsQ* in strain CSFR5 was studied in comparison to that in the wild type. Nitrate-grown filaments of the wild type and strain CSFR5 were washed and incubated for 2 days in media with nitrate or ammonium or without combined nitrogen.

RNA samples were isolated from each condition and retro-transcribed. Levels of *ftsQ* were quantified by real-time PCR using primers alr3857-1 and alr3857-2. The expression of *alr0599* and *all5167*, which is not affected by nitrogen deprivation (Flaherty *et al*., 2011), was used to normalize the values obtained for *ftsQ* (Fig. 3.13.A). The expression of *ftsQ* in the wild type showed a limited change depending on the nitrogen source. In strain CSFR5, *ftsQ* was found repressed in media containing nitrate and over-expressed in the absence of combined nitrogen. Compared to the wild type, strain CSFR5 showed 65 % of *ftsQ* expression in media containing nitrate, but expression was increased almost 2-fold and 3-fold in media containing ammonium or no source of combined nitrogen, respectively. However, none of these changes were statistically significant. In order to know whether altered expression of *ftsQ* affects the expression of downstream genes, *ftsZ* expression was analyzed in strain CSFR5 (Fig. 3.13.B). Expression of *ftsZ* was higher than that in the wild type when the filaments were incubated in the presence of nitrate or in the absence of combined nitrogen. This observation might indicate that *ftsZ* expression in strain CSFR5 was influenced by transcription from P_{ND}, although no NtcA-dependent regulation was evident for *ftsQ*. As described above, there is no evidence for co-transcription of *ftsQ* and *ftsZ* in the wild type, but insertion of a regulated promoter upstream of *ftsQ* could affect expression of both genes.

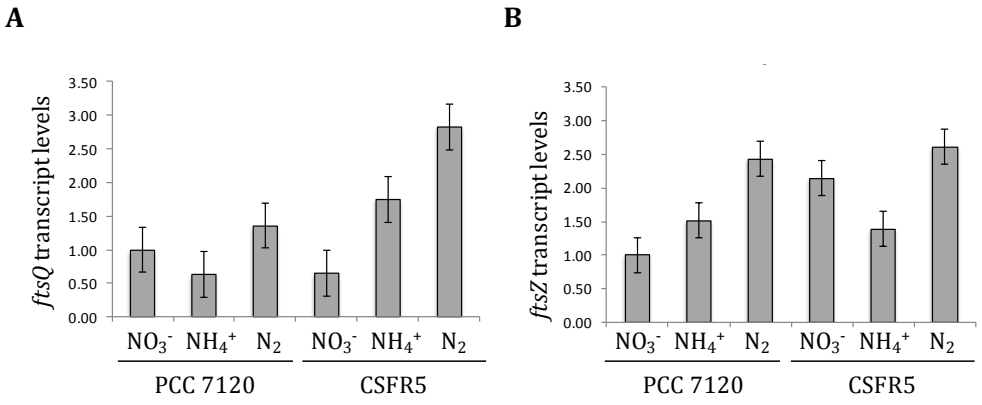

Fig. 3.13. Expression of *ftsQ* and *ftsZ* in *Anabaena* strains PCC 7120 and CSFR5. (**A**) Levels of the *ftsQ* transcript in strains CSFR5 and PCC 7120, relative to those in nitrate-grown PCC 7120 (wild-type) cells. RNA was isolated from BG11-grown filaments incubated for 48 h under culture conditions with the indicated nitrogen source. After that, RT-qPCR was performed. (**B**) Levels of the *ftsZ* transcript relative to those in nitrate-grown PCC 7120 cells.

Despite the fact that in strain CSFR15 *ftsQ* was not significantly downregulated, we inquired about the effect of its altered expression in *Anabaena*. A growth test in solid medium indicated no deficit in growth of CSFR5 (Fig. 3.14.A). When strain CSFR5 was grown in liquid media with different nitrogen sources, no alterations in growth or in cell morphology were observed (Fig. 3.14.B). In this case the area of the cells after 5 days of incubation in different media was not different to that in the wild type (Table 3.3). Therefore, strain CSFR5 was not further characterized.

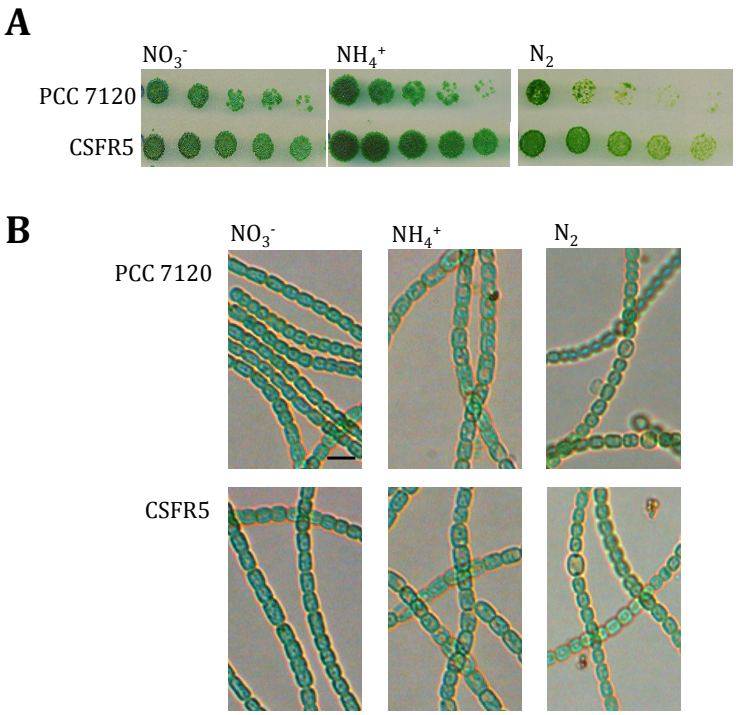

Fig. 3.14. Growth of strain CSFR5 in solid and liquid media. (**A**) Samples from BG11-grown filaments of strains PCC 7120 and CSFR5 were spotted at different dilutions (spots containing 5, 2.5, 1.25, 0.625 and 0.3125 ng of Chl *a* respectively) on solid media with the indicated nitrogen source, incubated under standard growth conditions and photographed after 7 days. (**B**) After 5 days of growth in liquid media with the indicated nitrogen source, filaments were visualized by light microscopy. The area of the cells was determined in the different liquid cultures (see the text for more details). Size bar, 3 µm.

Table 3.3. Area of the cells observed under the microscope in cultures grown in liquid medium containing the indicated nitrogen source for 5 days (mean ± SD; 37 cells measured in each culture). Student's *t* tests indicated that there were no significant differences between the mutant and the wild type under the tested conditions.

Strain	Nitrogen source	Cellular area (µm²)
PCC 710	NO_3^-	9.64 ± 0.39
	NH_4^+	9.83 ± 0.44
	N_2	8.10 ± 0.28
CSFR18	NO_3^-	10.17 ± 0.37
	NH_4^+	12.01 ± 0.45
	N_2	7.72 ± 0.27

3.1.4. Subcellular localization of SepJ

The subcellular localization of SepJ has been previously described using a GFP fusion (Flores *et al*., 2007). Different versions of the protein have been used to determine which domain(s) of SepJ are important for its correct localization and its cell-cell binding and transfer functions (Mariscal *et al*., 2011). Its localization as a ring in dividing cells suggested that SepJ correct localization at the cells poles depends on the division machinery. For this reason, localization of the native SepJ protein was studied in the *ftsZ* conditional mutant described above, strain CSFR18.

In strain CSFR18, the regulated expression of *ftsZ* permitted to establish conditions that resulted in production of low FtsZ cellular levels. Localization of SepJ under those

conditions was studied by immunofluorescence analysis (see *Mat&Meth* section 2.7.2) (Fig. 3.15.). Subcellular localization of native SepJ was tested after 48 h of incubation in the presence of nitrate or ammonium or without combined nitrogen using antibodies raised against the coiled-coil domain of the protein. SepJ was localized at the cell poles in filaments of the wild-type strain under every condition tested. Moreover, SepJ could be seen as a ring in the middle of dividing cells (see N_2-grown cells in Fig. 3.15.).

In strain CSFR18, SepJ could be specifically observed at the cell poles in filaments incubated for 48 h without combined nitrogen (Fig. 3.15.). After incubation in ammonium-containing medium, the SepJ signal could be seen delocalized as disperse spots (likely in the membrane). In filaments incubated with nitrate, the main SepJ signals were detected at the cell poles, but some disperse signals were also seen. These observations indicate that the correct localization of SepJ at the cell poles needs the presence of FtsZ in the cells at normal, or close to normal, levels.

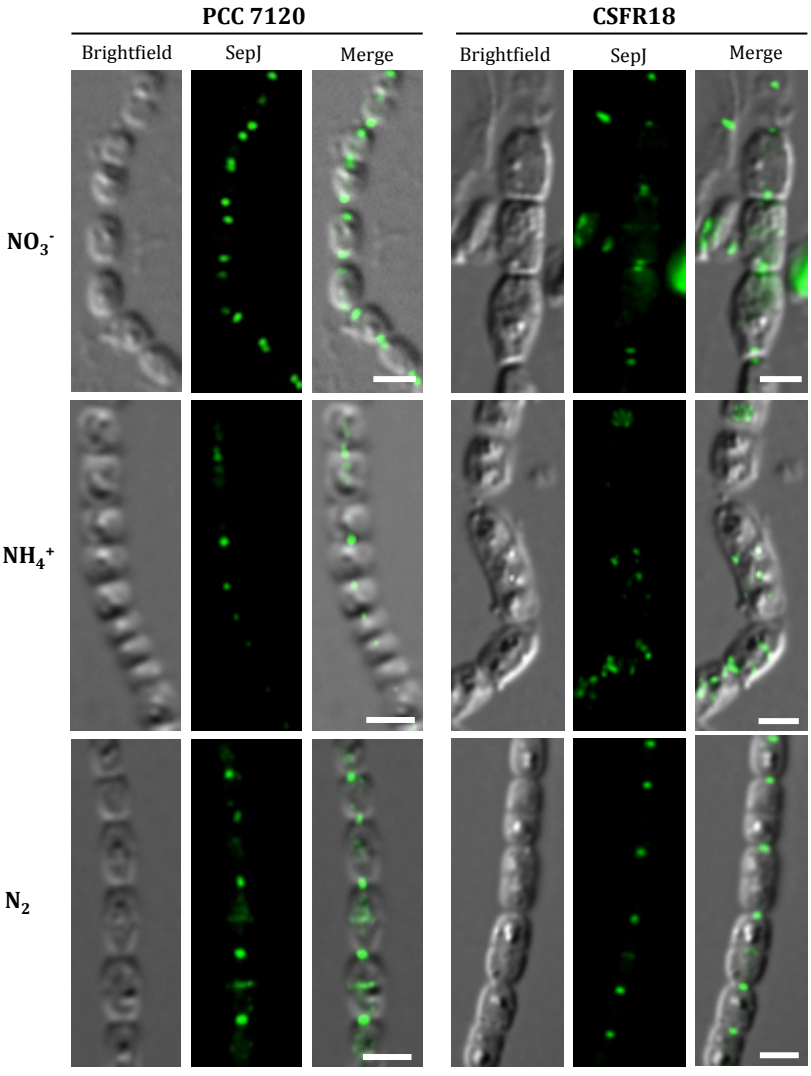

Fig. 3.15. Immunofluorescence localization of SepJ in *Anabaena* strains PCC 7120 and CSFR18. Filaments from BG11 medium were incubated for 48 h under culture conditions with de indicated nitrogen source, and after fixation to microscopy slides, they were incubated with antibodies against the coiled-coil domain of the *Anabaena* SepJ protein (see *Mat&Meth* section 2.7.2) Bright-field, fluorescence (SepJ), and merged images are shown. Size bars, 3 μm.

3.1.5. Treatment with berberine impairs SepJ localization

Berberine is an alkaloid produced by some plants that has been shown to interfere with the assembly of the FtsZ ring (Domadia *et al*., 2008; Boberek *et al*., 2010). To study with a different approach the role of the division machinery in the localization of SepJ, *Anabaena* cells were treated with berberine (see *Mat&Meth* section 2.8.6) and SepJ localization was analyzed by immunofluorescence using anti SepJ coiled-coil antibodies. Localization of FtsZ was also tested using anti *Anabaena* FtsZ antibodies to ensure that Z rings were not assembled (Fig. 3.16).

Formation of the FtsZ ring was hampered after incubating cells grown in nitrate-containing medium with 0.1 mM berberine for 24 h (Fig. 3.16). Longer incubations (≥ 48 h) or incubation with higher berberine concentrations (≥ 0.2 mM) resulted in cell lysis. The filaments with cells lacking an FtsZ ring showed SepJ labeling more spaced than the non-treated filaments (Fig. 3.16). In untreated filaments, mean distance between SepJ spots was 3.0 ± 0.7 μm (n=76) and this distance increased up to 5.1 ± 2.5 μm (n=74) in berberine-treated filaments. This difference was significant (Student's *t* test $P < 10^{-10}$). Spots observed with the anti SepJ coiled-coil antibodies might correspond to SepJ proteins placed at the septa before the treatment with berberine. When no SepJ signal was detected, in the elongated cells, this could result from lack of SepJ at the intercellular septa due to lack of FtsZ assembly. Although indirect effects cannot be discarded, these results are consistent with a dependence of SepJ localization on the FtsZ ring.

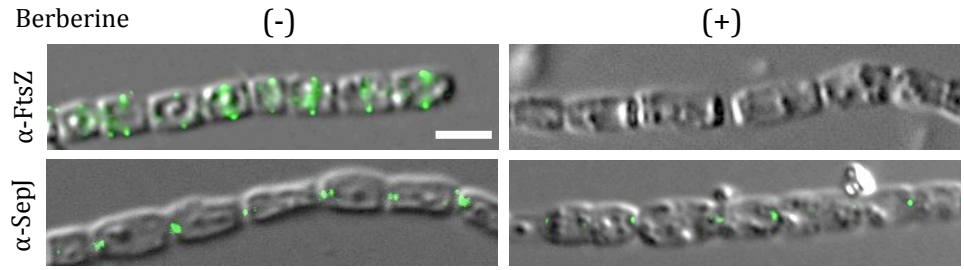

Fig. 3.16. Localization of FtsZ and SepJ in berberine-treated *Anabaena* filaments. Filaments grown in nitrate-containing medium were treated (+) or not (-) with 0.1 mM berberine for 24 h and then subjected to immunofluorescence. Merged bright-field and fluorescence images are shown. Size bar, 3 μm

3.2. STUDY OF SepJ COMPLEXES

3.2. STUDY OF SepJ COMPLEXES

As a possible component of septal junctions in *Anabaena*, the SepJ protein is needed to make long filaments in both media containing and media lacking a source of combined nitrogen, although its effect is most stringent in the absence of combined nitrogen. Although metazoan gap junctions are only formed by connexins, the formation of the septal junctions likely requires other proteins, and candidates are FraC and FraD, whose mutation alters SepJ localization and function (Merino-Puerto *et al*., 2010).

SepJ bears four differentiated domains (Herrero *et al*., 2016) (see Fig. 1.9): (I) an N-terminal sequence that could contain topological signals; (II) a coiled-coil domain; (III) a central linker domain rich in proline and serine residues; and (IV) an integral membrane (permease) domain that shows homology to proteins of the drug/metabolite exporter (DME) family. Immunofluorescence assays show that each cell likely contributes with a SepJ complex to the septal junctions (Mariscal, 2014). Moreover, the coiled-coil and linker domains of SepJ, predicted to be periplasmic, might be involved in the formation of intercellular complexes (Mariscal *et al*., 2011). In this chapter, we inquired whether SepJ is able to form stable complexes and whether other septal proteins are involved in such complexes.

3.2.1. SepJ self-interactions

As mentioned earlier, SepJ contains a coiled-coil domain that is predicted to reside in the periplasm. Coiled-coil motifs are present in a wide range of proteins and they are described to be involved in oligomerization and protein-protein interactions (Ciani *et al*., 2010; Mahrenholz *et al*., 2011). This made us wonder whether SepJ could form oligomers in addition to interacting with other different proteins. In this part of the work, we studied the ability of SepJ to make oligomers and which domain of the protein is involved in oligomerization.

3.2.1.1. Oligomerization properties of the coiled-coil domain

We first focused on the study of the oligomerization properties of the SepJ coiled-coil domain. To do this, a construct consisting of a C-terminal His-tagged coiled-coil domain of SepJ was expressed in *E. coli* BL21 and purified as described in *Mat&Meth* section 2.5.1.2. The identity of the purified SepJ coiled-coil domain was confirmed by MALDI-TOF analysis. Once the purified coiled-coil domain was available, we tested if it could form oligomers. The purified SepJ coiled-coil domain was studied by size-exclusion chromatography. A solution containing the purified domain at 1 mg mL^{-1} was loaded into a Superdex 200 column in order to separate proteins by their size. Superdex 200 has a separation range for molecules with molecular weights between 10 kDa and 600 kDa. Fractions obtained from the chromatography were subjected to SDS-PAGE and, after transferring the proteins to a PVDF membrane, western blot analysis was carried out using antibodies raised against the His-tag (Fig. 3.17). Protein standards of known size were also subjected to the chromatography to estimate the size corresponding to each fraction.

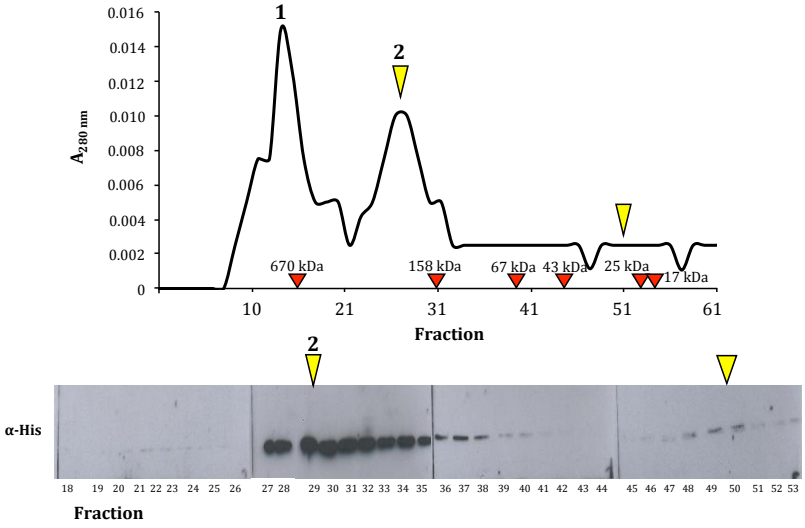

Fig. 3.17. Size-exclusion chromatography of purified SepJ coiled-coil domain. The coiled-coil domain was expressed in *E. coli* BL21 and purified as described in *Mat&Meth* section 2.5.1.2. Chart shows absorbance at 280 nm of each fraction obtained after chromatography. Two peaks were evident. The fractions were subjected to SDS-PAGE and western blot analysis was carried out using anti-His tag antibodies. The first peak contains multimeric forms whose estimated size was 759 kDa; the second peak (identified with a yellow arrow head) contains oligomeric forms whose estimated molecular weight was 240 kDa. Elution of monomeric form is also indicated with a yellow arrow head. Elution of protein standards is indicated by red lines in the chart. Proteins used as standard were thyroglobulin (670 kDa), gamma globulin (158 kDa), albumin (67 kDa), ovalbumin (43 kDa), chymotrypsinogen A (25 kDa), myoglobin (17 kDa) and ribonuclease A (13.5 kDa).

Results obtained in size-exclusion chromatography show that the SepJ coiled-coil domain can form multimers. The high amount of protein in peak 1 could correspond largely to precipitated coiled-coil domain that cannot be separated by SDS-PAGE. Peak 2 has an estimated molecular weight of 240 kDa. Because SepJ-CC-His_6 has an estimated size of 26.5 kDa, this multimeric form could correspond to 9 subunits. However, the accurate number of subunits cannot be deduced, since the isolated coiled-coil domain is predicted to fold as a cylinder and its size is likely over-estimated.

3.2.1.2. SepJ complexes in *Anabaena* membranes

In order to study whether the whole SepJ protein is able to form a stable complex, we designed a strategy to isolate SepJ from *Anabaena* membranes. An *Anabaena* strain (CSVM135) expressing a SepJ version fused to a double tag, containing His_{10}-tagged GFP (SepJ-GFP-His_{10}), was used (Fig. 3.18.A). The ability of strain CSVM135 to develop heterocysts was tested by incubating filaments for 48 h under diazotrophic conditions and staining the heterocysts using Alcian blue. Strain CSVM135 produced heterocysts and grew diazotrophically (Fig. 3.18.B). The subcellular localization of the fusion protein was analyzed by fluorescence microscopy. BG11-grown filaments of strain CSVM135 showed the SepJ-GPF-His_{10} protein correctly focused at the middle of the intercellular septa (Fig. 3.18.C).

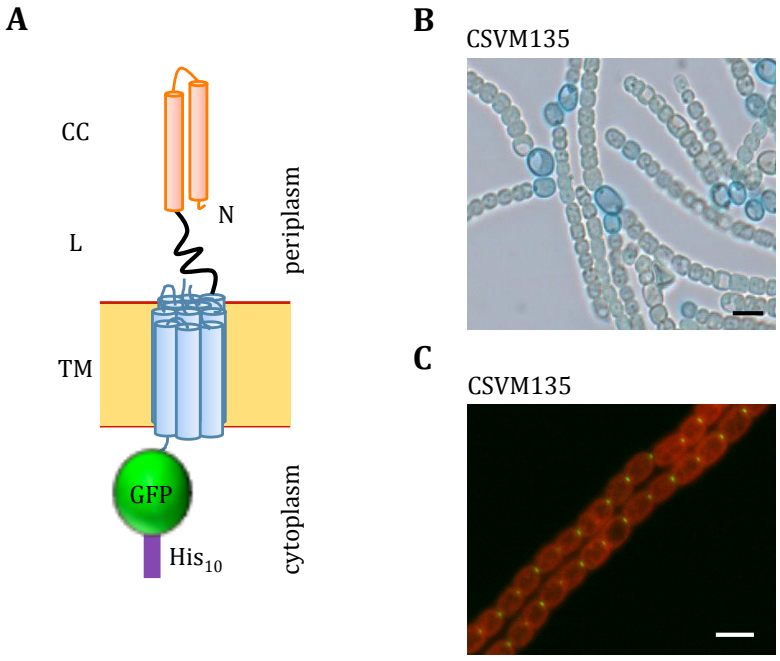

Fig. 3.18. An *Anabaena* strain expressing a double-tagged SepJ protein. **(A)** *Anabaena* strain CSVM135 produces a double-tagged SepJ version. The GFP protein is fused to the SepJ C-terminus and a His_{10}-tag is in turn fused to the GFP. **(B)** Filaments of strain CSVM135. Heterocysts were stained with Alcian blue, which highlights the polysaccharide layer of the heterocyst envelope. (**C**) Micrograph showing the localization of SepJ-GFP-His_{10} by fluorescence microscopy. The fusion protein is correctly focused at the cell poles in the intercellular septa.

In order to isolate the SepJ complexes from strain CSVM135, a two-step procedure was set up using a strain expressing single GFP-tagged SepJ (CSAM137) and the wild type as controls (Fig. 3.19). Total membrane fractions from *Anabaena* filaments were obtained by breaking down using glass beads (see *Mat&Meth* section 2.5.2.1). After solubilization of membrane proteins with 1% *n*-dodecyl β-D-maltoside (DDM), samples were mixed with a nickel resin in which His-tagged proteins get retained (Fig. 3.19). After washing the resin four times with buffer containing 1% DDM and 20 mM imidazole, retained proteins were eluted by using a 300 mM imidazole solution. The eluted material was then subjected to Blue Native-PAGE (Fig. 3.20.A), proteins were transferred to a PVDF membrane, and western blot analysis was performed using antibodies against the coiled-coil domain of SepJ (anti-SepJCC). Material reacting with the antibodies could be observed, but only in the strain in which SepJ was His-tagged. This material would correspond to SepJ-containing complexes with estimated sizes of 258.55 kDa, 346.82 kDa, 476.76 kDa and 655.38 kDa (Fig. 3.20.B).

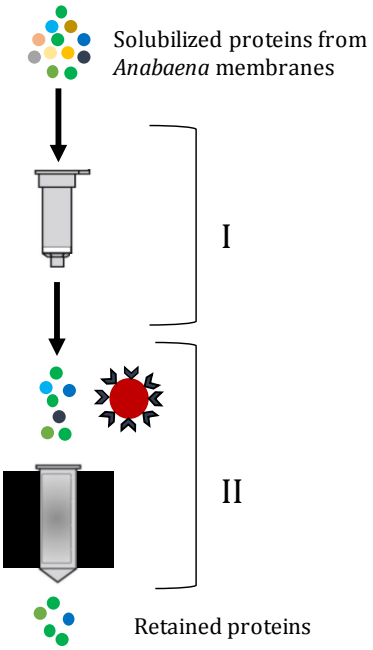

Fig. 3.19. Isolation of SepJ complexes from *Anabaena* membranes using a double-tagged SepJ protein. After solubilization of membranes from *Anabaena* using 1% DDM, the proteins were incubated with a nickel resin (I) in which His-tagged proteins get retained. These proteins were eluted from the resin using imidazole. The resulting eluate was then incubated with anti-GFP Microbeads (II), represented as a red circle surrounded by antibodies in the picture. The mixture was then loaded into a MACS column where microbeads remain together with GFP-tagged proteins bound to the antibodies. The elution was carried out using denaturalizing conditions (*Mat&Meth* section 2.5.2.2).

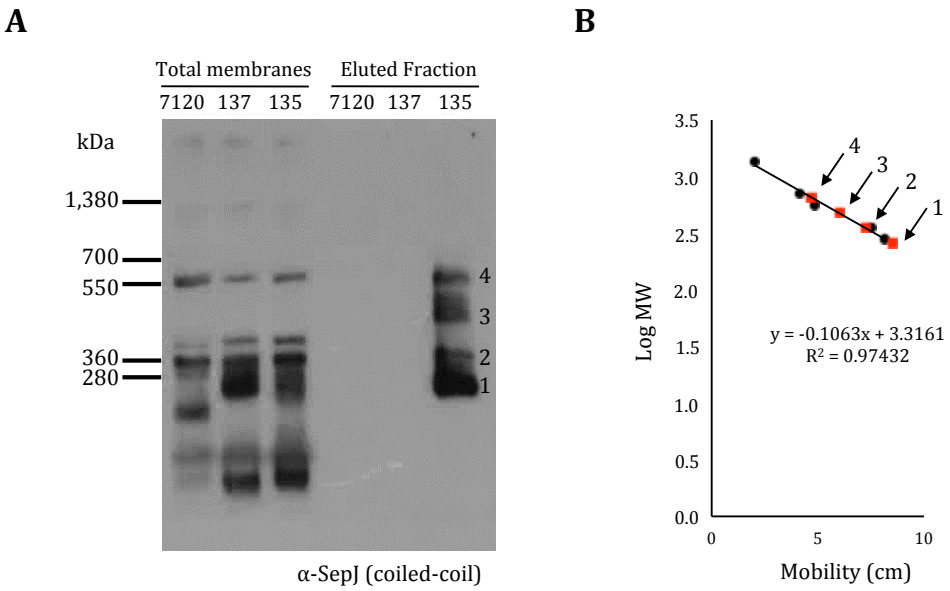

Fig. 3.20. Analysis of the fraction eluted from the nickel resin. (**A**) Membrane fractions and material eluted from step I were subjected to BN-PAGE, proteins were transferred to a PVDF membrane, and western blot analysis using anti-SepJCC antibodies was carried out. SepJ was found as high MW material (putatively forming complexes) in the *Anabaena* membranes. 7120, material from wild-type strain PCC 7120; 137, from strain CSVM137 producing SepJ-GFP; 135, from strain CSVM135 producing SepJ-GFP-His_{10}. After the resin column step, complexes containing SepJ were only found in material eluted from strain CSVM135. (**B**) For molecular size estimation, logarithm of standards' molecular weight and their corresponding mobility (expressed as cm from the upper part of the gel) were plotted into a graph in order to obtain an equation for molecular size prediction. Complexes of four different sizes could be seen, indicated as 1, 2, 3 and 4. The estimated size for each of these complexes was 258.55, 346.82, 476.76 and 655.38 kDa respectively.

After observation of SepJ complexes, the material eluted from the nickel resin was incubated with anti-GFP Microbeads and passed through a MACS column. The presence of the double-tagged SepJ protein was tested by analyzing eluted fractions in a SDS-PAGE gel, transferring proteins to a PVDF membrane and incubating this membrane in the presence of anti-SepJCC antibodies (Fig. 3.21.A). SepJ was observed only in eluted material that originated from strain CSVM135. When proteins in material eluted from the MACS column were separated by SDS-PAGE and stained with silver, six bands were detected in material from strain CSVM135, but four of them (black arrows) were detected in material from the negative controls too (Fig. 3.21.B). The estimated size of the upper band (upper red arrow) corresponded to SepJ-GFP-His_{10} (108.8 kDa). The two bands indicated red arrows were analyzed by mass spectrometry and SepJ-GFP was found to be present in both of them. The different mobility could result from the large hydrophobic region of the SepJ permease domain, which could bind different amounts of SDS depending on its state of folding. These results indicate that a stable complex would be formed by SepJ monomers in *Anabaena* and give no indication of other proteins interacting strongly with SepJ.

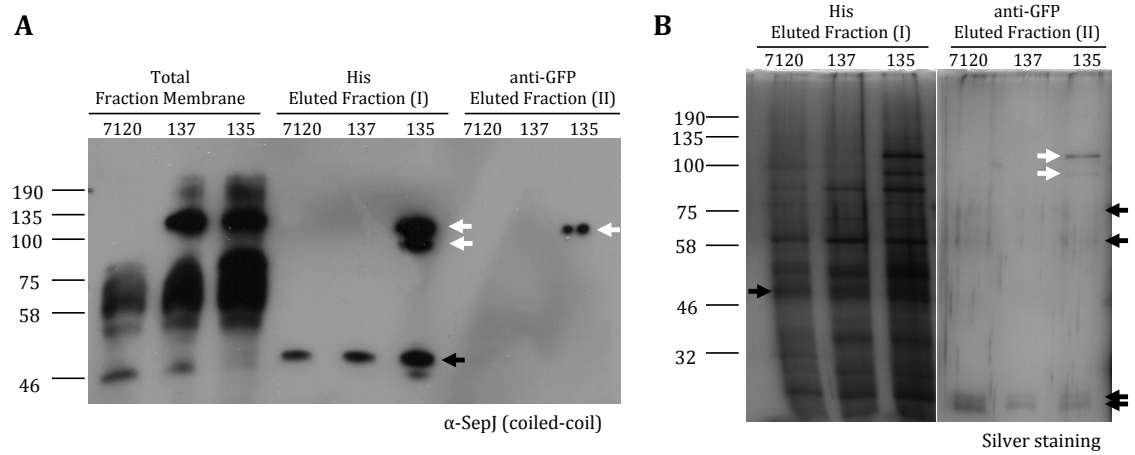

Fig. 3.21. Analysis of proteins isolated after SepJ pull down. **(A)** Western blot analysis using anti-SepJCC antibodies with samples from *Anabaena* strains PCC 7120 (wild type), denoted as 7120, CSAM137 (SepJ-GFP), denoted as 137, and CSVM135 (SepJ-GFP-His_{10}), denoted as 135. White arrows point to the SepJ-specific band in the eluates. The black arrow points to an unspecific band that we have frequently seen to interact with the anti-SepJCC antibodies. **(B)** Proteins contained in eluted fractions separated by SDS-PAGE. White arrows point to SepJ fused to GFP-His_{10} tag, and black arrows point to unspecific proteins present in eluted fractions from the three strains.

3.2.1.3. Analysis of SepJ self-interaction by BACTH

To get a deeper insight into SepJ-self interactions and the SepJ domains involved in such interactions, we used the Bacterial Adenylate Cyclase Two-Hybrid (BACTH) assay (Karimova *et al.*, 1998). This method is based on the reconstitution of an adenylate cyclase activity to study protein–protein interactions (Fig. 3.22). An interaction between test proteins results in reconstitution of an adenylate cyclase that produces cyclic AMP (cAMP), which binds to the catabolite activator protein (CAP [CRP]) activating transcription of a *lacZ* reporter gene encoding β-galactosidase.

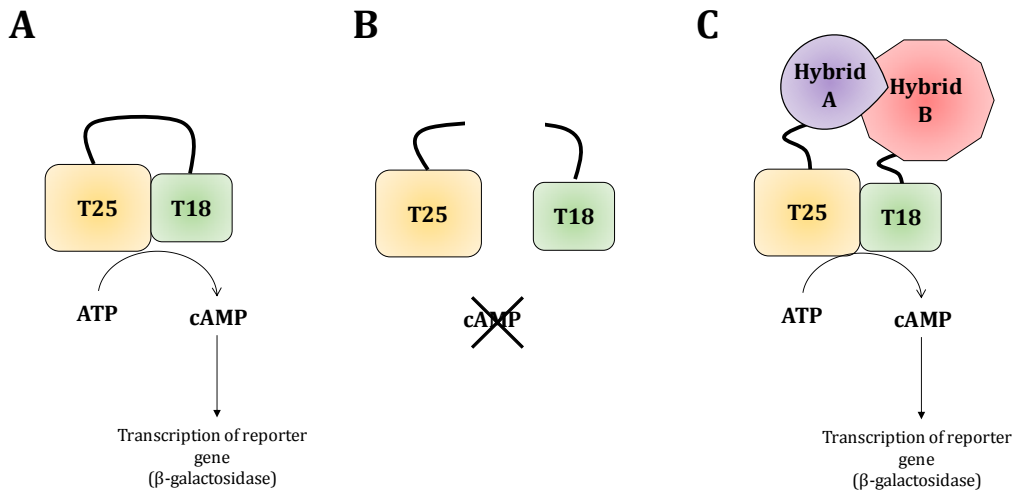

Fig. 3.22. Rational of the BACTH method. (A) The adenylate cyclase (CyaA) from *Bordetella pertussis* that catalyzes the production of cAMP from ATP can be divided into two domains (T25 and T18). **(B)** These two fragments have no catalytic activity when they are produced separately. **(C)** Fusions to interacting polypeptides, A and B, bring together T25 and T18 to reconstruct adenylate cyclase (CyaA) activity. cAMP acts as secondary metabolite activating transcription of *lacZ* encoding β-galactosidase.

Different fusions of SepJ to the catalytic domains T18 and T25 were prepared in order to corroborate SepJ oligomerization and to study the domains of SepJ involved in protein-protein interaction. In all the fusions, T25 or T18 fragments were added to C-terminal end of SepJ, which resides in the cytoplasm (Fig. 3.23.A). The full SepJ protein was first tested. SepJ-T25 and SepJ-T18 were together produced in *E. coli* and β-galactosidase activity was quantified. Plasmids encoding the T18 and T25 fragments alone were used as negative controls. A strong β-galactosidase activity was observed that clearly indicated SepJ self-interactions (Fig. 3.23.B).

To study the domains of SepJ involved in this interaction, four different truncated versions of SepJ were constructed (Fig. 3.23.A). We first prepared a SepJ version lacking a substantial part of the permease domain (amino acid residues 463 to 748 removed). This protein, denoted SepJ(ΔTM), bears the entire periplasmic part anchored to the plasma membrane by only one putative transmembrane segment. We also prepared a complementary SepJ version, denoted SepJ(Δpp), lacking most of the predicted periplasmic part of the protein (amino acid residues 40 to 410 removed) but keeping the entire permease domain. Two more SepJ versions were prepared: one of them, denoted SepJ(Δlinker) lacked the linker domain (amino acid residues 223 to 410 removed), and the other one, denoted SepJ(ΔCC), lacked the coiled-coil domain (amino acid residues 40 to 201 removed). All of these truncated versions were fused to the N-termini of both T25 and T18 fragments.

β-galactosidase activity of the different combinations of the SepJ versions is shown in Table 3.5 and summarized in Fig. 3.23.B**.** As controls we included combinations of each of the fusions with non-fused T25 or T18 fragments. None of the controls showed appreciable β-galactosidase activity. As reference for analysis of the tested SepJ versions, we used the double negative control in which none of the plasmids has an insert,

producing non-fused T25 and T18 fragments. SepJ(ΔTM) versions did not show any significant increase in β-galactosidase activity in any of the combinations tested with respect to the control. However, because SepJ(ΔTM) only shows one transmembrane segment, it might not be properly incorporated into the membrane. The SepJ(Δpp) version produced significantly increased β-galactosidase activity, but in a very small amount compared to the other statistical significant combinations. Because this deleted version bears the entire permease domain, these results suggest that the periplasmic part of SepJ is important for self-interaction. Both SepJ(ΔCC) and SepJ(Δlinker) showed appreciable β-galactosidase activity in all the combinations tested, indicating that both the coiled-coil and linker domains of SepJ contribute to SepJ-self interaction. Nonetheless, the linker domain appears to be more important for the SepJ self-interaction that the coiled-coil domain.

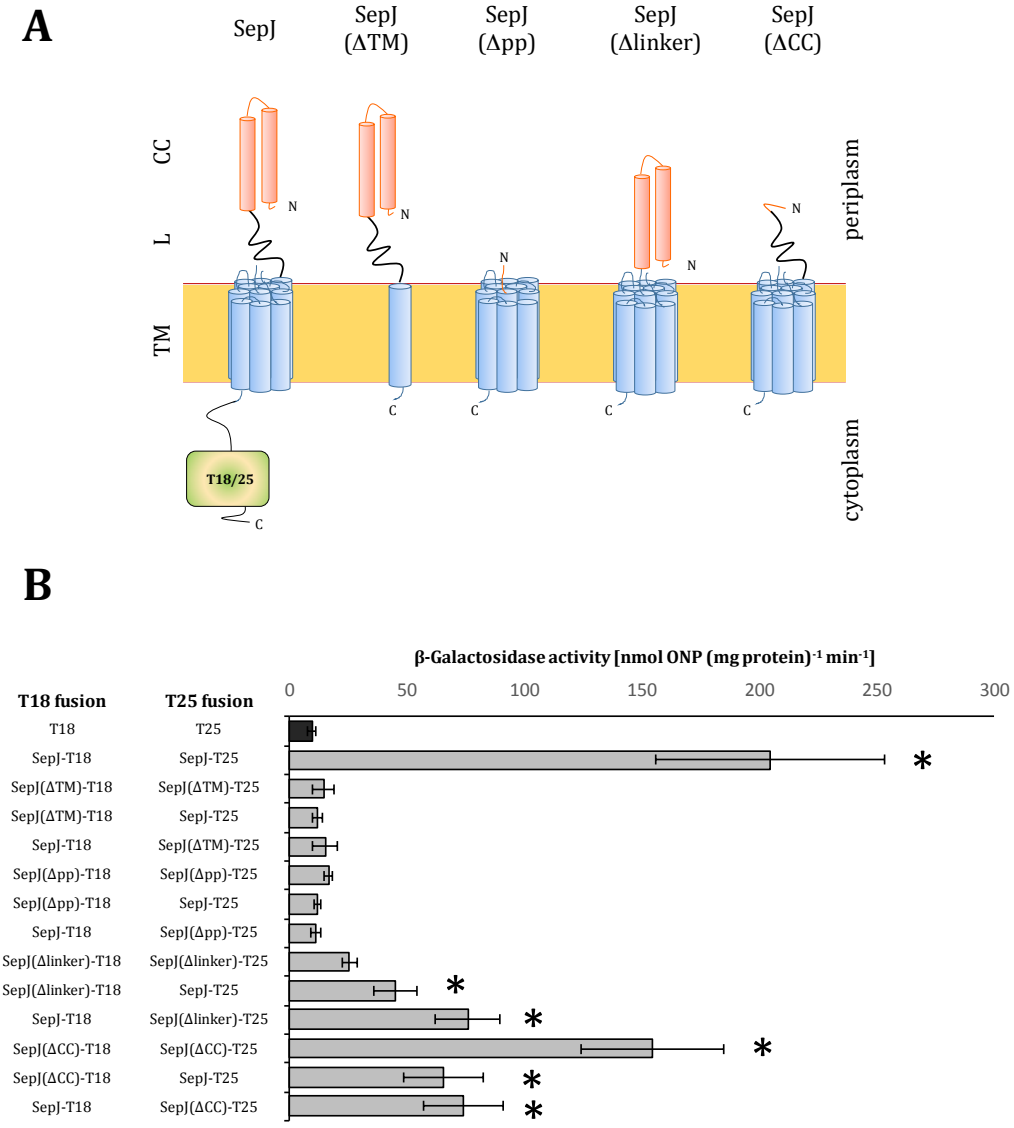

Fig. 3.23. Analysis of SepJ self-interactions by BACTH. (A) Schematics of the different SepJ protein fusions used for BACTH analysis. The N-terminal sequence and the coiled-coil domain (CC) are represented in orange, the linker domain (L) is indicated in black and the permease or transmembrane domain (TM), predicted to bear 11 TMSs, is represented in blue. T25 and T18 fragments of the catalytic subunit of adenylate cyclase are represented as a rectangle fused to the C-

terminus of SepJ. N- and C- terminal ends of the proteins are indicted in the figure. Deleted versions of SepJ lacking most of the transmembrane domain, all the periplasmic part but the N-terminal sequence, the linker domain or the coiled-coil domain, respectively, are also represented; the T18 and T25 fragments were fused in every case to the C terminus (not depicted). **(B)** β-galactosidase activity of the different combinations used. Asterisks highlight combinations that produced activity significantly different to that of the T18/T25 control at $P < 0.0005$. The complete set of quantitative data is shown in Table 3.5.

Table 3.4. Quantification of SepJ self-interactions assessed by BACTH analysis. The mean and standard deviation of the results from the number of independently isolated transformants indicated (*n*) are presented. The difference between strains carrying each plasmid combination and the T18/T25 plasmid pair was assessed by the Student's *t* test (*P* indicated in each case); asterisks and garnet color highlight differences significant at $P \leq 0.0005$.

T18 fusion	T25 fusion	β-Galactosidase activity [nmol ONP (mg protein)$^{-1}$ min^{-1}]	Student's t test (*P*)
T18	T25	9.32 ± 1.99 (10)	
SepJ-T18	T25	10.32 ± 2.86 (13)	0.3543
T18	SepJ-T25	9.02 ± 1.72 (13)	0.7087
T18	SepJ(ΔTM)-T25	10.76 ± 0.63 (4)	0.1893
T18	SepJ(Δpp)-T25	12.05 ± 1.81 (4)	0.0353
T18	SepJ(Δlinker)-T25	9.76 ± 1.10 (4)	0.6859
T18	SepJ(ΔCC)-T25	12.44 ± 1.65 (4)	0.0171
SepJ(ΔTM)-T18	T25	10.18 ± 4.17 (6)	0.5792
SepJ(Δpp)-T18	T25	9.32 ± 2.09 (6)	0.9975
SepJ(Δlinker)-T18	T25	10.51 ± 4.25 (6)	0.4528
SepJ(ΔCC)-T18	T25	11.47 ± 3.74 (6)	0.1520
SepJ-T18	SepJ-T25	204.86 ± 48.54 (10)	2 E-10*
SepJ(ΔTM)-T18	SepJ(ΔTM)-T25	14.33 ± 4.34 (4)	0.0100
SepJ(ΔTM)-T18	SepJ-T25	11.85 ± 1.89 (4)	0.0498
SepJ-T18	SepJ(ΔTM)-T25	15.16 ± 5.36 (4)	0.0092
SepJ(Δpp)-T18	SepJ(Δpp)-T25	16.69 ± 1.81 (4)	3 E-05*
SepJ(Δpp)-T18	SepJ-T25	11.48 ± 1.41 (4)	0.0730
SepJ-T18	SepJ(Δpp)-T25	11.27 ± 2.02 (4)	0.1245
SepJ(Δlinker)-T18	SepJ(Δlinker)-T25	25.50 ± 3.39 (4)	9 E-08*
SepJ(Δlinker)-T18	SepJ-T25	45.16 ± 9.31 (4)	4 E-08*
SepJ-T18	SepJ(Δlinker)-T25	75.83 ± 14.08 (3)	5 E-09*
SepJ(ΔCC)-T18	SepJ(ΔCC)-T25	154.65 ± 30.36 (3)	3 E-09*
SepJ(ΔCC)-T18	SepJ-T25	69.36 ± 16.90 (3)	2 E-07*
SepJ-T18	SepJ(ΔCC)-T25	74.01 ± 17.07 (4)	3 E-08*

3.2.2. Interaction of SepJ with cell division proteins

As has been previously shown, SepJ localization at the intercellular septa requires the cell division machinery. Among cyanobacterial proteins involved in cell division, FtsZ and FtsQ appear to play a central role in early and late steps, respectively, recruiting other elements involved in this process. We therefore selected these proteins to test possible interactions with SepJ. Additionally, FtsW, a divisome-linked peptidoglycan glycosyltransferase (Meeske *et al*., 2016) that contributes to building the cell wall in the late steps of cell division, was also included in this analysis.

Heterologous cell division proteins have been described to interfere with the *E. coli* cell division machinery, and production of *Anabaen*a FtsZ in *E. coli* results in a filamentation phenotype (Kuhn *et al*., 2000). Because of this, cell division proteins were fused to the T25 fragment, since pKT25-derived plasmids are in lower copy numbers than pUT18-derived plasmids. Moreover, topology predictions together with previous data obtained using *E. coli* homologs (Karimova *et al*., 2005) provided relevant information to decide which end of the proteins were appropriate for fusion to the T25 fragment.

FtsZ is the most widely conserved cell division protein among prokaryotes. Topology prediction of *Anabaena* FtsZ shows that it is a soluble protein. As it has been done before to test FtsZ in *E. coli* by BACTH (Karimova *et al*., 2005), the T25 fragment was fused to the C terminus of FtsZ (Fig. 3.26.A). To construct the plasmid bearing the fusion protein, *Anabaena ftsZ* gene (ORF *alr3858*) was amplified using primers alr3858-13 and alr3858-14 and the PCR product was cloned in pKNT25 using PstI and BamHI generating plasmid pCSFR32.

Secondary structure prediction of *Anabaena* FtsW showed that this protein contains 8 transmembrane segments with both N- and C-termini predicted to be cytoplasmic (Fig. 3.24). Because of that, we fused the T25 fragment to the N-terminus of the protein (Fig 3.26.A). To construct the plasmid encoding the fusion protein, *Anabaena ftsW* (ORF *all0154*) was amplified using primers all0154-9 and all0154-10 and the PCR product was cloned in pKT25 using PstI and BamHI, producing plasmid pCSFR31.

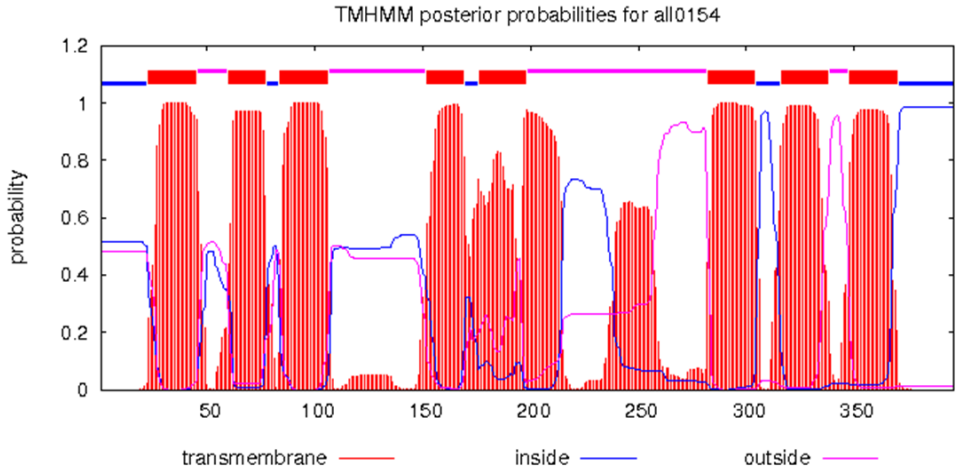

Fig. 3.24. Topology of *Anabaena* FtsW. Predicted topology of FtsW from *Anabaena* using the TMHMM program. FtsW (All0154) is predicted to contain eight transmembrane segments and both N- and C-termini are likely to be located in the cytoplasm.

Bioinformatics analysis of *Anabaena* FtsQ showed a secondary structure similar to that of its *E. coli* homolog (van den Ent *et al*., 2008) (Fig. 3.25), including the two subdomains α and β. The α subdomain is predicted to contain a Polypeptide Transport Associated (POTRA) motif. This protein shows a transmembrane segment, locating most of the protein in the periplasm. We fused the T25 fragment to the N-terminus of FtsQ (Fig. 3.26.A). To construct the plasmid encoding this fusion protein, *ftsQ* from *Anabaena* (ORF *alr3857*) was amplified using primers alr3857-7 and alr3857-8 and cloned in pKT25 using BamHI and PstI, generating plasmid pCSFR30.

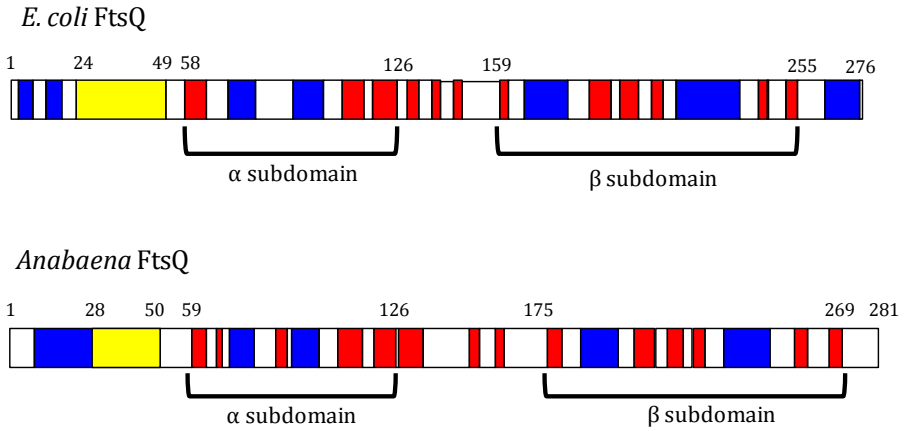

Fig. 3.25. Schematic representation of FtsQ from *E. coli* and *Anabaena*. *E. coli* FtsQ after van den Ent *et al.* (2008). *Anabaena* FtsQ is the product of ORF *alr3857* from the *Anabaena* genomic sequence (Kaneko *et al.*, 2001). *Anabaena* FtsQ secondary structure is presented as predicted by PSIPRED and drawn taking as a model the protein from *E. coli.* Yellow, transmembrane segment; blue, α-helix; red, β-strand.

3.2.2.1. Analysis of interaction between SepJ and cell division proteins by BACTH

We first tested interactions between SepJ and FtsZ, FtsW and FtsQ (Fig. 3.26.C; Table 3.6). No interaction was detected between SepJ and FtsZ. However, a weak (though significant, $P = 0.0161$) positive interaction was found between SepJ and FtsW and a very strong interaction between SepJ and FtsQ. To investigate further the interaction between SepJ and FtsQ, we studied whether different SepJ versions (with specific domain deletions) showed interaction with the entire FtsQ protein. Only SepJ(ΔCC) appeared to interact strongly with FtsQ. Thus, again the linker domain of SepJ was found to be important for a protein-protein interaction. On the other hand, we prepared different FtsQ versions with deleted domains to be tested with the SepJ protein. As described above, the periplasmic part of FtsQ bears two different domains: the α domain, containing a POTRA motif, and the β domain involved in recruitment of some divisome components. Two FtsQ deleted versions were fused at their N terminus to T25: a version lacking the α domain (residues 60 to 127) and another one lacking the β domain (residues 128 to 281). Interaction with SepJ was only lost when the α domain was deleted (Fig. 3.26.C; Table 3.6). These results indicate that the α domain, but not the β domain, of FtsQ is involved in the interaction with SepJ.

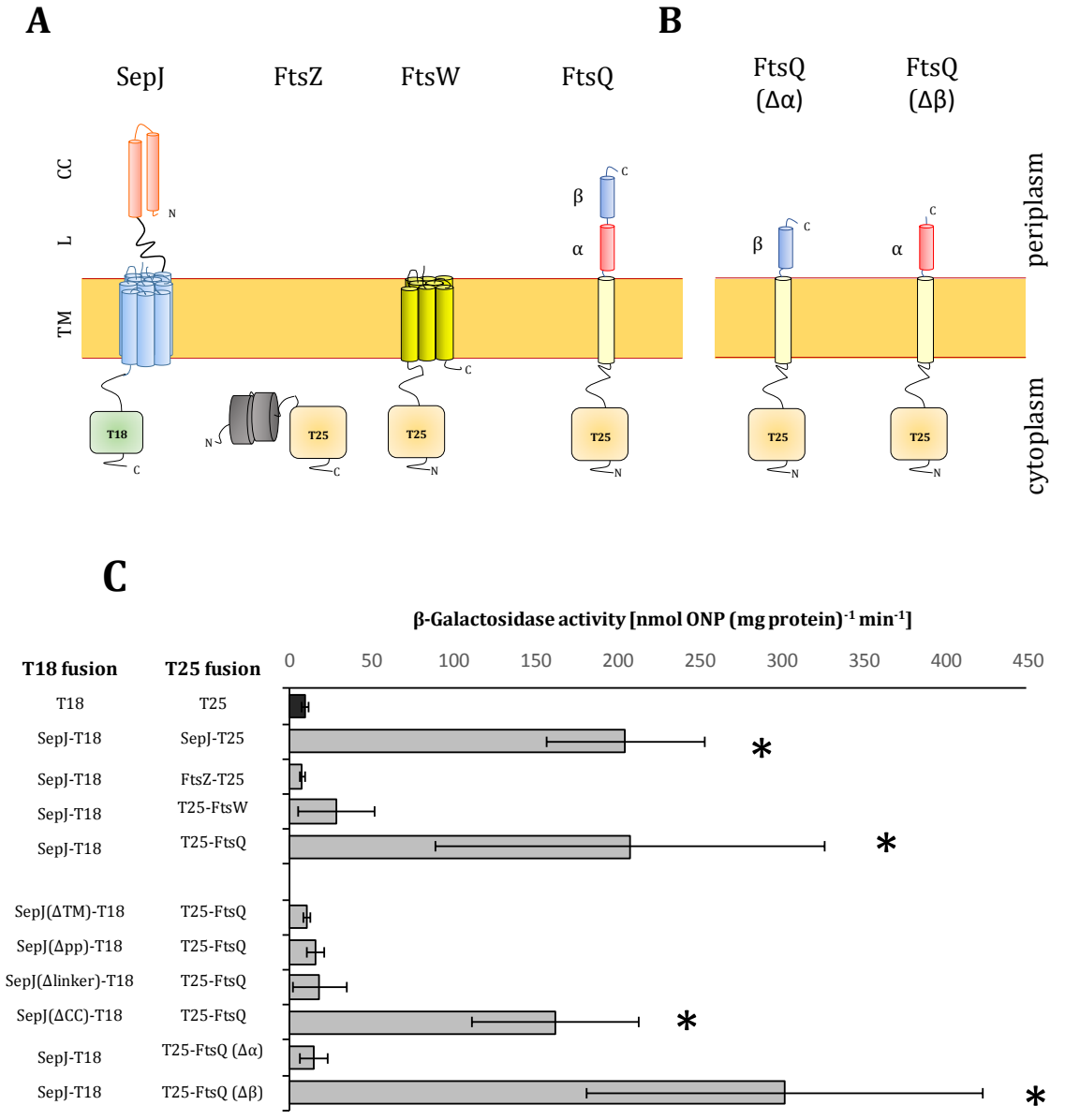

Fig. 3.26. BACTH analysis to test interactions between SepJ and division proteins. (A) Schematics of proteins used in BACTH analysis. The T25 and T18 fragments of the catalytic subunit of adenylate cyclase are represented as blocks. FtsZ (428 amino acid residues), predicted to be a soluble protein, is represented in grey fused to the T25 fragment by its C terminus. FtsW (396 amino acid residues) is represented in yellow and fused to T25 by its N terminus. FtsQ (281 amino acid residues) secondary structure is predicted to have one transmembrane segment (light yellow) and two periplasmic subdomains, α (represented in red) and β (represented in blue). FtsQ was fused through its N terminus to T25. The N and C termini of the proteins are indicated. **(B)** Domain deletion versions of FtsQ used in BACTH analysis. The FtsQ(Δα) version lacks amino acids residues 60 to 127, and the FtsQ(Δβ) version lacks amino acid residues 128 to 281. (**C**) β-galactosidase activity of the different combinations used. Asterisks highlight combinations that were significantly different with respect to the control at $P < 0.0001$. The complete set of quantitative data is shown in Table 3.6.

Table 3.5. Quantification of interactions between divisome proteins and SepJ assessed by BACTH analysis. The mean and standard deviation of the results from the number of independently isolated transformants indicated (*n*) are presented. The difference between strains carrying each plasmid combination and the T18/T25 plasmid pair was tested by the Student's *t* test (*P* indicated in each case); asterisks and garnet color highlight differences significant at $P \leq 0.0001$.

T18 fusion	T25 fusion	β-Galactosidase activity [nmol ONP (mg protein)$^{-1}$ min^{-1}]	Student's t test
T18	T25	9.32 ± 1.99 (10)	
SepJ-T18	T25	10.32 ± 2.86 (13)	0.3543
SepJ(ΔTM)-T18	T25	10.76 ± 0.63 (4)	0.1893
SepJ(Δpp)-T18	T25	12.05 ± 1.81 (4)	0.0353
SepJ(Δlinker)-T18	T25	9.76 ± 1.10 (4)	0.6859
SepJ(ΔCC)-T18	T25	12.44 ± 1.65 (4)	0.0171
T18	FtsZ-T25	8.51 ± 1.70 (4)	0.4929
T18	T25-FtsW	9.30 ± 1.19 (4)	0.9883
T18	T25-FtsQ	8.69 ± 2.32 (6)	0.5749
T18	T25-FtsQ (Δα)	5.72 ± 4.01 (2)	0.0681
T18	T25-FtsQ (Δβ)	7.14 ± 4.49 (2)	0.2607
SepJ-T18	SepJ-T25	204.86 ± 48.54 (10)	2 E-10*
SepJ-T18	FtsZ-T25	7.50 ± 1.53 (4)	0.1297
SepJ-T18	T25-FtsW	28.68 ± 23.14 (4)	0.0161
SepJ-T18	T25-FtsQ	207.50 ± 118.67 (5)	1 E-04*
SepJ(ΔTM)-T18	T25-FtsQ	10.34 ± 1.86 (4)	0.3965
SepJ(Δpp)-T18	T25-FtsQ	15.64 ± 5.42 (4)	0.0061
SepJ(Δlinker)-T18	T25-FtsQ	18.34 ± 16.64 (4)	0.0979
SepJ(ΔCC)-T18	T25-FtsQ	161.87 ± 50.86 (4)	3 E-07*
SepJ-T18	T25-FtsQ (Δα)	15.09 ± 8.48 (4)	0.0541
SepJ-T18	T25-FtsQ (Δβ)	302.06 ± 121.31 (3)	3 E-06*

3.2.2.2. Analysis of SepJ-FtsQ interaction by Co-IP

In order to validate the interaction between SepJ and FtsQ, co-immunopurification was tried. For this purpose, an *E. coli* strain carrying compatible plasmids expressing SepJ-GFP and His_6-FtsQ was prepared. Additionally, we generated a Δpp-SepJ-GFP version, lacking most of the periplasmic part of SepJ (residues 40 to 410 removed). To construct the His_6-FtsQ-encoding plasmid, the *Anabaena ftsQ* gene was cloned using primers alr3857-13 and alr3857-14, and the PCR product was cloned in pACYCDuet using BamHI and XhoI producing pCSFR50 (six histidine residues added to the N terminus of FtsQ). To produce SepJ-GFP and Δpp-SepJ-GFP version, a SacI-EcoRI fragment from pCSAL33 (bearing the *gfp-mut2* gene) was cloned in pCSE221 or in pCSE227, producing pCSFR51 and pCSFR52 respectively. As negative controls, we used a strain expressing this Δpp-SepJ-GFP version and His_6-FtsQ and other strains expressing only one of the proteins tested (SepJ-GFP, Δpp-SepJ-GFP or His_6-FtsQ). Each pair of plasmids were introduced in *E. coli* BL21 (Table 2.1) in order to induce the expression of both proteins. Co-purification assays were carried out as described in *Mat&Meth* section 2.6.1.

GFP was used as a tag for purification of the fusion protein from *E. coli* cell-free extracts generated by passage through a French pressure cell. Samples, which should consist of inside-out membrane microvesicles (Altendorf & Staehelin, 1974), were incubated with anti-GFP MicroBeads. Microbeads were then attached to a magnetic-activated cell sorting (MACS) column, and the material retained was released from the Microbeads by eluting with loading buffer (containing SDS and DTT) and subjected to SDS-PAGE. The presence of FtsQ in the samples was tested by western blot analysis using antibodies against His_6-tag (Qiagen) following the protocol described in *Mat&Meth* section 2.5.3.7 (Fig 3.27.A). The presence of GFP-tagged SepJ in the samples was verified by western blot analysis using anti-GFP antibodies (Invitrogen) (Fig. 3.27.B).

We found a positive signal corresponding to the His-FtsQ expected size in the sample containing also the entire SepJ protein, but a very weak or no signal in the samples containing the Δpp-SepJ version or the other negative controls, respectively. This result confirmed a stable interaction between FtsQ and SepJ, and emphasized the importance of the periplasmic part of SepJ in that interaction.

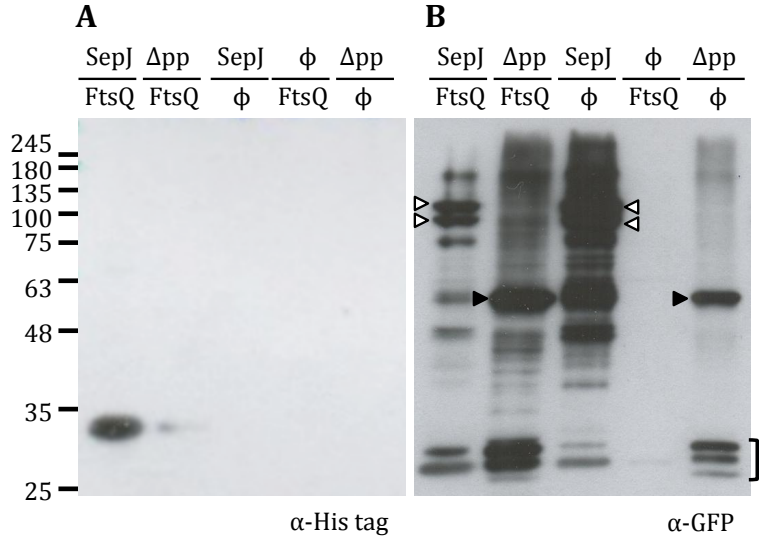

Fig. 3.27. Co-IP of SepJ-GFP and His_6-tagged FtsQ. Samples were allowed to interact with anti-GFP MicroBeads and loaded into a MACS column, and the material retained was then eluted and subject to western analysis with an anti-His_5 antibody **(A)** or an anti-GFP antibody **(B)**. For each lane, the proteins expressed in the corresponding *E. coli* strain are indicated; SepJ refers to SepJ-GFP; Δpp, SepJ-GFP without the periplasmic region; FtsQ, His_6-tagged *Anabaena* FtsQ; ϕ, plasmid vector without insert. White triangles point to signals corresponding to the SepJ-GFP fusion protein (about 108 kDa), and black triangles point to Δpp-SepJ-GFP (about 68 kDa). The SepJ protein generates forms moving to different extents in SDS-PAGE gels (Mariscal *et al*., 2011). Some degradation of the SepJ-GFP fusion proteins releasing at least two forms of GFP (about 27 kDa; bracket) and, in the case of the complete protein, possibly also a protein lacking the predicted periplasmic section appears to have taken place.

3.2.3. Other possible SepJ interactors

3.2.3.1. Test of interaction with Fra proteins

As is the case for SepJ, FraC and FraD are septal proteins in *Anabaena* (Merino-Puerto *et al.*, 2010). It has been shown that deletion of FraC or FraD delocalize SepJ, with the result of spreading it along the intercellular septa (Merino-Puerto *et al*., 2010), and impairs septal peptidoglycan nanopore formation as well (Nürnberg *et al*., 2015).

Fra proteins are encoded by the *fraC-fraD-fraE* operon and they are needed for filament integrity mainly in diazotrophic conditions (Merino-Puerto *et al*., 2010). FraC is predicted to be an integral membrane protein containing three transmembrane segments with the C terminus located in the cytoplasm. FraD has two domains: an integral membrane N-terminal domain containing five transmembrane segments, and a periplasmic C-terminal domain with two predicted coiled-coil motifs (Merino-Puerto *et al*., 2010). Based on these predictions, T18 or T25 fragments were fused to the C terminus or N terminus of FraC and FraD, respectively (Fig. 3.28.A).

To test interactions between the Fra proteins and SepJ, T18 and T25-fused versions FraC and FraD were prepared and used in BACTH analysis together with T25 and T18 versions of SepJ (Fig. 3.28.B; Table 3.7). No significant interaction was found between SepJ and FraC or FraD fusion proteins. Neither self-interactions nor interactions between the Fra proteins were found. These results provide no evidence for an interaction of FraC or FraD with SepJ.

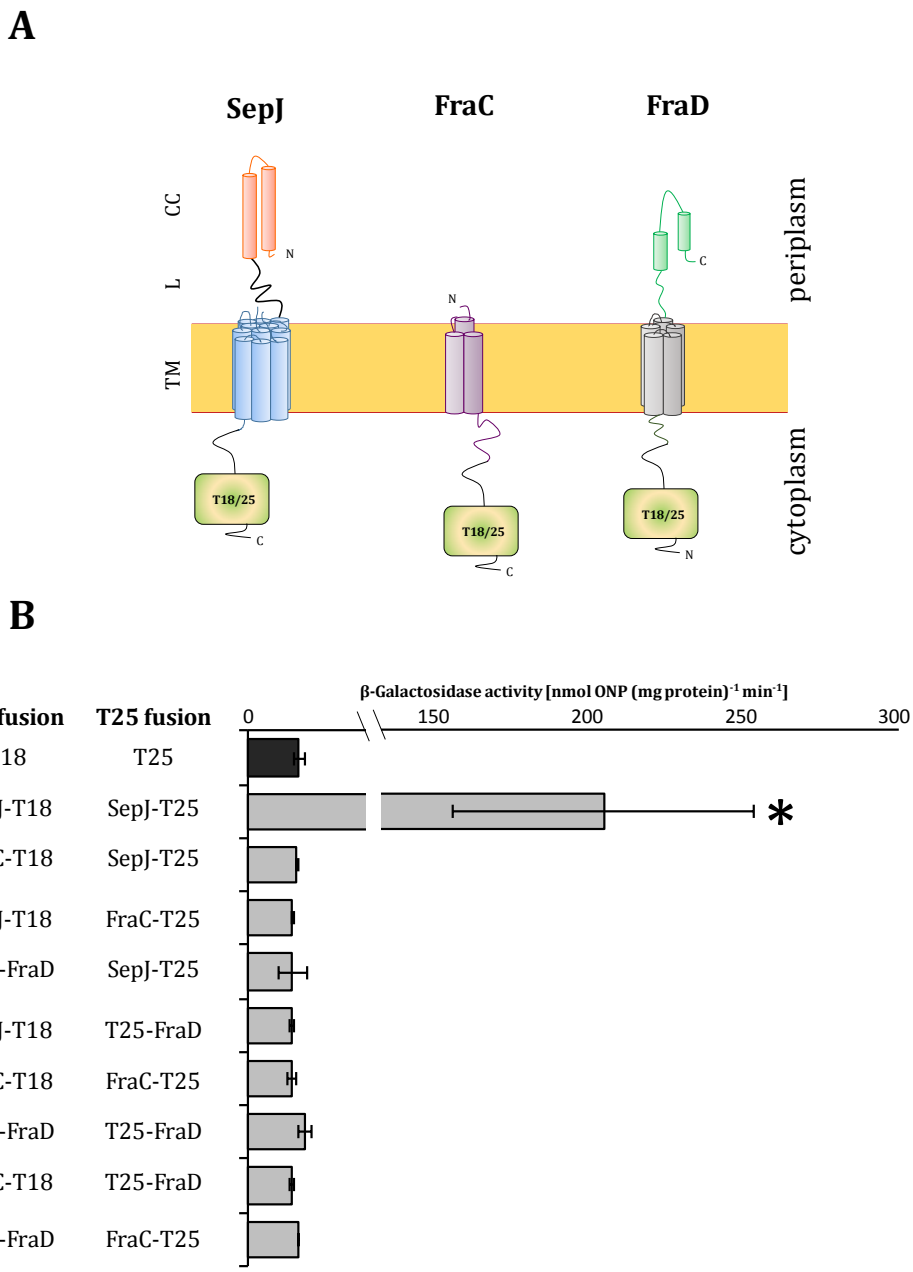

Fig. 3.28. Analysis of interaction between SepJ and Fra proteins by BACTH. (A) Schematics of the proteins tested by BACTH. The FraC protein (179 amino acid residues) is an integral membrane protein (represented in purple) which is predicted to contain 3 transmembrane segments. The FraD protein (343 amino acid residues) has two domains: an N-terminal integral membrane domain, composed of 5 predicted transmembrane segments (in grey), and a C-terminal coiled-coil domain (in green). T18 or T25 was fused to C and N termini of FraC and FraD respectively. **(B)** β-galactosidase activity of the different combinations tested. The asterisk highlights a combination that was significantly different. The complete set of quantitative data is shown in Table 3.6.

Table 3.6. Quantification of SepJ-Fra protein interactions assessed by BACTH analysis. The mean and standard deviation of the results from the number of independently isolated transformants indicated (*n*) are presented. The difference between strains carrying each plasmid combination and the T18/T25 plasmid pair was assessed by the Student's *t* test (*P* indicated in each case); an asterisk and garnet color highlights a difference that was highly significant, that of the SepJ/SepJ positive control.

T18 fusion	T25 fusion	β-Galactosidase activity [nmol ONP (mg protein)$^{-1}$ min^{-1}]	Student's t test
T18	T25	16.50 ± 1.79 (2)	
SepJ-T18	T25	20.99 ± 3.88 (2)	0.2756
T18	SepJ-T25	14.78 ± 0.86 (2)	0.3465
T18	FraC-T25	16.61 ± 0.58 (2)	0.9393
T18	T25-FraD	16.84 ± 0.25 (2)	0.8139
FraC-T18	T25	16.41 ± 1.22 (2)	0.9601
T18-FraD	T25	14.80 ± 1.42 (2)	0.4026
SepJ-T18	SepJ-T25	204.86 ± 48.54 (10)	2 E-10*
FraC-T18	SepJ-T25	15.68 ± 0.27 (2)	0.5900
SepJ-T18	FraC-T25	14.49 ± 0.07 (2)	0.2531
T18-FraD	SepJ-T25	14.39 ± 4.80 (2)	0.6189
SepJ-T18	T25-FraD	14.26 ± 0.73 (2)	0.2437
FraC-T18	FraC-T25	14.16 ± 1.26 (2)	0.2706
T18-FraD	T25-FraD	18.21 ± 2.03 (2)	0.4656
FraC-T18	T25-FraD	13.97 ± 0.75 (2)	0.2067
T18-FraD	FraC-T25	16.33 ± 0.21 (2)	0.9083

3.2.3.2. Interaction with SjcF1

SjcF1 was first identified in proteomic analysis of the cell wall from *Anabaena* (Moslavac *et al.*, 2005). This protein is involved in nanopore formation, since its inactivation alters the size of nanopores and intercellular communication (Rudolf *et al.*, 2015). SjcF1 contains an N-terminal transmembrane segment, an SH3 domain for protein-protein interactions and two peptidoglycan-binding domains. To test interaction between SjcF1 and SepJ, FaC and FraD, N-terminal fusions of SjcF1 to T18 and T25 fragments were prepared (Fig. 3.29.A). Although a strong interaction was not found between these proteins, statistically significant SjcF1/SepJ and SjcF1/FraC interactions were observed (Fig. 3.29.B; Table 3.7). Of note, SepJ and FraC contain predicted SH3 binding motifs (in SepJ, residues 326 to 331: PLTPEK; in FraC, residues 66 to 72: FVEPVLP). Interaction between SjcF1 and SepJ or FraC has also been observed by fluorescence anisotropy (Rudolf *et al.*, 2015). However, no significant interaction was found between SjcF1 and FraD or SjcF1 with itself. The weak interactions involving SjcF1 might result from a short residence time of this protein in the cytoplasmic membrane, since its destiny is the periplasm, where it interacts with the peptidoglycan.

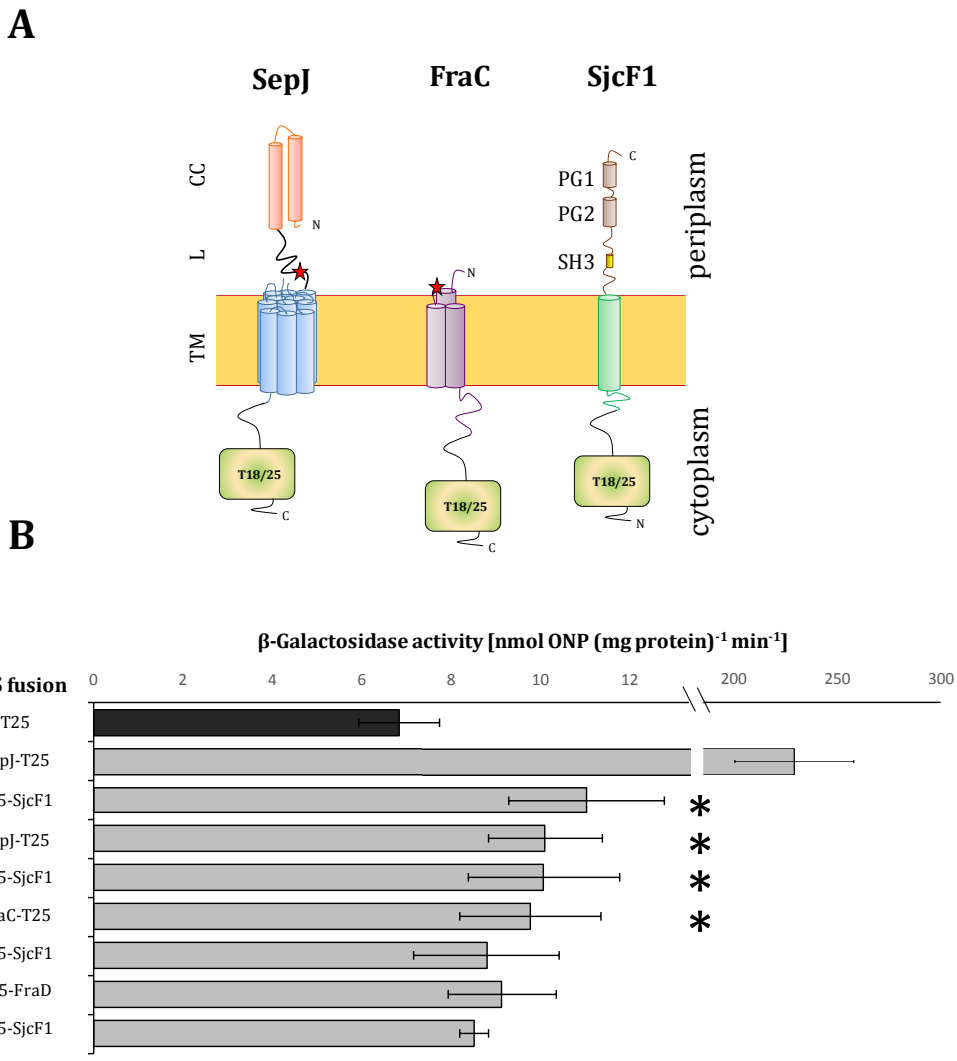

Fig. 3.29. Analysis of interactions between SjcF1 and SepJ or the Fra proteins. (A) Schematics of the SepJ, FraC and SjcF1 fusion proteins used in BACTH. SjcF1 (269 amino acid residues) bears two PG-binding domains, in brown and denoted as PG1 and PG2, and a SH3 domain, represented in yellow, that could be involved in protein-protein interactions. T18 and T25 fragments, represented as blocks, were fused to the N terminus of SjcF1. SH3-biding motifs are represented as red stars in SepJ and FraC. **(B)** β-galactosidase activity of the different combinations tested. Asterisks highlight combinations, other than the positive SepJ/SepJ control, that were significantly different to the control at $P < 0.005$. The complete set of quantitative data is shown in Table 3.7.

Table 3.7. Quantification of interactions between SjcF1 and septal proteins SepJ, FraC and FraD assessed by BACTH analysis. The mean and standard deviation of the results from the number of independently isolated transformants indicated (*n*) are presented. The difference between strains carrying each plasmid combination and the T18/T25 plasmid pair was tested by the Student's *t* test (*P* indicated in each case); asterisks and garnet color highlight differences significant at $P \leq 0.005$.

T18 fusion	T25 fusion	β-Galactosidase activity [nmol ONP (mg protein)$^{-1}$ min^{-1}]	Student's t test
T18	T25	6.85 ± 0.89 (5)	
SepJ-T18	T25	8.11 ± 0.43 (3)	0.0663
T18	SepJ-T25	7.88 ± 0.66 (3)	0.1371
T18	T25-SjcF1	7.91 ± 0.14 (3)	0.0961
T18	FraC-T25	8.92 ± 1.74 (3)	0.0631
T18	T25-FraD	8.07 ± 1.04 (3)	0.1262
T18-SjcF1	T25	7.97 ± 0.20 (3)	0.0833
FraC-T18	T25	8.07 ± 1.52 (3)	0.1931
T18-FraD	T25	8.98 ± 0.75 (3)	0.0137
SepJ-T18	SepJ-T25	204.86 ± 48.54 (10)	2 E-10*
SepJ-T18	T25-SjcF1	11.04 ± 1.75 (7)	0.0006*
T18-SjcF1	SepJ-T25	10.12 ± 1.28 (5)	0.0015*
FraC-18	T25-SjcF1	10.09 ± 1.70 (7)	0.0031*
T18-SjcF1	FraC-T25	9.78 ± 1.58 (7)	0.0041*
T18-FraD	T25-SjcF1	8.82 ± 1.63 (7)	0.0353
T18-SjcF1	T25-FraD	9.16 ± 1.21 (5)	0.0089
T18-SjcF1	T25-SjcF1	8.53 ± 0.33 (4)	0.0094

3.2.3.3. Interaction with peptidoglycan

A predicted topology of SepJ shows that the coiled-coil and linker domains are located in the periplasm (Flores *et al.*, 2016; Herrero *et al.*, 2016), although such location has been challenged (Omairi-Nasser *et al.*, 2015). In the places where SepJ is likely located, perforations traversing the septal peptidoglycan layers are found (Wilk *et al.* 2011; Nürnberg *et al.*, 2015). It is thought that SepJ, traversing those perforations, makes a communication conduit (Herrero *et al.*, 2016). We inquired whether, as is the case for SjcF1, SepJ could interact directly with peptidoglycan.

To test for a SepJ-peptidoglycan interaction, the entire SepJ protein and its coiled-coil domain were produced in *E. coli* as His_6–tagged proteins and purified as described above (*Mat&Meth* section 2.5.1.2). Murein sacculi (peptidoglycan) were isolated from *Anabaena* grown in BG11 medium also as described in *Mat&Meth* section 2.6.3.1. The protocol described in 2.6.3.2 and summarized in Fig 3.30.A was followed and, as negative controls, bovine serum albumin (BSA) and horseradish peroxidase (HRP) were used. The same amount of each protein (in molar terms) was incubated with a fixed amount of peptidoglycan as indicated in the legend to Fig. 3.30. Samples were then subjected to centrifugation (170,000 x *g*), and the precipitate, containing peptidoglycan and putative interacting proteins, was washed to minimize non-specific interactions. Samples were then analyzed by SDS-PAGE (Fig. 3.30.B) and protein content of the peptidoglycan precipitates was quantified. Both the entire SepJ protein and the coiled-coil domain were

present in the sedimented fraction of peptidoglycan. Controls without peptidoglycan, or with BSA or HRP instead of SepJ, did not show protein precipitation. (Fig. 3.30.B). These results show that SepJ interacts with the peptidoglycan, and that the coiled-coil domain alone can also interact.

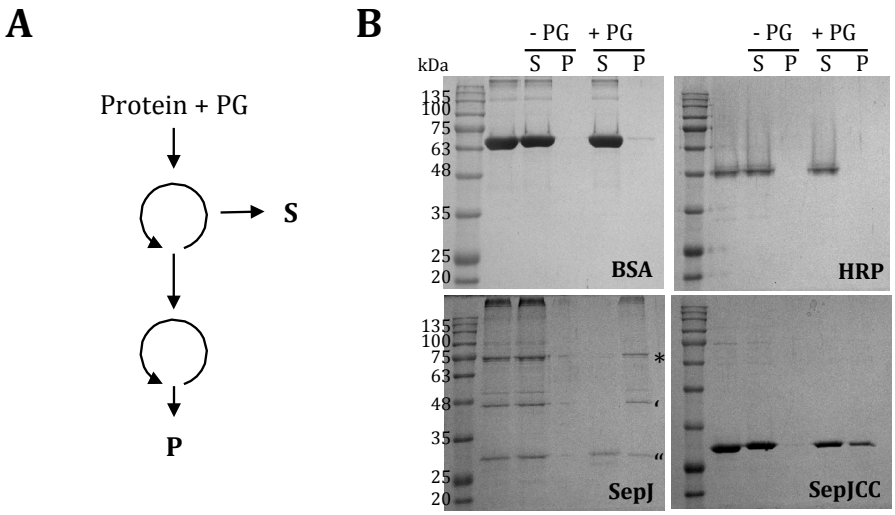

Fig. 3.30. Analysis of the SepJ-peptidoglycan interaction. (A) Schematic of the procedure used. An amount of 30 µL of a peptidoglycan preparation (OD_{600} 0.83) was mixed with 20 µL of the indicated protein to give a final concentration of 5 µM and incubated at room temperature for 1 h under gentle shaking. The mixture was then centrifuged at 170,000 *x g* for 30 min. The precipitate was resuspended in PBS containing 1% DDM and collected again by centrifugation. **(B)** The first supernatant (S), where proteins unbound to peptidoglycan remain, and the second precipitated peptidoglycan (P) were loaded into SDS-PAGE gels, and after electrophoresis the gels were stained with Coomasie Blue G-250. The first line in each gel contains a sample of the protein added to the incubation. The identity of the proteins was confirmed by MALDI-TOF. In the SepJ SDS-PAGE gel: *, full-length SepJ protein (determined MW, 79.4 kDa; expected MW, 82 kDa); ' and ", degradation products of estimated 50.9 and 30.9 kDa, respectively, that together make a full-length SepJ protein. PG, peptidoglycan.

Quantification of protein in the samples subjected to SDS-PAGE is shown in Table 3.8. The amount of protein in fraction S, corresponding to unbound proteins, and in fraction P, corresponding to peptidoglycan-bound proteins, was quantified by the Lowry assay. As peptidoglycan reacts giving increased absorbance, we corrected the samples containing protein and PG for the presence of peptidoglycan. A significant percentage of SepJ (about 65%) was bound to the peptidoglycan, and the ability of binding peptidoglycan was also significant for the isolated coiled-coil domain, since 55% of the added amount was recovered with the peptidoglycan. A very small percentage of control proteins (5%) were found together with the peptidoglycan in the precipitates, indicating that the interactions with SepJ and the coiled-coil domain were specific.

Table 3.8. Quantification of protein in each fraction after the peptidoglycan-binding assay. The amount of protein present in the first supernatant (S) and in the precipitated fractions (P) was quantified by the Lowry assay (mean ± SD from three technical replicates). Samples containing only isolated PG with no added protein were also quantified and the resulting estimation (7.33 ± 0.44 µg of protein) was subtracted to those fractions that contained PG in order to avoid overestimation of the amount of protein. The percentage of protein is presented relative to the amount added to the assay. Asterisks indicate those conditions in which the amount of protein in Fraction P was significantly different from that found in the BSA control (assessed by Student's *t* test, $p < 0.05$). PG, peptidoglycan.

		Protein in each fraction (µg)		
		Initial	Fraction S	Fraction P
BSA	- PG	8.96 ± 0.41	6.53 ± 0.21 (73%)	0.07 ± 0.09 (1%)
	+ PG	8.96 ± 0.41	4.02 ± 0.40 (45%)	0.41 ± 0.77 (5%)
HRP	- PG	6.65 ± 0.39	4.05 ± 0.40 (61%)	0.11 ± 0.18 (2%)
	+ PG	6.65 ± 0.39	4.10 ± 0.30 (62%)	0.32 ± 0.24 (5%)
SepJ	- PG	10.54 ± 0.77	9.90 ± 3.21 (94%)	0.08 ± 0.10 (1%)
	+ PG	10.54 ± 0.77	3.45 ± 0.60 (33%)	6.90 ± 1.80 (65%)*
Coiled-coil	- PG	3.67 ± 1.07	2.67 ± 0.84 (73%)	0.36 ± 0.58 (10%)
	+ PG	3.67 ± 1.07	1.55 ± 0.31 (42%)	2.01 ± 0.34 (55%)*

3.3. ROLE OF THE SepJ PERMEASE DOMAIN IN INTERCELLULAR COMMUNICATION

3.3. ROLE OF THE SepJ PERMEASE DOMAIN IN INTERCELLULAR COMMUNICATION

SepJ has been suggested to be involved in intercellular molecular transfer providing a path for the exchange of small water-soluble compounds. To trace intercellular molecular transfer in *Anabaena*, fluorescent makers such as calcein and 5-carboxifluorescein (5-CF) have been used (Mullineaux *et al*., 2008; Mariscal *et al*., 2011). Whereas a knock-out mutant of *fraC* and *fraD*, the genes encoding two other important septal proteins, is similarly impaired in transfer of 5-CF and calcein (Nürnberg *et al.*, 2015), a knock-out mutant of *sepJ* is more affected in the transfer of calcein than of 5-CF (Mariscal *et al*., 2011; Nürnberg *et al.*, 2015). This and other observations suggest that at least two types of communication conduits may exist in *Anabaena*, one related to SepJ and one related to FraC and FraD (Merino-Puerto *et al.*, 2011), and that calcein is a good tracer to test intercellular transfer mediated by SepJ-related conduits.

In addition to impaired transfer of calcein, a knock-out *sepJ* mutant arrests heterocyst differentiation at an early stage (Flores *et al*., 2007), indicating that SepJ could play a role mediating exchange of signals involved in heterocyst differentiation. Evidences for the involvement of SepJ in the transfer of diffusible regulatory signals have already been published (Rivers *et al*., 2014; Corrales-Guerrero *et al.*, 2015; Mariscal *et al*., 2016).

SepJ bears an integral membrane domain, which shows similarity to proteins of the Drug/Metabolite Transporter (DMT) superfamily (Jack *et. al*., 2001), specifically to the Drug/Metabolite Exporter (DME) family (Transporter Classification Database (TCDB) number 2.A.7.3). Proteins belonging to this group are involved in efflux of metabolites and different sorts of toxic compounds (Jack *et al*., 2001). In this part of the work, we addressed the SepJ communication function by studying its permease domain in detail. We first generated a *sepJ* mutant lacking most of its permease domain, containing only the first transmembrane segment. We used this strain as recipient to reconstruct the entire protein with versions of the permease domain containing point mutations or deletions, looking for mutants that discriminate between the cell-cell binding and communication functions of SepJ.

3.3.1. Analysis of the SepJ permease domain

The permease domain of the *Anabaena* SepJ protein extends from residue 412 to residue 751 of the protein. To gain a better understanding of this domain, we analyzed its possible topology by 6 different prediction programs (Table 3.9). Predictions of 9, 10 or 11 transmembrane segments (TMS) were generated depending on the program used. Some programs did not predict TMS1 and TMS3. However, most programs predicted quite consistently the last 8 TMSs. We selected the model of 11 TMSs, predicted by the TMHMM program (Fig. 3.31), because available experimental evidence supports this topology (Flores *et al.*, 2016; Herrero *et al.*, 2016). Thus, a SepJ-GFP-mut2 fusion (Flores *et al*., 2007) and BACTH analysis (see Results section 3.2.2) support a cytoplasmic localization of the C-terminus of SepJ, and interaction of SepJ with with FtsQ, SjcF1 and PG (see Results sections 3.2.2 and 3.2.3) supports the placement of the N-terminal part of the protein in the periplasm. The topological model shown in Fig. 3.31 indicates that the permease domain could be composed of two regions, the first one denoted TM1 and including the

first three TMSs, which are topologically less conserved, and the second one denoted TM2 and including the last eight TMSs, which is topologically very conserved.

Table 3.9. Prediction of the transmembrane segments in *Anabaena* SepJ. The program used and the position of the individual TM segments are indicated (see also Rudolf *et al.*, 2015).

Program	TM1	TM2	TM3	TM4	TM5	TM6	TM7	TM8	TM9	TM10	TM11
TMHMM	412 434	446 465	469 488	512 534	539 561	566 588	592 614	626 648	663 685	692 714	719 738
PHOBIUS	413 433	453 479		512 534	540 560	567 585	597 615	627 649	661 682	694 713	719 738
TMPred		434 452	483 506	538 557	559 581	594 614	618 637	650 671	683 704	718 735	744 760
TM-Finder	414 435	443 480		515 534	541 559	571 587	600 619	628 644	664 682	699 735	
HMMTOP		435 454	481 504	535 554	561 580-	593 612	617 635	648 667	684 702	715 734	739 758
DAS	415 430	458 481		518 534	540 556	575 584	600 616	628 646	664 681	697 713	721 734

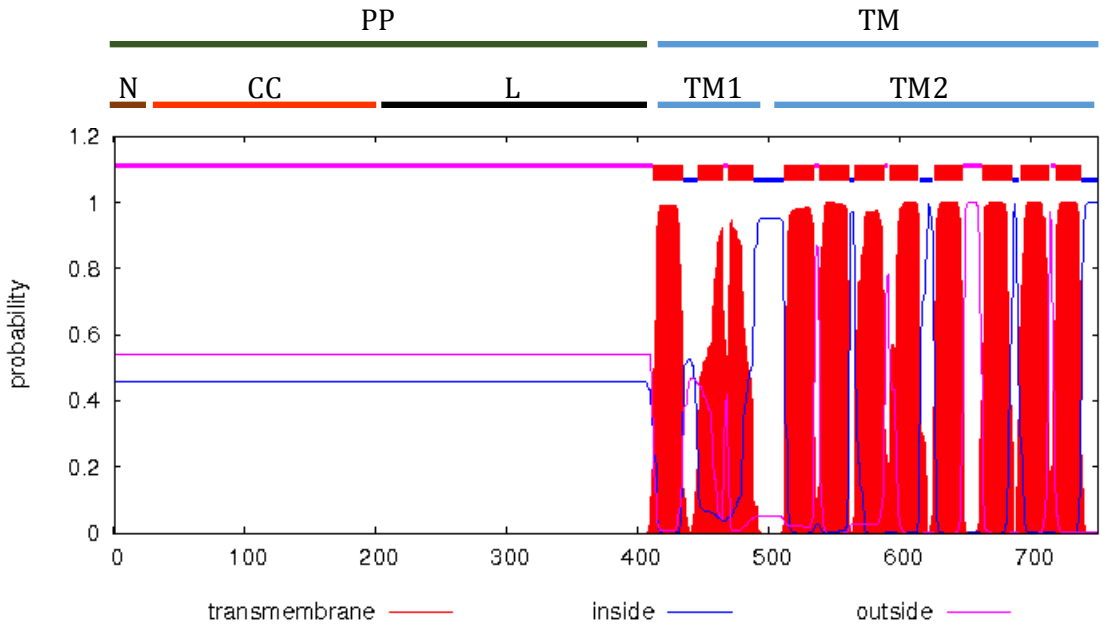

Fig. 3.31. Topological model for *Anabaena* SepJ according to TMHMM prediction. The predicted periplasmic section is indicated as PP and it would be composed of the conserved N-terminal sequence (N), the coiled-coil domain (CC) and the linker domain (L). The integral membrane section is indicated as TM (for transmembrane). Analysis of SepJ from many cyanobacterial strains showed that the region indicated as TM1 is topologically less conserved than the TM2 region, which is predicted by most of the programs to include 8 transmembrane segments. In our model, the eleven TMSs correspond to the amino acid residues indicated in Table 3.9 (TMHMM).

Alignment of the SepJ permease domain or a homologous protein from other representative cyanobacteria belonging to sections I to V shows that the permease domain is very conserved. Except for the case of *Cylindrospermopsis raciborskii* that would produce a shorter protein that lacks the last four TMSs (Plominsky *et al.*, 2015), most of the proteins show 9, 10 or 11 TMSs. Homology to proteins in the Drug/Metabolite Exporter

(DME) Family (TCDB number 2.A.7.3), in particular to EamA, also known as YdeD, is most evident in the last part of the permease, from residue 597 to the end of the protein.

Alignment of SepJ from heterocyst-forming cyanobacteria shows that it is a very conserved protein. Fig. 3.32 shows a phylogenetic tree of SepJ from heterocyst-forming cyanobacteria using SepJ from the non-heterocyst former *Trichodesmium erythraeum* as outgroup. All the SepJ homologs from heterocyst-forming cyanobacteria form a consistent group. This phylogenetic tree captures the general evolution of cyanobacteria, grouping together SepJ proteins from cyanobacteria of Section V (*Fischerella*, *Mastigocladus* and *Chlorogloeopsis*) and putting close to each other those that belong to the Nostocaceae (including *Nostoc* and *Anabaena*). Fig. 3.33 shows an alignment of the permease domains of SepJ from 35 heterocyst-forming cyanobateria, illustrating that about 1/3 of the amino acid residues are highly conserved.

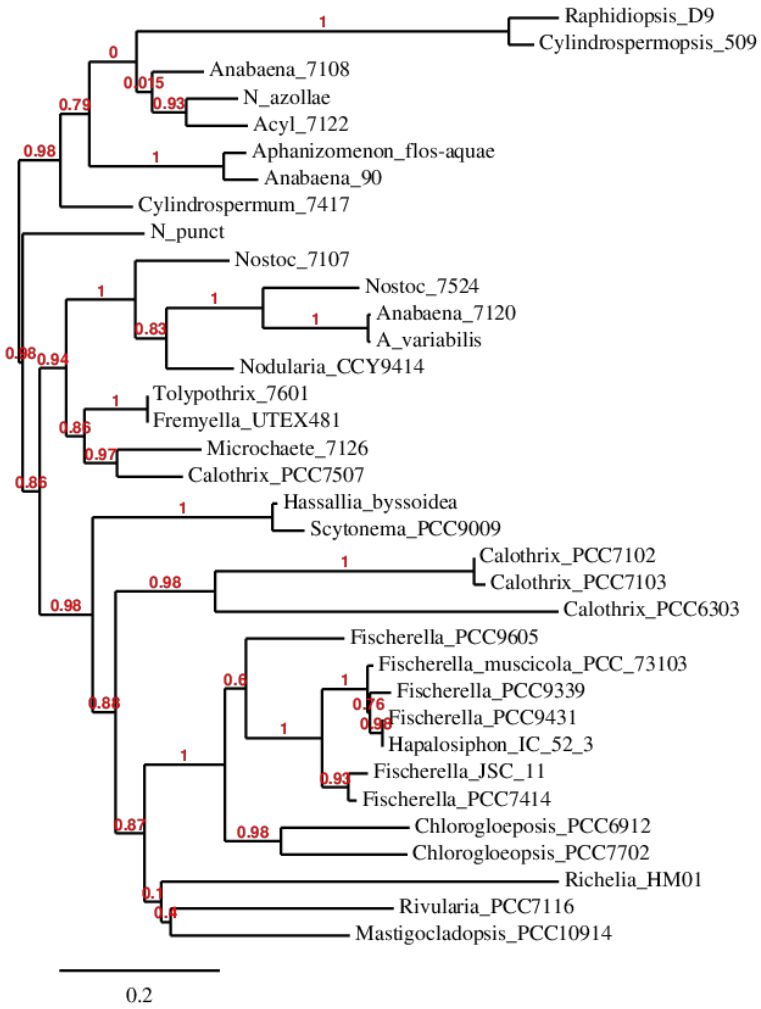

Fig. 3.32. Phylogenetic tree of SepJ proteins from heterocyst-forming cyanobacteria. Sequence of SepJ from the indicated cyanobacteria were aligned and analyzed using the program at www.phylogeny.fr with default parameters. Red numbers are bootstrap values.

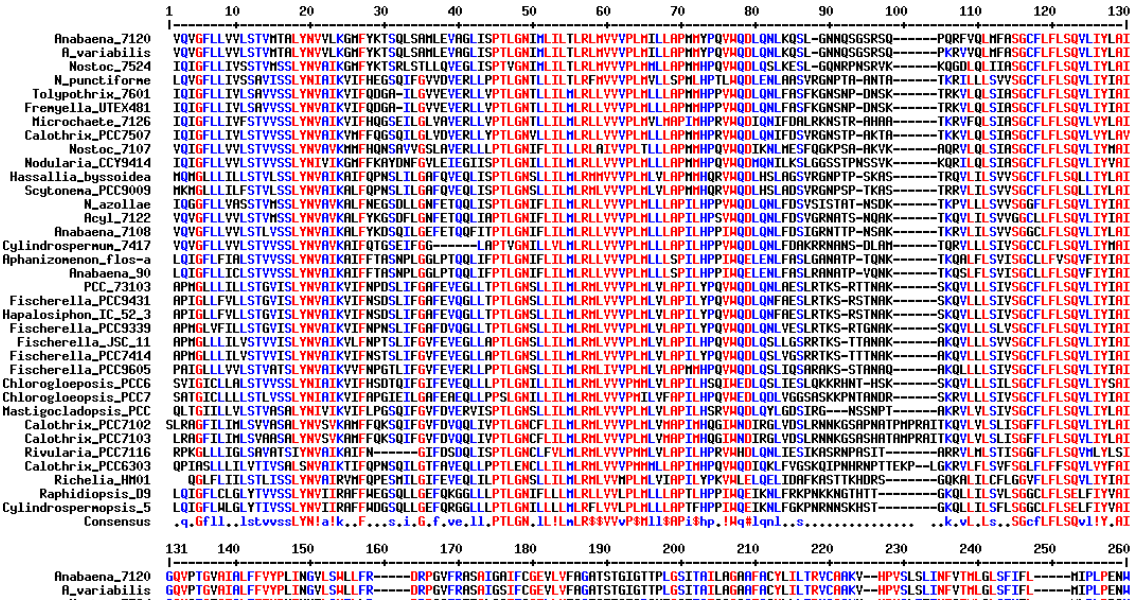

Fig. 3.33. Alignment of the permease section of SepJ from 35 heterocyst-forming cyanobacteria. The sequence of strain PCC 7120 SepJ includes amino acid residues 412 to 751. The alignment was performed at MultAlin (http://multalin.toulouse.inra.fr/multalin/) with default parameters. Color code: red, amino acid residues conserved in more than 90% of the sequences; blue, amino acid residues conserved in more than 50% but less than 90% of the sequences. The SepJ proteins aligned are from the following cyanobacteria: *Anabaena* sp. PCC 7120, *Anabaena variabilis* ATCC29413, *Nostoc* sp. PCC 7524, *Nostoc punctiforme* PCC 73102, *Tolypothrix* sp. PCC

7601, *Fremyella diplosiphon* UTEX 481, *Microchaete* sp. PCC 7126, *Calothrix* sp. PCC 7507, *Nostoc* sp. PCC 7107, *Nodularia spumigena* CCY9414, *Hassallia byssoidea*, *Scytonema* sp. PCC 9009, *Nostoc* (*Anabaena*) *azollae*, *Anabaena cylindrica* PCC 7122, *Anabaena* sp. PCC 7108, *Cylindrospermum stagnale* PCC 7417, *Aphanizomenon flos-aquae*, *Anabaena* sp. 90, *Fischerella muscicola* PCC 73103, *Fischerella* sp. PCC 9431, *Hapalosiphon* sp. IC-52-3, *Fischerella* sp. PCC 9339, *Fischerella* sp. JSC-11, *Fischerella* sp. PCC 7414, *Fischerella* sp. PCC 9605, *Chlorogloeopsis* sp. PCC 6912, *Chlorogloeopsis* sp. PCC 7702, *Mastigocladopsis* sp. PCC 10914, *Calothrix* sp. PCC 7102, *Calothrix* sp. PCC 7103, *Rivularia* sp. PCC 7116, *Calothrix* sp. PCC 6303, *Richelia intracellularis* HH01, *Raphidiopsis brookii* sp. D9, *Cylindrospermopsis* sp. 509.

3.3.2. Construction and characterization of a mutant expressing a permease-deleted version of SepJ

In the *Anabaena* chromosome, *sepJ* (ORF *alr2338*) occupies positions 2,818,434 to 2,820,689 (2,256 bp including its stop codon) (Kaneko *et al.*, 2001). To gain a better understanding of the function of the different domains of SepJ, mutants producing SepJ with deleted domains have been generated and analyzed (Mariscal *et al.*, 2011). One of those mutants contained a SepJ version lacking two transmembrane segments of the permease domain. That strain produced an aberrant SepJ protein that was found in the cytoplasm instead of in the cytoplasmic membrane at the cell poles (Mariscal *et al.*, 2011). We aimed at constructing a new SepJ version lacking most of the permease domain but keeping the coiled-coil domain, the linker domain and the first predicted TMS of the permease ($SepJ_{\Delta 463\text{-}748}$; Fig. 3.34).

A

>SepJ(Δ463-748)
MGRFEKRPDNDPRVRGELSRAAETALWAVVEDLESLQQNVLRSFQEEIKKLQ
TEKDRLTDEVQQLIEEKEHLQEVRRITEQQVLIRQLSEALAKHICSQLQSSLAKI
ANQTESQIAALKSAQSIGPAIENNEQVEKMLGSLDDNLTIAFNSLQQELKNYQS
NLSQQLSRMYNQQQQGETIVEELIDRLRGELTRAIQETSTAKAQLSPPTVLQP
PELQPPSSPVVVNLSPPTVLQFPDQQSPNPLQASTPLEETSTTKPSVSITPPEK
STPVTIVPPPQETRPETKSVIPKVSPDSETKLQSSQEKAAEPSSVINRELSAGA
AKSPLTPEKPPEPISTSKTKFSPSSEKPPEPISTSKTKFSPSSEKPPEPVSVLSR
DSSASKASTPPPAPVVRRGSTPSSSRSRKSSNLSPVQVGFLLVVLSTVMTALY
NVVLKGMFYKTSQLSAMLEVAGLISPTLGNIMNSNAEG

B

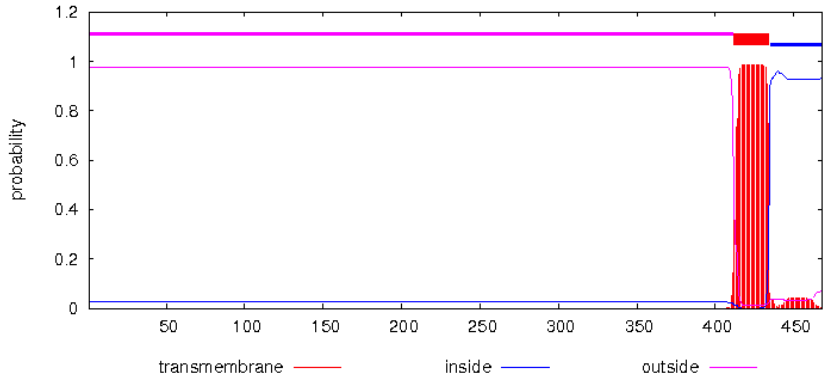

Fig. 3.34. SepJ protein bearing a deletion in the permease domain ($SepJ_{\Delta 463\text{-}748}$). (A) Sequence of the SepJ version produced by strain CSVM90. The coiled-coil domain is highlighted in red, and the liker domain in green. A three-amino-acid-residue insertion (NSN) is present in this protein as a result of the construction of the plasmid. (B) TMHMM prediction of the only transmembrane segment present in the $SepJ_{\Delta 463\text{-}748}$ protein.

For construction of strain CSVM90, a 5' fragment from the *sepJ* gene was amplified by PCR using primers alr2338-25 and alr2338-30, and a 3' fragment using primers alr2338-29 and alr2338-34 (Table 2.6). Both fragments were digested with EcoRI, ligated, and the resulting product was amplified using primers alr2338-25 and alr2338-34. The PCR product was digested with SpeI/XbaI and cloned in XbaI-digested vector pCSRO, which can be mobilized by conjugation and bears an Ω cassette, which confers resistance to Sm and Sp, and the *sacB* gene for positive selection (see *Mat&Meth* section 2.4.2). The resulting plasmid, pCSVM90, was transferred to *Anabaena* by conjugation. Exconjugants were selected by their resistance to Sm and Sp and double recombinants were then selected by their resistance to sucrose (Fig. 3.35). The presence of only mutant chromosomes was tested by amplifying the genomic region and sequencing of the amplified product. It could be confirmed that strain CSVM90 contained only mutant chromosomes (bearing the deleted version of *sepJ*) and no further mutations in *sepJ*.

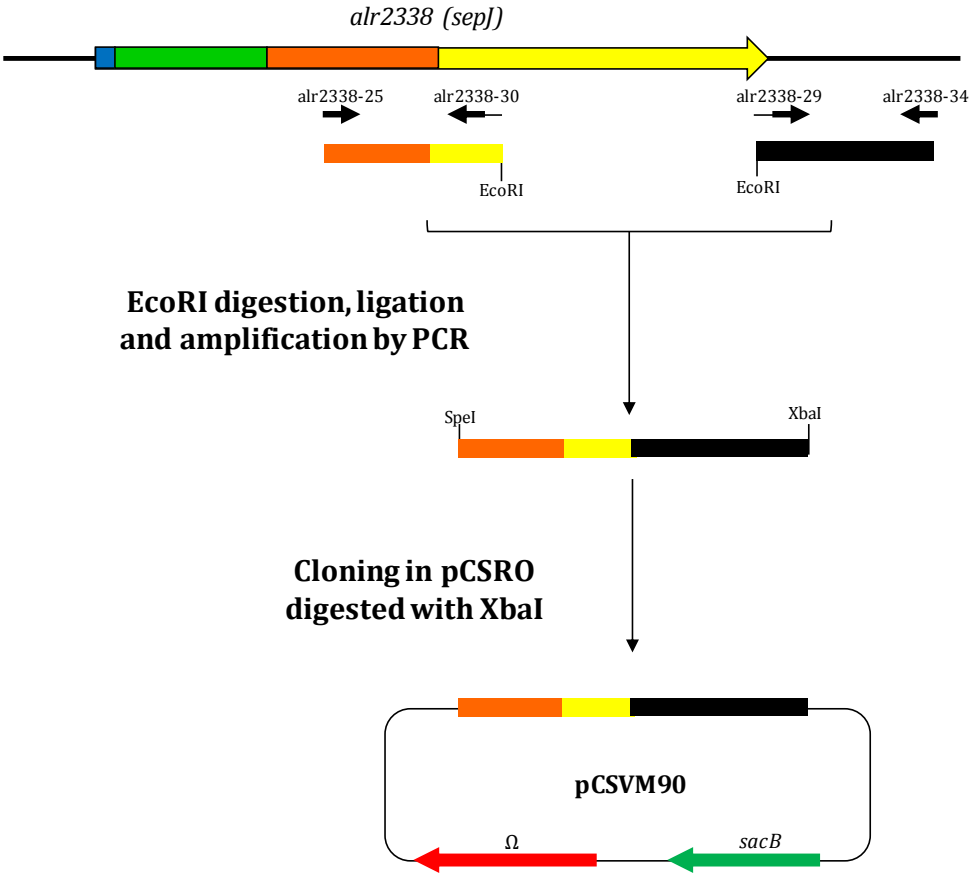

Fig. 3.35. Construction of the plasmid used for generation of *Anabaena* strain CSVM90. Two fragments from *sepJ* were amplified using primers alr2338-25/alr2338-30 (fragment encoding part of the linker domain and the first predicted TMS) and alr2338-29/alr2338-34 (encoding the 3' end and downstream region of *sepJ*). Both fragments were digested with EcoRI, ligated and the product was amplified using alr2338-25 and alr2338-34. The PCR product was digested with SpeI and XbaI and cloned in XbaI-digested pCSRO generating plasmid pCSVM90 that was transferred to *Anabaena* by conjugation. Double recombinants were selected as described in the text and *Mat&Meth* section 2.4.2.

To characterize the phenotype of CSVM90 ($SepJ_{\Delta 463\text{-}748}$), diazotrophic growth and nitrogenase activity were assessed using strain PCC 7120 (wild type) as a positive control

and strain CSVM34 (Δ*sepJ*) as a negative control. Strain CSVM90 ($SepJ_{\Delta 463-748}$) did not grow under diazotrophic conditions, neither in solid nor in liquid $BG11_0$ medium (Fig. 3.36). Nitrogenase activity was analyzed in cultures incubated for 48 h in $BG11_0$ medium. Strain CSVM90 ($SepJ_{\Delta 463-748}$) did not show any nitrogenase activity (Table 3.11).

We also addressed whether the deletion in $SepJ_{\Delta 463-748}$ influenced any of the two main SepJ functions: cell-cell anchoring and intercellular communication. Inspection of filaments from strain CSVM90 ($SepJ_{\Delta 463-748}$) showed that they were short in the presence of nitrate as nitrogen source, and they were extensively fragmented under nitrogen deprivation (Fig. 3.37). To study further the cell-cell anchoring function, filament length was studied in strain CSVM90 ($SepJ_{\Delta 463-748}$) in comparison to the wild-type and the SepJ deletion mutant CSVM34 in BG11 medium and after 48 h of incubation in $BG11_0$ medium (Fig. 3.38 and Fig. 3.39). Both in BG11 and $BG11_0$ medium, strain CSVM90 ($SepJ_{\Delta 463-748}$) showed a pattern of filament sizes similar to that of strain CSVM34 (Δ*sepJ*). To study the function of intercellular transfer, we measured intercellular transfer of calcein in BG11-grown filaments of the three strains (Table 3.10). Calcein transfer was clearly impaired in both strains, CSVM34 and CSVM90, but CSVM90 showed a higher recovery constant than CSVM34. These results indicate that strain CSVM90 ($SepJ_{\Delta 463-748}$) is impaired in intercellular transfer of calcein but not as much as a deletion mutant of *sepJ*.

The subcellular location of $SepJ_{\Delta 463-748}$ was then investigated to try to understand if the phenotype observed in strain CSVM90 resulted from an improper localization or lack of production of the protein. The localization of SepJ in strain CSVM90 ($SepJ_{\Delta 463-748}$) was studied by immunofluorescence using antibodies raised against the SepJ coiled-coil domain. The wild-type strain and the *sepJ* deletion mutant CSVM34 were used as controls (Fig. 3.40). SepJ was localized at the cell poles in filaments of the wild-type strain whereas it was observed scattered apparently in the surface of the cells (and sporadically in the intercellular septa) in strain CSVM90. No SepJ signal was detected in filaments of strain CSVM34 (Δ*sepJ*), corroborating that signals observed in strain CSVM90 ($SepJ_{\Delta 463-748}$) were not unspecific. These results indicate that CSVM90 ($SepJ_{\Delta 463-748}$) shows an impaired SepJ localization.

We also looked at septal peptidoglycan nanopores in strain CSVM90. The occurrence of these structures has been associated with the presence of SepJ in the septum (Nürnberg *et al*., 2015; Mariscal *et al.*, 2016). Murein sacculi (peptidoglycan) from filaments of strain CSVM90 grown in BG11 medium were isolated and visualized by transmission electron microscopy (Fig. 3.41). Strain CSVM90 ($SepJ_{\Delta 463-748}$) produced a low number of nanopores, which was nonetheless about 2-fold higher than the number in the *sepJ* deletion strain CSVM34 (Nürnberg *et al*., 2015). Diameter of nanopores in strain CSVM90 was not significantly different from that of a control strain (see below, Table 3.10).

From the phenotypic analysis of strain CSVM90 ($SepJ_{\Delta 463-748}$) it can be concluded that the permease domain of SepJ is necessary for the proper subcellular localization of the protein. Likely as a consequence of improper localization of SepJ, strain CSVM90 produces a low number of septal peptidoglycan nanopores and shows decreased intercellular transfer of calcein.

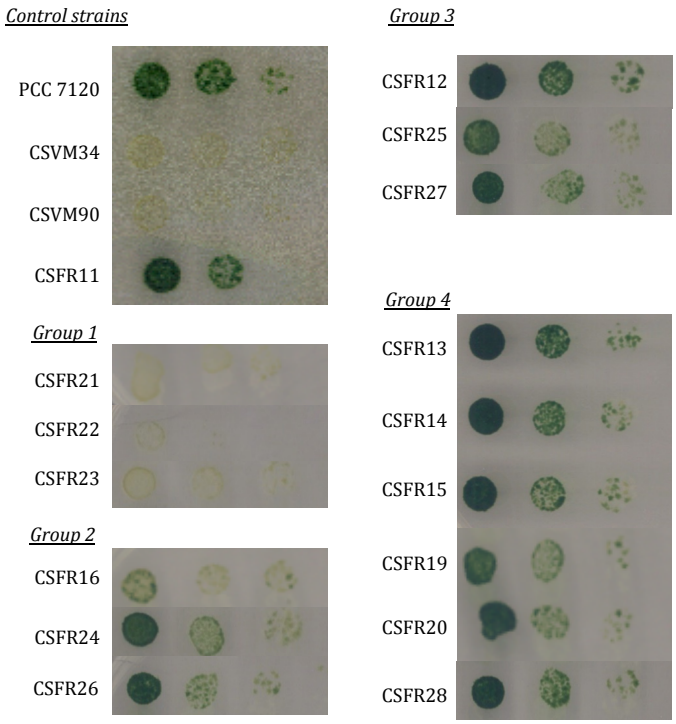

Fig. 3.36. Growth of *Anabaena* strains on solid BG11$_0$ medium. Filaments of the indicated strains grown in BG11 medium, containing antibiotics in the case of CSFR mutants, were washed, resuspended in BG11$_0$ medium at 1 μg of Chl ml^{-1}, and 5 μL of successive dilutions were spotted on solid BG11$_0$ medium. Photographs were taken after 10 days of incubation under growth conditions. Definitions of the groups are detailed in the text.

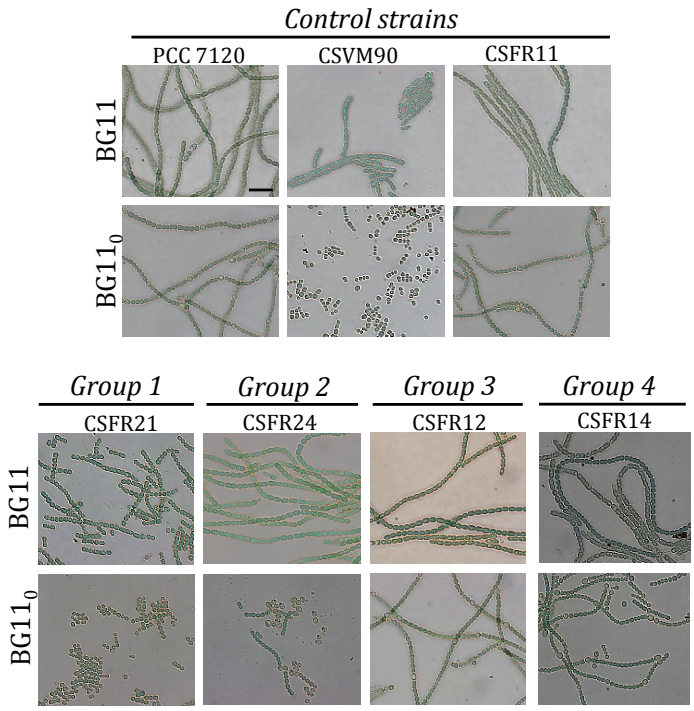

Fig. 3.37. Appearance of filaments of *Anabaena* strains grown in liquid BG11 or BG11$_0$ medium. Micrographs showing filaments of strains PCC 7120 (wild type) and CSVM90, as well as examples of phenotypic groups 1, 2, 3 and 4, grown in BG11 medium or incubated in BG11$_0$ for 48 h. Definitions of the groups are detailed below. Scale bar 10 μm.

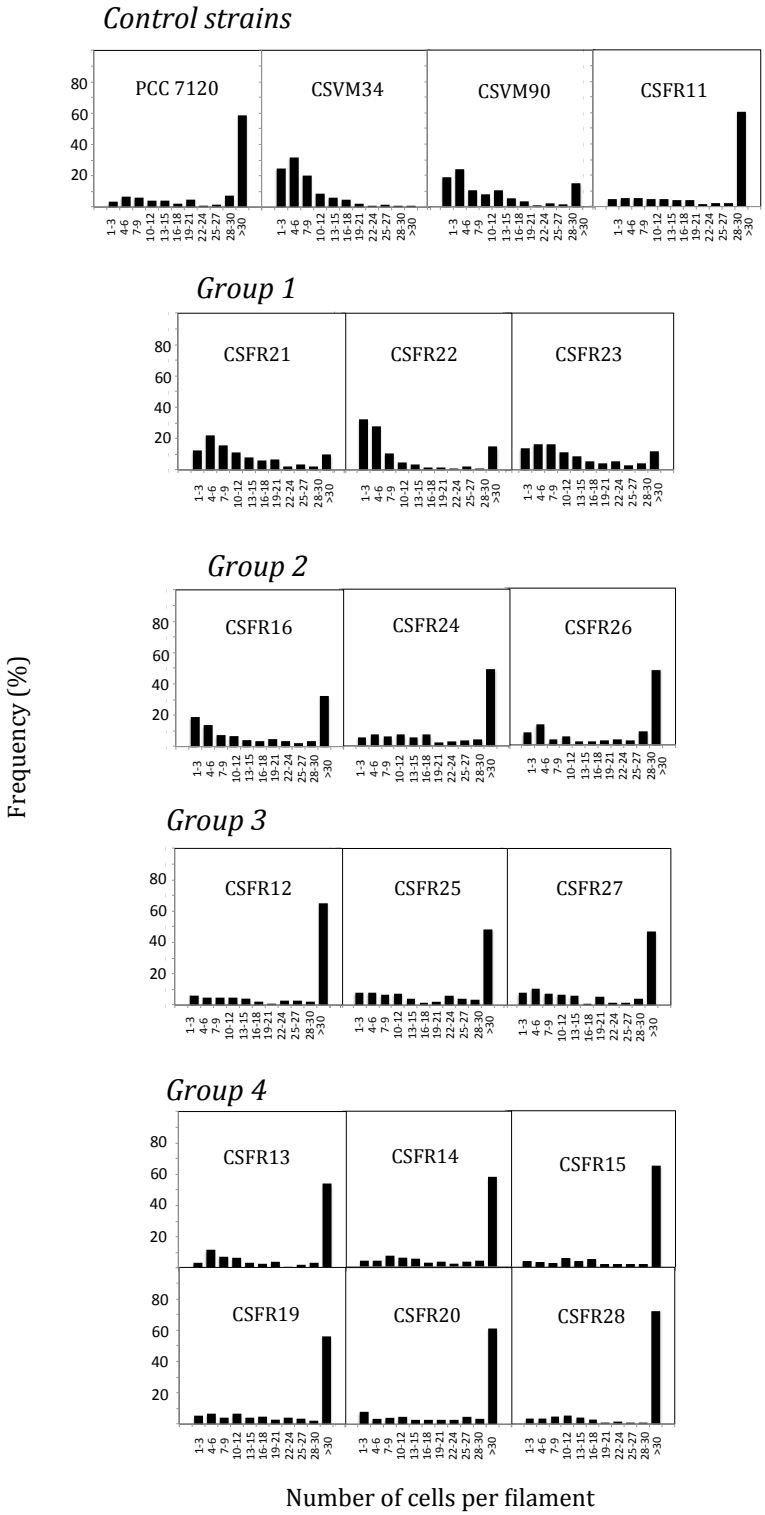

Fig. 3.38. Filamentation phenotype of *Anabaena* strains in BG11 medium. Samples from filaments grown in BG11 medium, containing antibiotics in the case of CSFR mutants, were harvested, observed by light microscopy and photographed. The number of cells per filament were counted. Graphs show the percentages of filaments with the indicated lengths. Definitions of the groups are detailed in the text.

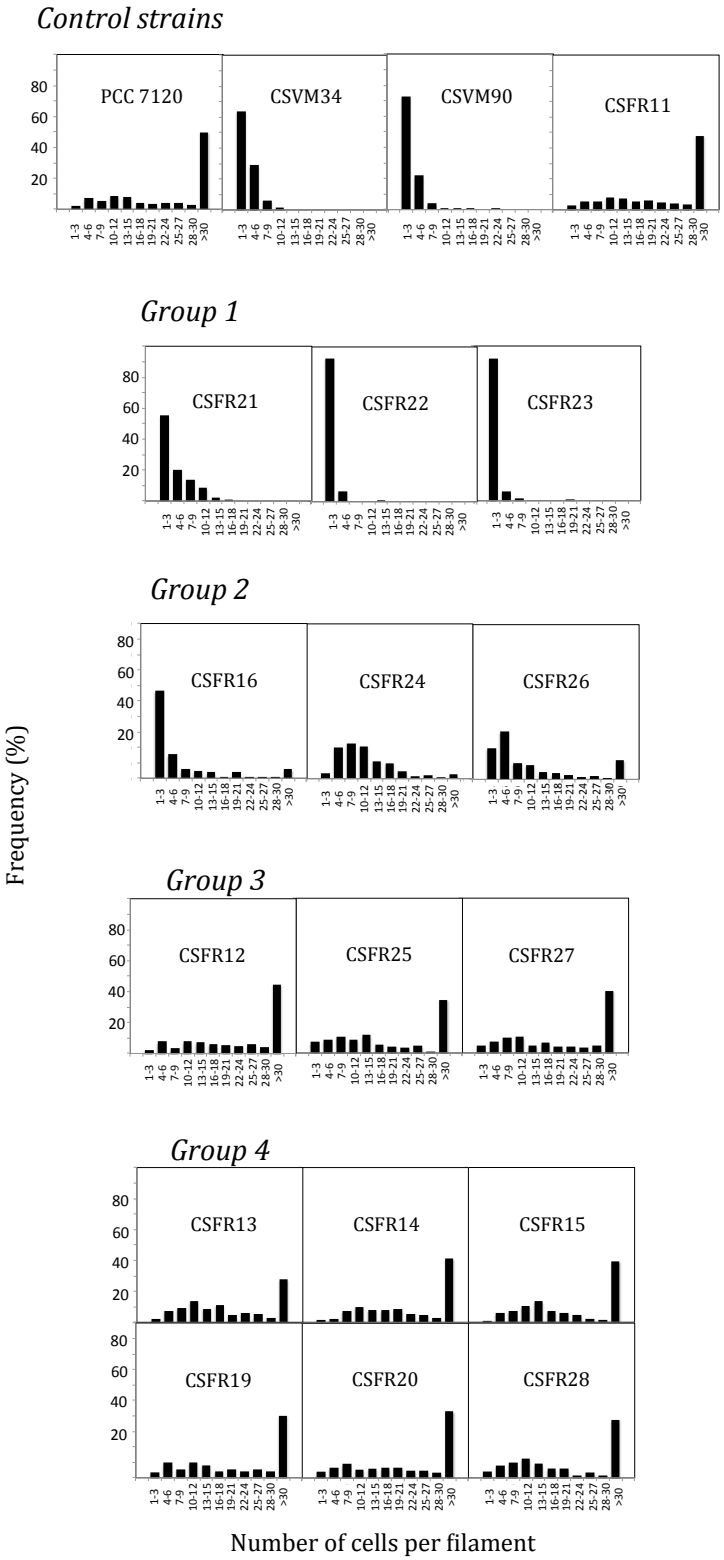

Fig. 3.39. Filamentation phenotype of *Anabaena* strains in $BG11_0$ medium. Filaments grown in BG11 medium were harvested, washed and re-inoculated at 1 μg of Chl ml^{-1} in $BG11_0$ medium. Micrographs were taken after 48 h of incubation in $BG11_0$ medium and the number of cells per filament were counted. Graphs show the percentages of filaments with the indicted lengths. Definitions of the groups are detailed in the text.

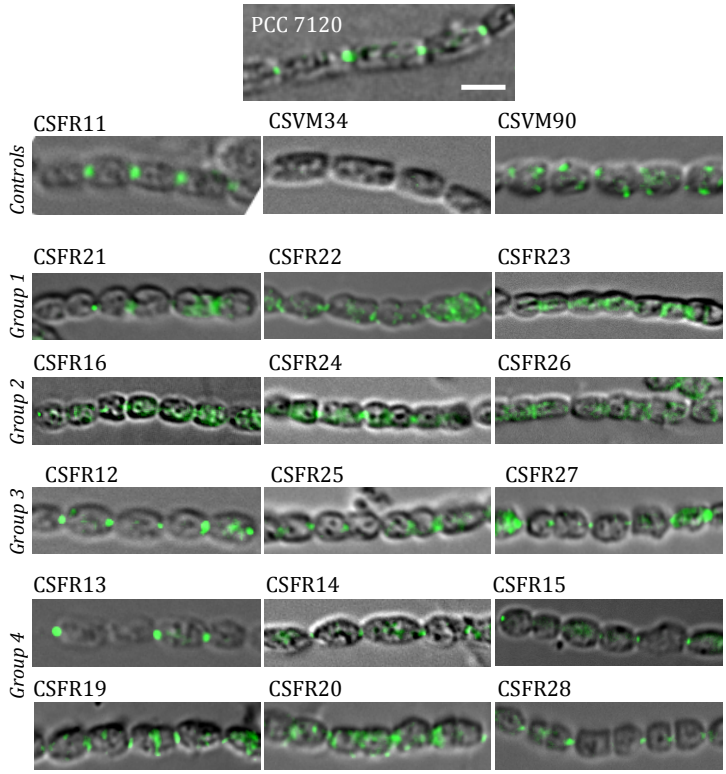

Fig. 3.40. SepJ localization in *Anabaena* strains. Filaments grown in BG11 medium were fixed and incubated with antibodies raised against the coiled-coil domain of the *Anabaena* SepJ protein as described in *Mat&Meth* section 2.7.2, and signals were visualized by fluorescence microscopy. Scale bar, 3 µm.

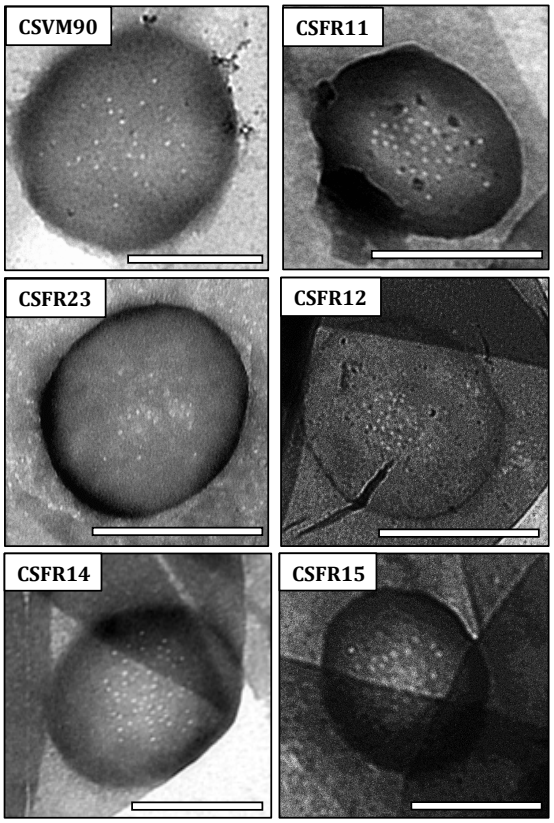

Fig. 3.41. Nanopore formation in *Anabaena* strains. Transmission electron micrographs showing septal peptidoglycan disks from strains CSVM90, CSFR11, CSFR23 (representative of Group 1), CSFR12 (representative of Group 3) and CSFR14 and CSFR15 (Group 4 representatives). PG was isolated from filaments grown in BG11 medium containing antibiotics for the CSFR strains. The number of nanopores and nanopore diameter are indicated in Table 3.10. Size bar, 1 µm.

Table 3.10. Filamentation phenotype, calcein transfer and nanopore analysis in *sepJ* mutant strains.

Strain (Genotype or SepJ protein)	Filamentation[a]		Calcein transfer[b]	Nanopores[c]	
	(BG11)	($BG11_0$)		Number per disk	Diameter (nm)
Controls					
PCC 7120 (WT)	+	+	0.034 ± 0.015	52.3 ± 6.2[d]	18.5 ± 3.5[f]
CSVM34 (Δ*sepJ*)	-	-	0.009 ± 0.004**	14.0 ± 7.6[e]	16.8 ± 5.0 [e]
CSVM90 ($SepJ_{\Delta 463-748}$)	-	-	0.018 ± 0.007**	27.3 ± 10.1 (9)*	14.3 ± 4.4 (52)
CSFR11 (SepJ)	+	+	0.048 ± 0.008	44.8 ± 6.3 (9)	15.4 ± 3.5 (57)
Group 1					
CSFR21 ($SepJ_{A542R}$)	-	-	0.038 ± 0.007		
CSFR22 ($SepJ_{\Delta 739-751}$)	-	-	0.032 ± 0.007		
CSFR23 ($SepJ_{\Delta 626-751}$)	-	-	0.044 ± 0.008	24.6 ± 10.1 (11)*	19.4 ± 12.3 (44)*
Group 2					
CSFR16 ($SepJ_{H624A}$)	[+]	-	0.013 ± 0.006**		
CSFR24 ($SepJ_{\Delta 690-751}$)	+	-	0.045 ± 0.010		
CSFR26 ($SepJ_{T616A}$)	+	-	0.017 ± 0.006**		
Group 3					
CSFR12 ($SepJ_{\Delta 498-507}$)	+	+	0.015 ± 0.006**	44.3 ± 4.9 (6)	14.1 ± 2.8 (46)
CSFR25 ($SepJ_{Y612A}$)	+	+	0.017 ± 0.006**		
CSFR27 ($SepJ_{R562A}$)	+	+	0.024 ± 0.006*		
Group 4					
CSFR13 ($SepJ_{R617A}$)	+	+	0.031 ± 0.010		
CSFR14 ($SepJ_{E663A}$)	+	+	0.038 ± 0.009	38.7 ± 12.3 (11)	19.3 ± 4.5 (46)*
CSFR15 ($SepJ_{S667A}$)	+	+	0.034 ± 0.010	41.9 ± 7.4 (9)	14.6 ± 4.4 (46)
CSFR19 ($SepJ_{G579A}$)	+	+	0.025 ± 0.010		
CSFR20 ($SepJ_{G724A}$)	+	+	0.042 ± 0.008		
CSFR28 ($SepJ_{E580A}$)	+	+	0.040 ± 0.011		

[a] Filamentation phenotype in BG11 or $BG11_0$ medium, as indicated: +, positive; -, negative; [+], weak positive.

[b] Intercellular transfer of calcein was determined by FRAP analysis performed with filaments that had been grown in BG11 medium (supplemented with antibiotics for the CSFR mutants). Data presented as the recovery constant R (s^{-1}), mean ± SEM of 12-29 filaments from 3 independent cultures. The difference between each strain and the complemented CSFR11 mutant (used for reference) was assessed with the Student's t test (*, $p < 0.05$; **, $p < 0.01$).

[c] Septal peptidoglycan nanopores were visualized in isolated murein sacculi by transmission electron microscopy (see Fig. 3.41). Number of nanopores per septal peptidoglycan disk is indicated as mean ± SD (n), where n is the number of counted disks. Diameter was measured using ImageJ software and is indicated as mean ± SD (n), where n is the number of measured nanopores. Number and size of nanopores in the different mutants were compared to those in strain CSFR11 using the Student's t test (*, $p < 0.05$). Data from the literature were not included in the statistical analysis. Blank space, not determined.

[d] Data taken from Mariscal *et al*. (2016).

[e] Data taken from Nürnberg *et al*. (2015).

[f] Data taken from Rudolf *et al*. (2015).

Table 3.11. Fox phenotype, nitrogenase activity and heterocyst pattern in *sepJ* mutant strains.

Strain (Genotype or SepJ protein)	Fox phenotype[a]	Nitrogenase activity[b]	24 h		48 h	
			% Hets[c]	% Cont Hets[d]	% Hets	% Cont Hets
Controls						
PCC 7120 (WT)	+	4.67 ± 0.53	7.41 ± 0.47	0.00	8.17 ± 0.18	0.73
CSVM34 (Δ*sepJ*)	-	0.00 ± 0.00**	0	nd[e]	0	nd
CSVM90 ($SepJ_{\Delta 463-748}$)	-	0.00 ± 0.00**	0	nd	0	nd
CSFR11 (SepJ)	+	5.26 ± 1.70	7.88 ± 0.48	0.50	9.02 ± 0.07	0.68
Group 1						
CSFR21 ($SepJ_{A542R}$)	-	0.00 ± 0.00**	0	nd	0	nd
CSFR22 ($SepJ_{\Delta 739-751}$)	-	0.00 ± 0.00**	0	nd	0	nd
CSFR23 ($SepJ_{\Delta 626-751}$)	-	0.00 ± 0.00**	0	nd	0	nd
Group 2						
CSFR16 ($SepJ_{H624A}$)	[+]	1.44 ± 0.62*	2.14 ± 0.78**	0.00	2.36 ± 1.49	0.00
CSFR24 ($SepJ_{\Delta 690-751}$)	+	1.41 ± 0.20*	7.16 ± 0.75[f]	0.00	12.01 ± 2.28[f]	0.00
CSFR26 ($SepJ_{T616A}$)	+	6.16 ± 2.80	3.07 ± 2.29*	0.00	7.77 ± 2.00	1.87
Group 3						
CSFR12 ($SepJ_{\Delta 498-507}$)	+	4.75 ± 1.97	7.26 ± 0.53	0.76	8.21 ± 1.29	4.53**
CSFR25 ($SepJ_{Y612A}$)	+	2.46 ± 1.35	5.43 ± 0.92*	0.76	8.27 ± 0.38	2.92**
CSFR27 ($SepJ_{R562A}$)	+	5.09 ± 1.91	7.08 ± 1.51	0.00	8.65 ± 0.80	2.21
Group 4						
CSFR13 ($SepJ_{R617A}$)	+	4.89 ± 1.41	6.64 ± 2.94	1.37	8.08 ± 0.86	7.77**
CSFR14 ($SepJ_{E663A}$)	+	2.02 ± 0.99*	8.31 ± 0.85	5.88**	9.96 ± 0.67	11.34**
CSFR15 ($SepJ_{S667A}$)	+	5.35 ± 1.65	6.00 ± 2.50	0.70	8.09 ± 1.97	6.59**
CSFR19 ($SepJ_{G579A}$)	+	3.90 ± 0.96	8.01 ± 1.45	1.25	8.86 ± 0.96	5.37**
CSFR20 ($SepJ_{G724A}$)	+	3.17 ± 1.63	8.61 ± 0.35	1.79	9.29 ± 0.53	6.79**
CSFR28 ($SepJ_{E580A}$)	+	7.37 ± 3.30	6.69 ± 1.04	2.03*	8.68 ± 1.31	3.50**

[a] Fox phenotype (growth on solid $BG11_0$ medium as shown in Fig. 3.36): +, positive; -, negative; [+], weak positive.

[b] Nitrogenase activity was determined as acetylene reduction in assays performed under oxic conditions with filaments that had been grown in BG11 medium (with antibiotics for the CSFR mutants) and incubated in $BG11_0$ medium (without antibiotics) for 48 h. Data presented as μmol $(mg\ Chl)^{-1}\ h^{-1}$, mean ± SEM of 2 (for strains which do not develop heterocysts), 3 (for all other strains except CSFR11) or 4 (for CSFR11) independent cultures. The significance of the difference between mutant and strain CSFR11 was assessed with the Student's t test (*, $p \leq 0.05$; **, $p < 0.01$).

[c] Heterocysts were visualized in filaments grown in BG11 medium (with antibiotics for the CSFR mutants) and incubated in $BG11_0$ medium without antibiotics for 24 or 48 h, as indicated. The percentage of heterocysts was determined for each of three independent cultures. At least 100 heterocysts from each culture were counted. Data are mean ± SD (n = 3). The significance of the difference between each mutant and strain CSFR11 was assessed with the Student's t test (*, $p \leq 0.05$; **, $p < 0.01$).

[d] Contiguous heterocysts refer to intervals with a size of zero vegetative cells. Data are the percentages of the intervals with size = 0 in filaments from three different cultures. Two categories were established (interval = 0; interval > 0), and the distribution in each mutant was compared to that in strain CSFR11 using the χ^2 test (*, $p \leq 0.05$; **, $p < 0.01$).

[e] Not determined because of the lack or low percentage of heterocysts, or because of released heterocysts (strain CSFR24)

[f] Numerous heterocysts were released from filaments of this strain: 61.3% at 24 h and 62.9% at 48 h.

3.3.3. Construction and characterization of mutants expressing SepJ proteins altered in the permease domain

As described above, strain CSVM90 ($SepJ_{\Delta 463-748}$) showed a phenotype similar (although not identical) to that of the *sepJ* deletion strain CSVM34, being impaired in both cell-cell anchoring and communication functions. In an attempt to discriminate between the two functions, we isolated *Anabaena* mutants producing SepJ proteins bearing point mutations or deletions in the permease domain. For this, we designed a strategy based on the reconstruction of the *sepJ* gene bearing the intended mutations using CSVM90 as parental strain (Fig. 3.42).

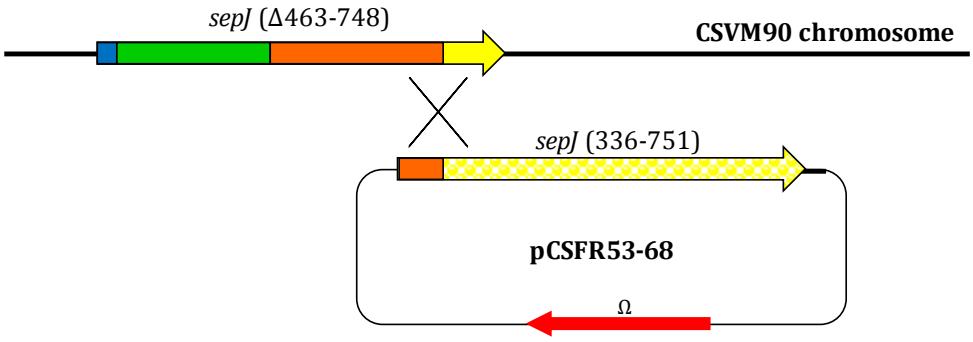

Fig. 3.42. Schematic of the genetic strategy followed to reconstruct *sepJ* using CSVM90 as parental strain. In strain CSVM90, the *sepJ* gene encodes a deleted version of SepJ ($SepJ_{\Delta 463-748}$). The regions encoding the N-terminal, the coiled-coil, the linker and the integral membrane domains are represented in blue, green, orange and yellow, respectively. Plasmids containing the region of the gene encoding from amino acid residue 336 to the end of the protein were used for reconstruction of the *sepJ* gene. The C.S3 cassette (a modified Ω cassette) is represented as a red arrow.

A number of site-directed mutations of *sepJ* were designed based in their conservation in the SepJ permease sequence (Fig. 3.33) We first constructed an *Anabaena* strain, CSFR12 that produces a SepJ protein lacking amino acid residues 498 to 507 ($SepJ_{\Delta 498-507}$), which are part of a predicted extra-membrane cytoplasmic loop in SepJ from heterocyst-forming cyanobacteria (see Fig. 3.43). We also prepared *Anabaena* strains with the following amino acid substitutions: $A_{542}R$ in strain CSFR21, $R_{562}A$ in strain CSFR27; $G_{579}A$ in strain CSFR19; $E_{580}A$ in strain CSFR28; $T_{616}A$ in strain CSFR26; $R_{617}A$ in strain CSFR13; $Y_{612}A$ in strain CSFR25; $H_{624}A$ in strain CSFR16; $E_{663}A$ in strain CSFR14; $S_{667}A$ in strain CSFR15; and $G_{724}A$ in strain CSFR20 (Fig. 3.43; Table 3.11).

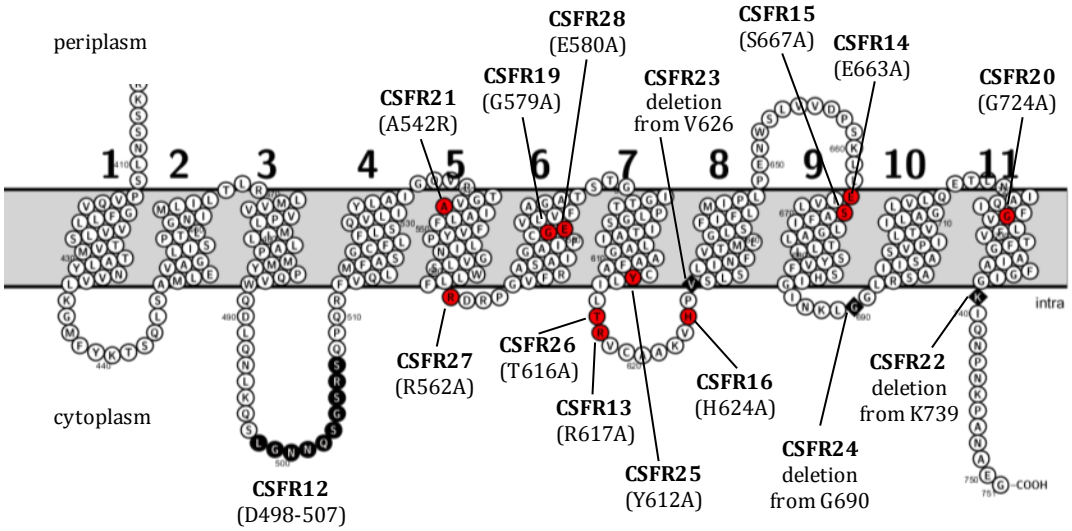

Fig. 3.43. Mutations in the permease domain of SepJ. Schematic of the permease domain of SepJ from *Anabaena* indicating the mutations introduced in this work. Transmembrane segments are numbered 1 to 11 according to the prediction of the TMHMM program. Black circles, residues deleted in strain CSFR12; red circles, specific amino acid mutations; black rhomboids, residues from which deletions started. All SepJ mutant proteins are also included in Table 3.12.

For construction of plasmids containing *sepJ* with point mutations or small deletions, a strategy based on two-step PCR site-directed mutagenesis was carried out (Fig 3.44). The amplified fragment bearing the mutation was cloned in a plasmid that also bears the Ω cassette. After transferring the plasmid to strain CSVM90 by conjugation, the mutants were selected by their resistance to Sm and Sp, resulting in the recovery of mutants generated by single cross-over as described above (Fig. 3.42).

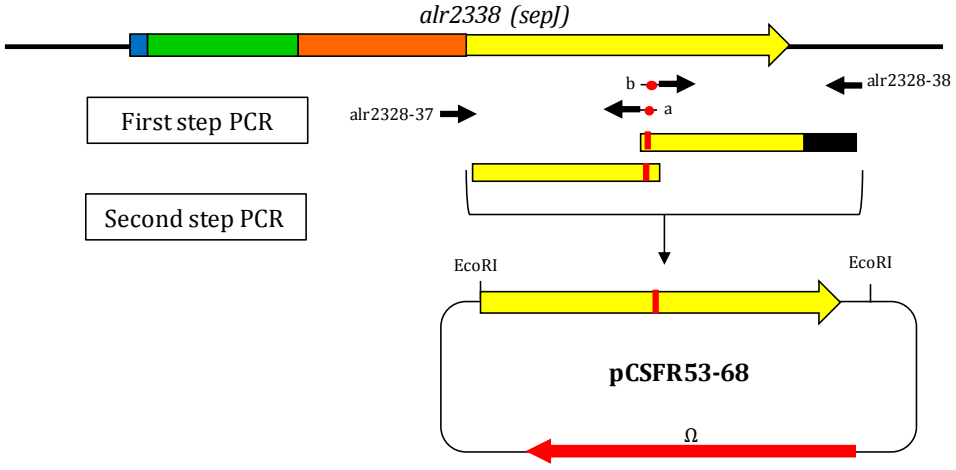

Fig. 3.44. Construction of mutants by two-step PCR site-directed mutagenesis. A first PCR step was carried out using primer alr2338-37 and a specific primer ("a") where nucleotide changes were introduced (represented as a red circle in the schematic), and primer alr2338-38 and another specific primer ("b") that overlapped primer "a" (See *Mat&Meth*, Tables 2.6 and 3.12). DNA from strain PCC 7120 was used as template in the first PCR steps. Then, an overlapping PCR was carried out using the products of the two previous PCR reactions as template and primers alr2338-37 and alr2338-38. The products of these PCRs, which contained site-specific mutations or small deletions, were cloned in EcoRI-digested pCSV3 producing plasmids pCSFR53 to pCSFR68 (Table 3.12). Plasmids were transferred to strain CSVM90 by conjugation.

Strains bearing constructs producing SepJ with C-terminal deletions were also prepared. Strain CSFR23 bears a C-terminal deletion from Val_{626} ($SepJ_{\Delta 626-751}$), which includes the last four TMSs; strain CSFR24 bears a C-terminal deletion from Gly_{690} ($SepJ_{\Delta 690-751}$) including the last two TMSs; and strain CSFR22 bears a deletion of the 13 C-terminal amino acids of the protein ($SepJ_{\Delta 739-751}$), which is a predicted cytoplasmic tail generally present in SepJ that however is not conserved in sequence. For plasmid construction, a stop codon was introduced in the reverse primer (See *Mat&Meth*, Table 2.6) and the amplification product was cloned in EcoRI-digested pCSV3 generating the plasmids listed in *Mat&Meth*, Table 2.6 and Table 3.12. These plasmids were transferred by conjugation to strain CSVM90 to generate strains CSFR22, CSFR23 and CSFR24. In addition, as a control, we created a strain bearing a wild-type version of the permease domain of SepJ, which was amplified by PCR using primers alr2338-37 and alr2338-38 (Table 2.6). The resulting PCR product was cloned in EcoRI-digested pCSV3 producing plasmid pCSFR53. This plasmid was transferred by conjugation to CSVM90, generating strain CSFR11.

Table 3.12. Plasmids and oligonucleotides used for strain construction.

Strain	Conjugated plasmid	Primer "a"	Primer "b"	SepJ version expressed
CSFR11	pCSFR53			wild type
CSFR12	pCSFR54	alr2338-40	alr2338-39	Δ(L498-S507)
CSFR13	pCSFR55	alr2338-42	alr2338-41	R617A
CSFR14	pCSFR56	alr2338-44	alr2338-43	E663A
CSFR15	pCSFR57	alr2338-46	alr2338-45	S667A
CSFR16	pCSFR58	alr2338-48	alr2338-47	H624A
CSFR19	pCSFR59	alr2338-50	alr2338-49	G579A
CSFR20	pCSFR60	alr2338-52	alr2338-51	G724A
CSFR21	pCSFR61	alr2338-54	alr2338-53	A542R
CSFR22	pCSFR62		alr2338-55	Δ(K739-G751)
CSFR23	pCSFR63		alr2338-56	Δ(V626-G751)
CSFR24	pCSFR64		alr2338-57	Δ(G690-G751)
CSFR25	pCSFR65	alr2338-58	alr2338-59	Y612A
CSFR26	pCSFR66	alr2338-60	alr2338-61	T616A
CSFR27	pCSFR67	alr2338-62	alr2338-63	R562A
CSFR28	pCSFR68	alr2338-64	alr2338-65	E580A

Exconjugants were screened by PCR using primers alr2338-10 and alr2338-25 (Fig. 3.45.A). The presence and segregation of chromosomes with a reconstituted *sepJ* gene was corroborated for all the mutants (Fig. 3.45.B).

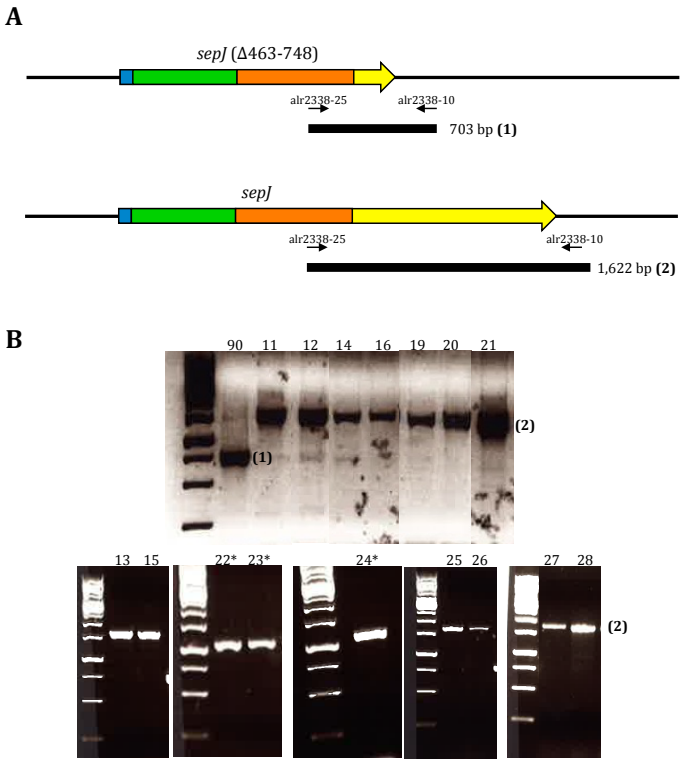

Fig. 3.45. PCR analysis of the genomic structure of strains bearing *sepJ* mutations. (**A**) Schematic of the *sepJ* genomic region in strain CSVM90 and the mutants with re-constructed *sepJ* genes, with indication of the primers used in the PCR reactions and expected PCR product sizes. (**B**) Products of the PCR reactions performed with primers alr2338-10 and alr2338-25 and, as template, DNA from the indicated strains grown in BG11 medium. Strains are denoted as 90 (CSVM90), 11 (CSFR11), 12 (CSFR12), etc. CSFR22 (22), CSFR23 (23) and CSFR24 (24) are highlighted with an asterisk indicating that the size of the PCR product is smaller than in the other strains because their *sepJ* gene contains a premature stop.

Once the strains bearing the different mutated *sepJ* genes were constructed, our goal was to characterize them for production and subcellular localization of SepJ, capability to make long filaments, diazotrophy (diazotrophic growth, nitrogenase activity and heterocyst formation and pattern), intercellular transfer of calcein and, for some strains, formation of nanopores. However, to ensure that the approach of reconstructing the *sepJ* gene was correct, we first investigated strain CSFR11 (SepJ) in detail.

The phenotypic features of strain CSFR11 were compared to those of its parental strain, CSVM90 ($SepJ_{\Delta 463\text{-}748}$) and of the wild type (strain PCC 7120). Strain CSFR11 (SepJ) could grow under diazotrophic conditions on solid medium in the same way as the wild type (Fig. 3.36). Inspection under the microscope did not show apparent differences between strain CSFR11 (SepJ) and the wild type (Fig. 3.37). Quantification of filament length showed that CSFR11 (SepJ), like the wild type, produced a high percentage of long filaments in both BG11 and $BG11_0$ media. In contrast, as expected, strain CSVM90 ($SepJ_{\Delta 463\text{-}748}$) produced shorter filaments (Fig. 3.38 and Fig. 3.39). SepJ localization was also studied in CSFR11 (SepJ) by immunofluorescence (Fig. 3.40). As in the wild type, the SepJ signal could be detected in the cell poles at the intercellular septa.

Regarding intercellular molecular transfer, calcein transfer in strain CSFR11 (SepJ) was not significantly different from that of the wild-type strain (Table 3.10). CSFR11 also showed a number of nanopores similar to that described by Mariscal *et al*. (2016) for the wild type, about 52 nanopores per disk, and they were distributed correctly centered in the septal disks (Fig. 3.41). Diameter of nanopores in strain CSFR11 was similar to that described by Nürnberg *et al*. (2015) for the wild type, about 15 nm (which is somewhat smaller than the diameter described by Rudolf *et al.*, 2015; Table 3.10).

Nitrogenase activity was measured after 48 h of incubation in medium lacking of combined nitrogen (Table 3.11). There was no significant difference between cultures from strain CSFR11 (SepJ) and the wild type, indicating that the ability of nitrogen fixation was restored in strain CSFR11 (SepJ). The percentage of heterocysts after 24 h and 48 h of diazotrophic growth was also determined (Table 3.11). We did not find any significant difference in the percentage of heterocysts between strain CSFR11 (SepJ) and the wild type at 24 h or 48 h.

The pattern of heterocysts in the filament was also analyzed in order to inquire whether the transfer of regulators was altered in strain CSFR11. The number of vegetative cells between two consecutive heterocysts was quantified (Figs. 3.46 and 3.47) and the presence of multiple contiguous heterocysts (Mch phenotype) was determined as the presence of heterocyst doublets (Table 3.11). Both parameters were not statistically different in CSFR11 (SepJ) and the wild type strain at 24 h and 48 h after nitrogen step-down (Figs. 3.46 and 3.47; Table 3.11). In conclusion, strain CSFR11 (SepJ) was complemented for all the features altered in the CSVM90 mutant. CSFR11 was used as the control strain for comparison with the permease mutants generated in this work.

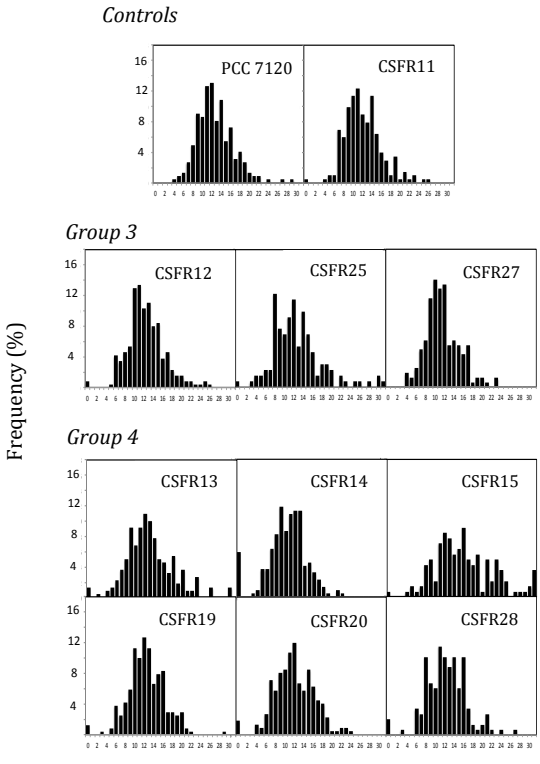

Fig. 3.46. Heterocyst pattern in *Anabaena* and *sepJ* mutants after 24 h of incubation in BG11$_0$ medium. Heterocyst pattern was approached as the length (number of cells) of the vegetative cell intervals between heterocysts. Interval zero denotes contiguous heterocysts. Strains CSFR16 and CSFR26, belonging to Group 2, are not shown because of the low percentage of heterocysts after 24 h of diazotrophic growth.

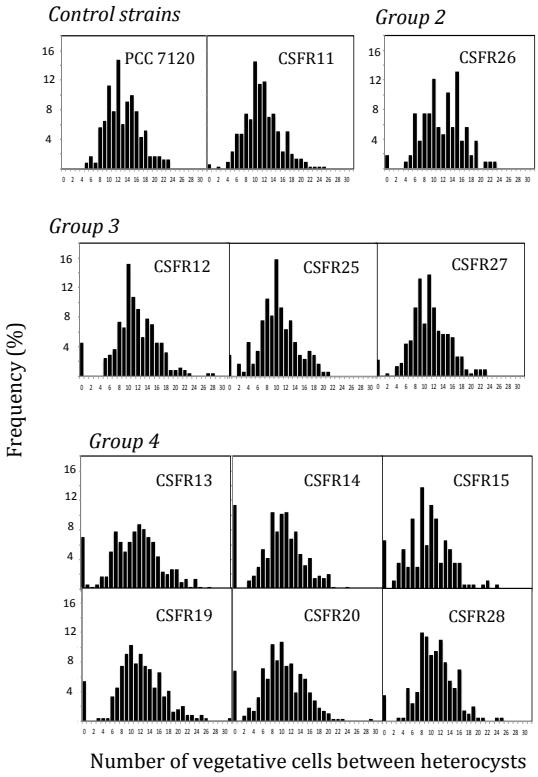

Fig. 3.47. Heterocyst pattern in *Anabaena* and *sepJ* mutants after 48 h of incubation in $BG11_0$ medium. Heterocyst pattern was approached as the length (number of cells) of the vegetative cell intervals between heterocysts. Interval zero denotes contiguous heterocysts. Only strains belonging to Groups 2, 3 and 4 are shown since they were able to develop heterocysts. Strain CSFR16, belonging to Group 2, is not included because of the low percentage of heterocysts after 48 h of diazotrophic growth. Note the presence of contiguous heterocysts in most of the mutants.

The phenotype of the SepJ permease mutants was then investigated. We used two positive controls, wild-type *Anabaena* and strain CSFR11 (SepJ), and two negative controls, strains CSVM34 (Δ*sepJ*) and CSVM90 ($SepJ_{\Delta 463\text{-}748}$). To simplify their presentation, we have grouped the mutants bearing deletions and point mutations according to their phenotypic traits. Mutants belonging to **Group 1** showed as main characteristic that they were impaired in filamentation, independently on the nitrogen source used; mutants belonging to **Group 2** were impaired in filamentation, mainly under diazotrophic conditions and some of them also showed a low calcein transfer; **Group 3** mutants showed impaired calcein transfer but they were not affected in filamentation; **Group 4** mutants showed a Mch phenotype indicative of impaired transfer of regulators but normal activity of calcein transfer. All the mutants and control strains could grow using nitrate as nitrogen source. Tables 3.10 and 3.11 summarize the phenotypic analysis, including filamentation and transfer functions (Table 3.10) and diazotrophic-related parameters (Table 3.11). The four groups are described in detail below.

3.3.3.1. Group 1 mutants.

Knock-out *sepJ* mutants show short filaments in media with combined nitrogen and fragment extensively upon incubation without combined nitrogen. We grouped together mutants CSFR21 ($SepJ_{A542R}$), CSFR22 ($SepJ_{\Delta 739-751}$) and CSFR23 ($SepJ_{\Delta 626-751}$) because they were affected in diazotrophic growth (Fig. 3.36) and showed short filaments both in BG11 and $BG11_0$ media (Fig. 3.37; Figs. 3.38 and 3.39). They were not able to form heterocysts, and, consistently, no nitrogenase activity could be detected (Table 3.11). As they showed the same phenotype as Δ*sepJ* mutants (Fox^- phenotype), we asked whether they were affected in production of SepJ.

To assess the production of SepJ in the mutants, immunolocalization with antibodies raised against the coiled-coil domain of the protein was performed. As shown above, SepJ was observed in the intercellular septa of filaments from the wild type and strain CSFR11 (SepJ), was missing from strain CSVM34 (Δ*sepJ*), and was observed scattered apparently in the surface of the cells in strain CSVM90 ($SepJ_{\Delta 463-748}$) (Fig. 3.40). SepJ could be detected in strains CSFR21 ($SepJ_{A542R}$), CSFR22 ($SepJ_{\Delta 739-751}$) and CSFR23 ($SepJ_{\Delta 626-751}$), indicating that the protein was produced at appreciable levels, but it was not as neatly located at the intercellular septa as in the positive control strains (Fig. 3.40).

Transfer of calcein between vegetative cells in filaments grown in BG11 medium was also tested. Surprisingly, strains CSFR21 ($SepJ_{A542R}$), CSFR22 ($SepJ_{\Delta 739-751}$) and CSFR23 ($SepJ_{\Delta 626-751}$) showed a normal activity of calcein transfer (Table 3.10). The nanopores were visualized in septal peptidoglycan disks from strain CSFR23 ($SepJ_{\Delta 626-751}$) (Fig. 3.41), in which the number of nanopores was lower than in the complemented strain CSFR11 (SepJ) and similar to that in strain CSVM90 ($SepJ_{\Delta 463-748}$), but nanopore diameter was increased by about 25% (compared to strain CSFR11) or 35% (compared to strain CSVM90) (Table 3.10).

From their phenotypic characterization, we conclude that mutants belonging to phenotypic Group 1 produce a SepJ protein that cannot fulfill its roles in filamentation and heterocyst differentiation.

3.3.3.2. Group 2 mutants

Strain CSFR16 ($SepJ_{H624A}$) formed long filaments but at a lower frequency that the positive controls (Figs. 3.37, 3.38 and 3.39). This strain together with strains CSFR24 ($SepJ_{\Delta 690-751}$) and CSFR26 ($SepJ_{T616A}$) fragmented appreciably upon incubation in $BG11_0$ medium (Fig. 3.39). This feature is defining the Group 2.

In the three strains SepJ was present, but it was only loosely associated to the intercellular septa (Fig. 3.40). Calcein transfer was impaired in strains CSFR16 ($SepJ_{H624A}$) and CSFR26 ($SepJ_{T616A}$) but not in CSFR24 ($SepJ_{\Delta 690-751}$) (Table 3.10). Strain CSFR26 ($SepJ_{T616A}$) produced a low percentage of heterocysts at 24 h but it got restored after 48 h of diazotrophic growth. This strain also produced nitrogenase activity at appreciable levels. Strains CSFR24 ($SepJ_{\Delta 690-751}$) also produced heterocysts at high levels, but a substantial fraction of them were released from the filaments and this strain showed low nitrogenase activity (Table 3.11). Both strains, CSFR24 and CSFR26, could grow under diazotrophic conditions (Fig. 3.36). Strain CSFR16 ($SepJ_{H624A}$) produced a low percentage

of heterocysts, low nitrogenase activity, and showed only weak growth under diazotrophic conditions, a weak Fox$^+$ phenotype (Table 3.11; Figs. 3.36).

According to their phenotypic analysis, SepJ in phenotypic Group 2 mutants provides filamentation function in BG11 medium and allows heterocyst differentiation, but fails to keep filamentation under nitrogen deprivation.

3.3.3.3. Group 3 mutants

Strains CSFR12 (SepJ$_{\Delta 498\text{-}507}$), CSFR25 (SepJ$_{Y612A}$) and CSFR27 (SepJ$_{R562A}$) formed long filaments when grown in BG11 or BG11$_0$ medium (Figs. 3.37, 3.38 and 3.39). However, they were impaired in calcein transfer (Table 3.10). Based on this, they were defined as Group 3 strains. In all these strains SepJ could be detected by immunofluorescence. It was well located at the intercellular septa in strain CSFR12 (SepJ$_{\Delta 498\text{-}507}$) and was also fairly located in CSFR25 (SepJ$_{Y612A}$) and CSFR27 (SepJ$_{R562A}$) (Fig. 3.40).

The presence of nanopores was analyzed in strain CSFR12 (SepJ$_{\Delta 498\text{-}507}$). Nanopores were located centered in the septal disks (Fig. 3.41) and the number of them per septal disk was similar to that in the control strain CSFR11 (SepJ) (Table 3.10). The diameter of nanopores was not altered either (Table 3.10). Hence, the SepJ mutations in these strains affected intercellular molecular transfer while hardly affecting morphology.

A relevant phenotypic feature of some Group 3 strains is that they produced some contiguous heterocysts, normally observed as heterocyst doublets (Fig. 3.48), which were more evident after 48 h than after 24 h of nitrogen deprivation (Figs. 3.46 and 3.47; Table 3.11). Because SepJ has been shown to be involved in the intercellular transfer of heterocyst pattern regulators (Rivers *et al*., 2014; Corrales-Guerrero *et al.*, 2015; Mariscal *et al*., 2016), these results suggest that the mutations of SepJ in Group 3 strains might affect transfer of some of those regulators.

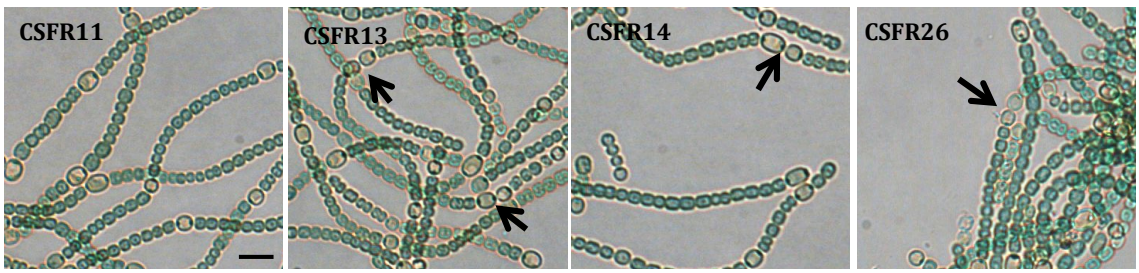

Fig. 3.48. Presence of heterocyst doublets in some *sepJ* mutant strains. Heterocysts in strains CSFR11 (SepJ), CSFR26 (SepJ$_{T616A}$), which belongs to Group 2, and CSFR13 (SepJ$_{R617A}$) and CSFR14 (SepJ$_{E663A}$), both belonging to Group 4, after 48 h growing under diazotrophic conditions. Arrows point to heterocyst doublets. Scale bar, 10 μm.

Therefore, in phenotypic Group 3 mutants, SepJ provides filamentation function in BG11 medium and allows heterocyst differentiation. However, the mutations in SepJ from Group 2 mutants affect transfer of calcein and some regulators.

3.3.3.4. Group 4 mutants

The strains belonging to this group were affected neither in diazotrophic growth nor in filamentation in BG11 or $BG11_0$ medium (Figs. 3.36-3.39). This group includes strains CSFR13 ($SepJ_{R617A}$), CSFR14 ($SepJ_{E663A}$), CSFR15 ($SepJ_{S667A}$), CSFR19 ($SepJ_{G579A}$), CSFR20 ($SepJ_{G724A}$) and CSFR28 ($SepJ_{E580A}$), which produced a higher percentage of contiguous heterocysts than Group 3 strains after 48 h of nitrogen deprivation, and also after 24 h (except strain CSFR15) (Table 3.11). Among them, strain CSFR14 ($SepJ_{E663A}$) presented the strongest phenotype showing a high percentage of contiguous heterocysts after both 24 h and 48 h of nitrogen deprivation (Figs. 3.46, 3.47 and 3.48; Table 3.11). CSFR14 also showed a lower nitrogenase activity than the other strains (Table 3.11).

In strains CSFR13 ($SepJ_{R617A}$), CSFR15 ($SepJ_{S667A}$) and CSFR28 ($SepJ_{E580A}$), SepJ was fairly located at the intercellular septa, whereas in CSFR14 ($SepJ_{E663A}$), CSFR19 ($SepJ_{G579A}$) and CSFR20 ($SepJ_{G724A}$) it was somewhat delocalized (Fig. 3.40). The presence of nanopores was also studied in strains CSFR14 ($SepJ_{E663A}$) and CSFR15 ($SepJ_{S667A}$) (Fig. 3.41; Table 3.10). Whereas strain CSFR14 ($SepJ_{E663A}$) showed a similar number of nanopores as the control strain CSFR11 (SepJ), 39 and 45 nanopores per disk, respectively, those nanopores were significantly wider in the mutant (19 nm for strain CSFR14 [$SepJ_{E663A}$] and 15 nm for strain CSFR11 [SepJ]). In contrast, nanopores from strain CSFR15 ($SepJ_{S667A}$) showed the same diameter as those of the control strain (about 15 nm), and their number (about 42 nanopores per disk) was similar to that of strain CSFR11 ($SepJ_{\Delta}$). All the strains showed an activity of calcein transfer not significantly different to that in the control strain CSFR11 (Table 3.10).

The results obtained with phenotypic Group 4 strains identify mutations of the SepJ permease that render a phenotype (production of heterocyst doublets) likely related with alterations in intercellular molecular transfer of heterocyst pattern regulators.

4. DISCUSSION

4.1. SepJ AS A KEY COMPONENT OF SEPTAL JUNCTIONS

The SepJ protein plays a very important role in multicellular cyanobacteria. It is required for anchoring cells to each other –thus contributing to filament integrity (Flores *et al*., 2007; Nayar *et al*., 2007)– and for intercellular molecular transfer as tested with the fluorescent tracer calcein (Mullineaux *et al*., 2008). In *Anabaena,* localization of SepJ has been previously studied with a GFP fusion to the C-terminal region of the protein. It has been shown that SepJ-GFP localizes very focused at the cell poles in the intercellular septa (Flores *et al*., 2007; Mariscal *et al*., 2011). In dividing cells, SepJ-GFP is also detected as a ring in the middle of the cell (Flores *et al*., 2007; Mariscal & Flores, 2010), similar to the Z ring made by proteins of the divisome such as FtsZ (Sakr *et al*., 2006). In this work, using 3D-deconvolution images, we have shown clearly that SepJ-GFP localizes to a ring in dividing cells. Importantly, localization at the cell poles and in a Z-like ring has been confirmed by immunolocalization of the native SepJ protein (Fig. 3.15).

The Z ring-like localization of SepJ and its progressive focusing to the cell poles suggested a relation between SepJ and the division process. Among the genes involved in cell division in bacteria, *ftsZ*, encoding a tubulin homolog, has been shown to be essential in most bacteria including *Anabaena* (Zhang *et al*., 1995). In many bacteria, this gene is included in a chromosomal region known as *dcw* cluster (division and cell wall), which also encompasses other genes such as *ftsL*, *ftsI*, *ftsW*, *ftsQ* and *ftsA* (Vicente *et al*., 1998). However, in cyanobacteria only *ftsQ* and *ftsZ* are adjacent in the genome. As shown in Fig. 3.2., the intergenic region between *ftsQ* and *ftsZ* is variable in length, being longer in heterocyst-forming than in other cyanobacteria (1,291 bp in *Anabaena*). In some cases, it contains a hypothetical ORF. The putative protein that might be encoded in this ORF does not show any significant similarity when compared with protein databases, and transcriptomic analysis in *Anabaena* (Flaherty *et al*. 2011) does not show transcription of this region. Therefore, there is no evidence for expression of this hypothetical ORF. This in turn rules out a possible co-transcription of *ftsQ* and *ftsZ*, at least under the growth conditions used by Flaherty *et al.* (2011).

To address the possible relation between SepJ and the cell division machinery, we constructed an *ftsZ* conditional mutant. Other *ftsZ* conditional mutants have been constructed in unicellular bacteria (e.g. Dziadek *et al*., 2003). However, to the best of our knowledge, attempts to create an *ftsZ* mutant in filamentous cyanobacteria have failed (Sakr *et al*., 2006). We constructed *Anabaena* strain CSFR18 in which, based on expression from a synthetic NtcA-dependent promoter, the FtsZ protein levels depend on the nitrogen source. The promoter was designed based on known features of Class II NtcA-activated promoters. Thus, the NtcA-biding site was located 23 bp upstream from the -10 promoter-box (Herrero *et al*., 2001). RT-qPCR and western analyses confirmed that expression of the *ftsZ* gene and production of the FtsZ protein followed the expected regulation in strain CSFR18: *ftsZ* RNA levels and the FtsZ protein were low when ammonium was present in the medium, increased in the presence of nitrate and were highest in the absence of combined nitrogen. The fact that FtsZ levels were moderate in nitrate-containing media made it possible the selection and maintenance of strain CSFR18. However, in this condition, strain CSFR18 showed lower FtsZ levels than the wild type, which could be the reason for the increased cellular area and difficulty to form Z rings (Fig. 3.7). In ammonium-containing media, FtsZ levels decreased substantially resulting in impairment

of cell division, increase of cell volume and, finally, cellular lysis, which could result from impairment in PG synthesis. Other bacteria, such as the rod-shaped bacterium *Escherichia coli*, are described to become filamentous when *ftsZ* is repressed (de Boer, 2016). The different shape of *Anabaena* cells under low levels of FtsZ compared to the rod-shaped bacterium *E. coli* indicates that the mechanisms responsible for shape maintenance in filamentous cyanobacteria are different from those in rod-shaped bacteria. On the other hand, as shown studying gene expression and protein levels (Fig. 3.6), *ftsZ* expression increases under diazotrophic conditions in the wild-type strain. When N_2-fixation starts after N step-down, cells initiate division synchronically, which could be the reason for this increase in *ftsZ* expression.

FtsQ is involved in the recruitment of late divisome components. To inquire whether SepJ is recruited to the septum by means FtsQ, we tried the same strategy as in the case of *ftsZ*. Thus, strain CSFR5 was constructed in which the *ftsQ* was expressed under the control of the synthetic NtcA-dependent promoter. Unfortunately, RT-qPCR analysis of the *ftsQ* gene in strain CSFR5 did not show the expected regulation. It has been described that FtsQ is a low abundance protein in *E. coli* (Carson *et al*., 1991). This also seems to be the case in wild-type *Anabaena*, which always showed lower *ftsQ* expression levels than strain CSFR5, independently of the nitrogen condition used (Fig. 3.13). However, over-expression of *ftsQ* in strain CSFR5 did not result in any altered cellular morphology indicating that cell division was not significantly affected.

SepJ localization was studied in CSFR18 under different nitrogen regimes. For that purpose, immunofluorescence localization was carried out. Our results have shown that the correct localization of SepJ requires the presence normal (or close to normal) FtsZ levels, which are best attained in the diazotrophic filaments of strain CSFR18 (Fig. 3.7; Fig. 3.15). A complementary approach was carried out to study the involvement of cell division machinery in septal localization of SepJ. We observed that treatment of *Anabaena* with berberine impedes FtsZ ring formation, as previously shown in *E. coli* (Domadia *et al*., 2008; Boberek *et al*., 2010), and impairs the correct localization of SepJ. Putting together all these results, we can conclude that the divisome has a role in the subcellular localization of SepJ. Whether, reciprocally, SepJ affects the operation of the divisome in heterocyst-forming cyanobacteria remains to be investigated.

The dependence of SepJ localization on FtsZ indicated that SepJ might be involved in transient interactions with proteins of the divisome. To investigate that, interaction of SepJ and some cell division proteins was addressed by BACTH analysis. Proteins involved in cell division that were assayed included FtsZ and two downstream divisome proteins, FtsQ and FtsW. Only FtsQ showed a strong interaction with SepJ (Fig. 3.26). In *E. coli*, FtsQ plays a role in recruiting late cell division components (Chen *et al*., 2002). Co-purification assays of SepJ and FtsQ confirmed the interaction between the two proteins and also showed a role of the periplasmic section of SepJ in this interaction (Fig. 3.27). This is consistent with the results of BACTH analysis, which suggest a role of the linker domain of SepJ in a specific interaction with the periplasmic α domain of FtsQ. This domain shows high similarity to polypeptide transport-associated (POTRA) domains (van den Ent *et a*l., 2008). The POTRA domain has been proposed to have a chaperone-like function (Sánchez-Pulido *et al*., 2003; Noinaj *et al*., 2013). Our results support a specific interaction between parts of the long extra-membrane section of SepJ and the periplasmic section of FtsQ. This

observation agrees with the prediction that the SepJ coiled-coil and linker domains are periplasmic (Flores *et al*., 2007). Putting together, all these results suggest that SepJ localization at the cell poles in the intercellular septa depends on the divisome. FtsQ would recruit SepJ at the division site as it does with late cell division components. Interactions of SepJ with other proteins of the divisome may also take place, and our results indeed suggest interaction with FtsW. Further analysis of interactions between SepJ and divisome proteins will give an increased knowledge of the mechanism involved in SepJ localization.

The SepJ protein contains four well-differentiated domains (Fig. 1.9). The 26 N-terminal amino acids are highly conserved in all SepJ proteins and our experience suggests that topological signals may reside in this sequence, although no signal peptide for the Sec system or other known secretion system such as TAT can be detected. The so-called coiled-coil domain extends from residues 28 to 207, and is highly conserved as well. This domain consists of two strongly predicted coiled-coil motifs (CC1, residues 28-95; and CC2, residues 127-207). Coiled-coil domains are commonly implicated in protein-protein interactions (Lupas & Gruber, 2005), and therefore the SepJ coiled-coil domain could have a role attaching to each other SepJ proteins from adjacent cells. Size-exclusion chromatography was used to assess if the coiled-coil domain is prone to self-interactions (Fig. 3.17). A peak corresponding to an oligomer with an estimated molecular weight of 240 kDa could be observed. However, single particle electron microscopy analysis of the coiled-coil domain protein preparation indicated that the coiled-coil complexes may have a cylindrical shape (unpublished data), implying that its real molecular weight could be over-estimated by size-exclusion chromatography. Thus, we can conclude that the SepJ coiled-coil domain can form multimers, but their accurate molecular weight and the subunits taking part in them are yet to be determined.

The SepJ protein in needed for formation of septal junctions in *Anabaena*, and the septal junctions likely traverse the septal peptidoglycan through nanopores (Nürnberg *et al.*, 2015). Reviewing available data, it has been suggested that the septal junctions may be 12 to 26 nm in length and 5.5 to 14 nm in diameter, which would fit well into the nanopores that have a diameter of about 15 to 20 nm (Herrero *et al*., 2016). Because of the large size of septal junctions, the proteins constituting these structures can be predicted to make large complexes. FraC and FraD are also necessary to make a normal number of nanopores in *Anabaena* (Nürberg *et al.*, 2015), but there is no evidence for the formation of SepJ-FraCD complexes (see below). Using a strain expressing a double-tagged SepJ (SepJ-GFP-His_{10}) we could find that the tagged SepJ protein can form complexes of a size up to 655 kDa, which could constitute hexamers, observed by BN-PAGE. Similar large complexes can also be detected in material isolated from membranes of wild-type *Anabaena*, but smaller forms of the complex could also be seen in the BN-PAGE gels that could result from disassembly during the isolation procedure. Further analysis of the material isolated with SepJ-GFP-His_{10} has given no indication of the presence in the complexes of proteins other than SepJ. However, we cannot rule out the participation in the SepJ-containing complexes of other proteins that do not interact strongly with SepJ and, therefore, could have been lost in the second step of purification (Fig. 3.21). Nonetheless, our BACTH analysis has unraveled a strong self-interaction of SepJ, for which the coiled-coil and linker domains appear to be very important, indicating that SepJ-containing complexes observed by BN-PAGE could correspond to SepJ multimers formed in a cell.

Other possible interactors of SepJ include the Fra proteins (Merino-Puerto *et al.*, 2011). These are proteins encoded by the *fraCDE* operon (Merino-Puerto *et al*., 2013). Localization of FraC and FraD has been studied by GFP fusions and, in the case of FraD also by immunogold analysis (Merino-Puerto *et al*., 2010; Merino-Puerto *et al*., 2011b). These proteins are also located at the cell poles in the intercellular septa, but their localization is not as focused in the middle of the septum as in the case of SepJ. FraD has a long extra-membrane section with a coiled-coil domain, which makes this protein a good candidate to interact with SepJ. Unfortunately, however, no interaction was detected by BACTH analysis between SepJ and FraC or FraD, nor self-interactions of the Fra proteins were detected. Nonetheless, previous results show that FraC and FraD are functionally related (Merino-Puerto *et al*., 2010). In summary, BACTH analysis has shown that SepJ is able to form stable complexes with itself, which is consistent with the detection of SepJ complexes discussed above. Such complexes could constitute the core of SepJ-related septal junctions. Fra proteins might be involved in the formation of a different type of septal junctions, which appear to influence SepJ localization (Merino-Puerto *et al.*, 2010, 2011b).

BACTH analysis also showed a faint, but significant interaction between SepJ and the peptidoglycan-binding protein SjcF1 (Table 3.7). SjcF1 was previously identified in cell wall preparations of both vegetative cells and heterocysts of *Anabaena* (Moslavac *et al*., 2005, 2007). The *sjcF1* mutant specifically deviates in the size of septal junction nanopores and is impaired in the intercellular transfer of calcein (Rudolf *et al*., 2015). SjcF1 contains two peptidoglycan-binding domains but does not contain a domain accounting for an enzymatic activity and thus is probably not involved in PG layer synthesis. However, it contains an SH3 domain for protein-protein interactions, and SepJ (as well as FraC) bear target peptides for the SH3 domain (Rudolf *et al.*, 2015). Proteins with the same architecture are exclusively present in filamentous cyanobacteria. Considering the results of Rudolf *et al.* (2015) and of our BACTH analysis, SjcF1 could act as a bridge between the septal junction complexes (both SepJ- and FraCD-containing complexes) and the peptidoglycan layer, since SjcF1 interacts with SepJ, FraC and peptidoglycan. Nonetheless, the complex formed between SjcF1 and SepJ could be transitory, and this interaction might take place before or during nanopore formation. Additionally, we have shown in this work that SepJ interacts with peptidoglycan by itself. SepJ complexes could be stabilized by their direct interaction with the septal PG. Moreover, we have shown that the SepJ coiled-coil domain is responsible, at least partially, for this interaction, although a role of the linker domain in the interaction of SepJ with PG cannot be ruled out.

The interaction results are summarized in Fig. 4.1. SepJ is involved in self-interactions probably forming hexamers. In this self-interaction, the coiled-coil and linker domains are involved. The interaction between the coiled-coil domain of SepJ with peptidoglycan could contribute to stabilize the SepJ complexes at the septum. We hypothesize that, like in metazoan gap junctions, hexamers from one cell could interact with hexamers from the adjacent cell. Alternativelly, SepJ could form trimers, and the hexamers observed in BN-PAGE could correspond to interacting trimers from adjacent cells. SepJ interacts with the SjcF1 protein, which is involved in regulation of nanopore size, and perhaps (although it has not been studied by us) it might also interact with AmiC amidases, which are involved in nanopore formation (Büttner *et al*., 2016). Additionally, SjcF1 also interacts with FraC, which might form, together with FraD, another type of septal junctions. Thus, SjcF1 would act as functional bridge between the two types of

septal junctions. Unfortunately, the composition of Fra-based septal junctions remains unknown.

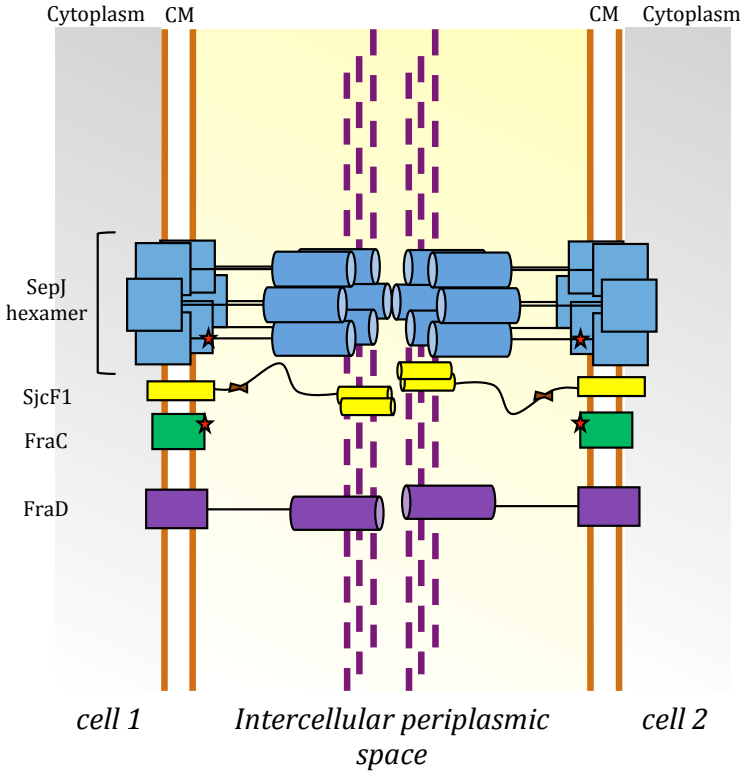

Fig. 4.1. Model for SepJ complex in the septal junctions. SepJ (blue) could form hexamers that are stabilized by SepJ self-interactions and by the interaction between, at least, the coiled-coil domain and the peptidoglycan layer of the septum (purple broken line). The SjcF1 protein (yellow) interacts with SepJ complexes by binding of its SH3 domain (represented as a brown figure) to a SH3-binding in SepJ peptide (red star). SjcF1 can also bind to FraC (green) but not to FraD (purple).

4.2. ROLE OF THE SepJ PERMEASE DOMAIN IN INTERCELLULAR COMMUNICATION

Knock-out mutants of *sepJ* are arrested in heterocyst differentiation, which may be related to a function of SepJ in transfer of regulators of heterocyst differentiation, as has been recently described (Rivers *et al*., 2014; Corrales-Guerrero *et al*., 2015; Mariscal *et al*., 2016). To investigate further the role of SepJ in the biology of *Anabaena*, we studied strains producing SepJ with different deletions or point mutations in its permease domain.

SepJ contains a permease domain homologous to transporters of the DME family. This domain might be involved in the transfer of compounds between cells (Mariscal *et al.*, 2011). *Anabaena* strain CSVM90 produces a SepJ protein that lacks the permease domain. Compared with strain CSVM34 (Δ*sepJ*), strain CSVM90 produces twice as much septal peptidoglycan nanopores and shows a two-fold increased intercellular transfer of calcein (Table 3.10). Thus, the poorly localized SepJ$_{\Delta 463\text{-}748}$ protein appears to allow the formation of some functional septal junctions, which however are insufficient to fulfill the filamentation and diazotrophic functions of SepJ. A wild-type *sepJ* gene was reconstituted using CSVM90 as parental strain obtaining strain CSFR11, which exhibits a complete wild-

type phenotype. SepJ versions with specific mutations were then introduced in *Anabaena*, and strains with altered phenotype were obtained.

Phenotypic group 1 mutants are impaired in filamentation and heterocyst differentiation but show high activity of intercellular transfer of calcein. Phenotypic group 2 mutants produce long filaments in BG11 medium and form heterocysts, but fail to produce long filaments under diazotrophic conditions; only one of the strains belonging to group 2, strain CSFR24, shows high levels of calcein transfer. Phenotypic group 3 mutants produce long filaments in the presence and absence of combined nitrogen, but do not show full activity of intercellular transfer of calcein. Phenotypic group 4 mutants show a wild type phenotype except for the presence of contiguous heterocysts.

The mutants in groups 1 and 3 show radically different phenotypes. Whereas group 1 strains show substantial calcein transfer but are morphologically altered (they are not able to form long filaments), group 3 strains are impaired in calcein transfer but do not show any filamentation defect. Group 3 strains appear to produce SepJ proteins allowing the formation of septal junctions that provide cell-cell binding function but fail to provide the full intercellular transfer function that can be traced with calcein. We hypothesize that the SepJ permease contributes to the formation of a conduit that mediates molecular transfer through the cytoplasmic membrane at the cell poles, and that the mutations in SepJ of group 3 strains affect such conduits. The mutations in SepJ of group 2 strains CSFR16 and CSFR26 may have a similar effect. In contrast, the SepJ proteins produced in group 1 strains, as well as that produced in group 2 strain CSFR24, do not provide full filamentation function but appear to allow the formation of septal junctions that are functional in the intercellular molecular transfer that can be traced with calcein. Whereas there is evidence for the existence of at least two types of septal junctions, those related to SepJ and those related to FraCD (Merino-Puerto *et al.*, 2011), both are together needed to produce a normal number of nanopores (Nürnberg *et al.*, 2015). It is possible that proteins such as FraC and FraD, and perhaps other proteins forming additional septal junctions (Nürnberg *et al.*, 2015), take over at least part of SepJ function when SepJ is present, likely participating in multiprotein complexes, but not fully functional. In this context, it is of interest that SepJ is found at least partly localized to the septum in all of our permease mutants. Interactions with the divisome protein FtsQ, which should be important for septal localization as shown above, involves the linker domain of SepJ, and interaction with PG involves the coiled-coil domain. None of these domains is affected in our permease mutants, providing a rationale for the presence of at least part of the protein correctly localized at the intercellular septa.

The mutations in SepJ of group 1, 2 and 3 strains are point mutations (A542R in strain CSFR21; H624A in CSFR16, T616A in CSFR26; Y612A in CSFR25; and R562A in CSFR27), small deletions (Δ498-507 in CSFR12 and Δ739-751 in CSFR22) or large deletions of the last two (Δ690-751 in CSFR24) or four (Δ626-751) predicted TMSs. A natural short form of SepJ has been recently reported: the terminal heterocyst-forming cyanobacterium *Cylindrospermopsis raciborskii* bears a *sepJ* gene that encodes a protein that lacks the last four TMSs (Plominsky *et al.*, 2015). Nonetheless, the *sepJ* gene is immediately followed by a gene encoding a predicted two-TMS protein that is homologous to the C-terminus of *Anabaena* SepJ. Thus, two polypeptides could interact to form a nearly complete standard SepJ protein in *C. raciborskii*. This cyanobacterium shows transfer

calcein between cells in the filament, supporting the fact that the incomplete versions of SepJ expressed by mutants of group 1 could carry out significant transfer activity.

Whereas the alteration in the transfer function that can be traced with calcein does not impair diazotrophic growth in phenotypic group 3 mutants, the corresponding mutations influence production of heterocysts, since these mutants show an increased number of contiguous heterocysts (the Mch phenotype) after 48 h of incubation without combined nitrogen. Six other strains, the phenotypic group 4 mutants, show filamentation and diazotrophic phenotypes similar to those of the positive control strains, but they exhibit an evident Mch phenotype (Table 3.11; Figs. 3.46 and 3.47). Calcein transfer is not affected in group 4 strains, but the effect of the point mutations on heterocyst pattern suggests an alteration in cell-cell communication specifically related with transfer of regulators. Insufficient transfer of inhibitors out of differentiating heterocysts may produce heterocyst doublets, but the phenotype is not as strong as that of inactivating inhibitor-encoding genes. Deletion mutants of *patS* and *hetN* genes show a Mch phenotype, but in *hetN* mutants contiguous heterocysts are more obvious at 48 h than at 24 h (Callahan *et al*., 2001; Corrales-Guerrero *et al*., 2014). The possible role of SepJ in the transfer of PatS and HetN morphogens has been recently reported (Rivers *et al*., 2014; Corrales-Guerrero *et al.*, 2015; Mariscal *et al*., 2016). Transfer of the HetN morphogen might be impaired in strains that belong to group 3 and CSFR15 since the Mch is only observed at 48 h. In group 4 strains (except CSFR15), the regulators affected could also include the PatS morphogen since the Mch phenotype can be also seen at 24 h. In general, the mutations in strains of phenotypic groups 3 and 4 allow to discriminate between the cell-cell binding (filamentation) and molecular transfer functions of SepJ, because all these strains form long filaments but appear to be impaired in the intercellular transfer of either calcein or heterocyst regulators or both.

Phenotypic analysis of group 3 and 4 strains suggests that the SepJ permease domain mediates some type of transport. , SepJ has been shown to be prone to self-interactions and form complexes in vivo (Results, section 3.2). Two options are possible: each SepJ subunit acts independently as a transporter or, alternatively, different subunits of SepJ make a complex that forms a conduit through which molecular transfer takes place. A model for these conduits could be the structures (connexons) formed by connexins in metazoan gap junctions (see above). The presence of a normal number of nanopores in group 3 and 4 strains suggests that the permease domain would be involved in the transfer function but not in nanopore formation.

Impairment of calcein transfer implies a deficiency in transfer of regulators, especially HetN morphogen, but not vice versa. Differential impairment in the transfer of calcein and regulators of heterocyst differentiation denotes the presence of residues in the permease domain of SepJ that provide some specificity or selectivity to the communication conduits of the septal junctions. Similarly, some connexin mutants that show altered permeability for some particular metabolites have been reported (Beltramello *et al*., 2005; Zhang *et al*., 2005; Santa Cruz *et al*., 2015).

In summary, septal junctions appear to join the cells in the filaments of heterocyst-forming cyanobacteria. SepJ is the core protein of at least one of the types of septal junctions that can be formed in *Anabaena*. Whereas the periplasmic part of SepJ appears to be involved in structural aspects such as complex formation, interaction with

peptidoglycan and filament integrity, the integral membrane domain seems to be involved in transfer of compounds between neighboring cells, since specific mutations in this domain result in impairment of the transfer of fluorescent tracers but also of regulators of cell differentiation.

Putting all the results of this work together, we hypothesize that SepJ is recruited to the division site with the likely participation of FtsQ, and that it could interact with some late components in the divisome that are involved in peptidoglycan remodeling. The extracellular part of SepJ could work as scaffold for proteins involved in nanopore formation. One of these proteins is SjcF1, which appears to be important for regulation of nanopore size. Once SepJ is at the intercellular septa, probably forming hexamers, these complexes would be involved in intercellular molecular exchange. Interaction between SepJ complexes and peptidoglycan could stabilize the septal junctions. Under diazotrophic conditions, SepJ would facilitate the diffusion of morphogens such as PatS- and, later, HetN-derived signals. Our results do not rule out the presence of other sorts of septal junctions that could be involved in transfer of different compounds or metabolites. Thus, septal junctions can be considered as functional analogs to metazoan gap junctions, since both of them mediate chemical communication between cells by simple diffusion (Nürnberg *et al*., 2015; Mullineaux *et al*., 2008; Nieves-Morión *et al*., 2017; Hervé & Derangeon, 2013). Gap junction channels are composed of two connexons (one from each cell) that connect the cells across the intercellular space (Hervé & Darangeon, 2013). Each connexon is made of six connexins, which are membrane proteins that constitute the only structural subunits of the channel. Connexins are intergral membrane proteins, with no extracellular domains. However, the presence of extracellular domains in septal junctions is necessary since communication between cells implies perforation of the peptidoglycan layers that are present in the intercellular space.

5. CONCLUSIONS

CONCLUSIONS

1. Subcellular localization of the septal protein SepJ in the heterocyst-forming cyanobacterium *Anabaena* requires normal cellular levels of FtsZ and, hence, depends on the divisome. SepJ interacts at least with the cell division protein FtsQ, and this interaction takes place through the periplasmic domains of both proteins.

2. SepJ oligomerizes "*in vivo*" putatively forming hexamers, and the coiled-coil and linker domains of the protein are involved in SepJ self-interactions.

3. Bacterial adenylate cyclase two-hybrid (BATCH) analysis shows that the recently discovered peptidoglycan-binding protein SjcF1 interacts independently with SepJ and FraC, another septal protein. SjcF1 may be a nexus between two different types of septal junctions in *Anabaena*, those containing SepJ and those containing FraC/D.

4. SepJ interacts directly with peptidoglycan, and its coiled-coil domain is at least partially responsible for this interaction.

5. The predicted periplasmic part of SepJ appears to be important for nanopore formation, since SepJ is needed to form a normal number of nanopores and mutants of the permease domain are able to form a substantial number of nanopores.

6. The SepJ permease domain is required for intercellular communication in the filaments of *Anabaena*, being involved at least in the transfer of regulators involved in heterocyst pattern formation.

7. Although cyanobacterial septal junctions lack stringent substrate specificity, some amino acid residues of the permease domain of SepJ provide some substrate selectivity to the septal junctions.

6. REFERENCES

Aarsman MEG, Piette A, Fraipont C, Vinkenvleugel TMF, NguyenDistèche M & den Blaauwen T (2005). Maturation of the *Escherichia coli* divisome occurs in two steps. *Mol Microbiol* 55: 1631–1645.

Abed RMM, Dobretsov S & Sudesh K (2009) Applications of cyanobacteria in biotechnology. *J Appl Microbiol* 106: 1-12.

Altendorf KH & Staehelin LA (1974) Orientation of membrane vesicles from *Escherichia coli* as detected by freeze-cleave electron microscopy. *J Bacteriol* 117: 888-99.

Bartual SG, Straume D, Stamsås GA, Muñoz IG, Alfonso C, Martínez-Ripoll M, Håvarstein LS & Hermoso JA (2014) Structural basis of PcsB-mediated cell separation in *Streptococcus pneumoniae*. *Nat Commun* 5: 3842.

Bauer CC, Buikema WJ, Black K & Haselkorn R (1995) A short-filament mutant of *Anabaena* sp. strain PCC 7120 that fragments in nitrogen-deficient medium. *J Bacteriol* 177: 1520-26.

Beltramello M, Piazza V, Bukauskas FF, Pozzan T & Mammano F (2005) Impaired permeability to Ins(1,4,5)P3 in a mutant connexin underlies recessive hereditary deafness. *Nat Cell Biol* 7: 63-9.

Berendt S, Lehner J, Zhang YV, Rasse TM, Forchhammer K & Maldener I (2012) Cell wall amidase AmiC1 is required for cellular communication and heterocyst development in the cyanobacterium *Anabaena* PCC 7120 but not for filament integrity. *J Bacteriol* 194: 5218-27.

Black TA, Cai Y & Wolk CP (1993) Spatial expression and autoregulation of *hetR*, a gene involved in the control of heterocyst development in *Anabaena*. *Mol Microbiol* 9: 77-84.

Boberek JM, Stach J & Good L (2010) Genetic evidence for inhibition of bacterial division protein FtsZ by berberine. *PLoS ONE* 5: e13745.

de Boer PAJ (2016) Classical spotlight: discovery of *ftsZ*. *J Bacteriol* 198: 1184.

Bonner JT (1998) The origins of multicellularity. *Int Biol* 1: 27-36.

Bos MP, Robert V & Tommassen J (2007) Biogenesis of the Gram-negative bacterial outer membrane. *Annu Rev Microbiol* 61: 191-214.

Boyer HW & Roulland-Dussoix DD (1969) A complementation analysis of the restriction and modification of DNA in *Escherichia coli*. *J Mol Bio* 41: 459-472.

Bradford MM (1976) A rapid and sensitive method for the quantification of microgram quantities of protein utilizing the principle of protein-dye binding. *Anal Biochem* 72: 248-254.

Buikema WJ & Haselkorn R (1991) Isolation and complementation of nitrogen fixation mutants of the cyanobacterium *Anabaena* sp. strain PCC 7120. *J Bacteriol* 173: 1879-85

Burnat M, Herrero A & Flores E (2014a) Compartmentalized cyanophycin metabolism in the diazotrophic filaments of a heterocysts forming cyanobacterium. *Proc Natl Acad Sci USA* 111: 3823-8.

Burnat M, Schleiff E & Flores E (2014b) Cell envelope components influencing filament length in the heterocyst-forming cyanobacterium *Anabaena* sp. strain PCC 7120. *J Bacteriol* 196: 4026-35.

Busby S & Ebright RH (1999) Transcription activation by catabolite activator protein (CAP). J Mol Biol 293: 199-213.

Bush MJ, Tschowri N, Schlimpert S, Flärdh K & Buttner MJ (2015) c-di-GMP signalling and the regulation of developmental transitions in streptomycetes. *Nat Rev Microbiol* 13: 749-60.

Büttner FM, Faulhaber K, Forchhammer K, Maldener I & Stehle T (2016) Enabling cell-cell communication via nanopore formation structure, function and localization of the unique cell wall amidase AmiC2 of *Nostoc punctiforme*. *FEBS J* 283: 1336-50.

Callahan SM & Buikema WJ (2001) The role of HetN in maintenance of the heterocyst pattern in *Anabaena* sp. PCC 7120. *Mol Microbiol* 40: 941-50.

Cameron JC, Sutter M & Kerfeld CA (2014) The carboxysome: function, structure and cellular dynamics. In Flores E & Herrero A (eds.), *The cell biology of Cyanobacteria*. Caiser Academic Press, Norfolk, UK, 171-188.

Carson MJ, Barondess J & Beckwith J (1991) The FtsQ protein of *Escherichia coli*: membrane topology, abundance, and cell division phenotypes due to overproduction and insertion mutations. *J Bacteriol* 173: 2187-95.

Cassier-Chauvat C & Chauvat F (2014) Cell Division in Cyanobacteria. In Flores E & Herrero A (eds) *The cell biology of Cyanobacteria*. Caister Academic Press, Norfolk, UK, 7-27.

Chen JC, Minev M & Beckwith J (2002) Analysis of *ftsQ* mutant alleles in *Escherichia coli*: complementation, septal localization, and recruitment of downstream cell division proteins. *J Bacteriol* 184: 695-705.

Ciani B, Bjelic S, Honnappa S, Jawhari H, Jaussi R, Payapilly A, Jowitt T, Stainmetz MO, Kammerer RA (2010) Molecular basis of coiled-coil oligomerization-state specificity. *Proc Natl Acad Sci USA* 46: 19850-5.

Claessen D, Rozen DE, Kuipers OP, Søgaard-Andersen L & van Wezel GP (2014) Bacterial solutions to multicellularity: a tale of biofilms, filaments and fruiting bodies. *Nat Rev Microbiol* 12: 115-124.

Corrales-Guerrero L, Mariscal V, Nürnberg DJ, Elhai J, Mullineaux CW, Flores E & Herrero A (2014a) Subcellular localization and clues for the function of the HetN factor influencing heterocyst distribution in *Anabaena* sp. PCC 7120. *J Bacteriol* 196: 3452-60.

Corrales -Guerrero L, Flores E & Herrero A (2014b) Relationships between the ABC-transporter HetC and peptides that regulate the spatiotemporal pattern of heterocyst distribution in *Anabaena*. *PLoS One* 9: e104571.

Corrales-Guerrero L, Mariscal V, Flores E & Herrero A (2013) Functional dissection and evidence for intracellular transfer of the heterocyst-differentiation PatS morphogen. *Mol Microbiol* 88: 1093-1105.

Corrales-Guerrero L, Tal A, Arbel-Goren R, Mariscal V, Flores E, Herrero A & Stavans J (2015) Spatial fluctuations in expression of the heterocyst differentiation regulatory gene *hetR* in *Anabaena* filaments. *Plos Genet* 11: e1005031.

Domadia PN, Bhunia A, Sivaraman J, Swarup S & Dasgupta D (2008) Berberine targets assembly of *Escherichia coli* cell division protein FtsZ. *Biochemistry* 47: 3225-34.

Dziadek J, Rutherford SA, Madiraju MV, Atkinson MA & Rajagopalan M (2003) Conditional expression of *Mycobacterium smegmatis ftsZ*, an essential cell division gene. *Microbiology* 149: 1593-603.

Ehira S & Ohmori M (2006) NrrA, a nitrogen-responsive regulator facilitates heterocyst development in the cyanobacterium *Anabaena* sp. strain PCC 7120. *Mol Microbiol* 59: 1692-1703.

Ehira S & Ohmori M (2014) NrrA directly regulates expression of the *fraF* gene and antisense RNAs for *fraE* in the heterocyst-forming cyanobacterium *Anabaena* sp. strain PCC 7120. *Microbiology* 160: 844-50.

Ekman M, Picossi S, Campbell EL, Meeks JC & Flores E (2013) A *Nostoc punctiforme* sugar transporter necessary to establish a cyanobacterium-plant symbiosis. *Plant Physiol* 161: 1984-92.

Elhai J & Wolk CP (1988a) A versatile class of positive-selection vectors based on the nonviability of palindrome-containing plasmids that allows cloning into long polylinkers. *Gene* 68: 119-38.

Elhai J & Wolk CP (1988b) Conjugal transfer of DNA to cyanobacteria. *Methods Enzymol* 167: 747-54.

Elhai J, Vepritskiy A, Muro-Pastor AM, Flores E & Wolk CP (1997) Reduction of conjugal transfer efficiency by three restriction activities of *Anabaena* sp. strain PCC 7120. *J Bacteriol* 179: 1998-2005.

van den Ent F, Vinkenvleugel TM, Ind A, West P, Veprintsev D, Nanninga N, den Blaauwen T & Löwe J (2008) Structural and mutational analysis of the cell division protein FtsQ. *Mol Microbiol* 68: 110-23.

Ermakova M, Battchikova N, Richaud P, Leino H, Kosourov S, Isojärvi J, Peltier G, Flores E, Cournac L, Allahverdiyeva Y & Aro EM (2014) Heterocyst-specific flavodiiron protein Flv3B enables oxic diazotrophic growth of the filamentous cyanobacterium *Anabaena* sp. PCC 7120. *Proc Natl Acad Sci USA* 111: 11205-10.

Ernst A, Black T, Cai Y, Panoff JM, Tiwari DN & Wolk CP (1992) Synthesis of nitrogenase in mutants of the cyanobacterium *Anabaena* sp. strain PCC 7120 affected in heterocyst development or metabolism. 174: 6025-32.

Errington J, Daniel RA & Scheffers DJ (2003) Cytokinesis in Bacteria. *Microbiol Mol Biol Rev* 67: 52-65.

Escudero L, Mariscal V & Flores E (2015) Functional dependence between septal protein SepJ from *Anabaena* sp. strain PCC 7120 and an amino acid ABC-type uptake transporter. *J Bacteriol* 197: 2721-30.

Fan Q, Huang G, Lechno-Yossef S, Wolk CP, Kaneko T & Tabata S (2005) Clustered genes required for synthesis and deposition of envelope glycolipids in *Anabaena* sp. PCC 7120. *Mol Microbiol* 58: 227-243.

Fan Q, Lechno-Yossef S, Ehira S, Kaneko T, Ohmori M, Sato N, Tabata S & Wolk CP (2006) Signal transduction genes required for heterocyst maturation in *Anabaena* sp. srain PCC 7120. *J Bacteriol* 188: 6688-93.

Fay P (1992) Oxygen relations of nitrogen fixation in cyanobacteria. *Microbiol Rev* 56: 340-73.

Feldmann EA, Ni S, Sahu ID, Mishler CH, Levengood JD, Kushnir Y, McCarrick RM, Lorigan GA, Tolbert BS, Callahan SM & Kennedy MA (2012) Differential biding between PatS C-terminal peptide fragments and HetR from *Anabaena* sp. PCC 7120. *Biochemistry* 51: 2436-42.

Feldmann EA, Ni S, Sahu ID, Mishler CH, Risser DD, Murakami JL, Tom SK, McCarrick RM, Lorigan GA, Tolbert BS, Callahan SM & Kennedy MA (2011) Evidence for direct binding between HetR from *Anabaena* sp. PCC 7120 and PatS-5. *Biochemistry* 50: 9212-24.

Fiedler G, Arnold M, Hannus S & Maldener I (1998) The DevBCA exporter is essential for envelope formation in heterocysts of the cyanobacterium *Anabaena* sp. strain PCC 7120. *Mol Microbiol* 27: 1193-202.

Flaherty BL, Johnson DBF & Golden JW (2014) Deep sequencing of HetR-bound DNA reveals novel HetR targets in Anabaena sp. strain PCC 7120. *BMC Microbiol* 14: 255.

Flaherty BL, Van Nieuwerburgh F, Head SR & Golden JW (2011) Directional RNA deep sequencing sheds new light on the transcriptional response of *Anabaena* sp. strain PCC 7120 to combined-nitrogen deprivation. *BMC Genomics* 12: 332.

Flemming HC, Wingender J, Szewzyk U, Rice SA & Kjelleberg (2016) Biofilms: an emergent form of bacterial life. *Nat Rev Microbiol* 14: 563-75.

Flores E & Herrero A (2010) Compartmentalized function through cell differentiation in filamentous cyanobacteria. *Nat Rev Microbiol* 8: 39-50.

Flores E, Frías JE, Rubio LM & Herrero A (2005) Photosynthetic nitrate assimilation in cyanobacteria. *Photosynt Res* 83: 117-33.

Flores E, Herrero A, Forchhammer K & Maldener I (2016) Septal junctions in filamentous heterocyst-forming cyanbacteria. *Trends Microbiol* 24: 79-82.

Flores E, Herrero A, Wolk CP & Maldener I (2006) Is the periplasm continuous in filamentous multicellular cyanobacteria? *Trends Microbiol* 14: 439-43.

Flores E, Pernil R, Muro-Pastor AM, Mariscal V, Maldener I, Lechno-Yossef S, Fan Q, Wolk CP & Herrero A (2007) Septum-localized protein required for filament integrity and diazotrophy in the heterocyst-forming cyanobacterium *Anabaena* sp. strain PCC 7120. *J Bacteriol* 189: 3884-90.

Frías JE, Flores E & Herrero A (1994) Requirement of the regulatory protein NtcA for the expression of nitrogen assimilation and heterocyst development genes in the cyanobacterium *Anabaena* sp. PCC 7120. *Mol Microbiol* 14: 823-32.

Gennaris A, Ezraty B, Henry C, Agrebi R, Vergnes A, Oheix E, Bos J, Leverrier P, Espinosa L, Szewczyk J, Vertommen D, Iranzo O, Collet JF & Barras F (2015) Repairing oxidized proteins in the bacterial envelope using respiratory chain electrons. *Nature* 528: 409-12.

Giddings TH & Staehelin LA (1978) Plasma membrane architecture of *Anabaena cylindrical*: occurrence of microplasmodesmata and chages associated with heterocyst development and the cell cycle. *Cytobiologie* 16: 235-49.

Giddings TH & Staehelin LA (1981) Observation of microplasmodesmata in both heterocyst-forming and non-heterocyst forming filamentous cyanobacteria by freeze-fracture electron microscopy. *Arch Microbiol* 129: 295-8.

Giovannoni SJ, Turner S, Olsen GJ, Barners S, Lane DJ & Pace NR (1988) Evolutionary relationships among cyanobacteria and green chloroplast. *J Bacteriol* 170: 3584-92.

Golden JW & Yoon HS (2003) Heterocyst development in *Anabaena*. Curr Opin Microbiol 6: 557-63.

Grosberg RK & Strathmann RR (2007) The evolution of multicellularity: a minor major transition? *Annu Rev Ecol Evol Syst* 38: 621-54.

Gupta M & Carr NG (1981) Enzymes activities related to cyanophycin metabolism in heterocysts and vegetative cells of *Anabaena* spp. *J Gen Microbiol* 125: 17-23.

Hahn A & Schleiff E (2014) The cell envelope. In Flores E & Herrero A (eds) *The cell biology of Cyanobacteria*. Caister Academic Press, Norfolk, UK, 29-87.

Hanahan D (1983) Studies on transformation of *Escherichia coli* with plasmids. *J Mol Biol* 166: 557-580.

Harry EJ (2001) Bacterial cell division: regulating Z-ring formation. *Mol Microbiol* 40: 795-803.

Haugland RP (2005) The Handbook—a Guidebook to Fluorescent Probes and Labelling Technologies. Carlsbad, CA, USA: Invitrogen Corp.

Herrero A & Burnat M (2014) Cyanophycin, a cellular nitrogen reserve material. In Flores E & Herrero A (eds) *The cell biology of Cyanobacteria*. Caister Academic Press, Norfolk, UK, 211-219.

Herrero A, Muro-Pastor AM & Flores E (2001) Nitrogen control in cyanobacteria. *J Bacteriol* 183: 411-25.

Herrero A, Muro-Pastor AM, Valladares A & Flores E (2004) Cellular differentiation and the NtcA transcription factor in filamentous cyanobacteria. *FEMS Microbiol Rev* 28: 469-87.

Herrero A, Picossi S & Flores E (2013) Gene expression during heterocyst differentiation. *Adv Bot Res* 65: 281-329.

Herrero A, Stavans J & Flores E (2016) The multicellular nature of filamentous heterocyst-forming cyanobacteria. *FEMS Microbiol Rev* 40: 831-54.

Hervé JC & Derangeon M (2013) Gap-junction-mediated cell-to-cell communication. *Cell Tissue Res* 352: 21-31

Huang G, Fan Q, Lechno-Yossef S, Wojciuch E, Wolk CP, Kaneko T & Tabata S (2005) Clustered genes required for the synthesis of heterocyst envelope polysaccharide in *Anabaena* sp. PCC 7120. *J Bacteriol* 187: 1114-23.

Ishikawa S, Kawai Y, Hiramatsu K, Kuwano M & Ogasawara N (2006) A new FtsZ-interacting protein, YlmF, complements the activity of FtsA during progression of cell division in *Bacillus subtilis*. *Mol Microbiol* 60: 1364-80.

Jack DL, Yang NM & Saier MH Jr (2001) The drug/metabolite transporter superfamily. *Eur J Biochem* 268: 3620-39.

Jakimowicz D & van Wezel GP (2012) Cell division and DNA segregation in *Streptomyces*: how to build a septum in the middle of nowhere. *Mol Microbiol* 85: 393-404.

Jüttner F (1983) 14C-labeled metabolites in heterocysts and vegetative cells of *Anabaena cylindrica* filaments and their presumptive function as transport vehicles of organic carbon and nitrogen. *J Bacteriol* 155: 628-33.

Kaneko T, Nakamura Y, Wolk CP, Kuritz T, Sasamoto S, Watanabe A, Iriguchi M, Ishikawa A, Kawashima K, Kimura T, Kishida Y, Kohara M, Matsumoto M, Matsuno A, Muraki A, Nakazaki N, Shimpo S, Sugimoto M, Takazawa M, Yamada M, Yasuda M & Tabata S (2001) Complete genomic sequence of the filamentous nitrogen-fixing cyanobacterium *Anabaena* sp. strain PCC 7120. *DNA Re*s 8: 205-13.

Karimova G, Dautin N & Ladant D (2005) Interaction network among *Escherichia coli* membrane proteins involved in cell division as revealed by bacterial two-hybrid analysis. *J Bacteriol* 187: 2233-43.

Karimova G, Pidoux J, Ullmann A & Ladant D (1998) A bacterial two-hybrid system based on a reconstituted signal transduction pathway. *Proc Natl Acad Sci USA* 95: 5752-56.

Kirkpatrick CL & Viollier PH (2011) New(s) to the (Z-)ring. *Curr Opin Microbiol* 14: 691-7.

Klint J, Rasmussen U & Bergman B (2007) FtsZ may have dual roles in the filamentous cyanobacterium *Nostoc/Anabaena* sp. strain PCC 7120. *J Plant Physiol* 164: 11-18.

Koebnik R, Locher KP & Van Gelder P (2000) Structure and function of bacterial outer membrane proteins: barrels in a nutshell. *Mol Microbiol* 37: 239-53.

Kuhn I, Peng L, Bedu S & Zhang CC (2000) Developmental regulation of cell division protein FtsZ in *Anabaena* sp. strain PCC 7120, a cyanobacterium capable of terminal differentiation. *J Bacteriol* 182: 4640-43.

Laemmli UK (1970) Cleavage of structural proteins during the assembly of the head of the bacteriophage T4. *Nature* 227: 680-5.

Lang NJ & Fay P (1971) The heterocysts of blue-green algae. II. Details of ultrastructure. *Proc Roy Soc Lond* 178: 193-203.

Lehner J, Berendt S, Dörsam B, Pérez R, Forschhammer K & Maldener I (2013) Prokaryotic multicellularity: a nanopore array for bacterial cell communication. *FASEB J* 27: 2293-2300.

Lehner J, Zhang YV, Berendt S, Rasse TM, Forchhammer K & Maldener I (2011) The morphogene AmiC2 is pivotal for multicellular development in the cyanobacterium *Nostoc punctiforme*. *Mol Microbiol* 79: 1655-69.

Li JH, Laurent S, Konde V, Bédu S & Zhang CC (2003) An increase in the levels of 2-oxoglutarate promotes heterocyst development in the cyanobacterium *Anabaena* sp. PCC 7120. *Microbiology* 149: 3257-63.

Liberton M & Pakrasi HB (2008) Membrane systems in cyanobacteria. In Herrero A & Flores E (eds) *The Cyanobacteria: molecular biology, genomics and evolution*. Caister Academic Press, Norfolk, UK. 271-287.

Lippa AM & Goulian M (2012) Pertubation of the oxidizing environment of the periplasm stimulates the PhoQ/PhoP system in *Escherichia coli*. *J Bacteriol* 194: 1457-63.

López-Igual R, Flores E & Herrero A (2010) Inactivation of a heterocyst-specific invertase indicates a principal role of sucrose catabolism in the heterocysts of *Anabaena* sp. *J Bacteriol* 192: 5526-33.

Lowry OH, Rosebrough NJ, Farr AL & Randall RJ (1951) Protein measurement with the Folin phenol reagent. *J Biol Chem* 193: 265-75.

Lupas AN & Gruber M (2005) The structure of alpha-helical coiled coils. *Adv Protein Chem* 70: 37-78.

Luque I, Flores E & Herrero A (1994) Molecular mechanism for the operation of nitrogen control in cyanobacteria. *EMBO J* 13: 2862-9.

Luque I & Forchhammer K (2008) Nitrogen assimilation and C/N balance sensing. In: Herrero A & Flores E (eds), The Cyanobacteria. Molecular biology, genomics and evolution. Caister Academic Press, UK, 335-382.

Lyons TW, Reinhard CT & Planavsky NJ (2014) The rise of oxygen in Earth's early ocean and atmosphere. *Nature* 506: 307-15.

Mackinney G (1941) Absorption of light by chlorophyll solutions. *J Biol Chem* 140: 109-12.

Mahrenholz CC, Abfalter IG, Bodenhofer U, Volkmer R & Hochreiter S (2011) Complex networks govern coiled-coil oligomerizatio- predicting and profiling by means of a machine learning approach. *Mol Cell Proteomics* doi:10.1074.

Maldener I, Summers ML & Sukenik A (2014) Cellular differentiation in filamentous cyanobacteria. In Flores E & Herrero A (eds) *The cell biology of Cyanobacteria*. Caister Academic Press, Norfolk, UK. 293-304.

Mandakovic D, Trigo C, Andrade D, Riquelme B, Gómez-Lillo G, Soto-Liebe K, Díez & Vásquez M (2016) CyDiv, a conserved and novel filamentous cyanobacterial cell division protein involved in septum localization. *Front Microbiol* 7: 94.

Marbouty M, Saguez C, Cassier-Chauvat C & Chauvat F (2009a) Characterization of the FtsZ-interacting septal proteins SepF and Ftn6 in the spherical-celled cyanobacterium *Synechocystis* strain PCC 6803. *J Bacteriol* 191: 6178-85.

Marbouty M, Saguez C, Cassier-Chauvat C & Chauvat F (2009b) ZipN, an FtsA-like orchestrator of divisome assembly in the model cyanobacterium *Synechocystis* PCC 6803. *Mol Microbiol* 74: 409-20.

Marbouty M, Saguez C & Chauvat F (2009c) The cyanobacterial cell division factor Ftn6 contains an N-terminal DnaD-like domain. *BMC Struct Biol* 9: 54.

Mariscal V (2014) Cell-cell joining proteins in heterocyst-forming cyanobacteria. In Flores E & Herrero A (eds). *The Cell Biology of Cyanobacteria*. Caister Academic Press, Norfolk, UK, 293-304.

Mariscal V & Flores E (2010) Multicellularity in a heterocyst-forming cyanobacterium: pathways for intercellular communication. *Adv Exp Med Biol* 675: 123-35.

Mariscal V, Herrero A & Flores E (2007) Continuous periplasm in a filamentous, heterocyst-forming cyanobacterium. *Mol Microbiol* 65: 1139-45.

Mariscal V, Herrero A, Nenninger A, Mullineaux CW & Flores E (2011) Functional dissection of the three-domain SepJ protein joining the cells in cyanobacterial trichomes. *Mol Microbiol* 79: 1077-88.

Mariscal V, Nürnberg DJ, Herrero A, Mullineaux CW & Flores E (2016) Overexpression of SepJ alters septal morphology and heterocyst pattern regulated by diffusible signals in *Anabaena. Mol Microbiol* 101: 968-81.

Markwell MA, Haas SM, Bieber LL & Tolbert NE (1978) A modification of the Lowry procedure to simplify protein determination in membrane and lipoprotein samples. *Anal Biochem* 87: 206-10.

Martín-Figueroa E, Navarro f & Florencio FJ (2000) The GS-GOGAT pathway is not operative in the heterocysts. Cloning and expression of *glsF* gene from the cyanobacterium *Anabaena* sp. PCC 7120. *FEBS Lett* 476: 282-6.

Meeks JC & Elhai J (2002) Regulation of cellular differentiation in filamentous cyanobacteria in free-living and plant associated symbiotic growth states. *Microbiol Mol Biol Rev* 66: 94-121.

Meeks JC, Wolk CP, Thomas J, Lockau W, Shaffer PW, Austin SM, Chien WS & Galonsky A (1977) The pathways of assimilarion of $^{13}NH_4^+$ by the cyanobacterium, *Anabaena cylindrica*. *J Biol Chem* 252: 7894-900.

Meeske AJ, Riley EP, Robins WP, Uehara T, Mekalanos JJ, Kahne D, Walker S, Kruse AC, Bernhardt TG & Rudner DZ (2016) SEDS proteins are a widespread family of bacterial cell wall polymerases. *Nature* 537: 634-38.

Merino-Puerto V, Herrero A & Flores E (2013) Cluster of genes that encode positive and negative elements influencing filament length in a heterocyst-forming cyanobacterium. *J Bacteriol* 195: 3957-66.

Merino-Puerto V, Mariscal V, Mullineaux CW, Herrero A & Flores E (2010) Fra proteins influencing filament integrity, diazotrophy and localization of septal protein SepJ in heterocyst-forming cyanobacterium *Anabaena* sp. *Mol Microbiol* 75: 1159-70.

Merino-Puerto V, Mariscal V, Schwarz H, Maldener I, Mullineaux CW, Herrero A & Flores E (2011a) FraH is required for reorganization of intracelular membranes during heterocyst differentiation in *Anabaena* sp. strain PCC 7120. *J Bacteriol* 193: 6815-23.

Merino-Puerto V, Schwarz H, Maldener I, Mariscal V, Mullineaux CW, Herrero A & Flores E (2011b) FraC/FraD-dependent intercellular molecular exchange in the filaments of a heterocyst-forming cyanobacterium, *Anabaena* sp. *Mol Microbiol* 82: 87-98.

Miyagishima S, Wolk CP & Osteryoung KW (2005) Identification of cyanobacterial cell division genes by comparative and mutational analyses. *Mol Microbiol* 56: 126-43.

Moslavac S, Bredemeier R, Mirus O, Granvogl B, Eichacker LA & Schleiff E (2005) Proteomic analysis of the outer membrane of *Anabaena* sp. strain PCC 7120. *J Proteome Res* 4: 1330-8.

Moslavac S, Nicolaisen K, Mirus O, Al Dehni F, Pernil R, Flores E, Maldener I & Schleiff E (2007) A TolC-like protein is required for heterocyst development in *Anabaena* sp. PCC 7120. *J Bacteriol* 189: 7887-95.

Mullineaux CW, Mariscal V, Nenninger A, Khanum H, Herrer A, Flores E & Adams DG (2008) Mechanism of intercellular molecular exchange in heterocyst-forming cyanobacteria. *EMBO J* 27: 1299-1308.

Mullineaux CW, Nenninger A, Ray N & Robinson C (2006) Diffusion of green fluorescent protein in three cell environments in *Escherichia coli*. *J Bacteriol* 188: 3442-8.

Muñoz-Dorado J, Marcos-Torres FJ, García-Bravo E, Moraleda-Muñoz A & Pérez J (2016) Myxobacteria: moving, killing, feeding, and surviving together. *Front Microbiol* doi:10.3389.

Muro-Pastor AM, Valladares A, Flores E & Herrero A (2002) Mutual dependence of the expression of the cell differentiation regulatory protein HetR and the global nitrogen regulator NtcA during heterocyst differentiation. *Mol Microbiol* 44: 1377-85.

Muro-Pastor MI, Reyes JC & Florencio FJ (2001) Cyanobacteria perceive nitrogen status by sensing intracellular 2-oxoglutarate levels. *J Biol Chem* 274: 38320-28.

Murray NE, Brammar WJ & Murray K (1977) Lambdoid phages that simplify the recovery of in vitro recombinants. *Mol Gen Genet* 150: 53-61.

Nagel de Zwaig R & Luria SE (1967) Genetics and physiology of colicin-tolerant mutants of *Escherichia coli*. *J Bacteriol* 94: 1112-23.

Nayar AS, Yamaura H, Rajagopalan R, Risser DD & Callahan Sm (2007) FraG is necessary for filament integrity and heterocyst maturation in the cyanobacterium *Anabaena* sp. strain PCC 7120. *Microbiology* 153: 601-7.

Ni S, Sheldrick GM, Benning MM & Kennedy MA (2009) The 2Å resolution crystal structure of HetL, a pentapeptide repeat protein involved in regulation of heterocyst differentiation in the cyanobacterium *Nostoc* sp. strain PCC 7120. *J Struc Biol* 165: 47-52.

Nicolaisen K, Mariscal V, Bredemeier R, Pernil R, Moslavac S, López-Igual R, Maldener I, Herrero A, Schleiff E & Flores E (2009) The outer membrane of a heterocyst-forming cyanobacterium is a permeability barrier for uptake of metabolites that are exchanged between cells. *Mol Microbiol* 74 58-70.

Nieves-Morión M, Lechno-Yossef S, López-Igual R, Frías JE, Mariscal V, Nürnberg DJ, Mullineaux CW, Wolk CP & Flores E (2017a) Specific glucoside transporters influence septal structure and function in the filamentous, heterocyst-forming cyanobacterium *Anabaena* sp. strain PCC 7120. *J Bacteriol* doi: 10.1128.

Nieves-Morión M, Mullineaux CW & Flores E (2017b) Molecular diffusion through cyanobacterial septal junctions. *mBio* 8: e01756.

Nikaido H (2003) Molecular basis of bacterial outer membrane permeability revisted. *Microbiol Mol Biol* Rev 67: 593-656.

Noinaj N, Kuszak AJ, Gumbart JC, Lukacik P, Chang H, Easley NC, Lithgow & Buchanan SK (2013) Structural insight into the biogenesis of β-barrel membrane proteins. *Nature* 19: 385-90.

Nürnberg DJ, Mariscal V, Bornikoel J, Nieves-Morión M, Krauβ N, Herrero A, Maldener I, Flores E, Mullineaux CW (2015) Intercellular diffusion of a fluorescent sucrose analog via the septal junctions in a filamentous cyanobacterium. *mBio* 6: e02109.

Nürnberg DJ, Mariscal V, Parker J, Mastroianni G, Flores E & Mullineaux CW (2014) Branching and intercellular communication in the Section V cyanobacterium *Mastigocladus laminosus*, a complex multicellular prokaryote. *Mol Microbiol* 91: 935-49.

Olmedo-Verd E, Muro-Pastor AM, Flores E & Herrero A (2006) Localized induction of the ntcA regulatory gene in developing heterocysts of *Anabaena* sp. strain PCC 7120. *J Bacteriol* 188: 6694-6699.

Omairi-Nasser A, Haselkorn R, & Austin JR 2nd (2014) Visualization of channels connecting cells in filamentous nitrogen-fixing cyanobacteria. *FASEB J* 28: 3016-22.

Omairi-Nasser A, Mariscal V, Austin JR 2nd & Haselkorn R (2015) Requirement of Fra proteins for communication channels between cells in the filamentous nitrogen-fixing cyanobacterium Anabaena sp. PCC 7120. *Proc Natl Acad Sci USA* 112: E4458-64.

Paz-Yepes J, Herrero A & Flores E (2007) The NtcA-regulated amtB gene is necessary for full methylammonium uptake activity in the cyanobacterium *Synechococcus elongatus*. J Bacteriol 189: 7791-98.

de Pedro MA, Quintela JC, Höltje JV & Schwarz H (1997) Murein segregation in *Escherichia coli*. *J Bacteriol* 179: 2823-34.

Pernil R, Herrero A & Flores E (2010) Catabolic function of compartmentalized alanine dehydrogenase in the heterocyst-forming cyanobacterium *Anabaena* sp. strain PCC 7120. *J Bacteriol* 192: 5165-72.

Pfaffl MW (2001) A new mathematical model for relative quantification in real-time RT-PCR. *Nucleic Acids Res* 29: e45.

Pfaffl MW, Horgan GW & Dempfle L (2002) Relative expression software tool (REST) for group-wise comparison and statistical analysis of relative expression results in real-time PCR. *Nucleic Acids Res* 30: e36.

Pfeffer C, Larsen S, Song J, Dong M, Besenbacher F, Meyer RL, Kjeldsen KU, Schreiber L, Gorby YA, El-Naggar MY, Leung KM, Schramm A, Risgaard-Petersen N, Nielsen LP (2012) Filamentous bacteria transport electrons over centimeter distances. *Nature* 491: 218-21.

Picossi S, Flores E & Herrero A (2013) Diverse roles of the GlcP glucose permease in free-living and symbiotic cyanobacteria. *Plant Signal Behav* 8: e27416.

Picossi S, Flores E & Herrero A (2014) ChIP analysis unravels an exceptionally wide distribution of DNA binding sites for the NtcA transcription factor in a heterocyst-forming cyanobacterium. *BMC Genomics* 15: 22.

Picossi S, Valladares A, Flores E & Herrero A (2004) Nitrogen-regulated genes for the metabolism of cyanophycin, a bacterial nitrogen reserve polymer: expression and mutational analysis of two cyanophycin synthetase and cyanophycinase gene clusters in heterocyst-forming cyanobacterium *Anabaena* sp. PCC 7120. *J Biol Chem* 279: 11582-92.

Pierson BK & Castenholz RW (1974) A phototrophic gliding filamentous bacterium of hot springs, *Chloroflexus aurantiacus*, gen. and sp. nov. *Arch Microbiol* 100: 5-24.

Plominsky AM, Delherbe N, Mandakovic D, Riquelme B, González K, Bergman B, Mariscal V & Vásquez M (2015) Intercellular transfer along the trichomes of the invasive terminal heterocyst forming cyanobacterium *Cylindrospermopsis raciborskii* CS-505. *FEMS Microbiol Lett* 362: fnu009.

Ramos-León F, Mariscal V, Frías JE, Flores E & Herrero A (2015) Divisome-dependent subcellular localization of cell-cell joining protein SepJ in the filamentous cyanobacterium *Anabaena*. *Mol Microbiol* 96: 566-80.

Ramakers C, Ruijter JM, Deprez RH & Moorman AF (2003) Assumption-free analysis of quantitative real-time polymerase chain reaction (PCR) data. *Neurosci Lett* 339:62-6.

Rico A, Krupka M & Vicente M (2013) In the beginning. *Escherichia coli* assembled the proto-ring: an initial phase of division. *J Biol Chem* 288: 20830-36.

Rippka R (1972) Photoheterotrophy and chemoheterotrophy among unicellular blue-green algae. *Arch Microbiol* 87: 93-98.

Rippka R, Deruelles J, Waterbury JB, Herdman M & Stainer RY (1979) Generic assignment, strain histories and properties of pure cultures of cyanobacteria. *J General Microbiol* 111: 1-61.

Rivers O, Videau P, Callahn S (2014) Mutation of sepJ reduces the intercellular signal range of a *hetN*-dependent paracrine signal, but not of a *patS*-dependent signal, in the filamentous cyanobacterium *Anabaena* sp. strain PCC 7120. *Mol Microbiol* 94: 1260-71.

Robson SA & King GF (2006) Domain architecture and structure of the bacterial cell division protein DivIB. *Proc Natl Acad Sci USA* 103: 6700-05.

Rubio LM & Ludden PW (2008) Biosynthesis of the iron-molybdenum cofactor of nitrogenase. *Ann Rev Microbiol* 93-111.

Rudolf M, Tetik N, Ramos-León F, Flinner N, Ngo G, Stevanovic M, Burnat M, Pernil R, Flores E & Schleiff E (2015) The peptidoglycan-binding protein SjcF1 influences septal junction function and channel formation in the filamentous cyanobacterium *Anabaena*. *mBio* 6: e00376-15.

Ruiz N (2016) Filling holes in peptidoglycan biogenesis of *Escherichia coli*. *Curr Opin Microbiol* 34: 1-6.

Ruiz N, Kahne D & Silhavy TJ (2006) Advances in understanding bacterial outer-membrane biogenesis. *Nat Rev Microbiol* 4: 57-66.

Sakr S, Thyssen M, Denis M & Zhang CC (2006) Relationship among several key cell cycle events in the developmental cyanobacterium *Anabaena* sp. strain PCC 7120. *J Bacteriol* 188: 5958-65.

Sambrook J & Russell DW (2001) *Molecular Cloning: A laboratory manual. Second Edition*. Cold Spring Harbor Laboratory Press, Cold Spring Harbor, NY.

Sánchez-Pulido L, Devos D, Genevrois S, Vicente M & Valencia A (2003) POTRA: a conserved domain in the FtsQ family and a class of β-barrel outer membrane proteins. *Trends Biochem Sci* 28: 523-6.

Santa Cruz A, Meşe G, Valiuniene L, Brink PR, White TW & Valiunas V (2015) Altered conductance and permeability of Cx40 mutantions associated with atrial fibrillation. *J Gen Physi*ol 146: 387-98.

Schamel WW (2008) Two-dimensional blue native polyacrylamide gel electrophoresis. *Curr Protoc Cell Biol*. Chapter 6: Unit 6.10.

Schirrmeister BE, Antonelli A & Bagheri HC (2011) The origin of multicellularity in cyanobacteria. *BMC Evol Biol* 11: 45.

Schirrmeister BE, de Vos, JM, Antonelli A & Bagheri HC (2013) Evolution of multicellularity coincided with the increased diversification of cyanobacteria and the Great Oxidation Event. *Proc Natl Acad Sci USA* 110: 1791-6.

Sherman DM, Tucker D & Sherman LA (2000) Heterocyst development and localization of cyanophycin in N_2-fixing cultures of *Anabaena* sp. PCC 7120 (cyanobacteria). *J Phycol* 36: 932-941.

Shih PM, Wu D, Latifi A, Axen SD, Fewer DP, Talla E, Calteau A, Cai F, Tandeau de Marsac N, Rippka R, Herdman M, Sivonen K, Coursin T, Laurent T, Goodwin L, Nolan M, Davenport KW, Han CS, Rubin EM, Eisen JA, Woyke T, Gugger M & Kerfeld CA (2013) Improving the coverage of the cyanobacterial phylum using diversity-driven genome sequencing. *Proc Natl Acad Sci USA* 110: 1053-8.

Snyder DS, Brahamsha B, Azadi P & Palenik B (2009) Structure of compositionally simple lipopolysaccharide from marine *Synechococcus*. *J Bacteriol* 191: 5499-5509.

Sperandeo P, Martorana AM & Polissi A (2016) Lipopolysaccharide biogenesis and transport at the outer membrane of Gram-negative bacteria. *Biochim Biophys Acta* doi: 10.1016.

Stal LJ & Zehr JP (2008) Cyanobacterial nitrogen fixation in the ocean: diversity, regulation and ecology. In Herrero A & Flores E (eds) *The Cyanobacteria: molecular biology, genomics and evolution*. Caister Academic Press, Norfolk, UK, 423-446.

Staron P, Forchhammer K & Maldener I (2011) Novel ATP-driven pathway of glycolipid export involving TolC protein. *J Biol Chem* 286: 38202-10.

Stewart WD, Fitzgerald GP & Burris RH (1967) *In situ* studies on nitrogen fixation with the acetylene reduction technique. *Science* 158: 536.

Studier FW & Moffatt BA (1986) Use of bacteriophage T7 RNA polymerase to direct selective high-level expression of cloned genes. *J Mol Biol* 189: 113-130.

Tanigawa R, Shirokane M, Maeda Si S, Omata T, Tanaka K & Takahashi H (2002) Transcriptional activation of NtcA-dependent promoters of *Synechococcus* sp. PCC 7942 by 2-oxoglutarate *in vitro*. *Proc Natl Acad Sci* USA 99: 4251-5.

Thomas J, Meeks JC, Wolk CP, Shaffer PW & Austin SM (1977) Formation of glutamine form [13N]ammonia, [13N]dinitrogen, and [14C]glutamate by heterocysts isolated from *Anabaena cylindrical*. *J Bacteriol* 129: 1545-55.

Thompson CL, Vier R, Mikaelyan A, Wienemann T, Brune A (2012) '*Candidatus Arthromitus*' revised: segmented filamentous bacteria in arthropod guts are members of *Lachnospiraceae*. *Environ Microbiol* 14: 1454-65.

Tomitani A, Knoll AH, Cavanaugh CM & Ohno T (2006) The evolutionary diversification of cyanobacteria: molecular-phylogenetic and paleontological perspectives. *Proc Natl Acad Sci USA* 103: 5422-47.

Turner RD, Waldemar V & Foster SJ (2014) Different walls for rods and balls: the diversity of peptidoglycan. *Mol Microbiol* 91: 862-74.

Typas A, Banzhaf M, Gross CA & Vollmer W (2012) From the regulation of peptidoglycan synthesis to bacterial growth and morphology. *Nat Rev Microbiol* 10 123-36.

Valladares A, Flores E & Herrero A (2008) Transcription activation by NtcA and 2-oxoglutarate of three genes involved in heterocyst differentiation in the cyanobacterium *Anabaena* sp. strain PCC 7120. *J Bacteriol* 190: 6126-33.

Valladares A, Flores E & Herrero A (2016) The heterocyst differentiation transcriptional regulator HetR of the filamentous cyanobacterium *Anabaena* forms tetramers and can be regulated by phosphorylation. *Mol Microbiol* 99: 808-19.

Valladares A, Herrero A, Pils D, Schmetterer G & Flores E (2003) Cytochrome *c* oxidase genes required for nitrogenase activity and diazotrophic growth in Anabaena sp. PCC 7120. *Mol Microbiol* 47: 1239-49.

Valladares A, Maldener I, Muro-Pastor AM, Flores E & Herrero A (2007) Heterocyst development and diazotrophic metabolism in terminal respiratory oxidase mutants of the cyanobacterium *Anabaena* sp. strain PCC 7120. *J Bacteriol* 189: 4425-30.

Valladares A, Montesinos ML, Herrero A & Flores E (2002) An ABC-type, high-affinity urea permease identified in cyanobacteria. *Mol Microbiol* 43: 703-15.

Vargas WA, Nishi CN, Giarrocco LE & Salerno GL (2011) Differential roles of alkaline/neutral invertases in *Nostoc* sp. PCC 7120: Inv-B isoform is essential for diazotrophic growth. *Planta* 233: 153-62.

Vázquez-Bermúdez MF, Flores E & Herrero A (2002) Analysis of binding sites for the nitrogen-control transcription factor NtcA in the promoters of *Synechococcus* nitrogen-regulated genes. *Biochim Biophys Acta* 1578: 95-8.

Vicente M, Gómez MJ & Ayala JA (1998) Regulation of transcription of cell division genes in the *Escherichia coli dcw* cluster. *Cell Mol Life Sci* 54: 317-24.

Villanelo F, Ordenes A, Brunet J, Lagos R & Monasterio O (2011) A model for the *Escherichia coli* FtsB/FtsL/FtsQ cell division complex. *BMC Struct Biol* 11: 28.

Vollmer W, Joris B, Charlier P & Foster S (2008) Bacterial peptidoglycan (murein) hydrolases. *FEMS Microbiol Rev* 32: 259-86.

Walsby AE (2007) Cyanobacterial heterocysts: terminal pores proposed as sites of gas exchange. *Trends Microbiol* 15: 340-9.

Wang Y & Xu X (2005) Regulation by *hetC* of genes required for heterocyst differentiation and cell division in *Anabaena* sp. strain PCC 7120. *J Bacteriol* 187: 8489-93.

Wildon DC & Mercer FV (1963) The ultrastructure of the vegetative cell of blue-green algae. *Aust J Biol Sci* 16: 585-96.

Wilk L, Strauss M, Rudolf M, Nicolaisen K, Flores E, Kühlbrandt W & Schleiff E (2011) Outer membrane continuity and septosome formation between vegetative cells in the filaments of *Anabaena* sp. PCC 7120. *Cell Microbiol* 13: 1744-54.

Wolk CP, Ernst A & Elhai J (1994) Heterocyst metabolism and development. In Bryant DA (ed) *The molecular biology of cyanobacteria*. Kluwer Academic Publisher, Holland, 769-823.

Wolk CP, Thomas J, Shaffer PW, Austin SM & Galonsky A (1976) Pathway of nitrogen metabolism after fixation of 13N-labeled nitrogen gas by the cyanobacterium, *Anabaena cylindrica*. J Biol Chem 251: 5027-34.

Wu X, Liu D, Lee MH & Golden JW (2004) *patS* minigenes inhibit heterocyst development of *Anabaena* sp. strain PCC 7120. *J Bacteriol* 186: 6422-9.

Xu X, Elhai J & Wolk CP (2008) Transcriptional and developmental responses by Anabaena to deprivation of fixed nitrogen. In Herrero A & Flore E (eds) *The Cyanobacteria: molecular biology, genomics and evolution*. Caister Academic Press, Norfolk, UK. 383-422.

Yoon HS & Golden JW (1998) Heterocyst pattern formation controlled by a diffusible peptide. *Science* 282: 935-8.

Yoon HS & Golden JW (2001) PatS and products of nitrogen fixation control heterocyst pattern. *J Bacteriol* 183: 2605-13.

Zhang CC, Huguenin S & Friry A (1995) Analysis of genes encoding the cell division protein FtsZ and a glutathione synthetase homologue in the cyanobacterium *Anabaena* sp. PCC 7120. *Res Microbiol* 146: 445-55.

Zhang Y, Tang W, Ahmad S, Sipp JA, Chen P & Lin X (2005) Gap junction-mediated intercellular biochemical coupling in cochlear supporting cells is required for normal cochlear functions. *Proc Natl Acad Sci USA* 102: 15201-06.

Zhu J, Jäger K, Black T, Zarka K, Koksharova O & Wolk CP (2001) HcwA, an autolysin, is required for heterocyst maturation in *Anabaena* sp. strain PCC 7120. *J Bacteriol* 183: 6841-51.